Dankwoord

Bij het afsluiten van dit onderzoek is het gepast de persoon van wijlen prof. Snoeys in herinnering te roepen die met een begeesterende overtuiging reeds van in het begin dit werk op een bepalende manier vorm en inhoud heeft gegeven. Verder is het de verdienste van prof. Peters dat dit onderzoek door zijn bijzondere impulsen succesvol is afgerond. De dagelijkse leiding werd waargenomen door prof. Sas die op een geestesverruimende manier en met een flegmatieke vindingrijkheid nieuwe ideeën en initiatieven in het onderzoeksdomein inpaste. De kansen op succes werden in belangrijke mate verhoogd door prof. Van Brussel die mij in zijn laboratorium onvoorwaardelijk de materiële en immateriële mogelijkheden heeft geboden gedegen wetenschappelijk werk te verrichten.

Bijzonder erkentelijk ben ik Theo Janter die met een grondig doorzicht en een stevige dosis redeneringsvermogen niet enkel zwakke plekken kon blootleggen maar ook verfijningen suggereren. Speciale dank gaat verder naar Francky Seys en Christophe Liefooghe die behulpzaam zijn geweest bij het uitvoeren van programmeerwerk en een materiaaltest. En ook het beschikbaar stellen van meetgegevens door Hubert Verelst en Eric Heublein heb ik bijzonder geapprecieerd.

Tenslotte spreek ik mijn gemeende waardering uit voor alle leden van de afdeling "Mechanische Constructie en Productie" met wie ik in een aangename sfeer heb mogen samenwerken en die zo een al dan niet tastbare bijdrage hebben geleverd tot het welslagen van dit werk.

Dirk Vandepitte
maart 1990

Contents

1 Introduction and survey of literature 7

1.1 Introduction 7

1.1.1 History of fatigue analysis 7

1.1.2 Fatigue and vibrations 8

1.1.3 Analytical versus experimental techniques 9

1.1.4 Requirements for a reliable method 10

1.1.5 Objectives of the method presented 12

1.2 Different types of fatigue 12

1.3 Numerical methods in fatigue analysis 13

1.3.1 Traditional method 13

1.3.1.1 Basic assumptions 13

1.3.1.2 Sequence of operations 17

1.3.1.3 Advantages and drawbacks 20

1.3.2 Local strain approach 21

1.3.2.1 Basic assumptions 21

1.3.2.2 Sequence of operations 26

1.3.2.3 Advantages and disadvantages 26

1.3.3 Linear fracture mechanics 27

1.3.3.1 Basic features 27

1.3.3.2 Recent developments 31

1.4 Numerical methods in structural analysis 32

1.4.1 Stress analysis 32

1.4.1.1 The finite element method 32

1.4.1.2 Boundary element method 33

1.4.2 Dynamic response 34

1.4.2.1 Direct integration 34

1.4.2.2 Modal analysis 35

1.5 Aspects of experimental analysis 35

1.5.1 Experimental techniques in fatigue analysis . . . 35
1.5.1.1 Full scale component testing 35
1.5.1.2 Material testing 37
1.5.2 Influencing factors 38
1.5.3 Comments on the accuracy of the results 40
1.6 Statistical methods of fatigue life predictions 40
1.6.1 Definition of the load signal 41
1.6.2 Distribution of level crossings and peak values . 42
1.6.3 Accumulation of damage 43
1.6.4 Wide band excitation 44
1.6.5 Use of statistical methods 45
1.7 Conclusion : formulation of the problem 45

2 Aspects of an analytical fatigue life estimation method 47
2.1 Purpose and capabilities of the method 47
2.1.1 Fields of application 48
2.1.2 Capabilities and restrictions 49
2.2 General overview of the method 51
2.2.1 Flowchart 51
2.2.2 Integration of experimental and analytical techniques 51
2.3 Consecutive steps in the method 55
2.3.1 Dynamic response of the structure 55
2.3.1.1 Flowchart 55
2.3.1.2 Necessary input data 55
2.3.1.3 Computation in the time domain 58
2.3.1.4 A fast computer algorithm 59
2.3.1.5 Superposition 61
2.3.2 Stress/strain analysis 62
2.3.2.1 Flowchart 62
2.3.2.2 Computation of spatial strain distribution 62
2.3.2.3 Direct computation of the stress/strain sequence using modal stresses or strains 68
2.3.3 Estimation of the fatigue lifetime 71
2.3.3.1 Flowchart 72
2.3.3.2 Selection of the critical areas on the structure 73

2.3.3.3 Conversion of nominal strain history to local strain history 75
2.3.3.4 Resolution into distinct hysteresis loops 76
2.3.3.5 Evaluation of accumulated damage . . . 76
2.3.4 Evaluation of design modifications 77
2.3.5 Comparison of statistical methods with the proposed method 78
2.4 Conclusion 80

3 Computation of the dynamic response of a structure 83
3.1 Introduction 83
3.2 A modal model of the structure 84
3.2.1 Determination of modal parameters 84
3.2.1.1 Analytical methods 84
3.2.1.2 Experimental methods 88
3.2.2 Accuracy of modal parameters 89
3.2.2.1 Sensitivity analysis 89
3.2.2.2 Correction of modal parameters 94
3.2.2.3 Coarseness of the modal model 95
3.2.2.4 Representation of the eigenmodes . . . 96
3.2.2.5 Example 96
3.3 Computation of the dynamic response 101
3.3.1 Frequency domain method 102
3.3.2 Time domain method 103
3.3.2.1 Impulse response 104
3.3.2.2 Arbitrary force input 105
3.3.2.3 Implementation of the algorithm 105
3.3.2.4 Static loads and higher modes 109
3.3.3 Comparison of frequency domain methods with time domain methods 110
3.3.3.1 Computational efficiency 111
3.3.3.2 Influence of a particular mode 111
3.3.3.3 Influence of static loads 112
3.4 Recent advances in dynamic modelling 112
3.4.1 Model updating techniques 112
3.4.2 Error localization 114
3.4.3 Nonlinearities 115
3.5 Conclusion 116

4 Strain computation in a dynamic context 119
4.1 Introduction 119
4.2 Numerical static elastic stress analysis 120
4.2.1 The finite element method 120
4.2.1.1 Basic features 120
4.2.1.2 Enhanced capabilities 124
4.2.1.3 Computational aspects 128
4.2.1.4 Comments on the use of the method . . 128
4.2.2 The boundary element method 129
4.2.2.1 Basic features 130
4.2.2.2 Enhanced capabilities 135
4.2.2.3 Computational aspects 137
4.2.2.4 Comments on the use of the method . . 138
4.2.3 Comparison of the boundary element method to the finite element method 139
4.2.3.1 The preprocessing phase 139
4.2.3.2 The continuous representation of geometry 140
4.2.3.3 The size of the matrices 140
4.2.3.4 Variables of mixed type 141
4.2.4 Example 141
4.3 Use of the boundary element method in elastic dynamic analysis 144
4.3.1 Time dependent integral formulation 144
4.3.2 Transform formulations 147
4.3.3 Nardini's method 148
4.3.4 Method based on modal parameters 150
4.3.4.1 Description of inertial loads 151
4.3.4.2 The concept of modal strains 152
4.3.4.3 Smoothing techniques 155
4.4 Computation of the effects of plasticity 156
4.4.1 Use of the finite element method 156
4.4.2 Use of the boundary element method 157
4.4.2.1 Coupling with the finite element method 158
4.4.2.2 Banerjee's technique involving particular integrals 159
4.4.3 Estimation of plastic deformation using elastic analysis 160

4.5 Conclusion 162

5 Estimation of fatigue lifetime **165**

5.1 Introduction 165
5.2 Local strain approach 166
5.2.1 Basic features 166
5.2.2 Material properties 167
5.2.2.1 Cyclic properties of the material 167
5.2.2.2 Strain–life -relation 169
5.2.2.3 Measurement of the material properties 171
5.2.3 Counting methods 175
5.2.3.1 Peak-valley method 175
5.2.3.2 Range-pair method 176
5.2.3.3 Rainflow method 176
5.2.3.4 Discussion of different methods 177
5.2.3.5 Storage of data 177
5.2.3.6 Reduction of noise 178
5.2.4 Influence of plasticity 180
5.3 Multiaxial fatigue 180
5.3.1 Failure mechanisms under multiaxial straining . 182
5.3.2 High cycle multiaxial fatigue 183
5.3.2.1 Proportional loading 183
5.3.2.2 Nonproportional loading 185
5.3.3 Low-cycle fatigue 187
5.3.3.1 Constitutive equations 188
5.3.3.2 Low-cycle multiaxial fatigue criterions . 191
5.3.4 A pragmatic approach 194
5.4 Comparison of the computed lifetime to experimental results 197
5.4.1 Sensitivity of the computed lifetime to variations of some parameters 197
5.4.1.1 Material properties 197
5.4.1.2 Mean stress level 199
5.4.1.3 Cyclic stress level 200
5.4.1.4 Comments on the accuracy of the computed lifetime 201
5.4.2 Tuning of the model 202
5.5 Conclusion 202

6 Practical examples **205**
6.1 Introduction 205
6.2 Notched cantilever beam 205
6.2.1 Description of the problem 206
6.2.2 Dynamic analysis 207
6.2.2.1 Experimental modal analysis 207
6.2.2.2 Numerical modal analysis 207
6.2.3 Modal strains 209
6.2.4 Fatigue life prediction 210
6.2.5 Fatigue life experiment 210
6.2.6 Justification of observed phenomena 212
6.2.7 Updating of the model 212
6.2.8 Modification of the setup 213
6.2.9 Conclusion 215
6.3 Hammer of a machine 215
6.3.1 Description of the problem 215
6.3.2 Fatigue analysis 217
6.3.3 Resonance fatigue 222
6.3.4 Resonance frequencies and modeshapes 224
6.3.5 Stress distribution 225
6.3.6 Design modifications 228
6.3.6.1 Radius of curvature 228
6.3.6.2 Damping 228
6.3.6.3 Mass/stiffness modification 229
6.3.6.4 Load input 230
6.3.6.5 Different material 231
6.3.7 Conclusion 231

A Basic features of the boundary element method **235**
A.1 Introduction 235
A.2 Boundary integral formulation of a problem of elastostatics 235
A.3 Numerical implementation 239
A.4 Displacements and stresses at points located inside the domain or on the boundary 245
A.4.1 Internal points 245
A.4.2 Stresses on the boundary 246

B Numerical evaluation of material characteristics **247**
B.1 Cyclic material properties 247
B.2 Fatigue properties 248
B.2.1 General procedure 248
B.2.2 General remarks 249
B.3 Statistical analysis 250

C Measurement of structural damping characteristics **251**
C.1 Logarithmic decrement method 251
C.2 Practical application 253

D Practical implementation **255**
D.1 General overview 255
D.2 Data preparation 257
D.3 Modal strain computation 258
D.3.1 Input data 258
D.3.2 Computational options 260
D.3.3 General remarks 262
D.4 Computation of dynamic response 262
D.4.1 Input data 262
D.4.2 Computational options 263
D.4.3 General remarks 263
D.5 Fatigue life estimation 264
D.5.1 Input data 264
D.5.2 Computational options 265
D.5.3 General remarks 267

List of Figures

N.1 Schema van de voorgestelde methode xxix
N.2 Opeenvolgende stappen in responsberekening xxxi
N.3 Schema van levensduurvoorspelling xli
N.4 Schema voor aanpassing van het vermoeiingsmodel . . . xlvi
N.5 Ingeklemde balk met groef xlvi
N.6 Uitvergroot beeld van de groef xlvii
N.7 Geometrie van de hamer xlix
0.1 Typical time schedule for the development and design of an automobile 2

1.1 Perfect elasto-plastic stress-strain behaviour 14
1.2 Example of a Wöhler-curve 14
1.3 Haigh–Soderberg -correction 16
1.4 Linear damage accumulation rule 17
1.5 Perfectly elastic state 18
1.6 One single plastic deformation (tension) 19
1.7 Hysteresis loops (positive mean strain) 19
1.8 One single plastic deformation (compression) 20
1.9 Hysteresis loops (negative mean strain) 20
1.10 Cyclic stress-strain -behaviour 23
1.11 Cyclic strain-life -relation 24
1.12 Stress-distribution around a crack tip 28
1.13 Crack growth rate 29

2.1 Consecutive steps in the fatigue life estimation method . 52
2.2 Integration of experimental and analytical techniques . . 54
2.3 Consecutive steps in the method of response prediction . 56
2.4 Definition of $\langle t-t_a\rangle^{-1}$, $\langle t-t_b\rangle^{0}$, $\langle t-t_c\rangle^{1}$ 60
2.5 Random load input 60

2.6 Superposition of static and dynamic load 62
2.7 General scheme of stress/strain- analysis 63
2.8 Modified scheme of the proposed method 72
2.9 Scheme of the life prediction technique from several strain sequences 73
2.10 Criterion of maximum strain amplitude 74
2.11 Determination of $\mathcal{S}$ 74
2.12 Elimination of noise on strain sequence 75

3.1 Assumption of constant curvature in beams 92
3.2 Small cube of material subjected to uniaxial loading . . 93
3.3 Hinged beam vibrating at 1^{st} resonance frequency, experimental mode shape 96
3.4 Load cases 2 and 3 and distribution of relative strain . . 101
3.5 Vibrating beam with backlash 116

4.1 Linear and quadratic meshes of rectangular elements . . 122
4.2 Location of Gauss-points in SYSTUS elements 2004 and 2008 123
4.3 Two examples of non-conforming elements 126
4.4 Hybrid element by FRAEYS DE VEUBEKE 127
4.5 Models of clamped T-plate 133
4.6 Four-noded linear surface element 134
4.7 Constant and quadratic discontinuous surface elements . 136
4.8 Examples of allowable linear surface meshes 136
4.9 Transformation of integration domain 137
4.10 Models and stress distribution of rotor disc 143
4.11 Notched beam vibrating at 1^{st} resonance frequency . . . 153
4.12 Model of prismatic notch effect 160

5.1 Specimen for measurement of cyclic material properties 171
5.2 Fatigue test specimen type "Moore" 173
5.3 The peak-valley method 176
5.4 Sensitivity of the peak-valley method to small load variations 176
5.5 The range-pair method 177
5.6 The rainflow method 178
5.7 Application of "racetrack"-method for reduction of noise 179
5.8 Local strain computation - a - NEUBER - b - alternative 181

5.9 Examples of proportional and nonproportional loading . 182
5.10 MOHR's circle for strains 183
5.11 Planes and directions of stages I and II crack growth . 184
5.12 a. Octahedral plane – b. Variation of τ_0 with θ 186
5.13 PRAGER's models for plastic behaviour 188
5.14 Piecewise linear stress–strain -law 189
5.15 Yield surfaces during proportional loading 189
5.16 Fatigue damage maps 195
5.17 Flowchart of fatigue updating procedure 203

6.1 Geometry of clamped beam 206
6.2 Enlarged view of notched area 206
6.3 Experimental mode shape 207
6.4 MSC-NASTRAN finite element model 208
6.5 Variation of resonance frequency with spring stiffness . . 208
6.6 Boundary conditions and inertial loading 210
6.7 Profile of the milled notch 212
6.8 Modified setup of clamped beam 213
6.9 Geometry of the hammer 216
6.10 Different phases of a cycle of operation of the hammer . 217
6.11 Relation between cyclic strain amplitude and number of cycles to failure 219
6.12 Measured strain sequence in point A 220
6.13 Measured strain sequence in point B 220
6.14 Static loadcase for determination of stress concentration factors 221
6.15 Iso-contour of equivalent VON-MISES -stress 221
6.16 Hysteresisloops in the critical area a of the body of the tail 222
6.17 Fourier transform of measured strain sequence point A . 223
6.18 Fourier transform of measured strain sequence point B . 223
6.19 Finite element mesh 224
6.20 Deformation of mode 1 226
6.21 Deformation of mode 2 226
6.22 Deformation of mode 3 226
6.23 Iso-contour of equivalent VON-MISES -stress for mode 1 227
6.24 Iso-contour of equivalent VON-MISES -stress for mode 2 227
6.25 Measured strain sequence in point A, hammer with elastomer cushion 231

A.1 Geometry of the bodies Ω and Ω^* 236
A.2 Example of discontinuous elements in two-dimensional analysis (clamped square plate with notch subjected to tension) 242

C.1 Impulse response function 252
C.2 Geometry of high pressure tube 253

D.1 Global scheme of computation 256
D.2 Isolated portion of crankshaft 261

List of Tables

N.1 Experimentele levensduur van de hamer xlix

1.1 Pros and cons of experimental and numerical methods . 11

3.1 Individual relative displacement components for each load 99
3.2 Distribution of relative strain along the length of the beam 100

4.1 Geometrical and material properties of rotor disc 142
4.2 Performance of FE and BE method on rotor disc 144

5.1 Material properties and loading conditions 198
5.2 Sensitivity of computed life to K' and n' for different K_t 199
5.3 Influence of mean stress 200
5.4 Sensitivity of computed life to stress concentration factor K_t 201

6.1 Material properties of steel 14NiCrMo13 211
6.2 Predicted life of notched beam 211
6.3 Material properties of carbonised material 214
6.4 Lives of test specimens to failure 218
6.5 Material properties of steel 14NiCrMo13, CN 0.20 . . . 218
6.6 Resonance frequencies 225
6.7 Resonance frequencies of modified hammer 229

A.1 Number of degrees of freedom (dof) 242
A.2 Dimension of influence matrices and vectors 243
A.3 Dimension of the set of equations 244

Nomenclature

The most important notations are summarised below. Symbols that occur only locally in one or a few sections are not mentioned here. All symbols used, including the ones below, are explained in the text.

General symbols and conventions

t	: time
$\dot{\bullet}$	: time derivative of quantity $\bullet$
$\ddot{\bullet}$	: second time derivative of quantity $\bullet$
x, y, z	: cartesian coordinate system
r, θ	: polar coordinate system
$\bullet_x$, $\bullet_y$, $\bullet_z$	: x-, y-, z- components of $\bullet$
$\bullet_i$, $\bullet_j$, $\bullet_z$	: x-, y-, z- components of $\bullet$ (used in summations)
$\underline{e}_i$	: unit vector in i-direction
I, J	: input and output locations
$\bullet_I$, $\bullet_J$	: quantity $\bullet$ taken in input and output locations
$\bullet_i \bullet_i$	: summation convention over indices that occur twice : $\bullet_i \bullet_i = \sum_i \bullet_i \bullet_i$
$\underline{\bullet}$	: vector, one-dimensional tensor $\underline{\bullet} = \bullet_x \underline{e}_x + \bullet_y \underline{e}_y + \bullet_z \underline{e}_z$
$\underline{\bullet}.\underline{\square}$	: vector product $\sum_{i=1}^{3} \bullet_i \square_i$
$\underline{\underline{\bullet}}$	: two-dimensional tensor
$\underline{\underline{\bullet}} : \underline{\square}$	: tensor product $\sum_{i=1}^{3} \sum_{j=1}^{3} \bullet_{ij} \square_{ij}$
$g(\xi)$	: general function of general variable ξ
$\Delta\xi$	: increment of variable ξ
w_i	: weighting factor in quadrature scheme

$O(\bullet^n)$: terms in $\bullet$ of order n and higher
$\delta(\bullet)$: DIRAC-function of scalar variable $\bullet$
$\Delta(\underline{\bullet})$: DIRAC-function of vector variable $\underline{\bullet}$
$\langle\bullet\rangle^n$: $\begin{cases} 0 & \bullet < 0 \\ \bullet^n & \bullet \geq 0 \end{cases} \quad n \neq -1$
$\bullet^*$: complex conjugate of $\bullet$
$*$: convolution operator
$[\bullet]$: matrix
$\{\bullet\}$: column vector
$[\bullet]^{-1}$: inverse of square matrix
j : imaginary unit $\sqrt{-1}$

Geometric properties

Ω : volume of body, domain
Ω^* : volume of containing body
Γ : boundary of body
Γ^* : boundary of containing body
$\Gamma_\bullet$: portion of boundary Γ where quantity $\bullet$ is imposed
l : length of beam
h : height of beam
I : geometrical cross sectional moment of inertia

Stress, strain, displacement

u, v, w : displacement in x-, y-, z- direction
σ : component of stress
σ_{ij} : component of stress i, $j = 1, 2, 3$
σ_i : principal stress $\sigma_1 \geq \sigma_2 \geq \sigma_3$
τ : shear stress
ε : component of strain
ε_{ij} : component of strain i, $j = 1, 2, 3$
ε_i : principal strain $\varepsilon_1 \geq \varepsilon_2 \geq \varepsilon_3$
γ : shear strain
$\bullet_e$: elastic portion of quantity $\bullet$
$\bullet_p$: plastic portion of quantity $\bullet$
M : bending moment

V : shear force
N : axial force
P : general force
M_t : torsional moment

Multiaxial states of stress

J_1' : 1^{st} invariant of stress tensor
J_2' : 2^{nd} invariant of stress tensor
τ_{crit} : limit of equivalent stress
$\bullet_{alt}$: alternating portion of quantity $\bullet$
$\bullet_{stat}$: static portion of quantity $\bullet$
$\Delta\sigma_{eq}$: variation of equivalent stress
s_{ij} : deviatoric stress
E_s : equivalent modulus of elasticity
$\hat{\sigma}$: equivalent stress
$\hat{\varepsilon}$: equivalent strain

Material properties

E : YOUNG's modulus of elasticity
G : shear modulus
ν : POISSON coefficient
λ, μ : LAMÉ coefficients
C_1, C_2 : material coefficients in equation of motion
σ_y : material yield stress
σ_u : material ultimate stress
RA : reduction of area
A_0 : nominal cross section of specimen
A_f : cross section of specimen at failure
ε_f : strain at rupture
σ_v : fatigue limit
n' : cyclic strain-hardening exponent
n : static strain-hardening exponent
K' : plastic stiffness modulus
σ_f' : fatigue strength coefficient

τ'_f	: shear fatigue strength coefficient
b	: fatigue strength exponent
ε'_f	: fatigue ductility coefficient
γ'_f	: shear fatigue ductility coefficient
c	: fatigue ductility exponent

Fatigue analysis

σ_N	: equivalent stress amplitude
σ_{nom}, ε_{nom}	: nominal stress, nominal strain
σ, σ_{real}	: real stress, local stress
ε, ε_{real}	: real strain, local strain
$\Delta\bullet$	: range of quantity $\bullet$
$\bullet_a$	: amplitude of $\bullet$
$\bullet_m$	: mean value of $\bullet$
$\bullet_{min}$	: minimum value of $\bullet$
$\bullet_{max}$	: maximum value of $\bullet$
N, N_i	: number of cycles to failure
n, n_i	: number of occurrences of cycle
C_{Miner}	: right hand side constant of MINER
W	: dissipated energy
W_f	: dissipated energy at fracture

Fracture mechanics

K	: stress intensity factor
σ	: engineering stress in notch area
a	: crack size
ΔK_0	: threshold value for crack propagation
K_c	: critical stress intensity factor
a_i	: initial crack size
a_c	: critical crack size
m	: exponent in PARIS equation
C	: coefficient in PARIS equation

Statistical analysis

$U(t)$	: stochastic process
$u_i(t)$	: sample i of process $U(t)$
t, t_j	: time of sampling
ν_a^+	: rate of positive crossing of level a
$\sigma_\bullet$	: standard deviation of quantity $\bullet$
m_i	: moment of order i
$\mathcal{E}(\bullet)$	: expected value of quantity $\bullet$
ω	: angular frequency
$S_u(\omega)$	: power spectral density op process $u(t)$
τ	: time variable
$R_u(\tau)$	: autocorrelation function of $u(t)$
M	: occurrence of maximum value of $u(t)$
D	: total damage
d_i	: damage at cycle i
S	: stress
$q(S)$	: probability density of stress S
$N(S)$	: number of cycles to failure for stress amplitude S
σ_S	: standard deviation on stress S
η	: dimensionless stress
f	: frequency
ω	: angular frequency
$W(f)$	: spectral density function
$G(\omega)$	: one-sided spectral density

Dynamics and modal analysis

m	: mass of single degree of freedom system
c	: damping of single degree of freedom system
k	: stiffness of single degree of freedom system
u	: displacement
$\dot{u}$	: velocity
$\ddot{u}$, a	: acceleration
s	: variable in LAPLACE-domain
$u_j^{(0)}$, $v_j^{(0)}$	: initial conditions

$J(u)$, $\mathcal{J}(d,t)$: energy functions HAMILTON's principle
P, P_i, P_e : potential energy, internal, external
T : kinetic energy
k : number of mode
f_k : natural frequency mode
ω_k : natural angular frequency
f_{dk} : damped resonance frequency
ν_k : damped angular resonance frequency
λ_k : complex eigenvalue
ζ_k : damping ratio
σ_k : damping factor
η_k : loss factor
Q_k : quality factor
ψ_k, $\{\psi_k\}$: mode shape, mode shape vector
ψ_k^u : mode shape expressed in terms of displacement
ψ_k^a : mode shape expressed in terms of acceleration
ψ_k^f : mode shape expressed in terms of inertial force
ψ_k^ε : mode shape expressed in terms of strain
$[M]$: mass matrix
$[C]$: damping matrix
$[K]$: stiffness matrix
R_{IJk} : residue mode k, input location I, output location J
a_k : modal scaling constant
H_{IJ}, $[H]$: frequency response function, matrix
$h_{IJ}(t)$: impulse response function
$U_{IJk} + jV_{IJk}$: complex modal displacement
L_{Jk} : modal participation factor for input location J
τ : time variable
$f(t)$: time variation of exciting force
$\mathcal{F}(\omega)$: excitation force in frequency domain
$x(t)$: output signal in time domain
$\mathcal{X}(\omega)$: output signal in frequency domain
$\mathcal{UR}_{IJ}$: upper residual term
$\mathcal{LR}_{IJ}$: lower residual term
Δt : time increment

Finite element method

$\{u\}$	: column vector of displacement degrees of freedom
$\{d\}$	: column vector of degrees of freedom
$[M]$	: global mass matrix
$[C]$	: global damping matrix
$[K]$	: global stiffness matrix
$[M]_i$	: mass matrix element i
$[C]_i$	: damping matrix element i
$[K]_i$	: stiffness matrix element i
$\{F\}$	: column vector of forces
$\varphi_i^{(j)}(\xi)$	: shape function for node j
$[N]$	: matrix of shape functions
$[\partial]$	: matrix of differential operators
$[B]$	: matrix of differences
$[D]$	: matrix expressing constitutive equations
Ω	: domain of the entire structure
Γ	: boundary of the entire structure
$\Gamma_\bullet$	: portion of boundary where quantity $\bullet$ is imposed
Ω_i	: domain of element i
Γ_i	: boundary of element i
$\bar{\bullet}$	: imposed value of $\bullet$
w	: deflection of plate element
$\partial w/\partial n$	: gradient of deflection of plate element
$\delta\bullet$	: virtual quantity $\bullet$
Π	: potential energy
Π'	: modified potential energy
Π_c	: complementary energy
Π_c'	: modified potential energy
$\mathcal{B}(\sigma)$	: potential energy of internal forces expressed in terms of stresses

Boundary element method

$\underline{x}$	: coordinate of field variable
$\underline{\xi}$	: coordinate of collocation point
$u_i(\underline{\xi})$	: displacement in i- direction at location $\underline{\xi}$

$p_i(\underline{\xi})$: traction in i- direction at location $\underline{\xi}$
$\{u\}$: column vector of displacements at collocation points
$\{p\}$: column vector of tractions at collocation points
$\{f\}$: column vector of volume loads at nodes of volume model
Ω : domain of the entire structure
Γ : boundary of the entire structure
Ω^* : domain of the surrounding structure $*$
Γ^* : boundary of the surrounding structure $*$
$\Gamma_\bullet$: portion of boundary where quantity $\bullet$ is imposed
Ω_i : domain of element i
Γ_i : boundary of element i
$\overline{\bullet}$: imposed value of $\bullet$
c_{ij} : constant number $(0 \leq c_{ij} \leq 1)$
u^*_{ij} : fundamental solution for displacements
p^*_{ij} : fundamental solution for tractions
$[H]$: influence matrix for displacements
$[G]$: influence matrix for tractions
$[W]$: influence matrix for volume loads
$[A]$: system matrix
$\{x\}$: column vector of unknowns
$\{y\}$: column vector of known right hand sides
$\underline{n}$: unit normal vector
r : distance between $\underline{x}$ and $\underline{\xi}$
$\varphi^{(j)}(\underline{\xi})$: shape function for node j
U^*_{ij} : time dependent fundamental solution for displacements
P^*_{ij} : time dependent fundamental solution for tractions
$\mathcal{L}(\bullet)$: LAPLACE- operator
$\{\mathcal{U}\}$: column vector of displacements in frequency domain
$\{\mathcal{P}\}$: column vector of tractions in frequency domain
$\mathcal{U}^*_{ij}$: fundamental solution for displacements in frequency domain
$\mathcal{P}^*_{ij}$: fundamental solution for tractions in frequency domain
$[T]$: conversion matrix of tractions to forces
$[\tilde{K}]$: stiffness matrix in FE–BE- coupling

Nederlandse samenvatting

N.1 Inleiding

N.1.1 Ontwerp tegen vermoeiing in industriële praktijk

Reeds in het midden van de negentiende eeuw werden ontwerpingenieurs geconfronteerd met vermoeiingsproblemen. Men slaagde er evenwel in de levensduur van mechanische produkten voldoende hoog te houden door de machine of de constructie op statische belasting te ontwerpen en grote veiligheidsfactoren (3 à 5) toe te passen. Naarmate constructies minder zwaar en met minder stijve materialen werden opgebouwd traden onaanvaardbare trillingsniveau's op en bleken vroeger gebruikte ontwerpmethodes niet langer toepasbaar. Men diende zijn toevlucht te nemen tot ver doorgedreven experimenten om de te verwachten levensduur van een constructie te kunnen bepalen vooraleer ze in bedrijf genomen werd. Enkel voor constructies van een vrij eenvoudige geometrie en met een welomschreven belastingsverloop bleken numerieke methoden nog toepasbaar te zijn. Van een complex geheel dat is opgebouwd uit meerdere onderdelen kunnen hooguit componenten worden doorgerekend die vrij eenvoudig kunnen afgezonderd worden uit de rest van de constructie. In de industriële praktijk worden daarbij vaak sterk vereenvoudigende hypothesen gesteld, bij voorbeeld wordt het dynamisch gedrag verwaarloosd. De enige methode van schatting van de levensduur waarop men betrouwt is een doorgedreven experiment waarbij de bestudeerde constructie in al dan niet gesimuleerde bedrijfsomstandigheden wordt belast. Daarbij blijkt het dikwijls moeilijk te zijn systematisch te werk te gaan. Om economische redenen worden testen soms vroegtijdig onderbroken. Zelfs wanneer een proefneming op een gedegen manier wordt doorgevoerd, is de interpretatie van de resultaten verre van eenvoudig.

N.1.2 Gebruikte technieken

De oudste methode — die heden nog het meest wordt toegepast — behandelt spanningsgrootheden op een manier die sterk verwant is met de klassieke methodes voor statische sterkteberekeningen. Met betrekking tot het gedrag van het materiaal zelf wordt doorgaans een hypothese van elastisch/perfect plastisch gedrag gesteld. Twee parameters beschrijven dit gedrag volledig : de elasticiteitsmodulus E en de vloeigrens σ_y. Fig.1.1 geeft een grafische voorstelling. De WÖHLER-curve geeft het verband tussen de amplitudo van de aangelegde spanning en het aantal cycli tot breuk. Er wordt nagegaan of een bepaalde cyclus die in het belastingspatroon optreedt al dan niet aanleiding geeft tot plastische vervorming. Er wordt onderscheid gemaakt tussen drie mogelijke gevallen :

- zuiver elastisch, fig.1.5
- eenmalige plastische vervorming, nadien elastisch, fig.1.6, 1.8
- plastische vermoeiing, met hysteresislussen, fig.1.7, 1.9

Voor alle cycli wordt een overeenstemmend aantal wisselingen tot breuk berekend uit de WÖHLER-curve en de geaccumuleerde schade wordt geschat volgens de regel van MINER.

De lokale-rekmethode verschilt van de traditionele methode op twee essentiële punten. Vooreerst wordt het cyclisch gedrag van een materiaal beschreven op een meer realistische wijze. Een plasticiteitsmodulus K' en een plastische exponent n' worden gedefinieerd om een meer nauwkeurige beschrijving van het materiaalgedrag in het plastische domein te bekomen. Anderzijds wordt niet langer de spanning maar eerder de rek als maatgevende grootheid gebruikt. Het vermoeiingsgedrag van een materiaal wordt uitgedrukt door een verband te leggen tussen de rek en het aantal cycli tot breuk. Een complex rekverloop wordt opgedeeld in elementaire cycli volgens de "regendrop"-teltechniek. Voor iedere cyclus worden de lokale rek en de lokale spanning bepaald, waarbij gebruik gemaakt wordt van de benadering van NEUBER. Voor elke cyclus wordt de elementaire schade bepaald en uiteindelijk wordt de geaccumuleerde schade begroot met de regel van MINER.

De traditionele method geeft aanvaardbare resultaten wanneer de amplitudo van de belasting zodanig is dat het materiaal in elasti-

sche toestand blijft. Wanneer plastische vervormingen optreden zijn de resultaten van de levensduurschatting onbetrouwbaar. De lokale-rekmethode komt aan deze tekortkomingen tegemoet door een betere beschrijving van het plastisch gedrag.

Zowel de traditionele methode als de lokale-rekmethode geven een schatting van het aantal cycli tot initiatie van een microscheur. Om het verschijnsel van scheuruitbreiding te beschrijven worden theorieën uit de breukmechanica toegepast.

N.1.3 Aanverwante technieken

Numerieke methoden kunnen worden gebruikt om bepaalde onderdelen van een algehele vermoeiingsanalyse uit te voeren. Het dynamisch gedrag van een constructie kan worden beschreven met behulp van een eindig-elementenmodel. Ook een spanningsberekening kan worden doorgevoerd met een eindig-elementenmodel, of alternatief met een randelementenmodel. Beide methoden die elk hun eigen karakteristieken hebben, bieden ook voor- en nadelen op verschillende domeinen. De praktische toepassing van elk van beide technieken laat in industriële middens vaak te wensen over. Zowel in de fundamentele keuze van de aard van de gebruikte methode, met elk hun bijzondere eigenheden, als in de concrete samenstelling van het model, dient een verantwoorde weg te worden ingeslagen. Het ligt voor de hand dat deze numerieke technieken in een computer ondersteunde simulatie bijzonder nuttig kunnen zijn, op voorwaarde echter dat de voordelen van elk van beide zo handig modelijk worden uitgebuit. Een voorbeeld is hier zeer illustratief. De globale stijfheid en het dynamisch gedrag van een tankschip kunnen worden gemodelleerd met een vrij ruw eindig-elementenmodel van het hele schip. Bij de controle van de spanningsniveau's in kritische zones van verbindingen of verstijvingselementen zal echter een zeer gedetailleerd model moeten worden samengesteld van een beperkte zone rondom de bestudeerde component.

N.1.4 Experimenteel vermoeiingsonderzoek

Proefondervindelijk onderzoek is een niet te omzeilen stap in vermoeiingsontwerp, en zal dit voor altijd blijven, alle ontwikkelingen van numerieke technieken ten spijt. Testopstellingen kunnen worden gebruikt om een gegeven probleem in zijn totaliteit te bestuderen, of om

een of meer deelaspecten te onderzoeken. Tevens is het mogelijk experimenteel onderzoek te combineren met numerieke analyse teneinde een grondig inzicht te verwerven in de meest kritische aspecten van het probleem.

Nochtans dient men in experimenteel werk met de meeste zorg te waken over de relevantie en het waarheidsgetrouwe karakter van de verschillende elementen en parameters uit de testopstelling, de te volgen belastingsprocedure en de bedrijfsomstandigheden. Het belang van deze laatste factoren dient niet te worden onderschat. Zo moet het proefmonster worden vervaardigd op precies dezelfde manier als de serieproductie om alle constructiedetails die voortspruiten uit de bewerkingstechnieken te laten overeenstemmen met de realiteit. Bij de test moet er voor gezorgd worden dat alle parameters als temperatuur, aggressiviteit van het omgevend milieu zo goed mogelijk worden gerealiseerd.

Vaak kan het uittesten van een volledige constructie nog op een relatief voor de hand liggende manier worden benaderd, hoewel de concrete realisatie van de testopstelling andere, technische problemen met zich brengt. Experimentele analyse van een component uit het geheel is soms verre van eenvoudig, omdat het afzonderen van die component maar kan gebeuren door de gepaste randvoorwaarden op te leggen.

N.1.5 Formulering van het probleem

In dit werk wordt een methode voorgesteld die toelaat om op een volledige en gefundeerde manier het vermoeiingsgedrag van een dynamisch belaste constructie te simuleren. Daarbij worden alle optredende parameters, gaande van het dynamisch gedrag van de constructie over invloeden van spanningsconcentratie tot cyclische plasticiteit en mogelijke mechanismen van scheurinitiatie onderzocht op hun relatief belang met betrekking tot de verwachte levensduur. Er wordt gepoogd de invloed van maatgevende parameters op een relevante manier te evalueren. De methode die uiteindelijk wordt voorgesteld houdt rekening met deze parameters zonder dat echter de complexiteit van het geheel te groot wordt. De eenvoud van de voorgestelde technieken is in een praktische toepassing in industriële middens van doorslaggevend belang. Met betrekking tot experimentele methoden wordt er naar gestreefd om de informatie die men bekomt uit proef-

ondervindelijk onderzoek op elk niveau van de analyse te kunnen vergelijken met numerieke resultaten. Door de methode modulair op te bouwen en stapsgewijze te werk te gaan is het mogelijk tussenresultaten te interpreteren en te valideren op basis van beschikbare meetresultaten.

N.2 Overzicht van de voorgestelde methode

De benadering die in volgende paragrafen N.3 tot N.5 wordt voorgesteld is opgebouwd uit drie grote stappen, zoals aangegeven in het schema fig.N.1.

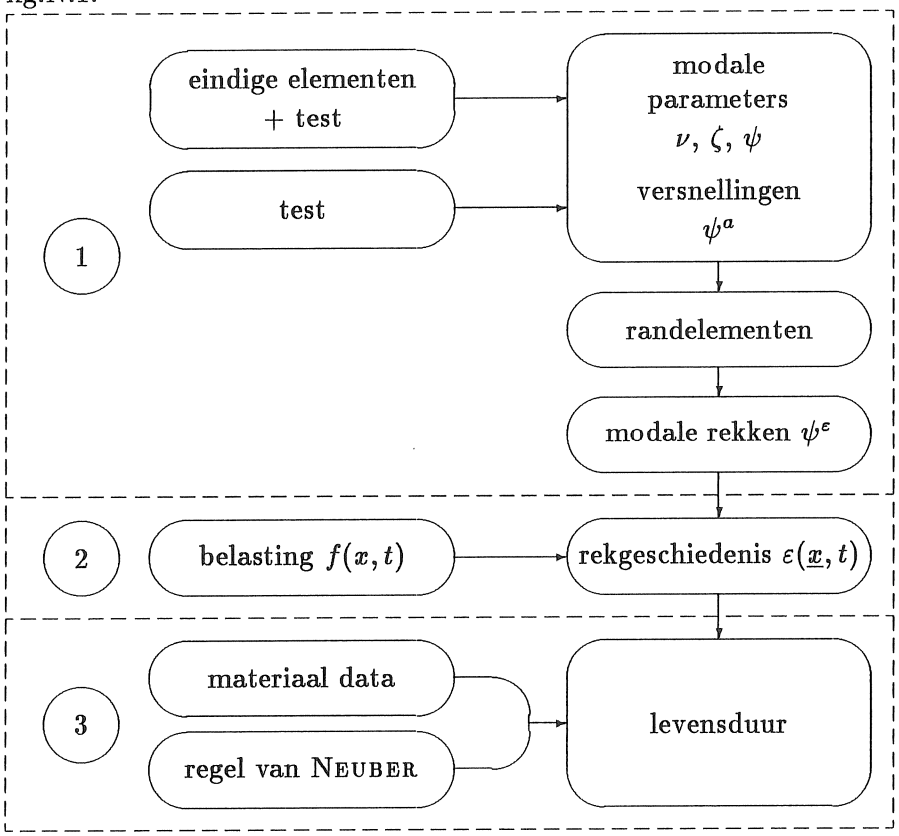

Figure N.1: Schema van de voorgestelde methode

Door de randelementenmethode op een originele manier te com-

bineren met het principe van de modale superpositie bekomt men op een snelle maar nauwkeurige manier de verlopen van de rek in de kritieke zones. Principes van de lokale-rekmethode worden nadien aangevuld met enkele bijkomende hulpmiddelen om de resultaten van de levensduurschatting grondig te evalueren.

Achtereenvolgens worden volgende stappen gezet :

modale rekken een of meerdere zones uit de constructie zijn potentieel kritiek, dit wil zeggen, in deze gebieden bestaat het gevaar voor vermoeiingsbreuk. Uit de beschrijving van de modevorm worden de overeenstemmende modale rekken in de kritieke zones berekend.

De modale rekken worden bekomen door aan de constructie de vervorming onder elke relevante modevorm op te leggen, en de overeenstemmende rekken in de bewuste gebieden te bepalen. De modevormen worden omschreven door de ruimtelijke verdeling van inertiekrachten als een statische belasting op te leggen en met de randelementenmethode de rekken te becijferen.

dynamische respons het verloop van de rek in functie van de tijd wordt in elk van de kritieke gebieden samengesteld door de convolutie-integraal te berekenen. Daarbij is het vereist dat het tijdsverloop van de aangelegde kracht volledig bekend is. Op basis van de frequentie-inhoud van deze kracht en van het dynamisch gedrag van de constructie zelf wordt het aantal eigenmoden bepaald dat in rekening dient genomen te worden. Door de modevormen uit te drukken in termen van modale rekken worden rechtstreeks de reksequenties in de kritieke zones bekomen. Een algoritme werd ontwikkeld om de convolutie-integraal op een snelle manier exact te berekenen.

schatting van de levensduur de lokale-rekmethode wordt toegepast om de schade te berekenen die wordt geaccumuleerd ten gevolge van de aangelegde reksequentie. Eerst wordt de meest kritieke zone geselecteerd. Nadien worden door combinatie van de benadering van NEUBER met de cyclische constitutieve curve van het materiaal de lokale rek- en spanningsverlopen afgeleid. Middels een correctie voor de gemiddelde spanning wordt dan voor elke cyclus de overeenstemmende elementaire schade bepaald, die dan uiteindelijk wordt gesommeerd volgens de regel van MINER.

Voor meerassige spanningstoestanden wordt een pragmatische benadering volgens SOCIE vooropgesteld.

Voor elk van de genoemde stappen is het aangewezen dat numerieke resultaten worden vergeleken met beschikbare experimentele waarden.

N.3 Dynamische respons

De dynamische respons van een constructie onder een wisselende belasting wordt berekend volgens het principe van de modale superpositie. Daartoe dient een grondige studie van het dynamisch gedrag de responsberekening vooraf te gaan. De opeenvolgende stappen worden schematisch voorgesteld in fig.N.2.

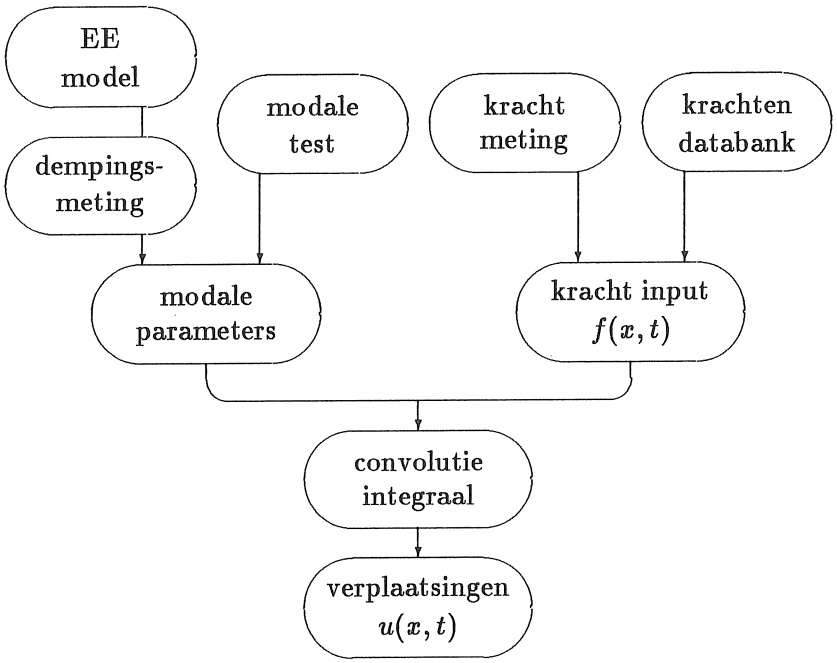

Figure N.2: Opeenvolgende stappen in responsberekening

Twee groepen van gegevens moeten worden ingevoerd, enerzijds de beschrijving van de ruimtelijke verdeling van het krachtverloop en anderzijds de modale parameters.

N.3.1 Het modaal model

Het dynamisch gedrag van een constructie kan worden bestudeerd met behulp van een numeriek model of een experimenteel model.

Met een eindig-elementenmodel wordt de bewegingsvergelijking van een constructie, na discretisatie in elementen en met verwaarlozing van demping, in een vrije trilling beschreven door de vergelijking.

$$\left([K] - \omega_k^2[M]\right)\{\psi_k\} = \{0\}$$

met $[K]$: de globale stijfheidsmatrix
$[M]$: de globale massamatrix
ω_k : de k^{de} eigenpulsatie
$\{\psi_k\}$: de k^{de} modevorm

Dit systeem heeft een aantal eigenwaarden, die men bekomt door de determinant van de matrix $[K]-\omega^2[M]$ nul te stellen. Achteraf worden dan de overeenstemmende modevormen berekend. Meestal worden de modevormen uitgedrukt in termen van verplaatsingen.

In een experimenteel model worden de transferfuncties gemeten tussen aangelegde kracht in een of meerdere punten en respons in een of meerdere punten. Van deze transferfuncties worden complexe polen berekend die bepalend zijn voor de resonantiefrequenties en de dempingswaarden. Nadien worden de modevormen geschat door de amplitudo's en de faseverschuivingen van de transferfuncties in verschillende punten met elkaar te vergelijken. De modevormen zijn bepaald in termen van de opgemeten responsgrootheden, doorgaans versnellingen.

Bij de vermoeiingsberekening zijn de optredende rekken bepalend voor de schade die wordt geaccumuleerd. Daartoe is het aangewezen in de convolutie-integraal grootheden als rekken als modevormcoëfficiënten in te voeren. Dit is het principe van de modale rekken, en het vereist de omzetting van modevormen uitgedrukt in termen van verplaatsingen, snelheden of versnellingen naar modale rekken.

N.3.1.1 Gevoeligheid van modale rekken

De gevoeligheid van modale rekken voor variaties van de individuele modevormcoëfficiënten is afhankelijk van de manier waarop de rekken worden berekend. De berekening gebeurt op basis van verplaatsingen

of versnellingen. Verplaatsingen lenen zich het best voor een vlotte visuele interpretatie. Rekken worden berekend uit verplaatsingen door afleiding, op voorwaarde dat een continue voorstelling beschikbaar is :

$$\varepsilon_{ij} = \frac{1}{2}\left(\frac{\partial u_i}{\partial x_j} + \frac{\partial u_j}{\partial x_i}\right)$$

De waarden van de verplaatsingen zijn evenwel enkel bepaald in de knopen van het modaal model. Differentiatie wordt gebruikt in plaats van afleiding :

$$\varepsilon_{ij} = \frac{1}{2}\left[\frac{u_i(\underline{x} + \Delta x_j \underline{e}_j) - u_i(\underline{x})}{\Delta x_j} + \frac{u_j(\underline{x} + \Delta x_i \underline{e}_i) - u_j(\underline{x})}{\Delta x_i}\right]$$

met $\underline{x}$: het punt waar de rek wordt berekend
Δx_i : increment van de coördinaat volgens de i-as
$\underline{e}_i$: eenheidsvector volgens de i-as

Differentiatie is een numeriek bijzonder instabiele bewerking en kleine wijzigingen van een knoopverplaatsing leiden tot zeer grote wijzigingen van de rekken. Zeker met opgemeten modevormen zijn de aldus berekende rekken helemaal onbetrouwbaar.

Modevormen uitgedrukt in termen van versnellingen worden eenvoudig omgezet naar inertiekrachten :

$$f_k(\underline{x}) = \rho(\underline{x}) a_k(\underline{x}), \qquad \forall \underline{x}$$

$\underline{x}$: coördinaat op de constructie
$\rho(\underline{x})$: massadichtheid van het materiaal in punt $\underline{x}$

De rekverdeling wordt bepaald door uitdrukking van het statisch evenwicht van inertiekrachten en inwendige spanningen :

$$\frac{\partial \sigma_{ij}}{\partial x_i} + f_j = 0$$

De oplossing van dit probleem gaat via een integratie van de inertiekrachten. In tegenstelling tot differentiatie is integratie een zeer stabiele bewerking en volstaat een vrij ruwe beschrijving van de modevorm om toch een behoorlijke nauwkeurigheid op de rekken te bekomen. Op deze manier is de gevoeligheid van modale rekken naar modale versnellingen klein.

N.3.1.2 Vereffening van de modevorm

De rekverdeling onder een bepaalde modevorm mag geen buitensporig hoge pieken vertonen opdat hij bruikbaar zou zijn voor verdere bewerkingen. Modevormen die vaak niet bijzonder glad zijn moeten dus worden vereffend om een goede schatting van de rekken te bekomen.

Beschouw een bepaalde mode k die wordt beschreven door de resonantiefrequentie ω_k en de modevorm ψ_k^u. Er wordt verondersteld dat schattingen $\omega_{k,e}$ en $\psi_{k,e}$ van de correcte modale parameters beschikbaar zijn. Doorgaans is de schatting voor de frequentie vrij goed, zodat kan worden aangenomen : $\omega_{k,e} = \omega_k$. De originele schatting van de modevorm $\psi_{k,e}$ wordt met een randelementenberekening vereffend.

Initieel is de modevorm $\psi_1^u = \psi_{k,e}^u$ uitgedrukt in termen van verplaatsingen. De inertiekrachten worden berekend in ieder van de knopen van het modaal model :

$$\psi_1^f = \rho\omega_k^2\psi_1^u$$

Deze inertiekrachten worden aangelegd als een statische belasting. De vervorming ψ_2^u die dan wordt bekomen is identiek met de originele vorm ψ_1^u op voorwaarde dat deze correct was. Wanneer ψ_1^u echter niet correct was, verschillen de vormen ψ_1^u en ψ_2^u van elkaar. De tweede vorm ψ_2^u is een betere schatting van de correcte vorm. De procedure begint nu opnieuw van deze tweede vorm.

Na een aantal iteratiestappen treedt convergentie op en wordt de correcte modevorm goed benaderd. Deze modevorm is een analytische modevorm. Geleidelijk wordt de informatie vervat in de originele modevorm $\psi_{k,e}$ vervangen door deze van de analytische vorm. Door de vermelde procedure slechts eenmaal te doorlopen blijft de oorspronkelijke informatie behouden en wordt de modevorm tevens vereffend.

Hiermee is dus aangetoond welk het belang is van een gepaste keuze van grootheden voor de modevormen : versnellingen of inertiekrachten laten een nauwkeuriger berekening van modale rekken toe dan verplaatsingen.

N.3.2 Berekening in het tijdsdomein

De berekening van de respons wordt doorgevoerd in het tijdsdomein volgens de uitdrukking :

$$x_I(t) = 2 \int_0^t \sum_{k=1}^{N} (U_{IJk} \cos \nu_k \tau - V_{IJk} \sin \nu_k \tau)\, e^{-\sigma_k t} f_J(t-\tau)\, d\tau$$

met : $x_I(t)$: respons in knoop I op tijdstip t
U_{IJk}, V_{IJk} : reëel en imaginair deel van de individuele component van de modevorm
ν_k : gedempte eigenpulsatie
σ_k : dempingswaarde
N : relevant aantal eigenmoden

Een recurrente betrekking laat toe de respons op een efficiënte manier te becijferen :

$$\mathcal{RS}_k(t+\Delta t) = e^{\lambda_k \Delta t} \mathcal{RS}_k(t) + \int_0^{\Delta t} e^{\lambda_k \tau} f(t+\Delta t-\tau) d\tau$$

met : $\mathcal{RS}_k(t)$: respons op tijdstip t
λ_k $= -\sigma_k + j\omega_k$, met j de imaginaire eenheid

Voor een brede klasse van belastingsfuncties $f(t)$ kan de convolutie-integraal exact worden becijferd, ongeacht de grootte van het tijdsincrement. Alternatief zou de respons ook kunnen worden berekend via het frequentiedomein om dan mits inverse FOURIER-transformatie terug te keren naar het tijdsdomein. Nochtans biedt de directe berekening in het tijdsdomein een aantal voordelen :

- de superpositie van statische belastingen gebeurt in het tijdsdomein
- de aanwezigheid, het oplopen en het afbouwen van residuele spanningen moet nauwkeurig worden beschreven, ook dit kan enkel in het tijdsdomein
- teneinde achteraf de resultaten goed te kunnen verwerken moet de overeenstemming tussen piekwaarden van de spanning en amplitudo's van de rek eenduidig worden beschreven

De invloed van een bepaalde mode op de respons wordt geëvalueerd door in de berekening de bewuste mode weg te laten en het resultaat te vergelijken met de volledige respons.

Recent werden belangrijke ontwikkelingen gerealiseerd op het gebied van modeloptimisatie, foutenlokalisering en niet-lineair gedrag.

N.4 Berekening van de modale rekken

Zoals zal blijken in paragraaf N.5 is de schatting van de levensduur bijzonder gevoelig voor het absolute rekniveau dat wordt bereikt. Zeker ter plaatse van geometrische spanningsconcentraties moeten lokale belastingsniveau's bijzonder nauwkeurig worden bepaald. Daartoe dient een geschikte numerische techniek te worden gekozen.

N.4.1 Statische elasticiteit

Twee grote numerische technieken zijn beschikbaar om grootheden als spanningen en rekken te bepalen in een elastisch medium dat is onderworpen aan een statische belasting.

De basisvergelijking van de eindige-elementenmethode luidt in de verplaatsingsformulering :

$$[K]\{u\} = \{F\} \tag{N.1}$$

In de randelementenmethode bekomt men :

$$[H]\{u\} = [G]\{p\} \tag{N.2}$$

Door een gepaste discretisatie van de constructie, door het invoeren van materiaalparameters en randvoorwaarden ontstaat in elk van beide methoden een vierkant stelsel van lineaire vergelijkingen in onbekende verplaatsingsgrootheden. In de eindige-elementenmethode bekomt men al gauw een systeemmatrix van een vrij grote dimensie die echter symmetrisch is en die een bandstructuur heeft. In de randelementenmethode is de dimensie van de systeemmatrix een grootteorde kleiner, maar de matrix is niet symmetrisch en hij bevat ook slechts toevallig nulelementen.

Eens het stelsel is opgelost kunnen de resultaten worden naverwerkt. Het is precies deze naverwerking die bepalend is voor de nauwkeurigheid waarmee rekken en spanningen worden bekomen. Hier moet

dus een belangrijk onderscheid worden gemaakt tussen beide genoemde technieken.

N.4.1.1 De eindige-elementenmethode

Na oplossing van het stelsel N.1 beschikt men over de verschillende componenten van de verplaatsingen in de knopen van het model. De rekken worden daaruit afgeleid door differentiatie :

$$\{\varepsilon\} = [\partial][N]\{u\} = [B]\{u\}$$

De graad van het rekverloop doorheen een element is een eenheid lager dan de graad van de vormfuncties voor de verplaatsingen. Zo is de rek constant in een lineair element. De rek wordt enkel correct berekend in enige discrete punten binnen het element, de zogenaamde Gauss-punten. Door extrapolatie naar de randen van het element onderschat men in de regel de piekwaarden die doorgaans aan de randen optreden. Bovendien worden door de numerieke differentiatie van primaire onbekenden bijkomende fouten geïntroduceerd.

Deze tekortkomingen worden grotendeels tenietgedaan door het gebruik van elementen van een bijzonder type of door het gebruik van alternatieve formuleringen van krachtenevenwicht en continuïteit. Bij de zogenaamde niet-conforme elementen is de impliciete continuïteit van verplaatsingen of hoekverdraaiingen over de randen van aanliggende elementen niet meer voldaan. En in de duale formulering van de eindige-elementenmethode vertrekt men bij de definitie van de vrijheidsgraden en de vormfuncties van een element van de eis van inwendig evenwicht eerder dan van de eis van continuïteit van verplaatsingen. Elk van beide opties verschaffen de gebruiker de mogelijkheid met een relatief ruw netwerk van elementen een nauwkeurige bepaling van de rekken te bekomen. Nochtans worden deze formuleringen in de praktijk slechts zelden toegepast.

N.4.1.2 De randelementenmethode

Bij de berekening van de rekken dient een onderscheid te worden gemaakt tussen punten op de rand en punten gelegen in het inwendige van het volume. In punten gelegen op de rand van de constructie treden verplaatsingen en spanningen als gelijkwaardige grootheden op

in de vergelijkingen. Dientengevolge behoeven sommige componenten van de rektensor niet langer te worden afgeleid uit verplaatsingen. Voor componenten gericht volgens de coördinaatassen van het element dient deze operatie nog wel te worden uitgevoerd. In punten gelegen in het inwendige van het domein kunnen de componenten van de rektensor rechtstreeks worden bepaald door integratie over heel de rand van spanningen en verplaatsingen gewogen met een geschikte fundamentele functie.

In het algemeen kan worden gesteld dat in gevallen met compacte geometrie met een randelementenmodel nauwkeuriger rekwaarden worden bekomen dan met een eindig-elementenmodel wanneer de rekentijden voor beide modellen vergelijkbaar zijn.

N.4.2 Elasticiteit in een dynamische contekst

Beide methoden vermeld in voorgaande paragraaf zijn ook hier toepasbaar. Elk van beide laat toe een responsberekening door te voeren in het frequentiedomein. Om redenen aangehaald in paragraaf N.3.2 is echter een berekening in het tijdsdomein aangewezen voor toepassingen van vermoeiingsanalyse. Weerom dient onderscheid te worden gemaakt tussen twee grote mogelijkheden, directe tijdsintegratie en modale superpositie.

Bij de directe tijdsintegratie worden de bewegingsvergelijkingen tijdsstap voor tijdsstap geïntegreerd, telkens rekening houdend met beginvoorwaarden of met de toestand op een voorgaand tijdsstip. Wanneer traagheidskrachten belangrijk worden is deze procedure vrij omslachtig en rekenintensief vermits het tijdsincrement dan erg klein moet worden gekozen. Wanneer het eindige-elementenmodel niet al te omvangrijk is kan een dergelijke berekening te verantwoorden zijn, een randelementenberekening daarentegen wordt al gauw oneconomisch vermits de optredende fundamentele oplossingen tijdsafhankelijk zijn. Sommige onderzoekers, zoals NARDINI, stellen alternatieve methoden voor, die evenwel weinig geschikt zijn voor praktische toepassing.

De methode met modale superpositie is beschikbaar in vele eindige-elementenpakketten. De eerste stap in een dergelijke berekening is de bepaling van resonantiefrequenties en modevormen. De dynamische respons wordt dan in een eerste fase uitgedrukt in termen van verplaatsingen, en rekken worden in elke tijdsstap uit de verplaatsingen afgeleid. In de in dit werk voorgestelde methode wordt gewerkt met

modale rekken, die worden bepaald uit een statische randelementenberekening. Daarbij dient in de basisvergelijkingen de invloed van de inertiekrachten mee te worden ingevoerd. Het stelsel N.2 wordt dan :

$$[H]\{u\} = [G]\{p\} + [W]\{f\}$$

Nochtans kan de discretisatie van het volume van de constructie op een vrij eenvoudige en ruwe manier worden doorgevoerd. Vermits de volume-elementen geen structurele functie hebben doch enkel moeten dienen om het verloop van de inertiekrachten doorheen de constructie te beschrijven, beschikt men bij de definitie van de elementen over een grote vrijheid. De geometrie van het model hoeft niet perfect overeen te stemmen met de geometrie van de werkelijke constructie. Zo mogen bij voorbeeld sommige delen van de constructie niet door elementen bedekt blijven terwijl andere delen mogen overlappen. Voor de vormfuncties in de elementen volstaat een polynoom van de eerste graad. De randvoorwaarden die aan de constructie worden opgelegd maken deze statisch bepaald.

In een goed ontworpen constructie treden slechts een beperkt aantal kritieke zones op. Men kan volstaan met een rekberekening die is beperkt tot enkele gebieden. Daartoe wordt uit de constructie een gebied afgezonderd dat de beschouwde kritieke plaats omsluit. De randen die aldus ontstaan door het wegsnijden van het beperkt gebied uit het geheel zijn meestal niet spanningsvrij. Daarom moeten de spanningsresultanten die werken op deze doorsneden worden aangelegd als randvoorwaarden op de randen van het beperkt gebied. Men zal hier verkiezen spanningsresultanten aan te leggen boven verplaatsingen, omdat de gevoeligheid van de berekende rek in de kritieke zone naar opgelegde krachten veel kleiner is dan de gevoeligheid naar opgelegde verplaatsingen. Steunend op het principe van DE SAINT-VENANT kan de verdeling van de spanningsresultanten over de doorsneden op een arbitraire manier gebeuren, op voorwaarde dat de randen niet al te dicht bij de bestudeerde kritieke plaats gelegen zijn. Weerom wordt een systeem van randvoorwaarden in verplaatsingen zo gekozen dat het beperkt gebied statisch bepaald is.

Aldus bestaat een volledig stel van randvoorwaarden en belastingen uit :

- inertiekrachten in het volumemodel
- spanningen op de doorgesneden randen

- een statisch bepaald systeem van opgelegde verplaatsingen

Een dergelijke berekening wordt doorgevoerd voor elke modevorm en voor elke kritieke zone.

N.4.3 Invloed van plasticiteit

Het optreden van plastische vervormingen introduceert niet-lineariteiten in de berekening. Doordat de stijfheid van de constructie in de plastische zones afhankelijk is van de grootte van de plastische vervormingen moet de berekening in stappen worden doorgevoerd. Deze techniek wordt toegepast in de eindige-elementenmethode (vergelijking N.1). Op basis van de reeds opgetreden plastische vervorming wordt de stijfheidsmatrix $[K]$ van de constructie telkens opnieuw becijferd. De nauwkeurigheid van de berekening neemt toe met het aantal stappen waarin de belasting wordt opgedeeld. Wanneer bovendien rekken moeten worden berekend dient een fijne verdeling van de constructie in elementen te worden gedefinieerd. Het hoeft geen betoog dat een dergelijke berekening bijzonder duur en tijdrovend is.

In de randelementenmethode zijn de fundamentele oplossingen niet langer bruikbaar gelet op de variabele stijfheid van de constructie. BANERJEE stelt een techniek voor die hieraan tegemoet komt. De conclusie is nochtans dat de randelementenmethode hier helemaal geen uitweg biedt.

NEUBER heeft in een theoretische ontwikkeling een verband bepaald tussen werkelijke spanning en werkelijke rek in een plastische vervorming. Combinatie van een uitdrukking van dit verband met de cyclische constitutieve wet van het materiaal laat toe de spanning en de rek te bepalen in het plastische domein vertrekkend van een theoretische veronderstelling van perfect elastisch gedrag. De regel van NEUBER wordt in zijn meest bruikbare vorm geformuleerd als :

$$\sigma.\varepsilon = \frac{(K_t\sigma_{nom})^2}{E} = (K_t\varepsilon_{nom})^2 E$$

waarin K_t de elastische spanningsconcentratiefactor voorstelt. Deze regel is slechts bruikbaar wanneer het overgrote deel van de constructie elastisch blijft en slechts in een beperkt gebied plastische vervormingen optreden. Iedere goed ontworpen constructie voldoet hieraan.

N.5 Schatting van de levensduur

Na vervollediging van de rek- en responsberekeningen beschikt men in elk van de kritieke zones van de constructie over het rekverloop als functie van de tijd. Toepassing van vermoeiingstheorieën laat toe een schatting te maken van de levensduur. Schematisch wordt het verloop van de berekening voorgesteld in fig.N.3.

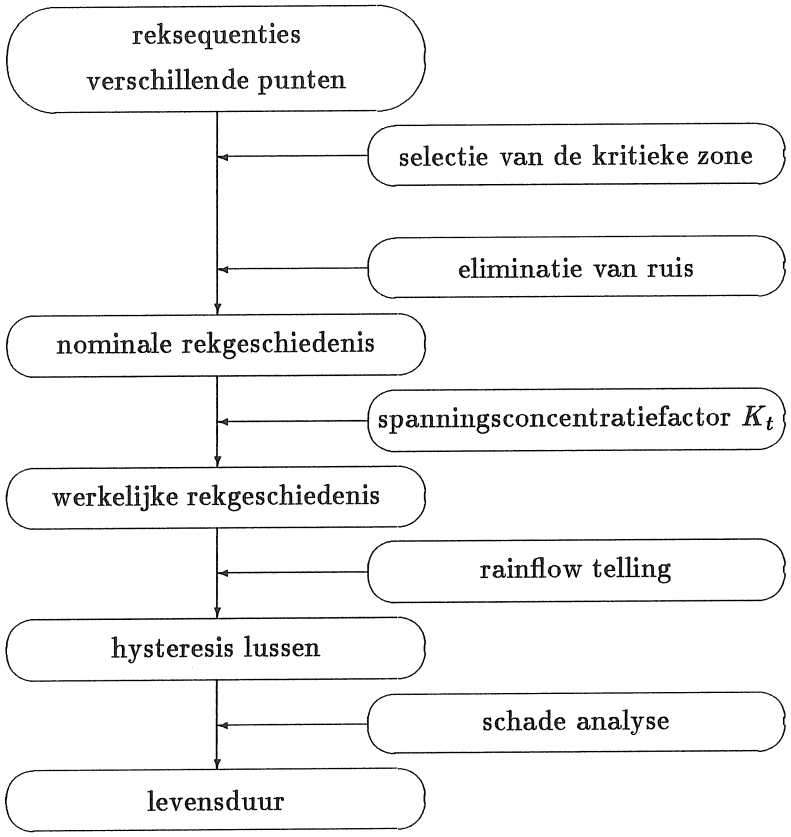

Figure N.3: Schema van levensduurvoorspelling

De lokale-rekmethode wordt hier aangevuld met een aantal hulpmiddelen die toelaten het bekomen resultaat te evalueren.

N.5.1 De lokale-rekmethode

De lokale-rekmethode is ontworpen om met een minimum aan experimentele informatie die afhankelijk is van het bestudeerde geval toch een realistische schatting van de levensduur te maken. De basisstelling waarvan men vertrekt bepaalt dat het verloop van de lokale rek, eerder dan de spanning determinerend is voor de schade die wordt geaccumuleerd. De drie factoren die bepalend zijn voor de levensduur, te weten het materiaal, de geometrie en de belasting, worden gekarakteriseerd door een aantal grootheden die eenduidig en onderling onafhankelijk zijn. Zo is men in staat het proces van schade-accumulatie te reconstitueren op basis van deze parameters.

materiaal de parameters E, K' en n' beschrijven het cyclisch constitutief gedrag, de parameters E, σ'_f, ε'_f, b en c beschrijven het verband tussen rekamplitudo en levensduur

geometrie de invloed van geometrische details wordt weerspiegeld door de elastische spanningsconcentratiefactor K_t

belasting de variatie in de belasting wordt beschreven op een globale manier, dit betekent dat niet de spanning of de rek ter plaatse van de kritieke zone moet worden gedefinieerd, maar wel de spanning σ_{nom} of de rek ε_{nom} in een punt ergens in de omgeving, dat via de spanningsconcentratiefactor rechtstreeks in verband staat met de kritieke zone.

Op deze manier kan men op basis van het verloop van de werkelijke rek het verband leggen tussen de accumulatie van schade in een reële constructie en in een glad proefmonster.

Vertrekkend van de sequenties van de nominale rekken of spanningen wordt eerst het meest kritieke punt geselecteerd. Indien gewenst wordt dan een zeker percentage ruis geëlimineerd dat de levensduur niet beïnvloedt en de berekening vertraagt. Met kennis van de spanningsconcentratiefactor, de constitutieve wet van het materiaal en met de regel van NEUBER worden dan de sequenties van werkelijke rek en werkelijke spanning bepaald. Een telalgoritme, vaak de "regenval"-techniek, elimineert gesloten hysteresislussen. Voor iedere lus wordt de schade bepaald en tenslotte worden deze geaccumuleerd met de regel van MINER.

Een van de essentiële karakteristieken van de lokale-rekmethode is dat de parameters die het materiaalgedrag beschrijven nauwkeurig moeten zijn gedefinieerd. Gespecialiseerde werken bevatten gegevens over vele technische materialen. Nochtans dient te worden opgemerkt dat de geringste wijziging van testomgeving of materiaaltoestand aanleiding kan geven tot belangrijke verschillen in parameters. In geval van onzekerheid omtrent de nauwkeurigheid van de beschikbare materiaaldata moeten de materiaalparameters onafhankelijk worden opgemeten.

N.5.2 Meerassige spanningstoestanden

De originele formulering van de lokale-rekmethode is slechts toepasbaar voor eenassige spanningstoestanden. Gevallen waar de spanningstoestand twee- of zelfs drie-assig is kunnen niet meteen worden behandeld. In de literatuur worden zeer vele methoden voorgesteld. Een dubbel onderscheid wordt gemaakt tussen hoge levensduur en lage levensduur enerzijds en proportionele en niet-proportionele belasting anderzijds. Een belastingspatroon wordt proportioneel genoemd als er een in de tijd constante verhouding bestaat tussen de verschillende componenten van de spanningstensor. In het tegenovergestelde geval variëren de onderscheiden componenten van de spanningstensor onafhankelijk van elkaar.

Een zeer elementaire benadering definieert een equivalente spanning, bij voorbeeld volgens het criterium van VON MISES. Deze methode geeft goede resultaten zolang de plastische vervormingen niet te groot worden en zolang het belastingspatroon ongeveer proportioneel is.

Een andere techniek waarnaar vaak wordt gerefereerd legt een verband tussen het aantal cycli tot initiatie van een scheur en de totale geaccumuleerde plastische rekenergie. Gebruik van dit criterium vergt een volledige becijfering van de tijdsverlopen van elke component afzonderlijk. Daartoe moet het constitutieve gedrag van het materiaal met de verschillende componenten van de spanningstensor volledig worden beschreven. De beschrijving volgens MROZ wordt meest algemeen aanvaard. Een aantal spanningsniveau's worden vastgelegd waarbinnen het materiaal met welbepaalde parameters wordt beschreven. Een dergelijke berekening vergt bijzonder veel rekentijd. Bovendien is deze methode ook niet algemeen toepasselijk vermits som-

mige materialen een afwijkend gedrag vertonen. Bovenal is de beschrijving van het gedrag op een dergelijke manier enorm omslachtig door de veelheid aan parameters, wat de kansen van deze methode op praktische toepassing zeker niet ten goede komt.

SOCIE heeft meer fundamenteel onderzoek verricht naar de verschillende mechanismen van scheurvorming en naar de verschillende omstandigheden waarin elk van deze mechanismen optreedt. Hij heeft vastgesteld dat het fysische mechanisme wordt bepaald door drie parameters :

- de aard van het materiaal
- de wijze van belasting, schuifspanning of normaalspanning, of een combinatie
- het aantal cycli tot breuk

De aard van de belasting wordt weerspiegeld door de parameter $J_1'/3\sigma_1$ waarin J_1' de eerste invariant van de spanningstensor voorstelt en σ_1 de grootste hoofdspanning. Deze parameter geeft eenduidig de verschillende mogelijke types en combinaties van belastingen weer. Op basis van experimenten zijn er kaarten opgesteld voor een aantal materialen die aangeven welk mechanisme optreedt bij de aangelegde belasting en bij de optredende levensduur. Bij elk van de drie mechanismen die worden onderscheiden hoort een wiskundig model dat een verband legt tussen de verschillende grootheden van de belasting en het aantal wisselingen tot breuk.

N.5.3 Enkele belangrijke parameters

Als resultaat van de vermoeiingsberekening bekomt men een enkel getal, het aantal maal dat het opgelegd rekverloop kan worden herhaald vooraleer een scheur geïnitieerd wordt. Teneinde dit resultaat grondig te kunnen interpreteren en op zijn betrouwbaarheid te kunnen beoordelen en met het oog op wijzigingen van het ontwerp is het wenselijk dat de invloed van de belangrijkste parameters wordt nagegaan. Een gevoeligheidsanalyse wijst de cruciale parameters aan die de grootste invloed op de levensduur uitoefenen.

De invloed van de parameters uit de rek–levensduur -curve is voor de hand liggend. De invloed van de cyclische parameters n' en K' is dat helemaal niet. Door een kleine wijziging aan deze constanten aan

te brengen en de bekomen levensduren te vergelijken verkrijgt men een inzicht in de nauwkeurigheid waarmee n' en K' zouden moeten bekend zijn. De invloed is slechts significant wanneer belangrijke plastische vervormingen optreden.

Een fysisch belangrijke parameter is de invloed van de gemiddelde spanning gedurende een cyclus en de manier waarop deze in het model wordt geïntroduceerd. De eenvoudigste benadering bestaat erin deze invloed gewoon over het hoofd te zien. Andere benaderingen zoals deze van HAIGH-SODERBERG en deze van MORROW zijn vermeldenswaard. De meest algemeen aanvaarde correctie is de parameter van SMITH-TOPPER-WATSON. In een grondige analyse schat men de levensduur best eens zonder gemiddelde spanning en eens met SMITH-TOPPER-WATSON om nadien op een gefundeerde manier de resultaten te vergelijken. De allerbelangrijkste parameter is echter het absolute rekniveau dat wordt bereikt. Wanneer de belasting in het domein van de hoge levensduren zit kan de gevoeligheid worden geschat met het verband :

$$\frac{dN}{N} = \frac{1}{|b|}\frac{d\varepsilon}{\varepsilon}$$

Dit verband toont aan dat een relatieve fout op het rekniveau vermenigvuldigd wordt met een factor $1/|b|$. De grootteorde van b ligt doorgaans tussen de grenzen -0.1 en 0. De nauwkeurigheid van de spanningsconcentratiefactor is determinerend voor de betrouwbaarheid van de analyse. Dit verklaart waarom bij de berekening van de modale rekken de grootst mogelijke zorg moet worden besteed aan de constructie van een degelijk structureel randelementenmodel.

Wanneer experimentele gegevens voorhanden zijn kan men deze gebruiken om het vermoeiingsmodel aan te passen. Fig.N.4 geeft schematisch aan hoe dit best kan gebeuren.

N.6 Praktische toepassingen

Twee praktische toepassingen illustreren de ideeën en de methoden die in de theoretische beschouwingen naar voor zijn gebracht. In het eerste geval wordt het belang van een precieze modellering van geometrische details geïllustreerd, en wordt een toepassing gegeven van een aanpassing van het model aan experimentele data. In het tweede geval wordt gepoogd het dynamisch gedrag van de constructie te wijzigen om de

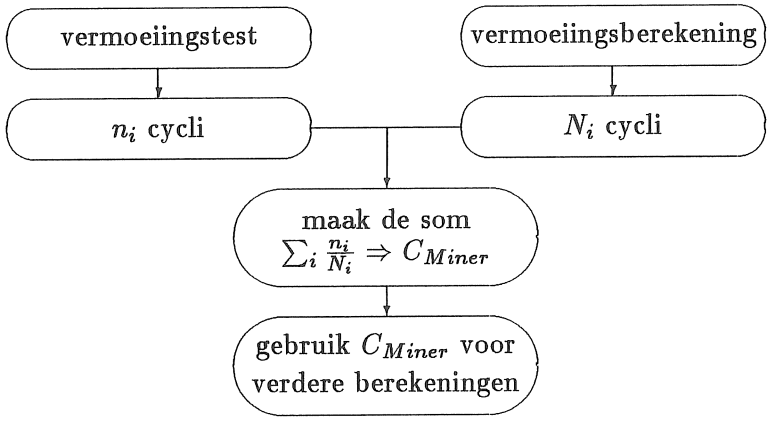

Figure N.4: Schema voor aanpassing van het vermoeiingsmodel

levensduur te verlengen. De enige daadwerkelijke verbetering is een verhoging van de vermoeiingsweerstand van het materiaal zelf.

N.6.1 Ingeklemde balk met groef

Een stalen balkje met vierkante doorsnede 10×10 mm^2 en een groef wordt ingeklemd op het tafeltje van een electrodynamische excitator, zoals getoond in fig.N.5. De belasting verloopt sinusoïdaal in de tijd op

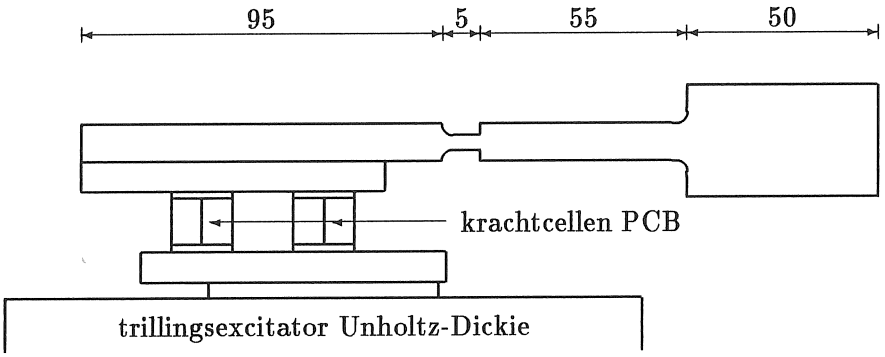

Figure N.5: Ingeklemde balk met groef

de tweede resonantiefrequentie met een amplitudo van 1.5 mm op het vrije uiteinde. Twee doorsneden zijn potentieel kritiek, die in sectie

a met een afrondingsstraal van 3 *mm* en die in doorsnede **b** met een straal van 0.1 *mm* (fig.N.6).

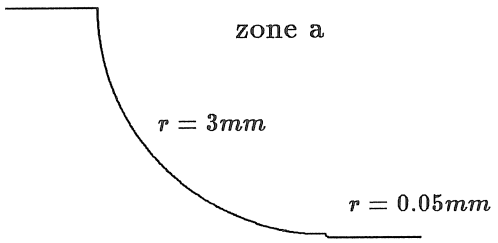

Figure N.6: Uitvergroot beeld van de groef

Een experimentele modale analyse toont een resonantiefrequentie van 146.1 *Hz* en een dempingsverhouding van 2.31%. De massa- en stijfheidseigenschappen van de balk zelf en van de toegevoegde massa ter plaatse van de bevestiging op de excitator zijn goed bekend en kunnen ook nauwkeurig in het model worden ingevoerd. De inklemming op de excitator is echter niet oneindig stijf. In het model moet dus een eindige vertikale stijfheid worden ingevoerd die moeilijk te schatten is zonder metingen uit te voeren. Daartoe is de stijfheid van deze veren zodanig bepaald dat de berekende resonantiefrequentie overeenstemt met de gemeten resonantiefrquentie van 146.1 *Hz* : $k = 7.45\ kN/m$.

De met deze modevorm corresponderende verplaatsingen worden nu omgezet naar inertiekrachten door te vermenigvuldigen met de factor $\rho\omega^2 u_i/u_{eind} \times 1.5mm$. De berekening van de modale rekken gebeurt met een tweedimensionaal randelementenmodel van het beperkte gebied (fig.N.6) dat de beide kritieke zones omvat. In de beide doorsneden waar het beperkte gebied aan de rest van de balk is bevestigd zijn de snedekrachten aangelegd als belastingen op de rand. Wegens de zeer kleine afrondingsstraal moet een bijzonder dicht randelementenmodel worden gegenereerd met in totaal 216 elementen. Als modale rekken, meteen geschaald naar de aangelegde belasting vindt men :

$$\varepsilon_a = 0.095\% \qquad \varepsilon_b = 0.224\%$$

Met deze waarden van de aangelegde belasting zijn de overeenstemmende levensduren in beide doorsneden **a** en **b** bepaald. De relevante karakteristieken van het materiaal zijn samengevat in tabel 6.1. De geschatte levensduren voor elk van beide doorsneden zijn :

$$N_a = 2.3 \times 10^{15} \qquad N_b = 1.98 \times 10^6$$

De levensduur van het balkje is ook experimenteel bepaald in dezelfde opstelling als voor de modale test. De respons van de balk wordt opgemeten met een accelerometer op het einde van de balk. Na zes minuten moet de frequentie worden bijgeregeld tot 138 *Hz* om weer in resonantie te komen. Verder moet de frequentie geleidelijk worden verlaagd tot breuk uiteindelijk optreedt in sectie **a** bij 45 *Hz* na 29 minuten. De scheur is dan 3.5 *mm* diep en de resterende 0.5 *mm* is de restbreuk. Het aantal cycli tot initiatie van de scheur bedraagt 75000.

Het feit dat de breuk optreedt in sectie **a** is onverwacht vermits de modale rek er veel kleiner is dan in sectie **b**. Bij nader toezicht blijkt echter dat de groef op een onverzorgde manier is gefreesd, en dat aan de voet van de afrondingsstraal van 3 *mm* een trapje bestaat van 0.05 *mm*, dat een hoge spanningsconcentratiefactor met zich brengt. Voor de aanpassing van het model rekent men in omgekeerde zin en wordt de spanningsconcentratiefactor bepaald uit de levensduur : $K_t = 4.14$. Een tweede gelijkaardige opstelling is gemaakt met echter een materiaal met hogere vermoeiingseigenschappen vermeld in tabel 6.3. De aangelegde amplitudo bedraagt 1.8 *mm*. Het geoptimaliseerde eindige-elementenmodel wordt opnieuw gebruikt en de hoger bepaalde factor $K_t = 4.14$ wordt toegepast in zone **a**. De overeenstemmende geschatte levensduur in zone **a** bedraagt 120000 cycli. De levensduurtest verloopt ruwweg op dezelfde manier als voor het oorspronkelijk geval met een levensduur van 270000 wisselingen tot initiatie van een scheur. De overeenstemming tussen voorspelde en gemeten levensduren is dus goed, dank zij de invoering van de spanningsconcentratiefactor.

Dit voorbeeld toont aan hoe belangrijk de invloed van zeer kleine geometrische details wel is.

N.6.2 Hamer van een machine

In dit geval wordt het ontwerp van de hamer van een machine geoptimaliseerd die wordt onderworpen aan een aantal schokbelastingen. De geometrie is voorgesteld in fig.N.7. Het vermoeiingsprobleem treedt op in de zones **a** en **b**. Vijf testen werden uitgevoerd, de resultaten zijn samengevat in tabel N.1. Het stuk is vervaardigd uit staal 14NiCrMo13. De reksequenties in de kritieke zones zijn opgemeten met rekstrookjes. De metingen zijn voorgesteld in fig.6.12 en 6.13. Vermits rekstrookjes slechts een gering aantal wisselingen van grote amplitudo (3000 à 7000 μstrain) kunnen weerstaan, moet de rek opgemeten

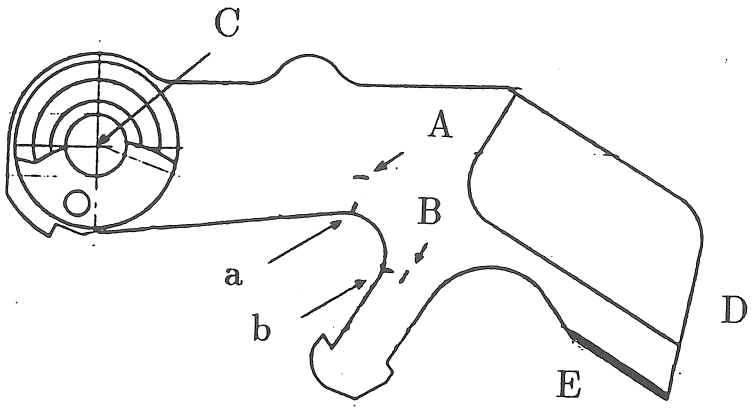

Figure N.7: Geometrie van de hamer

nr.	aantal cycli	plaats
1	3820	lichaam
2	2410	lichaam
3	1970	staart
4	4020	staart
5	3050	lichaam

Table N.1: Experimentele levensduur van de hamer

worden in een punt waar een lagere amplitudo optreedt.Het verband tussen de rekken op beide plaatsen dient te worden uitgedrukt door een spanningsconcentratiefactor door de verhouding te nemen van de rekken berekend met een statisch randelementenmodel. Als belasting wordt een statische kracht aangelegd op het uiteinde van het staartje en als randvoorwaarden worden de verplaatsingen op de as en op het uiteinde van het lichaam nul gesteld. De aldus bekomen factoren worden op de reksequenties toegepast en de levensduren worden geschat :

$$N_a = 3820 \qquad N_b = 1940$$

De spreiding op de resultaten is deels te wijten aan een spreiding op de intensiteit van de schokbelastingen.

De FOURIER-getransformeerden van beide signalen (fig.6.17, 6.18.) onthullen twee pieken, bij 9.8 *kHz* en bij 21.0 *kHz*. Wegens de kleine schaal van het stuk moet een numerieke modale analyse worden uitgevoerd. Met het commercieel pakket SYSTUS is een eindig-elementen-

model opgebouwd (fig.6.19). Dempingskarakteristieken zijn in dit probleem onbelangrijk. De berekende natuurlijke frequentie van 18.4 *kHz* stemt overeen met een buiging van de staart. De modale rekken die behoren bij elk van beide modevormen worden berekend met een randelementenmodel. De rekverdelingen voor elk van beide moden vertonen piekwaarden ter plaatse van de kritieke punten. Deze vaststelling bevestigt het vermoeden dat beide breukfenomenen te wijten zijn aan resonantievermoeiing.

Teneinde de levensduur te verhogen zijn verschillende mogelijkheden onderzocht. Door het aanbrengen van dempend materiaal in het contactoppervlak van de schok wordt de frequentie-inhoud van de schok drastisch gereduceerd en de levensduur verhoogd. Nochtans is het elastomeer materiaal na een duizendtal cycli uitgesleten, en geschiedt het contact opnieuw tussen staal en staal. De enige haalbare oplossing is een verbetering van de materiaaleigenschappen. Door een meer intense carbonitruratie stijgt de vermoeiingsductiliteitscoëfficiënt.

N.7 Conclusies

In dit werk wordt een methode voorgesteld om het vermoeiingsgedrag te simuleren dynamisch belaste metalen constructies. De methode is modulair opgebouwd en laat aldus steeds een vergelijking met experimentele gegevens toe. Voor elke stap die in de berekening wordt gezet worden beschikbare technieken vergeleken en de selectie van de te volgen methode gebeurt op basis van haalbare precisie en efficiëntie.

Fatigue design in industrial practice

Fatigue is a point of major concern in the design phase of a new product that will be subjected to variable loads. Numerical analysis is sometimes used to assess fatigue life of small components with fairly simple geometry that are subjected to well defined loading. Several methods are established for the analysis of fatigue phenomena in rather simple structures. Experimental experience is expressed in numerical expressions only for cases of little complexity, where the origin and the nature of the failure mechanism can be identified fairly easily.

Industrial products are assemblies of pieces, components and substructures connected by mechanical joints. Geometry, material properties, service conditions and loading together determine the fatigue behaviour of the assembly. The interaction of all these factors may be quite complex. Historically only experimental methods were generally accepted as a verification tool for the reliability and continuing effectiveness of a new engine or machine. Numerical methods offer some alternative opportunities in the analysis of structures, still they are unable to fully substitute for experimental techniques. This clearly impedes a quick and efficient development of industrial products, thus confronting technical requirements with serious economical constraints. Figure 0.1 presents a scheme that is typical for the development and design of a new automobile [1]. Testing phases appear only in the later stages of development 1 and 2. If modifications of the original design are necessary they can be evaluated only in the next prototype. Numerical methods are helpful since they predict the influence of modifications quickly. Both experimental and numerical procedures are iterative, but a single iteration step takes very little

time when it can be done in computer simulation. The major portion of the time required for a numerical analysis is generally taken by the construction of the original model. A well constructed model can afterwards be modified fairly easily. Companies that are involved in the development and design of mechanical structures strongly desire to account for fatigue phenomena as early as possible in the process of development by eliminating or shortening some iteration phases. They spend considerable effort in establishing a general methodology that is capable of accelerating the procedure. Distinction is made between "direct" methods and "step by step" methods.

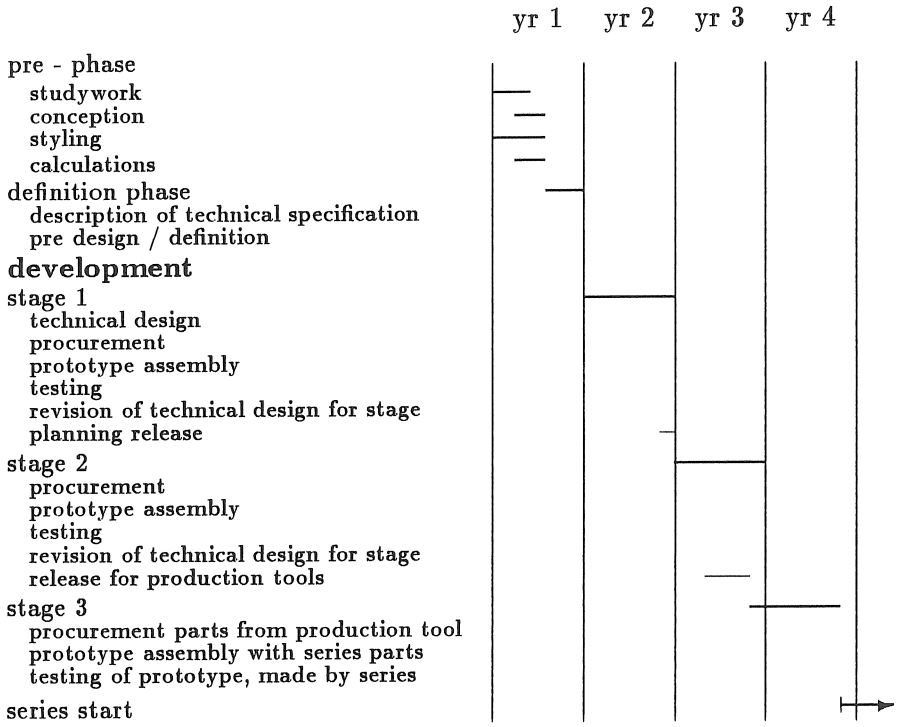

Figure 0.1: Typical time schedule for the development and design of an automobile

Methods of the former type adopt a kind of black box approach that extracts an estimation of lifetime from a number of inputs on load, geometry and material. Physical interpretation of results usually is not

obvious. A number of assumptions is made on how materials behave under cyclic loading and on the mechanisms of damage accumulation. Complex load sequences are represented by a restricted set of numbers. Statistical evaluation of results is an essential step in the validation process.

Step by step methods consider the separate influences of each input in a more systematic way. Consecutive evaluation of the effects of load with respect to dynamic behaviour, of geometry and of material properties allows for a localization of the problem. A more profound investigation of structural modifications is feasible. Comparison of intermediate results with experimental data leads to an efficient updating of the model. The global method is built up of a number of consecutive steps. For some of those steps, fair theories are available, others still lack consistency in accuracy or usefulness.

The latter kind of approach is clearly preferable from an engineering point of view. That is why most companies tend to adopt such an approach, in combination with experimental testing. Careful consideration of the methods employed in industrial practice reveals significant discrepancies and even hiatuses. A valid global approach first considers the crucial elements in an analysis together with the factors that lifetime is most sensitive to. For each single step an appropriate method is selected that reflects physical reality closely without overcomplicating theoretical and computational aspects. Each of those steps merges in a global system that is both consistent and complete, both reliable and practical in use.

The global method is built up of three essential steps :

- response prediction
- stress and strain computation
- lifetime prediction

For each of those steps, literature provides plenty of methods. They all have their own advantages and drawbacks. Some of them are fairly simple whilst others are more complicated. In subsequent chapters the author develops a global methodology by selecting appropriate techniques for each step. Existing methods are modified and together with some original developments they form a new global approach that is powerful and flexible.

The first chapter introduces the general concepts of fatigue analysis as it is being performed in current practice. An overview of literature is presented together with some more detailed information on the basic elements of fatigue theory and criterions. Relevant numerical methods are briefly reviewed. The advantages and drawbacks of experimental methods are compared to the capabilities of numerical techniques.

The second chapter presents the general aspects of an integrated fatigue life assessment method. It is explained which operations have to be made consecutively and how data flow from one module to the next one. Each module is again subdivided into a number of elementary operations. Flowcharts are very illustrative here. It is argued why a perfect interaction between analytical and experimental methods is possible. Hence, an efficient updating of analytical models is feasible. Although temptation may be very strong, shortcuts are not trustworthy. The dynamic behaviour of an aircraft may well be analysed with a finite element model. Stress concentrations in the landing gear can be evaluated with the same technique; however, the model is totally different from the dynamic model. The dynamic behaviour of an assembly is determined by the global stiffness and mass, whereas stresses and strains are governed only by very local characteristics of geometry, loading and material properties. Two separate computations have to be performed.

The third chapter deals with the computation of dynamic response. After a brief review of time domain and frequency domain methods and a comparison of both, it is shown that the convolution integral method offers most advantages in a context of fatigue life assessment, where effects of plasticity and residual stresses have to be taken into account. Computation of the convolution integral is rather time-consuming however, and therefore a fast algorithm is developed that is based on a recursion formula. The concept of modal strains is used throughout. A new smoothing technique that is based on dynamic equilibrium allows an accurate evaluation of modal strains. Finally some recent advances in dynamic modelling are discussed.

Chapter four provides details on how stresses and strains are computed. The accuracy of computed strain levels is crucial to the success of the method. The ability of the finite element technique with regard to stress and strain computation is discussed. The conventional displacement formulation seriously underestimates stress concentra-

tions unless a very dense mesh is used. The dual formulation is much more efficient in stress and strain analysis but its use is confined to highly knowledgeable analysts. The boundary element method offers some superior capabilities in stress and strain analysis. The original combination of the concept of modal strains, that are computed by boundary integral techniques, together with a convolution method gives a quick estimation of strain response with a very high degree of accuracy. Further it is shown why elastic analysis conveys sufficient information, even for the evaluation of plastic local stress and strain.

The fifth chapter discusses the local strain approach. Evaluation of cyclic material properties has to be performed very carefully. Literature provides plenty of models that describe a material's behaviour when it is subjected to multiaxial loading. A pragmatic approach is adopted that encompasses most situations that are encountered in practice. The parameters that fatigue lifetime is most sensitive to are enumerated and a general procedure for updating the damage accumulation model is presented.

Chapter six illustrates the proposed method on a number of examples. Finally some conclusions are drawn on the accuracy and the usefulness of the global approach, and some ideas for future developments are summarized.

Appendix A describes some theoretical backgrounds of the boundary element method. Appendix B explains the numerical operations that are used to determine cyclic and fatigue material properties from experimental data. Appendix C gives some details on the measurement of damping characteristics of structures. Appendix D elaborates on a numerical implementation of the proposed method.

Chapter 1

Introduction and survey of literature

1.1 Introduction

1.1.1 History of fatigue analysis

In many branches of mechanical industry, most cases of failure are due to fatigue. The first occurrences of fatigue fracture of components were recognized already in the middle of the nineteenth century. In those days, the determination of the dimensions of all kinds of mechanical equipment was based only on considerations of static strength. Soon these conventional methods did not meet the requirements of a well-functioning product. At a meeting of the Institution of Mechanical Engineers, STEPHENSON cautioned the members that breakage of this type was a subject "of serious importance" and noted that in one case a railway axle failure had led to charges of "manslaughter against the engineer and superintendent" [2]. However, the engineers did not have a thorough understanding of the physical mechanisms of crack nucleation and crack growth. They contented themselves with the introduction of safety factors which they hoped would cover the mysterious peculiarities of fatigue phenomena. Gradually the conviction rose that only experimental verification was able to give proof of the reliability of a new product. Any kind of experiment is time-consuming and is quite expensive for the manufacturer. For many types of structures rules and standards were established, based upon the experience that

was gathered by the engineers throughout many years. Still these directives are being updated continuously according to the most recent experiences [3,4,5,6,7,8]. The very existence of those standards that are generally accepted may give rise to unconscious, unmerited and erroneous self-confidence of the engineer. Thoughtless application of those rules that are believed infallible may cause unexpected and even disastrous events. The dramatic pictures of the ravaged oil-platform Alexander Kielland [9, pp.119] and the wrecked flight JAL123 [10] will perpetually remain the mournful mementoes of man's shortcomings in mastering seemingly trivial technology.

All of these considerations illustrate vividly that although the basic understanding of the nature of fatigue phenomena has ameliorated considerably, each separate case has to be studied thoroughly. Care should be taken not to overlook any single aspect of a particular problem and no shortcut is trustworthy.

1.1.2 Fatigue and vibrations

In the early stages of mechanical design, engineers unconsciously assumed a linear relation between external load and stress at the critical areas. In a majority of cases this assumption is valid. The very first occurrences of fatigue fracture that were reported are related to railroad industry. In these applications components were largely oversized and engines ran at moderate speeds. There was no interaction between the dynamic characteristics of the structure and the applied load. This and similar phenomena will be called quasi-static or forced.

As technological evolution produced gradually more advanced materials and as economical demands required cheaper light-weight design, the dynamic characteristics of the component needed a closer attention of the engineer. Moreover operating speeds of machinery increased consistently. The coincidence of these phenomena became an important matter of concern to every engineer involved in mechanical design.

In the fifties scientific research was started in the field of vibrations of structures. Techniques of modal analysis were developed in order to be able to cope with many kinds of trouble which are all related to the dynamic behaviour of structures. Problems of driving comfort in an automobile, problems of noise produced by engines, problems of geometrical stability of precision machinery, problems of distortions

in light-weight structures can all be handled by techniques of modal analysis [11]. The problem of fatigue of a structure that is excited at or near one or several of its resonance frequencies is an important problem that modal analysis can be used for as a diagnostics tool.

Today many examples of current industrial practice exist where an excessive level of vibrations is the source of fatigue problems. Among others, every branch of transportation industry often faces vibration trouble causing the lifetime of the structure to be unacceptably low :

- engine mounting system in the body of an automobile
- suspension system of an automobile
- hub, blades, joints, ... of the rotor of a helicopter
- panels of a fixed wing aircraft or spacecraft, which are excited acoustically by the noise pressure from its jet-engine
- components of weapon systems and their mounting assemblies
- ...

In each of these examples, the dynamic characteristics of the structure not only multiply the number of cycles, the quasi-absence of significant damping increases the level of cyclic stress considerably. The number of cycles to fracture may thus be reduced tremendously. Industrial needs urgently require a global methodology that incorporates the dynamic aspects of structure and loading in fatigue prediction techniques. A large amount of effort is spent by many companies in the development of a general approach to estimate the lifetime of the structure [12,13,14,15,16,17].

1.1.3 Analytical versus experimental techniques

Throughout the last 150 years, several techniques have been developed that analyse the structure's behaviour of crack initiation and growth. Historically only experimental methods were used in the design and verification of new products. Gradually engineers gained a more thorough understanding of physical mechanisms of fatigue phenomena, and they came up with rules that matched experimental observation. Distinction between a variety of methods classifies them in three categories :

- strictly experimental methods
- analytical methods
- mixed methods

Strictly experimental techniques are most straightforward but not necessarily easiest in use. It is attempted to create real-life circumstances for the examined component to operate in. The applied loading is the same as the loading that the component is subjected to in real-service conditions. The response of the component is monitored. Either the accumulated damage from a partial sequence of loading, or the total number of cycles to failure is measured. The required availability of a prototype is inherent to the method and a new test must be performed for every single modification of the structure. This procedure is costly and very time-consuming.

Analytical techniques use mathematical models that reflect physical phenomena as closely as possible. An appropriate model of the component has to be built and an accurate description of the operating loads must be available. Computer algorithms then yield an estimation of lifetime. At least some experimental work is necessary in order to have an appropriate description of the material properties. Alternatively one can learn about them from publications or from often simplified experimental relations. It is generally very difficult to incorporate the influences from surrounding conditions like residual stresses, effects of temperature and corrosion.

Mixed methods combine experimental and analytical techniques in any order. One can either start from an experimentally obtained stress response, and then estimate lifetime using analytical tools, or one can first use numerical methods to generate a load set, and then apply this load set as an input for measurements.

Both numerical and experimental methods have their own advantages and disadvantages. They are summarized in table 1.1. Mixed methods can be situated in between the two other kinds. The author has attempted to use sound engineering judgement in combining the best possible conditions in order to replace the "?" by a "++".

1.1.4 Requirements for a reliable method

Nowadays economical demands have made analytical methods prevail over experimental ones. In order for them to gain general acceptance

item	experimental	analytical
cost	−	+
time	−	+
prototype	−	+
loading conditions	+	−
material properties	+	−
environmental conditions	+	−
modifications	−	+
accuracy	+	?
overall usefulness	?	
engineering judgment	!	

Table 1.1: Pros and cons of experimental and numerical methods

among designing engineers, they should meet a number of requirements :

limitation of experimental effort : it will clearly never be feasible to eliminate all experimental investigations, still one should endeavour to restrict them to studies that are completely case-independent. In this way engineers will be able to obtain the data they need from experience acquired by their colleagues. As experimental and analytical techniques are complementary, the advantages of both should be fully used.

accurate description of loading conditions : there are two types of loads that are important to the analysis :

- static loads : it will be shown that they have an important impact on the fatigue behaviour of the structure
- dynamic loads : any type of dynamic loading, periodic or non-periodic, random, ...must be modelled accurately. The dynamic behaviour of the model should correspond fairly well with the actual characteristics of the structure.

stress level : since the fatigue life of a component is very sensitive to the absolute stress level, it is of the utmost importance that refined tools are used to compute the stress level at critical areas of the component

material behaviour : this includes two separate aspects :

- characteristics of the virgin material : the engineer should have an accurate model of the way the virgin material responds on the macroscopic level to the applied loading. Not only the so-called constitutive equations but also the strain-life equation of the material are vitally important in fatigue analysis.
- disturbances by external conditions : environmental conditions, special operating conditions, temperature, technological processes, ...may influence the nominal behaviour of the material

usefulness and practicality : in spite of all intricacies that may complicate the method, it must above all be useful and reasonably easy in practice

1.1.5 Objectives of the method presented

A global method is presented that helps the designing engineer in developing a new product and in evaluating structural modifications. The procedure of designing against fatigue can be run in a fully automated way with a minimum of experimental input. Experimental data are complementary to analytical results, it is preferable that experimental experience is used to its full benefit in updating the analytical model.

It is the author's intention to devise a global scheme that meets the basic requirements in a way that is pragmatic, yet not sacrificing reliability.

1.2 Different types of fatigue

Among others, like thermal fatigue, environmental fatigue, corrosion fatigue, ..., two different types of mechanical fatigue should be distinguished :

forced fatigue is characterized by a linear relation between external loads and internal stresses. The only dominant factor for this type of behavior is the stiffness of the structure. The frequency

content of the external load is irrelevant. This type is also called "quasi-static".

resonance fatigue is characterized by a more complex relation between external load and the deformation of the structure. Not only the stiffness, but also the mass distribution of the structure, and the frequency content of the external load are important. Fatigue phenomena then originate from an unsuitable dynamic behavior of the component. The applied load excites one or more resonance frequencies of the structure, which results in very large displacements, and thus, the structure is heavily strained.

In the former case, the relation between external load and internal stress can be determined with a static analysis. This is the kind of approach that has been used for many years when dealing with fatigue phenomena. In the latter, traditional fatigue analyses can no longer be applied. Transient response has to be determined. This can be done either experimentally, or computationally.

1.3 Numerical methods in fatigue analysis

Three classes of numerical methods can be distinguished. This section highlights their basic features. The consecutive computational steps that are taken and their main advantages and drawbacks.

1.3.1 Traditional method

The general approach of this method is a direct reflection of the old traditional methods that are used in the theory of elasticity. Refs. [18, Chap. 4], [19, Chap. 7] provide details on its characteristics.

1.3.1.1 Basic assumptions

1.3.1.1.1 Constitutive equations

A perfect elasto-plastic behaviour of the material is assumed. For many materials the behaviour in compression is similar to the behaviour in tension. The material is then characterized by two quantities, Young's modulus of elasticity E and the yield stress σ_y. A graphical representation of this behaviour is shown in fig. 1.1.

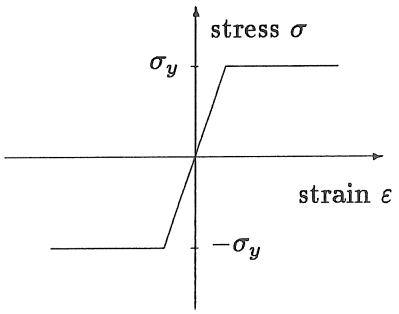

$$\begin{cases} |\sigma| \leq |\sigma_y| & : \quad \varepsilon = \frac{\sigma}{E} \\ |\sigma| > |\sigma_y| & : \quad \varepsilon = ? \end{cases}$$

Figure 1.1: Perfect elasto-plastic stress-strain behaviour

1.3.1.1.2 Stress–life relation

The Wöhler-curve (fig. 1.2) is the graphical representation of the relation between stress-amplitude and number of cycles to failure. The axis of abscissas is logarithmic. The relation is obtained by fitting the best curve through a number of individually measured points.

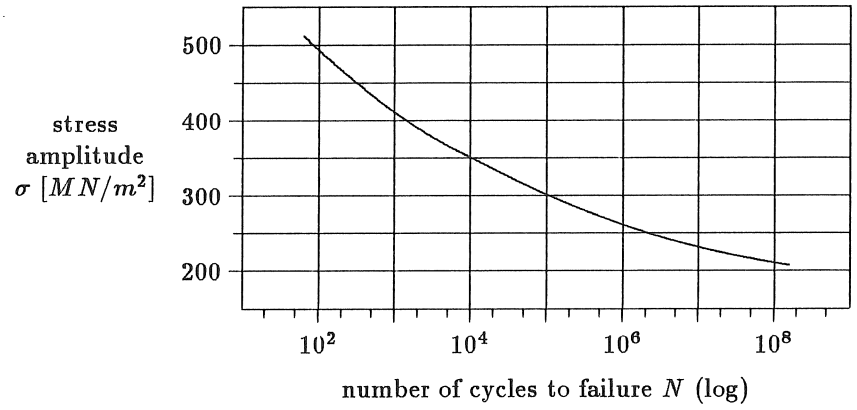

Figure 1.2: Example of a Wöhler-curve

Initially Wöhler-curves were measured only for purely elastic deformation. Due to effects of plasticity in the area of low-cycle fatigue the accuracy at low numbers of cycles to failure may be doubtful. Some materials exhibit a fatigue limit σ_v. Depending upon the nature of the material a particular type of mathematical formula may be best

suited. Following types are common :

$$\text{no fatigue limit :} \quad a \log \sigma + \log N = C^{te}$$
$$\text{fatigue limit } \sigma_v : \quad a \log(\sigma - \sigma_v) + \log(N - N_0) = C^{te}$$

where : a, C^{te}, N_0 : constant numbers
σ : amplitude of cyclic stress
N : number of cycles to failure of the specimen

In these formulations the quantity σ has a definite dimension, which must be specified explicitly (N/mm^2, N/m^2, ...).

Several types of machines are used for the measurement of the relation between stress amplitude and number of cycles : cyclic tension–compression, rotative bending, cyclic torsion, ... It takes a long time to perform this experiment and it is very expensive. Therefore some approximative representations of the stress–life -curve have been presented :

$$\text{MANSON} \quad \Delta\varepsilon = 3.5 \frac{\sigma_u}{E} N^{-0.12} + \left(\ln \frac{100}{100 - RA}\right)^{0.6} N^{-0.6}$$
$$\text{COFFIN} \quad \Delta\varepsilon = 2 \frac{\sigma_u}{E} + 0.5 \left(\ln \frac{100}{100 - RA}\right) N^{-0.5}$$

where : $\Delta\varepsilon$: cyclic strain variation
σ_u : ultimate strength
RA: reduction of area at the instant of rupture of the specimen $RA = \frac{A_0 - A_f}{A_0}$

$\Delta\varepsilon$ is a more general representation of the cyclic load. Unlike the quantity σ in fig. 1.2, it is meaningful in states of plastic deformation. MANSON's equation is used for materials that do not possess a fatigue limit and COFFIN's equation is used for materials that do exhibit a fatigue limit. Both equations, together with some others are merely approximative. They are useful though, when only information about the static characteristics of the material is available.

1.3.1.1.3 Influence of mean stress

Conventional Wöhler-curves fig. 1.2 are obtained for perfectly reversed loading, i.e. for a mean value of load equal to zero. In practice one

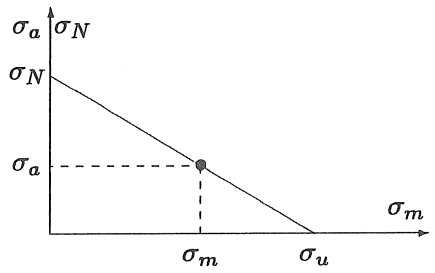

$$\sigma_N = \sigma_a \frac{\sigma_u}{\sigma_u - \sigma_m} \qquad (1.1)$$

Figure 1.3: Haigh–Soderberg -correction

often encounters load cycles with mean values different from zero. In such cases the Wöhler-curves can not be used immediately, and corrections are necessary. HAIGH and SODERBERG proposed a correction formula 1.1 :

where : σ_a : cyclic stress amplitude ($\sigma_a = \frac{\sigma_{max} - \sigma_{min}}{2}$)
σ_m: mean stress ($\sigma_m = \frac{\sigma_{max} + \sigma_{min}}{2}$)
σ_N: equivalent stress amplitude

σ_N is a fictitious quantity without any physical meaning, it is simply used to read the damage that corresponds with the values σ_a and σ_m from the Wöhler-curve. In case of a compressive mean stress, its influence is assumed to be nonexistent.

1.3.1.1.4 Stress concentration factor

The geometry of the notch and the type of loading influence the level of stress at the root of the notch. The relation between nominal stress and real stress is expressed by the linear stress concentration factor 1.2 :

$$K_t = \frac{\sigma_{notch}}{\sigma_{notch,nom}} \qquad (1.2)$$

where : σ : real value of stress
σ_{nom} : nominal value of stress

The nominal value of stress is obtained by application of the conventional formulas from the theory of elasticity.

1.3.1.1.5 Accumulation of damage

A stress variation similar to the one shown in fig. 1.4 is split into a distinct number of blocks. Each of these blocks has a certain amount of damage associated with it. MINER [20] stated that the total damage is found from a linear accumulation rule 1.3 :

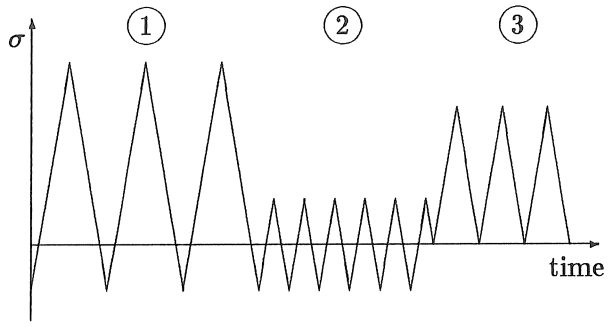

$$\Sigma = \sum_{i=1}^{m} \frac{n_i}{N_i} \qquad (1.3)$$

Figure 1.4: Linear damage accumulation rule

where : m : the number of blocks
n_i : the number of cycles in block i
N_i: the number of cycles to failure for a cycle i
Σ : measure of accumulated damage

The value Σ should be compared to 1. MINER states that failure will not occur unless Σ exceeds 1.

1.3.1.2 Sequence of operations

The first step is the separation of the complete stress variation into a number of elementary stress cycles, each cycle being characterized by its extreme values σ_{max} and σ_{min} of nominal stress. Amplitude and mean stress are denoted by σ_a and σ_m. Real stresses are found by multiplication with stress concentration factor K_t :

$$\sigma_{max} = K_t \sigma_{nom,max} \qquad \sigma_{min} = K_t \sigma_{nom,min} \qquad \sigma_a = K_t \sigma_{nom,a}$$

Depending upon the maximum and minimum values σ_{max} and σ_{min} and amplitude σ_a three separate cases can be identified :

1. $\sigma_{max} < \sigma_y$ and $\sigma_{min} > -\sigma_y$, perfectly elastic (case 1.3.1.2.1)
2. $\sigma_{max} \geq \sigma_y$, plastic in tensile area (case 1.3.1.2.2)
3. $\sigma_{min} \leq -\sigma_y$, plastic in compressive area (case 1.3.1.2.3)

Each of these cases will be outlined briefly below.

1.3.1.2.1 Perfectly elastic state

This case is shown in fig. 1.5.

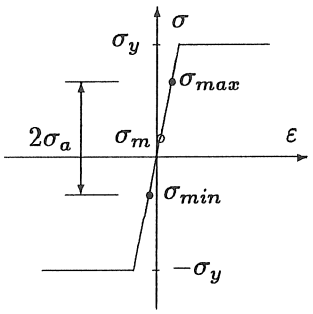

the value of mean stress is given by :

$$\sigma_m = K_t \sigma_{nom,m}$$

and equation 1.1 then yields :

$$\sigma_N = \sigma_a \frac{\sigma_u}{\sigma_u - \sigma_m}$$

Figure 1.5: Perfectly elastic state

1.3.1.2.2 Plastic deformation in tensile area

In the plastic domain strains need to be computed to describe the state of deformation uniquely :

$$\varepsilon_{max,min} = K_t \frac{\sigma_{nom,max,min}}{E} \qquad \Delta\varepsilon = \frac{2K_t\sigma_{a,nom}}{E} \qquad \varepsilon_m = \frac{K_t\sigma_{m,nom}}{E} \tag{1.4}$$

Again, distinction is made between different cases :

1. elastic deformation $\Delta\varepsilon \leq \frac{2\sigma_y}{E}$
2. reversed plastic deformation $\Delta\varepsilon > \frac{2\sigma_y}{E}$

1. one single plastic deformation occurs and all subsequent cycles remain in a fully elastic state (fig. 1.6).
2. every single load variation causes the material to yield, alternatively in tension and compression. Hysteresis loops are followed (fig. 1.7).

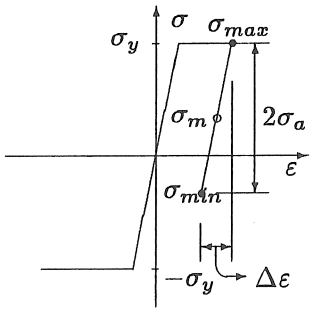

the value of mean stress is given by :

$$\sigma_m = \sigma_y - \frac{E\Delta\varepsilon}{2}$$

and equation 1.1 then yields :

$$\sigma_N = \frac{E\Delta\varepsilon}{2}\frac{\sigma_u}{\sigma_u - \sigma_y + \frac{E\Delta\varepsilon}{2}}$$

Figure 1.6: One single plastic deformation (tension)

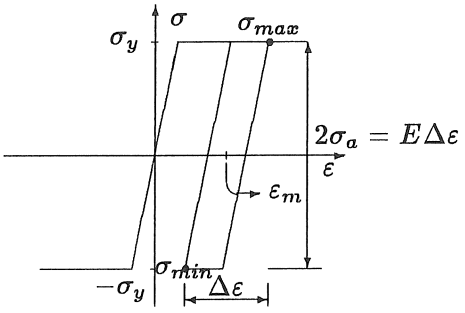

the mean value of strain ε_m is taken into account, and equation 1.1 is written as :

$$\begin{aligned}\sigma_N &= \frac{E(\Delta\varepsilon)_N}{2} \\ &= \frac{E\Delta\varepsilon}{2}\frac{\epsilon_f}{\epsilon_f - \varepsilon_m}\end{aligned}$$

Figure 1.7: Hysteresis loops (positive mean strain)

1.3.1.2.3 Plastic deformation in compressive area

As in the plastic tensile domain (case 1.3.1.2.2) strains need to be computed with equations 1.4. Again, distinction is made between different cases :

1. elastic deformation $\Delta\varepsilon \leq \frac{2\sigma_y}{E}$

2. reversed plastic deformation $\Delta\varepsilon > \frac{2\sigma_y}{E}$

1. one single plastic deformation occurs and all subsequent cycles remain in a fully elastic state (fig. 1.8).

2. every single load variation causes the material to yield, alternatively in tension and compression. Hysteresis loops are followed (fig. 1.9).

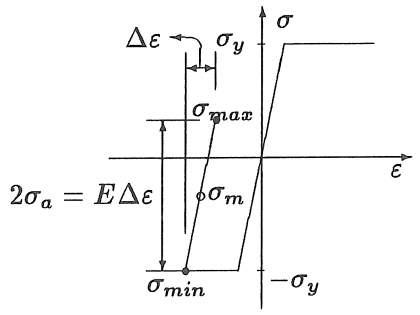

as the mean stress is in the compressive area, it is not taken into account, and thus :

$$\sigma_N = \sigma_a$$

Figure 1.8: One single plastic deformation (compression)

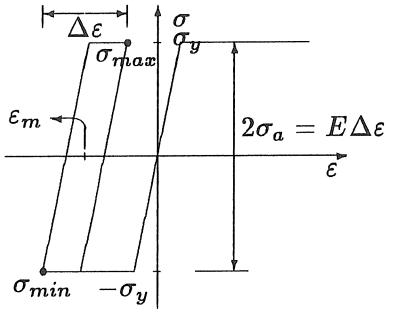

the mean value of strain ε_m is taken into account, and equation 1.1 is written as :

$$\begin{aligned} \sigma_N &= \frac{E(\Delta\varepsilon)_N}{2} \\ &= \frac{E\Delta\varepsilon}{2}\frac{\epsilon_f}{\epsilon_f - \varepsilon_m} \end{aligned}$$

Figure 1.9: Hysteresis loops (negative mean strain)

1.3.1.2.4 Accumulation of damage

One of these cases applies for each elementary cycle from the complete stress–history, and each time the corresponding value of N is obtained. The accumulated damage is then found from MINER's rule 1.3.

1.3.1.3 Advantages and drawbacks

This procedure is a logical extension to the conventional methods of analysis of static strength and deformation. Therefore it is very simple. The simplicity is its main advantage. It does not recognize however, the peculiarities of cyclic loading, especially in the area of plastic deformation. The cyclic behaviour of the material is very much different from its static behaviour. It can no longer be represented by the static material properties σ_y, σ_u and E. Moreover, it is a rather poor practice to relate the number of cycles to failure merely to an elastically determined quantity, stress. The approach of relating the

lifetime of a material to stress, as it is measured in the traditional Wöhler-curves, is not founded on any physical principle. Particularly in the region of plasticity, it is erroneous. Similar considerations apply to the determination of real stresses from nominal stresses. The elastic stress concentration factor K_t does not relate real stresses to nominal stresses correctly. In case plastic deformation occurs, the real stress concentration factor K_t^σ may be very much different from the real strain concentration factor K_t^ε.

The conclusion from all of these shortcomings may be stated roughly as follows : "the predicted lifetime for load variations in the domain of high-cycle fatigue may be fairly good, whereas in the areas of low-cycle fatigue the accuracy of the traditional method is very doubtful".

Another important consideration is concerned with the way of handling variable amplitude load–histories. MINER's linear accumulation rule is characterized by a rather severe lack of physical evidence.

A number of alternative formulations are presented in literature [19], [21]. Although they may accentuate some aspects in a slightly different fashion, they basically follow the same way of reasoning. They all have similar shortcomings in modelling cyclic plastic behaviour of the material appropriately.

1.3.2 Local strain approach

This approach is a more elaborate version of the traditional method. Essentially it follows the same way of reasoning, although its description of the cyclic behaviour of the material is much closer to reality, and also, much more complicated. The method was developed at the University of Waterloo, Ontario, Canada at the end of the sixties. Pioneering work was done by TOPPER, DOWLING, CONLE, LANDGRAF, LAPOINTE, MORROW and SOCIE. Details of the method can be found in [18, Chap. 5], [22,23,24,25,26].

1.3.2.1 Basic assumptions

1.3.2.1.1 Constitutive equations

A cyclic load variation may alter the characteristics of the material considerably. The adequate relation between cyclic stress and strain has to be modified in order to give an accurate description of the local

states of stress and strain, especially in conditions of plasticity. This relation is a measure of the stationary response of the material.

Comparison of the monotonic behaviour of the material with its cyclic behaviour shows that inelastic deformations occur at stress levels below the static yield stress. For some materials this difference may be important (up to 50%).

The variation $\Delta\varepsilon$ of deformation ε is composed of two terms, one elastic term $\Delta\varepsilon_e$ and one plastic term $\Delta\varepsilon_p$:

$$\Delta\varepsilon = \Delta\varepsilon_e + \Delta\varepsilon_p \tag{1.5}$$

The relation between stress σ and deformation ε is well known :

$$\frac{\Delta\sigma}{2} = E\frac{\Delta\varepsilon}{2} \tag{1.6}$$

Experimental analysis showed that relation 1.7 is valid in regions of cyclic plasticity :

$$\frac{\Delta\sigma}{2} = K'\left(\frac{\Delta\varepsilon}{2}\right)^{n'} \tag{1.7}$$

where : K' : plastic modulus (MN/m^2)
n' : cyclic exponent

Joining equations 1.5, 1.6, 1.7 yields :

$$\frac{\Delta\varepsilon}{2} = \frac{\Delta\sigma}{2E} + \left(\frac{\Delta\sigma}{2K'}\right)^{\frac{1}{n'}} \tag{1.8}$$

Equation 1.8 is the representation of hysteresis loops in stationary situations. The quantities E, K', n' fully describe the cyclic behaviour of the material. The cyclic relation between stress σ and deformation ε is written in equation 1.9 :

$$\varepsilon = \frac{\sigma}{E} + \left(\frac{\sigma}{K'}\right)^{\frac{1}{n'}} \tag{1.9}$$

This relation is indicated by the dotted line in fig. 1.10. It joins the tips of the hysteresis loops. This curve is called the virgin curve. Since the shapes of the loop curves equation 1.8 are known, the stress-strain -response can be predicted if it is possible to identify which strain

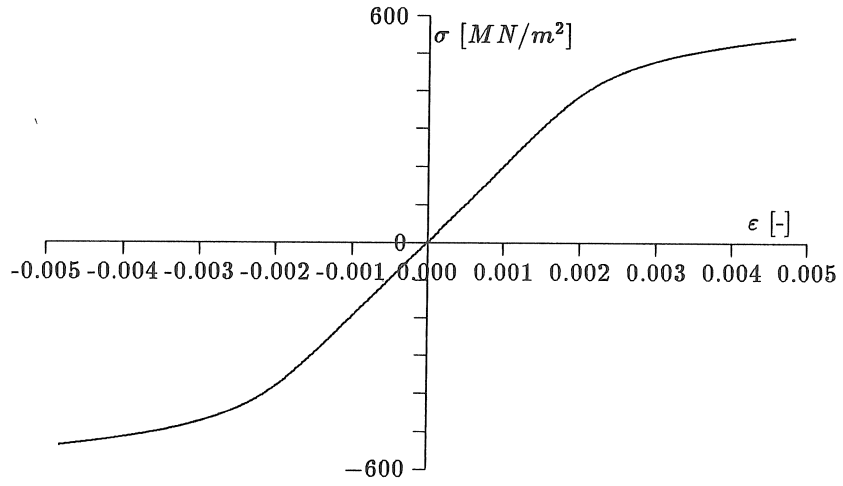

Figure 1.10: Cyclic stress-strain -behaviour

excursions result in closed loops. The key to this is the fact that the stress-strain -behaviour exhibits a memory effect. This memory effect can be characterized in a general manner. For the case of repeatedly applied strain history, the following two rules are needed :

- when the strain next reaches a value at which the direction of straining was previously reversed, a hysteresis loop is closed and the stress-strain -path beyond this point is the same as if the direction of straining had not been reversed
- once a strain excursion forms a closed loop, this excursion does not affect the subsequent behaviour

The hysteresis looping and memory behaviour is exhibited by the rheological model of IWAN [27].

1.3.2.1.2 Strain-life -relation

The same data from the Wöhler-curve fig. 1.2 are used. However, the quantity that is represented in the axis of ordination is cyclic strain. This quantity describes the state of deformation uniquely not only in the elastic but also in the plastic domain, whereas stress is indicative only in the elastic domain. Two distinct representations were established for the relation between the number of cycles to failure on the one hand, and elastic and plastic portions of cyclic strain on the other

hand.

$$\frac{\Delta\varepsilon_e}{2} = \frac{\sigma'_f}{E} N^b \qquad \frac{\Delta\varepsilon_p}{2} = \varepsilon'_f N^c \tag{1.10}$$

where : σ'_f : fatigue strength coefficient
b : fatigue strength exponent
ε'_f : fatigue ductility coefficient
c : fatigue ductility exponent

The total resistance of the material is given by equation 1.11 :

$$\frac{\Delta\varepsilon}{2} = \frac{\sigma'_f}{E} N^b + \varepsilon'_f N^c \tag{1.11}$$

The quantities σ'_f, ε'_f, b, c are characteristics of the material. The relations 1.10 and 1.11 are represented in fig. 1.11. Close observation of MANSON's and COFFIN's equations and relation 1.11 shows that they are all very much alike, however, equation 1.11 is the most generally valid.

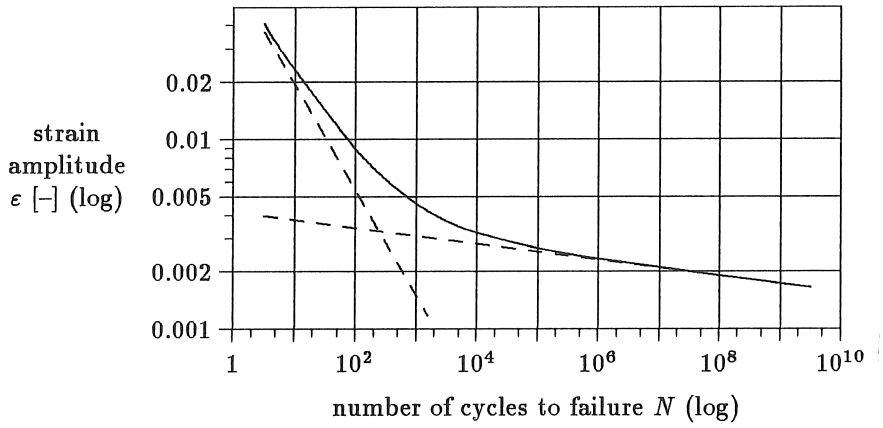

Figure 1.11: Cyclic strain-life -relation

1.3.2.1.3 Influence of mean stress

Often mean stresses at the root of the notch have little influence because they are reduced considerably by cyclic plasticity. The mean stresses that result from the static component of the external load are transferred to the surrounding material that behaves elastically.

This observation is particularly valid in situations of low-cycle fatigue. ELLYIN [135] shows that the influence of mean values of strain is not significant.

For cases of high-cycle fatigue, the stress variation is predominantly elastic and the influence of mean stress is important. Tensile mean stresses are taken into account. Compressive mean stresses tend to close a crack, and so they have a beneficial influence on the lifetime of a component. The lifetime may be estimated using equation 1.12 :

$$\varepsilon_a = \frac{\sigma'_f - \sigma_m}{E} N^b + \varepsilon'_f N^c \tag{1.12}$$

SMITH, TOPPER and WATSON [29] have presented another formulation 1.13 which is almost generally accepted :

$$\sigma_{max}\varepsilon_a = \frac{\sigma'^2_f}{E} N^{2b} + \sigma'_f \varepsilon'_f N^{b+c} \tag{1.13}$$

where σ_{max} is the maximum value of stress in the cycle. Close observation of equations 1.12 and 1.13 learns that only the elastic term of the equation 1.11 is modified.

1.3.2.1.4 Influence of stress concentrations

Fatigue cracks generally initiate at the root of a notch or at a geometric discontinuity of the structure. The major part of the structure behaves elastically whereas one or more minor parts are subjected to cyclic plasticity. These parts are located close to a notch. It is now necessary to assume a certain hypothesis about the local behaviour of stress and strain.

NEUBER [30] presents an approach which states that the geometric mean value of stress concentration factor and strain concentration factor is equal to the elastic concentration factor :

$$\sqrt{K_t^\sigma \, K_t^\varepsilon} = K_t$$

This law relates the local values of amplitudes of stress $\Delta\sigma$ and strain $\Delta\varepsilon$ to the nominal values of stress amplitude :

$$\sqrt{\Delta\sigma \, . \, \Delta\varepsilon \, E} = K_t \Delta\sigma_{nom} \tag{1.14}$$

where σ_{nom} is the nominal stress variation.

1.3.2.2 Sequence of operations

The nominal load sequence is converted into sequences of local stresses and strains. The nominal load sequence may be given in terms of external force, nominal stress, nominal strain, ... The conversion into local values is performed by solving a set of equations that relate local stress and strain to external load.

The state of stress and strain in the first load cycle is governed by the virgin curve 1.9 and the appropriate formulation of NEUBER's rule 1.14 :

$$\begin{cases} \varepsilon &= \frac{\sigma}{E} + \left(\frac{\sigma}{K'}\right)^{\frac{1}{n'}} \\ \sigma \,.\, \varepsilon &= \frac{(K_t\, \sigma_{nom})^2}{E} \end{cases} \tag{1.15}$$

Substitution of the first equation into the second one yields the coordinates in the σ-ε -plane at the instant of the first load maximum. At this time the memory effect shows up, causing the material to follow the stress-strain -paths described in paragraph 1.3.2.1.1. A different set of equations 1.16 now governs the states of stress and strain :

$$\begin{cases} \frac{\Delta\varepsilon}{2} &= \frac{\Delta\sigma}{2E} + \left(\frac{\Delta\sigma}{2K'}\right)^{\frac{1}{n'}} \\ \Delta\sigma \,.\, \Delta\varepsilon &= \frac{(K_t\, \Delta\sigma_{nom})^2}{E} \end{cases} \tag{1.16}$$

Consecutive solution of the appropriate sets of equations convert the nominal load sequence into sequences of local stress and strain. Finally one ends up with a series of hysteresis loops, like the ones presented in fig. 1.10. It is then very easy to extract elementary cycles from the complex load variation.

Each of these cycles is now handled independently. The damage that is associated to a cycle is evaluated with the SMITH–TOPPER–WATSON -parameter 1.13. The total accumulated damage is found from MINER's rule 1.3.

1.3.2.3 Advantages and disadvantages

The local strain approach presents some major advantages over the traditional method.

Only a limited amount of information is needed which is based on experimental data. This consists entirely of material properties from small laboratory specimens or from published literature. Specifically, a cyclic stress-strain -curve 1.8 and a strain-life -curve 1.11 are needed.

Given these, life estimates may be made for any number of different component geometries or load histories. An important drawback, however, is that it may be hard to find the necessary information on the characteristics of the material. The experimental work that has to be done is not a standard procedure. Few publications provide details on the cyclic behaviour of the material. Few companies are willing to share with their competitors the information they have gathered laboriously. It is yet essential for the engineer to have a fair knowledge of the characteristics of the material.

The method serves as a basis for rationally accounting for interactions among material behaviour, geometry and load history. Life calculations based on constant amplitude load-life -data for notched components do not share this advantage. Notched component data which reflect such interactions may of course be obtained for a particular combination of material, geometry and load history. But, if one relies on notched component data alone, there is no rational basis for transferring such effects to different materials, geometries, or load histories. Hence, notched component data under a variety of conditions would be needed to cover all possibilities.

The critical areas on the structure must be selected on a rational basis. Some experimental techniques are available, that show the locations of maximum strain variation. An interesting technique is based on the principle of brittle lacquers. It is described by BEAUFRONT in [31].

1.3.3 Linear fracture mechanics

This approach is completely different from the two previous methods. It starts from essentially experimental data as it observes the behaviour of crack growth of a component. The analytical elements of the method are based on some generalized experimental laws. Many publications are available [18, Chap. 6],[32].

1.3.3.1 Basic features

The fracture mechanics approach differs from other methods in that it makes a clear distinction between physically different phenomena, crack initiation, crack growth and fracture. The fracture mechanics approach studies the phase of crack propagation. It uses an analytical

description of the stress pattern in the vicinity of the crack tip, and it establishes a relation between external load, magnitude, shape and orientation of the flaw.

1.3.3.1.1 Stress intensity factor

Theory of linear elasticity provides solutions of spatial stress distribution in the vicinity of a crack tip for different geometries. Some formulas can be found in publications by PARIS et al. [33] and DECHAENE [34]. These formulations can only be written in an explicit form for points that are close to the crack tip (fig. 1.12).

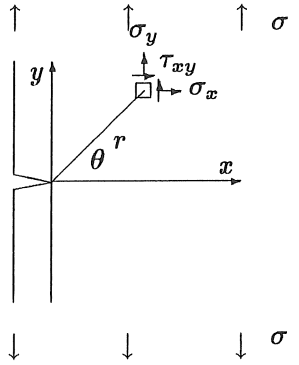

$$\begin{aligned} \sigma_x &= \frac{K}{\sqrt{2\pi r}} \cos\frac{\theta}{2}\left(1 - \sin\frac{\theta}{2}\sin\frac{3\theta}{2}\right) \\ \sigma_y &= \frac{K}{\sqrt{2\pi r}} \cos\frac{\theta}{2}\left(1 + \sin\frac{\theta}{2}\sin\frac{3\theta}{2}\right) \\ \tau_{xy} &= \frac{K}{\sqrt{2\pi r}} \cos\frac{\theta}{2}\sin\frac{\theta}{2}\cos\frac{3\theta}{2} \end{aligned} \quad (1.17)$$

Figure 1.12: Stress-distribution around a crack tip

where : σ_x : normal stress in x-direction
σ_y : normal stress in y-direction
$\tau_{x,y}$: shear stress
r, θ: polar coordinates of considered point

In general, equations 1.17 are written :

$$\sigma_{ij} = \frac{K}{\sqrt{2\pi r}} \mathcal{F}_{ij}(\theta)$$

The stress intensity factor is expressed as (equation 1.18) :

$$K = C\sigma\sqrt{\pi a} \quad (1.18)$$

where : C_{geom} : a dimensionless factor that expresses the influence of geometry
σ : nominal loading stress
a : half the length of the crack

The factor K describes the spatial stress distribution around the crack in a unique way. For points close to the tip of the crack, the distance r is very small, and plastic deformation occurs. Still, K is a fairly good measure of the stress intensity. A relation of type 1.18 is generally valid, and only the value of the factor C_{geom} depends on geometry. Literature provides formulas, tables and graphs with these values for many types of geometry and loading [35,36,37,38].

1.3.3.1.2 Relation between stress intensity factor and crack growth rate

Definition 1.18 relates the cyclic variation of K to a cyclic variation of loading stress σ. The variation of K is characterized by its maximum and minimum values K_{max} and K_{min}. It is observed experimentally that load variations characterized by a certain value $\Delta K = K_{max} - K_{min}$ exhibit the same crack growth rate. This relation can be measured experimentally (fig. 1.13). The dimensions of K and a must

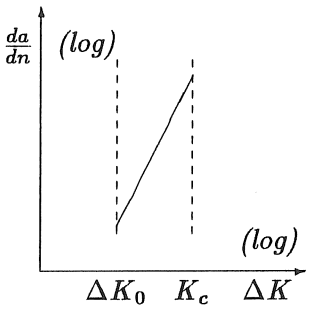

A mathematical formulation for this experimental observation is given by PARIS [33] :

$$\frac{da}{dn} = C(\Delta K)^m \qquad (1.19)$$

Figure 1.13: Crack growth rate

be mentioned explicitly. Relation 1.19 is valid only in the region :

$$\begin{cases} \Delta K > \Delta K_0 \\ K < K_c \end{cases}$$

where : ΔK_0 : a threshold value
K_c : critical value of stress intensity
C, m, ΔK_0, K_c : material characteristics

Outside these limits, equation 1.19 is not valid :

$$\begin{array}{rcll} \Delta K & < & \Delta K_0 & \text{no crack growth} \\ K & \geq & K_c & \text{sudden failure} \end{array}$$

Some other types of equations similar to 1.19 were presented.

After the relation between stress intensity and crack growth rate has been established, the number of cycles for a crack to grow from an initial length a_1 to a final length a_2 can be computed. This is done by integration of the PARIS–equation 1.19 :

$$\int_{a_1}^{a_2} \frac{da}{C(\Delta K)^m} = \int_0^N dn = N$$

Depending on whether the way by which the stress intensity factor is expressed in terms of crack length, the integration can be performed explicitly or numerically. In the latter case the domain of integration is split in an appropriate number of intervals.

1.3.3.1.3 Sequence of computations

In practice the lifetime of a component is predicted as follows :

1. estimation of initial crack length a_i : in case the real dimensions of the crack can not be measured, a conservative estimate is formed
2. computation of the stress intensity factor : K_{max} and K_{min} are computed from the load and the crack size data
3. verification of boundaries : it is checked whether K_{max} and K_{min} lie inside the region of crack growth
4. determination of critical crack length : the value a_c is computed from equation 1.18 such that $K = K_c$
5. integration of PARIS' equation 1.19 : with the integration limits $a_1 = a_i$ and $a_2 = a_c$ the final number of cycles to failure is found

1.3.3.2 Recent developments

1.3.3.2.1 Crack closure

ELBER [39] explained a number of rather unexpected observations as phenomena of crack closure. Close to the tip of the crack plastic strains occur when the load is applied. After the load is taken away compressive residual stresses tend to close the crack. When the next cycle of loading is applied a certain portion of the load is necessary to compensate for the residual stresses, and only the remainder of the load variation is able to strain the material. The effect is that the load variation which is responsible for opening the crack is reduced.

1.3.3.2.2 Crack growth retardation

A single overload in a sequence of constant amplitude causes temporary crack retardation. Due to the peak load a relatively vast plastic zone (par. 1.3.3.2.1) is created. Residual compressive stresses exist in this area, which retard the growth of the crack. This effect may be very important.

1.3.3.2.3 Small cracks

It is observed that short cracks may exhibit a behaviour that is completely different, from the one that is expected (equation 1.19). NOWACK [40] explains why the growth rate of small cracks may be considerably higher than the growth rate that is common to long cracks. The threshold value ΔK_0 may as well be much lower than the value for long cracks.

1.3.3.2.4 Variable amplitude loading

The procedure described in section 1.3.3.1.3 is based on data of constant amplitude loading. It does not account for phenomena like crack closure and crack growth retardation. Some alternative approaches were proposed recently, the WILLENBORG–model [41,42], the WHEELER–model [43,44], the DUGDALE–model [45]. In an overview paper [46], SCHIJVE mentions 14 different models and he concludes that every single model has its own advantages and disadvantages. Although many models may have a few common characteristics, the mere fact that such a multitude of models exist, proves that it is very hard to combine all normal and exceptional aspects of crack growth behaviour in one single model that is generally valid. The efforts that

are spent are very recent, and a huge lot of research is still to be done. Nevertheless it is highly doubtful that a model can be constructed encompassing every single peculiar phenomenon.

1.4 Numerical methods in structural analysis

Numerical methods are being developed, that give the engineer a powerful tool in the analysis of complex structures. The first step in discretising a structure is the finite difference method, the more evolved finite element method followed. Today the boundary element method offers some superior capabilities.

1.4.1 Stress analysis

1.4.1.1 The finite element method

For beam-like structures, trusses, frames, grillages, the displacement method is known for a long time [47, Chap. 44]. For two-dimensional and three-dimensional structures, the finite element method was developed as a fairly straightforward extension to the displacement method.

The publications on the finite element method are innumerable. Refs. [48], [49], [47, Chap. 44], [50], [51] provide basic characteristics together with some advanced features. The basic idea behind the method is a discretization of the full domain of unknowns into small pieces, or elements. Each of these elements has some characteristics that can easily be modelled in mathematical equations. The equations are grouped together in the element stiffness matrix $[k]$. The coordinates of the nodes of each element are transformed to the global system of axes and all the elementary stiffness matrices are joined in one global stiffness matrix $[K]$.

$$[K]\{u\} = \{F\}$$

These equations relate the load force $\{F\}$ to the displacements $\{u\}$ in the nodes. Introduction of the boundary conditions then yields a number of linear equations equal to the number of unknowns. This system has a unique solution. The displacements of all points on the structure are known. In fatigue analysis however, stress is determinative for the life that can be expected. Stresses are obtained from displacements by derivation.

More recently, an advanced variant of the finite element method emerged that eliminated the error induced by mathematical differentiation considerably. Stresses are independent variables on a level equivalent to displacements. This alternative formulation is called the hybrid theory.

1.4.1.2 Boundary element method

The theory of boundary elements was introduced by MASSONNET [52]. Due to a prohibitive lack of computational power, however, its practical use was doomed. Only in the mid seventies research concentrated on practical implementations and only in the early eighties its use left academic spheres.

The boundary element method is essentially based on a strongly mathematical background. Some mathematical transformations are used in order to transform the basic equations to a formulation that involves only unknown quantities on the boundary of the structure. Appendix A shows which transformations are used and how they lead to the boundary integral formulation. Tractions and displacements are independent variables that appear next to each other. Some important conclusions show up :

- the field of unknowns is restricted to the boundary of the structure
- stresses are obtained directly
- there is no discretization of the volume of the body, unless body forces have to be taken into account
- the states of stress and displacement are piecewise continuous, but they are not discretized, distinct discontinuities are allowed

The original formulation of the boundary integral equation is only valid when the entire structure is in a state of elastic deformation. Initially the method is conceived to analyse isotropic and homogeneous media, i.e. structures that are built from only one material. It is very well possible though, to model structures consisting of different materials. In this case different zones need to be defined, which are at first analysed separately. The separate zones are then joined together by imposing interface conditions.

1.4.2 Dynamic response

There are two methods for the analysis of the response of a structure to arbitrary time-dependent loading :

- direct solution of the differential equations
- modal analysis, using previously computed eigenvalues and eigenvectors

1.4.2.1 Direct integration

The dynamic response of a system with one degree of freedom is governed by the equation 1.20 :

$$m\ddot{u} + c\dot{u} + ku = f(t) \tag{1.20}$$

where : u : displacement k : stiffness
$\dot{u}$: velocity c : damping
$\ddot{u}$: acceleration m : mass

For structures with multiple degrees of freedom all the equations of type 1.20 are assembled in one general matrix equation 1.21 :

$$[M]\{\ddot{u}\} + [C]\{\dot{u}\} + [K]\{u\} = \{f(t)\} \tag{1.21}$$

where : $[M]$: mass matrix
$[C]$: damping matrix
$[K]$: stiffness matrix
$\{u\}$: vector of components of displacements at nodes
$\{f(t)\}$: vector of components of external forces at time t

These equations are solved by a time-stepping procedure. Given the values of $\{u\}$, $\{\dot{u}\}$ and $\{\ddot{u}\}$ at time t satisfying equation 1.21, values of $\{u\}$, $\{\dot{u}\}$ and $\{\ddot{u}\}$ are sought such that the equation is still satisfied at time $t + \Delta t$. Initial conditions for $\{u\}$, $\{\dot{u}\}$ and $\{\ddot{u}\}$ have to be defined in advance. A recursive algorithm is used, in which at each time step all the components of the displacements are known. Any type of loading can be evaluated, and even non-linear analysis is possible. The computational effort rapidly becomes very large with the time increment Δt.

1.4.2.2 Modal analysis

Previously computed eigenvalues and eigenvectors are used in the calculation of transient response by projection in the space defined by the eigenvectors. In the computation of modal parameters of the structure, damping is neglected, and the eigenvalue problem is formulated in equation 1.22 :

$$\left([K] - \omega^2[M]\right)\{u\} = \{0\} \tag{1.22}$$

where $\omega = 2\pi f$, f being the undamped resonance frequency. An eigenvalue solver is used for the consecutive computation of eigenfrequencies and eigenmodes $\{\psi\}$. The modes are always expressed in terms of displacements. The response of the structure is computed as a linear superposition of the different modes of the structure. The system of equations to be solved must in principle be linear. The method of modal analysis is more efficient because the equations are decoupled, and because it is often sufficient to integrate for a small number of modes, much smaller than the number of eigenvalues of the system.

1.5 Aspects of experimental analysis

The experimental duties one has to perform will always remain a factor of crucial importance to the accuracy of the obtained result, regardless of the ratio between analytical and experimental parts of the analysis (section 1.1.3). It will always be inevitable for the engineer to have experimental data that he can rely on.

1.5.1 Experimental techniques in fatigue analysis

Experimental analysis involves full scale testing and testing of small size laboratory specimens. The former type of tests is used to evaluate the life of the full structure when it is subjected to real service loads. Tests of the latter type are performed to determine the properties of the material.

1.5.1.1 Full scale component testing

Some of the earliest fatigue studies involved full-scale testing. After a period of concentration on small testpiece data, the second half of

this century has seen an increasing trend towards full-scale testing, aided by the ready availability of appropriate testing equipment. It is instructive at this stage, to examine the justification for such testing today, since it is a very expensive procedure. A series of decisions have to be taken on the approaches and alternatives in applying testing techniques for evaluating component durability.

test objectives : first the engineer needs to define the results that he expects from the test. An important point to be noticed is the in-service environment of the component. The conditions of the test must match the real-life operating conditions, in order to allow field-related life estimates to be made. In case experience from previous tests is available, modifications can be evaluated. Otherwise a preliminary test is required to show the location and the mode of fatigue failure.

test specimen : generally, the smaller the specimen, the less expensive the test equipment for mechanical testing. It is important to note, however, that as the size of the specimen is reduced the finesse to conduct the test usually increases. In case the critical component cannot be isolated a sample of the complete structure is required. In case it can, the question rises whether the fatigue sensitive area is understood. The answer to this question determines whether a sample of the component section at the critical location is sufficient.

data collection locations : digital computers are utilized to store the simulated service history data banks. When the environmental loading is not independent of the specimen, data must be collected to aid in preparing test system inputs. When specimen inputs cannot be recorded the specimen's response must be measured. When specimen responses are measured and recorded, a compensation technique for controlling parameters remote from the inputs is necessary.

data collection techniques : when the specimen strain responses are affected by the specimen dynamics, the frequency contents must be maintained. When the specimen inputs are not stationary Gauss-distributed a time history recording is necessary to maintain both frequency content and amplitude distribution.

When the specimen dynamics are irrelevant and multiaxial loading is important then the question rises whether the strain responses between channels are dependent. If so a time history recording is necessary to maintain channel interdependency and peak accuracy. If not, an amplitude distribution recording is possible.

programming and control methods : it is desirable that laboratory tests can be accelerated. Such a procedure must however be viewed with caution. An accelerated test is possible when dynamic effects are irrelevant, simply by increasing the exciter's operating speed, thus reconstructing the original time response history in a shorter span of time. The gain in testing time is limited by the dynamic effects of both specimen and exciter. Still, it is possible to accelerate the test but it may be required to compensate for the dynamic effects by modifying the inputs to the exciter. DE VIS et al. [53] present some generalized test simulation procedures that replace the actual field operation by controlled shaker testing.

These are some general considerations on how the test should be performed. MARSH [9] comments on aspects that are peculiar to a very broad range of industrial applications.

1.5.1.2 Material testing

A number of small size specimen tests are necessary in order to evaluate the characteristics of the material. The results of these tests are utilized in subsequent analysis. The local strain approach intends to make fatigue predictions flexible in a sense that knowledge of only a limited number of material properties is necessary, regardless of the complexity of load variation and regardless of the notch geometry. It requires seven parameters to describe cyclic material behaviour, four to establish a fatigue damage curve and three to define a cyclic stress–strain -curve. For the purpose of fatigue life assessment, these data may be obtained in one of three ways :

direct measurement : some methods for determining the required material properties are established. They are, however, not a

standard test that is performed by every laboratory. If maximum accuracy is required, then there is no substitute for obtaining these material parameters by direct measurement for the material of interest.

indirect measurement and calculation : approximation methods for the calculation of fatigue properties from more easily measurable parameters have been developed for situations where direct measurement is impractical. However, the results may not always be reliable, and these techniques should only be used for general assessments and comparisons, rather than for accurate fatigue life calculations.

from existing databases : as with service data, material data can be organized on a computer database form. Unlike service data, however, material information is common to many industries so that over the past fifteen to twenty years much information has been accumulated. Companies have spent large amounts of money in laboriously gathering experience and organizing an efficient database. In a recent publication, SEEGER covers some 600 materials. Interpretation of these data is not always straightforward, as materials may be slightly different over country's bounds.

1.5.2 Influencing factors

Many factors exert an influence on the fatigue behaviour of a component. Material properties, geometric characteristics and load variation are predominant quantities. Their influence is modelled by the mathematical representations of physical reality. Some other factors, however, appear to affect the fatigue behaviour considerably :

residual stress : many technological processes induce residual stresses at the critical areas of a structure. The welding and the grinding processes both create heat affected zones, characterized by tensile residual stresses near the surface of the component and compressive stresses inside the volume. Cold forming processes also give rise to residual stresses. Their sign may either be positive or negative. Generally these residual stresses are unknown,

since they depend very strongly on the technological process and on the competence of the workman.

When testing a component, one should make sure that the component has the same internal stresses as a component that is taken from industrial production. Especially when measures are taken to induce residual stresses artificially one should wonder whether the repetitive nature of the technological process is sufficient in order for the residual stresses to be consistently the same for all samples.

temperature effects : materials behave differently when subjected to extreme temperature conditions. Especially for those structures that operate in strongly variable conditions, care should be taken that test conditions match the real operating conditions, and that temperature effects are simulated well.

ductility and embrittlement of the material : some technological processes exert an important influence on these material properties. Hardening techniques, welding processes and carbonizing technologies tend to embrittle the material. Variance on these properties may have an important effect on the fatigue behaviour of the component. The test sample should have the same characteristics that are typical to industrial production.

surface quality : microcracks initiate much faster on a rough material surface, while the influence of surface quality is not significant for macrocracks. The surface roughness should be well controlled when performing tests in the region of high-cycle fatigue.

environmental aspects : some environmental conditions may accelerate the accumulation of damage on structures that are poorly protected. Structures that are exposed to corrosion exhibit fatigue behaviour that may be extremely harmful to the structure. Components that are expected to operate in severe environmental conditions should be tested likewise.

scale effects : the size of the test specimen affects its resistance to fatigue. Thinner specimens tend to have longer lives than thicker specimens for equal stress. Data collection should be done using specimens with appropriate dimensions.

All of the aforementioned aspects influence the fatigue behaviour of the component to some extent. It is very difficult to predict their influence, and for some of them it is particularly difficult to quantify the impact they have on fatigue life. The most important point however, is the fact that they are characterized by a large value of variance. This observation may cause the relevancy of the result of a test to be doubtful.

1.5.3 Comments on the accuracy of the results

It is a well established fact that large values of variance are inherent to any result in fatigue analysis. Many reasons make this statement to be disappointing, yet true. The major cause may be found in the imperfections and irregularities that characterize any material. Besides, mechanical technology is unable to manufacture two products that are completely identical. Every single hole in the rotor disc of a jet engine is drilled in exactly the same material, with exactly the same technology, using exactly the same machinery, still, they should all be examined separately.

Engineers involved in fatigue design, are not wasting their time, whatsoever. They should be aware of the fact that although a whole lot of uncertainties cannot be removed, sound engineering judgment can reveal major tendencies. They should not attempt to forecast the number of cycles to failure within a margin of 5%, yet they are able to predict the relative gain caused by structural modifications.

1.6 Statistical methods of fatigue life predictions

Many reasons complicate an engineering description of fatigue behaviour, variability in failure data from experiments, temperature effects, residual stresses, complicated stress processes, ... While many uncertainties in the fatigue problem exist, some probabilistic design methods provide a mechanism of treating such uncertainty in a rational manner. The methods described here present a global approach, starting from the statistical characteristics of a variable load and incorporating uncertainty about the material characteristics. CRANDALL and MARK [54], ROBSON [55], KARLIN [56] NEWLAND [58] and

KASHYAP [57] give overviews of the techniques that are used to study random vibrations. GRISARD [59] applies these methods to fatigue life prediction.

The first approach for a theoretical treatment of the problem of sonic fatigue in aircraft structures which considers the aspects which have to be taken into account was made by MILES in 1954 [60]. Later a random fatigue design algorithm for stationary gaussian processes has been proposed by WIRSCHING and HAUGEN [61,62]. This procedure is based upon the assumption that each tensile peak of the same magnitude causes an equal amount of fatigue damage. Investigations of random fatigue design later included work of ANG and MUNSE on bridges [63], NOLTE and HANSFORD on offshore platforms [64], LANDGRAF and LAPOINTE [22] and WETZEL [65] on automotive structures, and DOWLING [24], GALLAGHER and STALNAKER [66], and YANG and TRAPP [67] on aircraft structures.

Sections 1.6.1 to 1.6.5 briefly introduce some concepts that are common to most of the approaches mentioned.

1.6.1 Definition of the load signal

A stochastic process consists of a theoretically infinite number of sample functions each of which can be thought of a resulting from a separate experiment. Suppose, for instance, that the air pressure $U(t)$ at some point on the fuselage behind the engine of a jet aircraft is the quantity being studied. It is necessary to know how the pressure varies during long-distance flying and so a large number of time histories $u_1(t)$, $u_2(t)$, ...are recorded for typical flights. This collection of sample functions constitutes an approximation for the theoretically infinite family of the random process. This process is characterised by its statistical properties, which may be viewed in two ways :

- for a given signal $u_i(t)$, which is one element of the entire group $U(t)$, the statistical characteristics are computed as a function of time t
- for a particular instant of time t_j, all the excitations of the family are considered at time t_j, and the statistical characteristics of this random variable are established

A random process is said to be stationary if the probability distributions obtained for the whole group do not depend on absolute time.

This implies that all the averages are independent of absolute time, and specifically, that mean value and standard deviation are independent of time.

A stationary process is called ergodic if, in addition to all the group averages being stationary with respect to a shift of the time scale, the averages taken along any single sample are the same as the total group averages. Each sample function $u(t)$ is then completely representative of the family $U(t)$ that characterises the stochastic process. Ergodic stationary random processes are studied in subsequent sections 1.6.2 to 1.6.5.

1.6.2 Distribution of level crossings and peak values

Consider a random signal $u(t)$. The mean rate of positive crossings ν_a^+ of a certain level $u = a$ is given by :

$$\nu_a^+ = \frac{1}{2\pi}\frac{\sigma_{\dot{u}}}{\sigma_u} e^{-\frac{a^2}{2\sigma_u^2}} = \frac{1}{2\pi}\sqrt{\frac{m_2}{m_0}} e^{-\frac{a^2}{2m_0}}$$

and the rate of positive zero crossings ν_0^+ :

$$\nu_0^+ = \frac{1}{2\pi}\frac{\sigma_{\dot{u}}}{\sigma_u} = \frac{1}{2\pi}\sqrt{\frac{m_2}{m_0}} \tag{1.23}$$

where :

$$\sigma_u^2 = \mathcal{E}[u^2] = \int_{-\infty}^{\infty} S_u(\omega)\, d\omega = m_0$$

$$\sigma_{\dot{u}}^2 = \mathcal{E}[\dot{u}^2] = \int_{-\infty}^{\infty} \omega^2 S_u(\omega)\, d\omega = m_2$$

$$S_u(\omega) = \frac{1}{2\pi}\int_{-\infty}^{\infty} R_u(\tau) e^{-j\omega\tau}\, d\tau$$

$$R_u(\tau) = \mathcal{E}[u(t)u(t+\tau)]$$

$\mathcal{E}[\bullet]$ stands for "the statistical expectation of", and $R_u(\tau)$ is the autocorrelation function for the random process $U(t)$. $S_u(\omega)$ is the mean square spectral density, ω being the angular frequency. Equation 1.23 is called "RICE's formula". ν_0^+ is the mean frequency or the central frequency. The mean rate of peak values $\mathcal{E}[M]$ is equally determined by RICE :

$$\mathcal{E}[M] = \frac{1}{2\pi}\sqrt{\frac{m_4}{m_2}}$$

where m_4 is the moment of 4^{th} order of the spectral density of the signal :

$$m_4 = \int_{-\infty}^{\infty} \omega^4 S_u(\omega)\, d\omega$$

1.6.3 Accumulation of damage

The expected value of the rate of damage accumulation $\mathcal{E}[D]$ is then :

$$\mathcal{E}[D] = \mathcal{E}[M] \int_0^{\infty} \frac{q(S)}{N(S)}\, dS \tag{1.24}$$

This expression is generally valid for any distribution $q(S)$ and any shape of the WÖHLER-curve $N(S)$ (fig.1.2). Supposing the WÖHLER-curve is represented in a simplified manner by :

$$N = C.S^{-\beta} \tag{1.25}$$

then the damage d_i for an elementary cycle i of amplitude $S = a$ is :

$$d_i = \frac{a^{\beta}}{C}$$

For a gaussian narrow band process, the distribution $q(S)$ is given by :

$$q(S) = \frac{S}{\sigma_S^2} e^{-\frac{S^2}{2\sigma_S^2}} \tag{1.26}$$

Introduction of 1.25 and 1.26 into 1.24 gives (with $\eta = S/\sigma_S$) :

$$\begin{aligned} \mathcal{E}[D] &= \mathcal{E}[M] \frac{\sigma_S^{\beta}}{C} \int_0^{\infty} \eta^{\beta} q(\eta)\, d\eta \\ &= \nu_0^+ \frac{(\sqrt{2}\sigma_S)^{\beta}}{C} \Gamma\left(1 + \frac{\beta}{2}\right) \end{aligned}$$

where $\Gamma(\xi)$ is the *Gamma*-function :

$$\Gamma(\xi) = \int_0^{\infty} z^{2\xi - 1} e^{-z^2}\, dz$$

1.6.4 Wide band excitation

The critical issue in this study becomes one of deriving the probability density of the amplitude of peak values for the case where the signal $U(t)$ is gaussian but not narrow band, in which case the distribution of stress b is not known. WIRSCHING and MOHSEN SHEHATA [68] characterize the spectral shape $W(f)$ by an irregularity factor α :

$$\alpha = \frac{\nu_0^+}{\mathcal{E}[M]}$$

with $0 \leq \alpha \leq 1$, and $\alpha = 1$ for $U(t)$ narrow band. Monte Carlo methods are then used to simulate $u(t)$ and estimate $q(S)$. Given an arbitrary function $W(f)$ which is obtained by measurement, a sample of $u(t)$ is simulated using the following form :

$$u(t) = \sum_{k=1}^{N} \sqrt{2G(\omega_k)\Delta\omega_k}\cos(\omega_k t + \phi_k)$$

$G(\omega)$ is the one sided spectral density function in terms of frequency : $G(\omega) = W(f)/2\pi$. Frequency is defined over the interval $[0, \omega_u]$ with partitions of length $\Delta\omega_k$ such that :

$$\omega_u = \sum_{k=1}^{N} \Delta\omega_k$$

ϕ_k is a random phase angle, uniformly distributed in the interval $[0, 2\pi]$. If all $\Delta\omega$ are equal, $U(t)$ will be periodic with a period of the reciprocal of the minimum frequency of the input spectral density. This problem is avoided by using random intervals for $\Delta\omega_k$.

Once a sample of the random process is generated the sequence of operations is the same as in section 1.6.3.

Another approach is presented by FENECH and RAO [69]. They consider the problem of fatigue failure due to flow noise excitations from a fracture mechanics point of view. The power spectrum of the stress induced by a narrow band and broad band flow noise on a panel is used to determine the fatigue failure probability of that panel. YANG and HEER [70] have shown that the material strength initially at R_0 decreases to R_n after n stress cycles according to the relationship :

$$R_n = R_0 e^{-\frac{k}{2}\sum_{j=1}^{n} S_j^b}$$

where : k : a constant representing the initial crack propagation rate
b : an experimentally obtained exponent
S : an applied positive peak stress

The statistical distribution of R_n depends on the statistical distribution of R_0 and of the stress peaks S_j, $j = 1, 2, \ldots, n$. A lognormal distribution of the material properties and a Raleigh distribution of the stress peaks are implied in the statistical model. The Poisson failure rate and reliability are computed for several crack propagation factors and statistical distributions of the initial strength of materials. The authors conclude that the panel's fatigue lifetime obtained by statistical analysis is generally shorter than the one given by a deterministic Palmgren-Miner cumulative model for narrow band and broad band excitations. The two models predict similar fatigue lifetime for cases corresponding to small initial material cracks or low rates of crack propagation.

1.6.5 Use of statistical methods

Statistical methods are used extensively in many applications, such as wind loading of bridges and buildings, water wave loading of offshore structures, acoustic loading of aircraft panels, rough road loading of automobile structures, ... The data that are input to the analysis may be either a strain sequence or the power spectral density of the external load. In the latter case the strain response still has to be computed. The power spectral density of the response S_{vv} is easily related to the power spectral density of the load input S_{uu} :

$$[S_{vv}] = [H^*(\omega)].[S_{uu}(\omega)].[H(\omega)]^t$$

HARTT and LIN [71] present an excitation spectrum for offshore structures subjected to seawave excitation and HERNRIED and LAU [72] provide data on earthquake spectra.

1.7 Conclusion : formulation of the problem

Today engineers have many techniques at their disposal to estimate the fatigue lifetime of a mechanical component. Some of them are rather complex, some others are fairly simple. Quite often only experimental analysis is able to yield results that are reliable. In recent

years the local strain approach is developed to be a powerful tool in fatigue life prediction. It specifies a number of characteristics that do not depend on the particular case that is considered, and that allow quick and accurate evaluation of all aspects of the problem. The lack of availability of material data and properties in readily accessible data bases remains a serious problem and continues to restrict wide-spread use of the newer life prediction technologies. Therefore an accurate yet simple technique should be devised that is accessible to laboratories which are willing to invest in advanced knowledge, rather than in expensive technology.

Many types of structures suffer excessive levels of vibrations, often giving rise to cracks and sometimes early fracture. When the interaction between dynamic characteristics of load and structure is relevant, the vibratory response of the structure has to be determined in an accurate fashion. This task is prohibitively time-consuming. Industrial practice currently neglects the dynamic behaviour of the structure.

Another important matter of concern in fatigue analysis is the accurate prediction of stresses that occur at the critical areas. Experimental analysis often fails to evaluate stress concentrations accurately. It is then necessary to compute local stresses and strains from the nominal quantities. Several numerical techniques exist for stress evaluation. They should be refined such that maximum accuracy is achieved.

The combined computation of the dynamic stress pattern may seem to be a commonplace procedure. However, careful investigation of existing methods, applied on practical cases, sometimes reveals deficiencies that are unacceptable in fatigue life prediction. The main effort in response prediction should be directed towards an accurate evaluation of stress levels.

In conclusion, the problem may be stated as follows : **develop an integrated methodology that analyses the dynamic behaviour of the structure, that computes the stress levels, that estimates the fatigue life and that integrates analytical and experimental experiences smoothly in a way that is flexible, fast and easy in use, yet not compromising the accuracy and the reliability of its results !**

Chapter 2

Aspects of an analytical fatigue life estimation method

2.1 Purpose and capabilities of the method

Current practice of resonance fatigue life assessment and design in large and highly technological companies nowadays still is awkward. It lacks consistency and theoretical background and only partial analyses are carried out. Quite often there is no collaboration between experimental and analytical groups of the company simply because there is no tool for interactive comparison of experimental and analytical data.

In this chapter an integrated fatigue life estimation method will be introduced. It is primarily designed for thorough evaluation of the fatigue behaviour of dynamically loaded structures and for detailed comparison of structural modifications. It is developed essentially to study phenomena of low-cycle and/or high-cycle fatigue, from the time of crack initiation to failure. The method is very flexible in a sense that it integrates any amount of experimental data smoothly into the analysis. It is essentially capable of handling resonant behaviour in a fast and accurate fashion. Static loads are easily superposed to the dynamic deformation.

The proposed method employs techniques of several branches of mechanical engineering. It implies three major parts, and for each

separate part a technique that performs efficiently is presented. Some techniques that function satisfactorily are optimized in quest of maximum performance. It is shown that some other methods that are used widespread are actually inaccurate or even erroneous. Those methods are modified and adapted in an effort of pursuing optimum accuracy and flexibility. Finally some model updating procedures are presented that allow interaction between experimental and analytical results.

The computation of the dynamic strain response is performed using an original dynamic boundary element analysis. A combined use of response computation in modal coordinates and static boundary element analysis form the basis of a particularly accurate and fast technique for constituting the multiaxial strain history of a structure that is subjected to dynamic loading. The concept of modal strains is used throughout. Analytical computation of modal strains is based on numerical differentiation of displacements. It will be shown that the accuracy is acceptable only when displacements are computed from inertial forces. A new procedure is developed that smooths and completes mode shapes. Only little information about the mode shapes is needed to allow a fair estimation of the strain history.

Conventional boundary element practice tries to avoid body terms as much as possible, mainly because of high computation times. It will be demonstrated why only little computational effort is involved in an accurate description of inertial forces. Even a coarse geometric model of volume cells is suitable for the purpose of computing modal strains.

This chapter introduces the major steps of the proposed method. The basic reasoning behind it is outlined only briefly. A more detailed justification of the whys and the wherefores of the different steps is given in chapters 3 – 5.

2.1.1 Fields of application

The local strain approach will be used. This method has received general acceptance among engineers in fatigue analysis. Mechanical structures are studied from the time they are manufactured up to failure. Typical examples of cases to be studied by this method are :

- components of production machinery
- components of ground vehicle transportation systems

- military equipment
- agricultural and heavy industry machinery
- most components of rotating wing aircraft
- landing gear of fixed wing aircraft
- ...

The proposed method needs further development to be capable of analysing phenomena which are essentially characterized by crack propagation. So far, only metallic structures can be studied. The method is a valuable tool in the design and modification of mechanical structures. It is designed to function in the development phase of a product, before any prototype is available. It can also be used to analyse the influence of modifications to the fatigue behaviour. The term "modification" should be understood in a very broad sense. Not only geometrical or material modifications can be evaluated, but also modifications to the dynamic characteristics of either structure or loading can be studied.

2.1.2 Capabilities and restrictions

One of the fundamental assumptions in theory and applications of modal analysis is the hypothesis of linearity and time invariance. Linearity comprises homogeneity and superposition. Schematically these principles can be represented as follows :

$$\begin{array}{lcccccc} \text{homogeneity} & : & f \rightarrow x & \Rightarrow & af & \rightarrow & ax \\ \text{superposition} & : & \left.\begin{array}{l} f_1 \rightarrow x_1 \\ f_2 \rightarrow x_2 \end{array}\right\} & \Rightarrow & f+g & \rightarrow & x_1+x_2 \\ \text{time invariance} & : & f(t) \rightarrow x(t) & \Rightarrow & f(t-t_0) & \rightarrow & x(t-t_0) \end{array}$$

where : f_1, f_2 : exciting loads applied to the structure
x_1, x_2 : response of the structure
a : constant scalar numbers
$\rightarrow$: yields a response of

The assumptions of linearity and time invariance are adopted here.

The method is not capable of handling non-linear systems. This is a restriction to the type of structure rather than to the properties of

the material. Non-linear structures such as joints and stops should be analysed with other techniques, in particular the method of direct integration (section 1.4.2.1), which is used for transient response analysis. The assumption of linearity implies that deformations of the structure essentially must be small, such that the constitutive equations of linear elasticity are still fulfilled.

Problems of resonance fatigue failure tend to occur most often in lightly damped structures rather than in strongly damped structures. For a lightly damped structure little force is needed to induce high levels of stress whereas strongly damped structures are characterized by peak levels of stress that are much lower. Stress levels are reduced to a negligible amplitude much slower in the former case than in the latter. As far as the accuracy of the result is concerned, a fair estimation of damping characteristics is vitally important, especially when the structure is lightly damped. This statement is not valid for structures subjected to static or quasi-static loading (section 1.2).

A series of assumptions concerns the characteristics of the material when it is subjected to cyclic loading :

- it is supposed to exhibit a "Masing behaviour" [135] A material is said to exhibit a "Masing description" when the peak to peak differences of the hysteresis loops are obtained from the cyclic stress-strain curve, equation 1.8, magnified by a factor of two. Variations of stress and strain are determined with respect to the origin placed at the compressive tip of the largest hysteresis loop. This observation affects the manner in which the absorbed plastic energy is calculated.

- the material properties are kept constant. They are assumed not to vary with surrounding conditions. The influence of temperature effects as described by VANSEVENANT [73] are not taken into account here. Corrosion effects can not be modelled analytically.

- the material characteristics are identical in the tensile area and in the compressive area.

All of these considerations do not introduce severe restrictions, since most technical metallic materials, steel alloys, aluminum alloys, titanium alloys, ... do exhibit the assumed nature.

2.2 General overview of the method

2.2.1 Flowchart

Three major steps have to be made when analysing the fatigue life of a component. The proposed method is modular, it is very flexible in a sense that it is very easy to depart from the second or the third step when information is available from previous analyses. The method consists of three modules that are executed consecutively :

1. response computation
2. stress analysis
3. fatigue life prediction

Figure 2.1 gives a schematic overview of the consecutive steps of the method of fatigue analysis. The dashed lines form the boundaries of each module.

where : ν : damped resonance frequencies
ζ : damping ratios
ψ : mode shapes
ψ^u in terms of displacements
ψ^ε in terms of strains
$u(t)$: displacement history
$\varepsilon(t)$: strain history
x : geometric location

2.2.2 Integration of experimental and analytical techniques

Experimental data can be used at any level of the analysis. One can switch from experimental techniques to analytical methods at any point of the analysis, and vice versa.

Modal parameters can be obtained either from experimental analysis, or from numerical analysis. In the latter case only resonance frequencies and mode shapes can be computed. It is clearly impossible to find damping values from numerical analysis. The user does have to perform some experimental work in order to determine damping ratios. They should be measured independently. Mode shapes

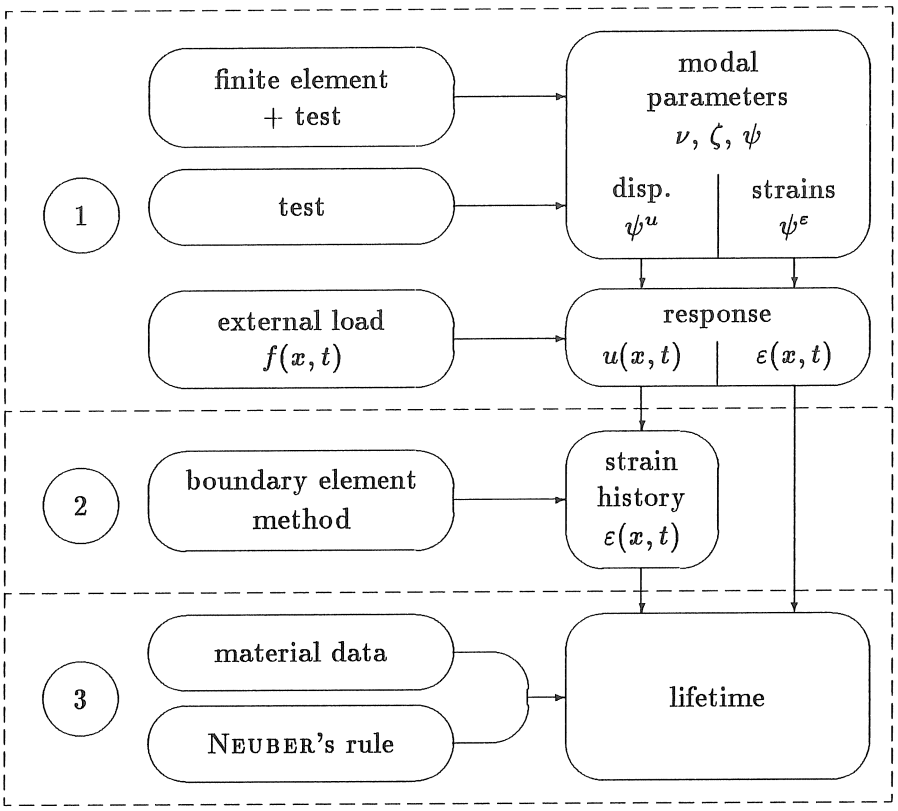

Figure 2.1: Consecutive steps in the fatigue life estimation method

may be expressed in terms of strains, displacements or accelerations. Numerical analysis yields mode shapes that are expressed in terms of displacements, while experimental data can have either type. Conventional measurements utilize accelerometers, or, alternatively, strain gauges.

Starting from the computed displacements $u(t)$, stress/strain analysis is performed using the boundary element method. It is crucially important that mode shapes are smooth. An appropriate smoothing technique based on the use of inertial forces is used here. Mode shape data expressed in terms of displacements ψ^u are used to compute inertial forces ψ^f. A static computation with inertial forces ψ^f gives modal strains. Direct computation of modal strains from mode shapes that

are not smooth may introduce severe errors. Therefore mode shapes are expressed preferably in terms of accelerations. This aspect will be explained thoroughly in section 3.2.2.4.

Stresses and strains can also be measured directly on the actual structure and the measured sequence is then recorded on some digital storing device. When strain gauges are used in the measurement of modal parameters, the step of strain computation can be skipped. However, strain gauges should be stuck in the critical areas of the structure, such that critical stresses are known directly. It is not at all obvious how to interpolate for stresses in intermediate points.

The strain history is used as an input to the fatigue life estimation module. First the nominal strain sequence is converted to a local strain sequence using NEUBER's rule (equation 1.14). The complex strain history is then resolved into a number of elementary cycles, each of which a certain amount of damage is associated to. Finally the total damage is estimated using an accumulation rule. When an experimental fatigue analysis is performed the structure is subjected to the actual strain history $\varepsilon(t)$. The accumulation of damage is monitored or, the structure is loaded until failure occurs.

The flexibility of the proposed method now emerges from the consideration that experimental and analytical techniques can be interwoven without any restrictions. Any path through consecutive main steps is feasible (figure 2.2).

The thicker arrows in fig.2.2 indicate the path that should be followed preferably.

In the development phase of a new product the original design is usually modified several times. Analytical methods usually accelerate the process of evaluating modifications. Experimental methods on the other hand are extremely valuable in establishing confidence in the mathematical models that are used. Extensive and involving projects can be split up in separate tasks and each of these tasks consists of experimental and analytical subtasks. Although they are fully independent, they may be complementary and they may be executed interactively.

Consider the example of the blade of a jet engine turbine. Blades suffer high stress concentrations near their roots, which may be critical when subjected to dynamic loading. The development phase of the blade may be run through in a sequence of three steps, after it has

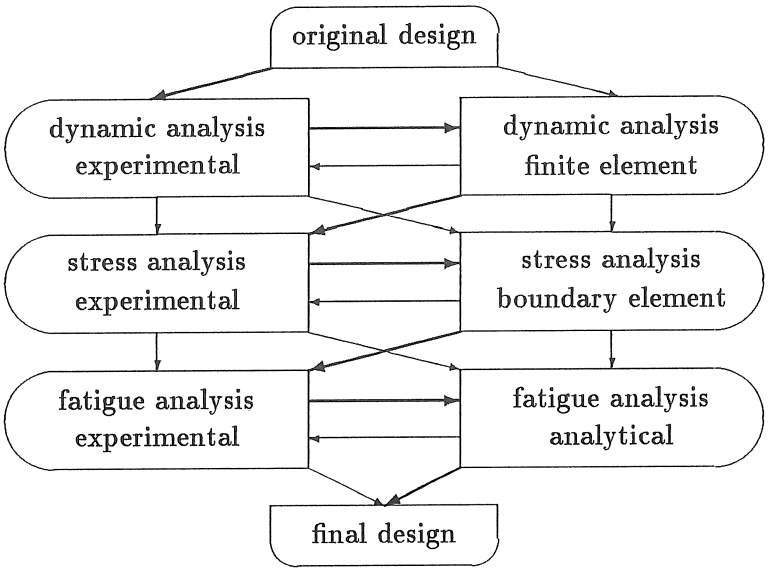

Figure 2.2: Integration of experimental and analytical techniques

been prepared by the CAD-division of the company :

dynamic characteristics : a prototype is built, together with a finite element model. The finite element model is tuned in such a way that its results match the experimentally determined ones. The updated model is used for evaluating modifications.

stress analysis : a boundary element model of the blade is constructed and the actual stresses are measured on the prototype. The boundary element model is refined in such a fashion that analytical and experimental results coincide. The boundary element model is used to optimize the geometry of the blade in search of a reduction of stress concentrations.

fatigue analysis : the blade is loaded cyclically until cracks initiate, or, it is verified whether the blade is capable of resisting the prescribed load variation. An analytical estimation of fatigue life is compared to the experimental one and the analytical model is used to evaluate modifications of material properties, e.g. heat treatments.

A fully interactive use of experimental and analytical techniques provides a useful and reliable tool for designing mechanical components.

For some types of structures, such as nuclear equipment and spatial vehicles, it is hardly feasible to build and test a prototype. In those cases, the designer has to estimate the lifetime on a purely analytical basis, with very little means of comparing the analytical results with experimental results. A powerful and perfectly reliable method is absolutely necessary for the engineer in order to come up with a well-functioning and safe product.

2.3 Consecutive steps in the method

The three consecutive steps mentioned in fig.2.1 are commented in this section.

2.3.1 Dynamic response of the structure

First the response of the structure is determined when it is subjected to the load variation.

2.3.1.1 Flowchart

Figure 2.3 presents an overview of the different elements of response prediction. Response computation is performed in the time domain by evaluating a convolution integral. Section 3.3.3 outlines the main advantages of a computation in the time domain over a computation in the frequency domain.

A modal model of the structure is built. It may either be analytical or experimental. The geometry of the structure is represented by a number of physical points, the nodes, and connections, commonly called connectivities. Finally one ends up with the displacement responses in the nodes of the modal model. In this way the behaviour of the entire structure is known in time.

2.3.1.2 Necessary input data

The information that should be entered to the analysis consists of two types :

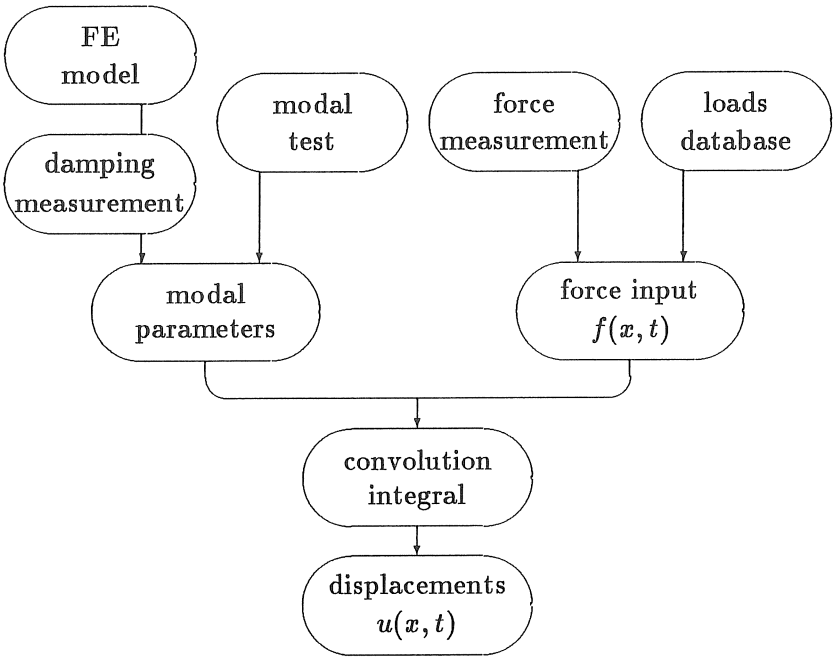

Figure 2.3: Consecutive steps in the method of response prediction

dynamic behaviour of the structure the dynamic characteristics of the structure are described completely by its modal parameters ν, ζ and ψ. Mode shapes ψ may be expressed in terms of displacements, accelerations, strains, ... It will be shown later that mode shapes are expressed preferably in terms of strains (section 3.2.2.4), which have to be computed from accelerations or inertial forces. Representation of mode shapes in terms of displacements is sufficiently accurate provided that strains are not merely computed by numerical differentiation of displacements. The operation of differentiation introduces very severe errors.

description of load input $f(t)$ the time variation of the applied external load must be known explicitly in order to be able to perform a computation in the time domain.

There are two sources of information where one can learn about the applied load. The force input can in general be measured with a load cell that is mounted in the load path. In the case of

an automobile for instance, the force that is transferred by the mounting of the engine is measured by a load cell which is fixed with a bolt between the body of the car and the engine block. The forces that are transferred through the wheels are measured with a specially designed force transducer which is mounted near the joints. These loads are measured and recorded on a digital storage device during a test trip. Very often the load sequences are similar, for similar products. Although a new type of an automobile may look totally different, the forces that are transferred through its wheels resemble very much the forces on another automobile of comparable size. Companies keep these data and use it for later developments. In such a fashion, a database is organized based on experience gathered over many years. The load sequence is used as an input to the response computation module. Care should be taken that next to the temporal variation of loads also the spatial variation is measured appropriately. Phase shifts between several load inputs have an influence on the response. Loads that are characterised by an in-phase variation may excite primarily symmetrical modes while out-of-phase loads are more likely to excite non-symmetrical modes.

In some cases practical reasons impede an accurate measurement of the applied loads. The forces that are exerted on the blades of a helicopter are distributed very unevenly over the length of the blade, and it is physically difficult to measure the aerodynamic effects of the rotating movement of the blades. In accordance with point 3 of section 1.5.1.1, the responses have to be measured. In the case of the helicopter strains are measured in several locations just below the rotor hub. A compensation technique then yields a force that is equivalent to the overall aerodynamic effects. This equivalent force can be used as an input to the subsequent analysis of the helicopter's components.

Another case of loading that is sometimes difficult to analyse is impact loading. Some types of structures exist, e. g. weapon systems, that are characterized basically by an impact type of loading. Several transducers are capable of measuring an impulse that comes close to a theoretical Dirac-impulse. It is, however, often extremely difficult to mount these devices in the machine during operation. These types of loading are modelled with an

acceptable accuracy as real Dirac-impulses. The magnitude of the impact still has to be estimated.

2.3.1.3 Computation in the time domain

Dynamic response of a mechanical structure can be computed with several procedures. The most important methods that are available are mentioned briefly in section 1.4.2. The direct method starts from the matrix notation of the equations of motion 1.21 :

$$[M]\{\ddot{u}\} + [C]\{\dot{u}\} + [K]\{u\} = \{f(t)\}$$

These equations are solved by a time stepping procedure, starting from $t = 0$, and proceeding gradually with an increment Δt. This method is extremely time-consuming, especially when the nature of the load variation is such that distinct peaks occur at very closely spaced intervals. The method is also very weak when impulse-like loads are applied. An advantage of the method consists in its ability to handle static loads together with dynamic loads.

The dynamic response of a linear structure can be evaluated much more directly by describing the dynamic behaviour in terms of modal parameters. Response prediction can be performed either in the time domain or in the frequency domain. As cycles of loading are characterized by consecutive maxima and minima, and as these phenomena of cyclic loading occur essentially in the time domain, the frequency domain is unsuitable for representing the stress variation. However, the dynamic response of the structure can be computed in the frequency domain, and it can be converted to the time domain afterwards by inverse Fourier-transformation. This procedure is time-consuming and inefficient. It is much more straightforward to compute the time response of the structure directly in the time domain, using the impulse response function $h_{IJ}(t)$ of the structure :

$$h_{IJ}(t) = \sum_{k=1}^{N} \left\{ R_{IJk} e^{\lambda_k t} + R^*_{IJk} e^{\lambda^*_k t} \right\}$$

where : R_{IJk} : the residue of mode k
λ_k : pole of mode k

For a force input $f(t)$ different from a Dirac-impulse, the response in the time domain is written in the form :

$$x(t) = \int_0^t f(\tau)h(t-\tau)\,d\tau \tag{2.1}$$

This equation yields the time response for any type of force function $f(t)$.

2.3.1.4 A fast computer algorithm

Equation 2.1 is generally valid and it can be used to compute the time-response under any type of load-input. Numerical integration schemes, such as Simpson-quadrature or Gaussian quadrature, are used [74], [171, App. C] :

$$\int_{-1}^{1} g(\xi)\,d\xi \approx \sum_{i=1}^{n} w_i f(\xi_i)$$

where : ξ_i : the coordinate of the i^{th} integration point
w_i: the associated weighting factor
n : the number of integration points

The error associated to a quadrature scheme is related to the $2n^{th}$ derivative of the function $g(t)$:

$$E_n = O\left(\frac{d^{2n}g}{dt^{2n}}\right)$$

These quadrature schemes may suffer an acute lack of accuracy, especially when the load is varying rapidly. This disadvantage can be overcome by selecting a higher number of integration points n.

Only a small number of distinct types of loads are commonly encountered in real-life situations :

- sinusoidal loading $f(t) = A\sin(\omega t - \phi)$

  where : ω : angular frequency of load input
  ϕ : phase shift of load input
  A : amplitude of load input

- impact loading $f(t) = A\delta(t-t_0) = A\langle t-t_0\rangle^{-1}$

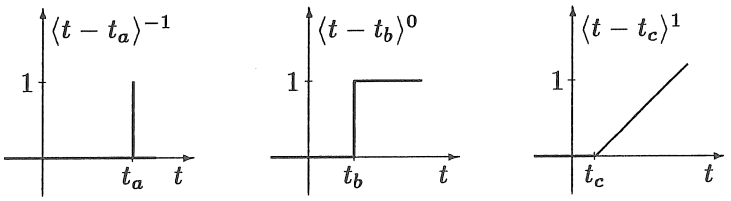

Figure 2.4: Definition of $\langle t - t_a \rangle^{-1}$, $\langle t - t_b \rangle^{0}$, $\langle t - t_c \rangle^{1}$

where : t_0 : instant of time of load-impulse
A : amplitude of impulse

The notation $\langle \bullet \rangle^n$ is explained in fig.2.4.

- random variation of load : such a type of load variation can be written approximatively as a linear combination of linear functions $\langle t - t_i \rangle^1$, after the full span of time has been divided in a number of intervals (fig.2.5).

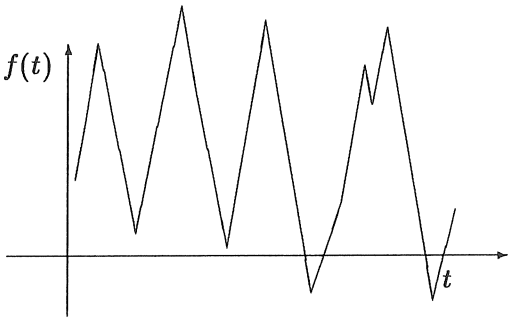

$$f(t) = \sum_{i=1}^{n} A_i \langle t - t_i \rangle^1$$

Figure 2.5: Random load input

where : A_i : constant coefficients
t_i : instant of time joining interval i to $i-1$

- any type of load that is represented by a function like :

$$f(t) = \sum_{i=1}^{m} A_i \, e^{a_i t} \, \langle t - t_i \rangle^{n_i} \, \sin(\omega_i t - \phi_i)$$

where : A_i, a_i, ω_i, ϕ_i : constant numbers
m : number of elementary functions
t_i : time instant that bounds interval i
n_i : non-negative exponent

As combinations of $\langle t - t_i \rangle^{n_1}$ and $\langle t - t_i \rangle^{n_2}$ are allowed, some values of t_i and t_{i+1} may be coincident.

For any of these types of functions the integration 2.1 can be performed explicitly.

Moreover the procedure is accelerated considerably since the integrand needs to be evaluated only in the limits of the time-interval. Each of these aspects, flexibility, speed and accuracy, turn the approach of computing dynamic response in the time domain into an extremely powerful tool.

2.3.1.5 Superposition of static and dynamic strains

A structure is often subjected to a set of static loads, next to dynamic loads. Evident examples are the static weight of an automobile that is carried by its suspension system or the centrifugal force which loads the rotating blades of a turbine engine. When relating to the different types of loading defined in the previous paragraph, it can be stated generally that any load represented by a function like $f(t) = A\langle t - t_0 \rangle^0$ is a static load.

Deformation of structures subjected to static loading should not be computed with equation 2.1. A separate computation of static deformation must be performed independently. The combined effect of static and dynamic deformations is obtained easily by linear superposition. A stepped load variation as shown on the left hand side of fig.2.6 is split up symbolically into a static part $f_s(t)$ and a dynamic part $f_d(t)$.

It will be pointed out later that static loads do have an important influence on fatigue lifetime. These static stresses are introduced into the fatigue analysis as mean stresses. Tensile mean stresses tend to reduce the lifetime of structure, whereas the influence of compressive mean stresses may be beneficial. The effect of mean stresses is especially important in the area of high cycle fatigue.

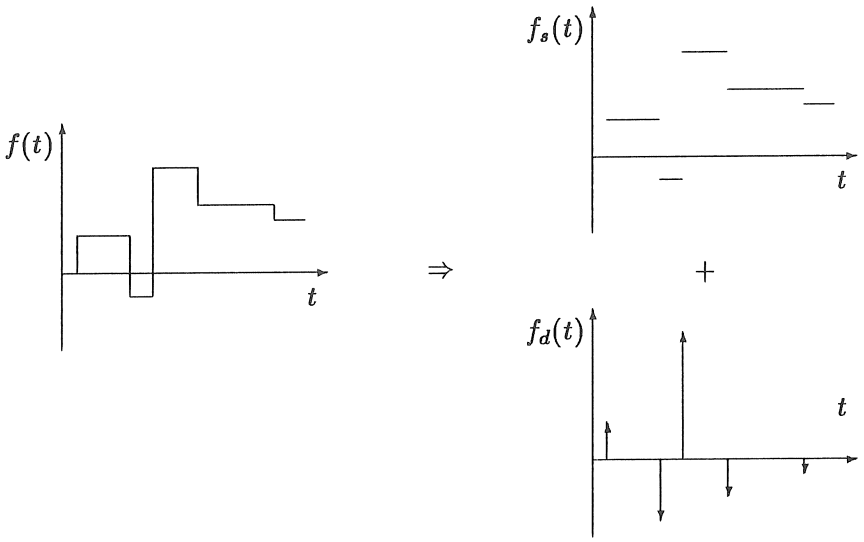

Figure 2.6: Superposition of static and dynamic load

2.3.2 Stress/strain analysis

The second step in the overall analysis of the structure is concerned with the computation of stresses and strains at the critical areas on the structure.

2.3.2.1 Flowchart

Fig.2.7 presents an overview of the different methods that can be used for computing the stresses and strains in several areas on the structure.

2.3.2.2 Computation of spatial strain distribution

Four different approaches are feasible :

imposed displacements : the displacements that result from the dynamic analysis are used as external loads to the structure. A finite element or a boundary element model of the structure must be built. This model will be called the "structural model". Care should be taken for the nodes of the structural model to coincide with the nodes of the modal model. The displacements of these nodes are found from the modal computation. The classical

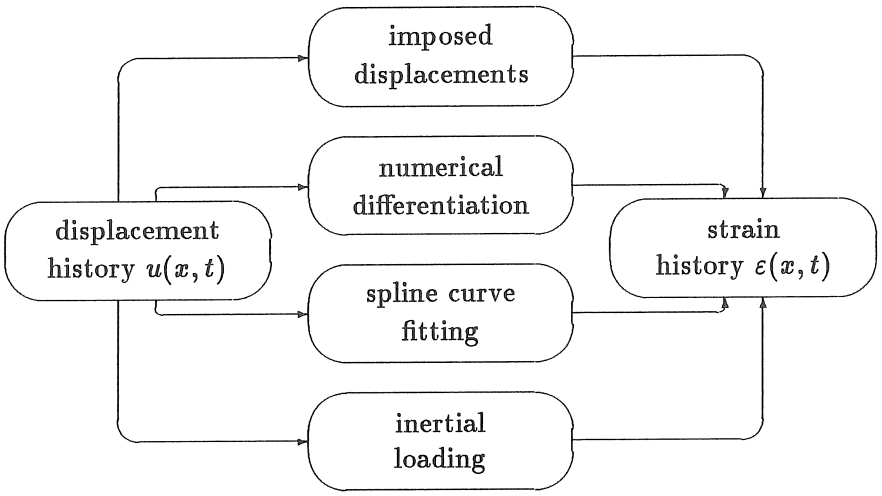

Figure 2.7: General scheme of stress/strain- analysis

finite element formulation is then written in matrix notation :

$$[K]\{u\} = \{f\}$$

where : $[K]$: the stiffness matrix
$\{u\}$: the vector of displacements at the nodes
$\{f\}$: the vector of reaction forces at the nodes

The boundary element formulation looks very similar :

$$[H]\{u\} = [G]\{p\}$$

where : $[H]$: the influence matrix for the displacements
$[G]$: the influence matrix for the tractions
$\{u\}$: the vector of displacements at the nodes
$\{p\}$: the vector of tractions at the nodes

Both formulations are very much alike, the vector of unknowns comprises the reactions — forces $\{f\}$ in the case of finite elements, and tractions $\{p\}$ in the case of boundary elements — in the nodes where the displacements are imposed, and the displacements $\{u\}$ in the other nodes. The system of equations has a unique solution. In the finite element method, strains are

obtained from displacements by mathematical derivation, and stresses are computed from the strains by applying HOOKE's law :

$$\{\varepsilon\} = [D]\{u\}$$

Theoretically, all the components of the stress tensor can be computed from the displacements. This can be done in any point on the structure. Thus, the stress history results for each point. It should be noted, however, that the boundary element method is far superior to the classical displacement formulation of the finite element method for these types of analysis.

The technique of representing a structure's state of deformation merely by its deformation in a few nodes is in general erroneous when used for the purpose of obtaining stresses. A definition of displacements at discrete nodes conveys insufficient information about the local behaviour of the structure at intermediate points. The result that is obtained from a computation based on imposed displacements is that particular shape of deformation that contains lowest overall energy, within the range of fields of displacements that is allowed by the interpolation functions.

numerical differentiation : this method can be used only for geometrically simple components, such as beam-like and plate-like structures. No structural model is necessary. The most straightforward way to obtain strains ε from displacements in the case of bending considers strains to be related to curvature χ, $\varepsilon = \chi y$:

$$\chi = \frac{\frac{d^2u}{dx^2}}{\sqrt{\left[1 + \left(\frac{du}{dx}\right)^2\right]^3}} \approx \frac{d^2u}{dx^2}$$

where : χ : curvature
u : transverse displacement
y : distance to neutral axis
ε : strain in the longitudinal direction

The curvature at a node i is obtained from the displacements at the neighbouring nodes $i-1$ and $i+1$:

$$\chi = 2\frac{u_{i-1}\Delta x_i - u_i(\Delta x_{i-1} - \Delta x_i) + u_{i+1}\Delta x_{i-1}}{\Delta x_{i-1}\Delta x_i(\Delta x_{i-1} + \Delta x_i)} \qquad (2.2)$$

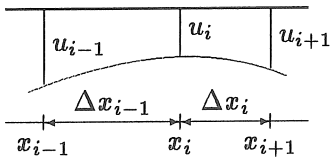

This representation of curvature is taken from the method of finite differences. Equation 2.2 is equivalent to the second derivative of displacement with respect to the coordinate x. The value of curvature χ that results from equation 2.2 is extremely sensitive to minor variations of the displacement at the nodes $i-1$, i, $i+1$. The process of numerical differentiation is particularly unstable, when it is based on data at discrete points rather than on continuous functions.

fitting a spline curve : this method can be used only for geometrically simple components such as beam-like and plate-like structures. No structural model is necessary. In order to represent the field of unknowns in intermediate points, a spline curve of a particular shape is fitted through the nodal values of the displacements. Strains are obtained by derivation of the function of displacements with respect to the appropriate coordinate. This approach has some clear advantages over the method of direct numerical differentiation as it is able to smooth some of the asperities of the strain pattern. This approach is essentially very similar to the approach of the finite element or the boundary element method where the interpolation functions are defined in advance. The technique of fitting a spline-curve through the nodal values is merely a variant. The same considerations apply that are valid for the finite element method and the boundary element method. This approach is not generally acceptable for strain computations. Some other techniques of smoothing and completion exist [77]. The same remark applies to them.

inertial load : the accelerations at the nodes of the modal model are found by derivation of the displacements with respect to time :

$$\text{for a particular mode } k: \quad a = -\omega_k^2 u \tag{2.3}$$

Equation 2.3 is valid only for one particular mode. When several modes are present in the frequency contents of the structure's

response, equation 2.3 can not be used any longer. Instead, response computation should be based on mode shapes defined in terms of accelerations. Inertial loads are proportional to accelerations :

$$f = \rho a$$

where : f : inertial force pro unit volume $[N/m^3]$
ρ : mass density $[kg/m^3]$
a : acceleration $[m/s^2]$

These inertial forces are applied as a static load case. Static equilibrium is expressed between body forces, resulting from inertial loading, and internal forces, resulting from the deformation of the structure. When the exact inertial forces are imposed, the resulting field of displacements that is computed from the static analysis coincide with the original mode shapes.

A finite element model or a boundary element model of the structure has to be built. Distinction should be made between both options :

finite element : it is mandatory that all the nodes of the structure where modal displacements are known from the dynamic analysis coincide with nodes of the finite element model. The inertial loads are represented in an incomplete manner unless all the nodes of the structural finite element model coincide with the nodes of the modal model. The distribution of the loads should be fully comprehensive, i.e. the appropriate value of acceleration should be assigned to each direction of every single node of the finite element model. If not, zero inertial load will be assigned to the superfluous nodes. This restriction has some grave consequences on how the inertial forces are defined, when mode shapes are measured experimentally. For beam-like and even for simple plate-like structures it is in general not that difficult to obtain a complete representation of the distribution of accelerations. In case of more complex geometries and rather compact structures it may be troublesome to describe the variation of accelerations through the thickness of the structure. Inertial loading has to be modelled sufficiently accu-

rate in order for the distribution of deformations to match the distribution of loads.

Another remark is concerned with the effect of discretization of the body forces f. The approach of the finite element method discretizes continuous body loads to a set of local point forces applied to the nodes. It concentrates a continuously distributed load in a number of distinct nodes.

boundary element : there is no need for nodes of the boundary element model to coincide with those of the modal model. The volume mesh only serves as a basis for an accurate description of volume loading. Results of tractions and displacements are computed only at the boundary. The body forces $\{f\}$ that result from inertial loading may be represented with a mesh that is totally independent of the mesh used to discretize the unknown displacements u and tractions p. This statement is illustrated by SOMIGLIANA's identity A.10 :

$$c_{ij}u_j(\underline{\xi}) = \int_\Gamma u^*_{ij}(\underline{\xi},\underline{x})p_j(\underline{x})\,d\Gamma(\underline{x}) - \int_\Gamma p^*_{ij}(\underline{\xi},\underline{x})u_j(\underline{x})\,d\Gamma(\underline{x}) + \int_\Omega u^*_{ij}(\underline{\xi},\underline{x})f_j(\underline{x})\,d\Omega(\underline{x})$$

where : c_{ij} : constant number ($0 \leq c_{ij} \leq 1$), depending upon the location of the field point $\underline{\xi}$ with respect to Γ and Ω
$u_j(\underline{\xi})$: displacement in j-direction at field point $\underline{\xi}$
u^*_{ij} : fundamental solution for displacements
p^*_{ij} : fundamental solution for tractions
$u_j(\underline{x})$: displacement in j-direction at coordinate $\underline{x}$
$p_j(\underline{x})$: traction in j-direction at coordinate $\underline{x}$
$f_j(\underline{x})$: inertial load in j-direction at coordinate $\underline{x}$

Tractions p are defined as the ratio of the force acting on a surface Γ over the area of the surface. Unlike the components of the two-dimensional stress tensor $\underline{\underline{\sigma}}$ the components of the one-dimensional tensor or vector $\underline{p}$ depend on the coordinate system they refer to.

Appendix A gives proof of this identity and it explains more thoroughly the meaning of the different notations. What imports here is the fact that the volume forces $f(\underline{x})$ appear only in the integrand of the volume-integral over the domain Ω, whereas the displacements u and the tractions p should be taken on the boundary Γ. The discretization of the volume is independent of the discretisation of the boundary.

As the variation of the inertial force through the thickness of the material is usually small, a linear shape function can be used. Interpolation functions should be introduced to represent the variation of the inertial load over the domain Ω. The variation of the body force f over the superficial directions of the structure on the other hand may be strongly variable. All the information that one obtains from the dynamic computation can be fully utilized, regardless of the discretization of the boundary. There are no requirements for the boundary element model to be compatible with the modal model.

It is noteworthy that, unlike in finite element approaches, volume loads (N/m^3) are represented in a continuous fashion, i.e. they are distributed over the entire volume, they are not concentrated in the nodes.

Section 3.2.2 shows that the approach of computing the strain pattern from accelerations is theoretically most accurate. The boundary element method is well suited for an efficient modelling of volume forces.

2.3.2.3 Direct computation of the stress/strain sequence using modal stresses or strains

The previous section shows how stresses and strains are computed from displacements or accelerations. It is stated there that preferably accelerations are used to obtain a stress pattern (section 3.2.2). The boundary element method provides better opportunities for stress analysis than any other method (section 4.2.3). The procedure starts from a distribution of accelerations over the entire structure. Multiplication of accelerations with mass density yields the inertial forces. At every single timestep a static computation has to be performed from

which the distribution of stress and strain result. For long load histories this implies a high number of consecutive computations. Consider the system of equations A.12 that is to be solved at a certain instant of time :

$$[H]\{u\} = [G]\{p\} + [W]\{f\}$$

where : $[H]$: matrix of influence coefficients for displacements
$[G]$: matrix of influence coefficients for tractions
$[W]$: matrix of influence coefficients for body forces
$\{u\}$: vector of displacements at boundary nodes
$\{p\}$: vector of tractions at boundary nodes
$\{f\}$: vector of volume forces $= \rho\{a\}$ at boundary nodes
$\{a\}$: vector of accelerations at boundary nodes

Appendix A explains how this matrix notation is developed. Depending on the type of boundary conditions — imposed displacements or imposed tractions — the unknown displacement or traction is written in vector $\{u\}$ or vector $\{p\}$. Reordering the equation A.12 and moving the unknowns to the left hand side, the system of equations is written :

$$[A]\{x\} = \{y\} + [W]\{f\} \tag{2.4}$$

Vector $\{y\}$ contains information on the boundary conditions : either displacement or traction is prescribed in each node. For pure inertial loading tractions p at free surfaces are zero. A structure that is subjected to inertial loading only and that has imposed displacements equal to zero at its fixation points is characterized by :

$$\forall t : \quad \{y\} = \{0\}$$

As the matrix $[A]$ depends only on the geometry of the structure, on the material properties and on the type of boundary conditions, it does not vary with time t. The system of equations 2.4 is then solved by inverting matrix $[A]$:

$$\{x\} = [A]^{-1}(\{y\} + [W]\{f\})$$

The unknowns $\{x\}$ are expressed directly in terms of the body forces $\{f\}$. It should be noted however, that the matrix $[A]$ is non-symmetrical and fully populated. Inversion of such a matrix is a time-consuming

task. Some powerful algorithms have been developed though [75], that solve these equations in a quick and accurate manner. Strains are found from displacements and tractions using the procedures of section A.4.

TOWNLEY [17] introduces the concept of "modal strains". They characterize a particular mode shape in terms of strains. A mode shape is represented by its strain distribution. The strain tensor is computed in a number of points on the structure and together they convey the same information as do the modal displacements. It is admitted however, that visual interpretation of modal strains is not particularly evident, especially when the state of deformation is multiaxial. As mode shapes contain information about the proportional pattern of deformations only, and not on the actual measures of displacement, a factor of proportionality should be introduced on the modal strains too. Modal strains are obtained from displacements via accelerations, with the boundary element method.

The pattern of accelerations that characterizes a particular mode shape is introduced in equation 2.4. The displacements $\{u\}$ that result should be proportional to the accelerations $\{a\}$. The factor of proportionality is the square of the eigenpulsation ω. The numerical procedure that is used to obtain strains from displacements and tractions is explained in section A.4. It is feasible to compute strains in any physical point on the structure. In practice, the modal strain distribution is represented in a limited number of distinct points. The selection of points where the strain tensor is computed should be based on two considerations :

- the global shape of deformations should be represented completely
- local peak values of strain must be included since they are usually the sources of problems

The former aspect is mainly important when modal strains are expected to represent the overall pattern of deformation, whereas the latter is preponderant in analyses of local effects, such as fatigue phenomena. All the areas where potentially critical stresses are expected should be included in the model. It will be shown later (section 4.4) that it suffices to select one point in a critical area such that its nominal stress level is related easily to its maximum stress level. This relation

is expressed by the elastic stress concentration factor (equation 1.2). It is found from the same boundary element analysis. Although modal strains do not have a direct physical meaning, as they are proportional to each other, the stress concentration factor is correct. The same scaling factors that are used for mode shapes expressed in terms of displacements apply for mode shapes expressed in terms of strains.

Modal strains are mainly useful to accelerate the procedure of constructing the strain history directly from the dynamic analysis. In doing so, the first and the second steps of section 2.2, fig. 2.1 are switched. The first step is now a boundary element computation of the modal strain distribution that corresponds to each mode shape. The dynamic analysis has moved to the second step, finally yielding the stress history at the critical locations. The flowchart presented in fig.2.1 is shaken up a bit, yet it comprises the same operations (fig.2.8).

Experimental modal analysis usually employs accelerometers. Parameter estimation yields mode shapes in terms of accelerations directly. Mode shapes may be either real or complex. Modal strains are obtained directly in the case of real mode shapes. In the case of complex modes, two separate computations are performed, one on the real portion of the mode and another one on the imaginary portion. They are combined afterwards into complex strains. One should be aware however, that problems of resonance fatigue most often occur in lightly damped structures. The modes of this kind of structures are almost normal modes, and they may be converted to normal modes without a significant loss of accuracy. Occasionally strain gauges are utilized when performing a modal test. Regardless of whether the modes are real or complex, modal strains are obtained directly. It should be noticed that the measurement errors that are introduced when straingauges are used may be much more significant than with other types of transducers.

2.3.3 Estimation of the fatigue lifetime

A number of strain histories at different locations on the structure results from the combined dynamic stress analysis. Each of those locations has its corresponding strain history. The strain history is in general multiaxial. This implies that a second order strain tensor is defined as a function of time. The location where the strain tensor is obtained does not necessarily coincide with the actual location of

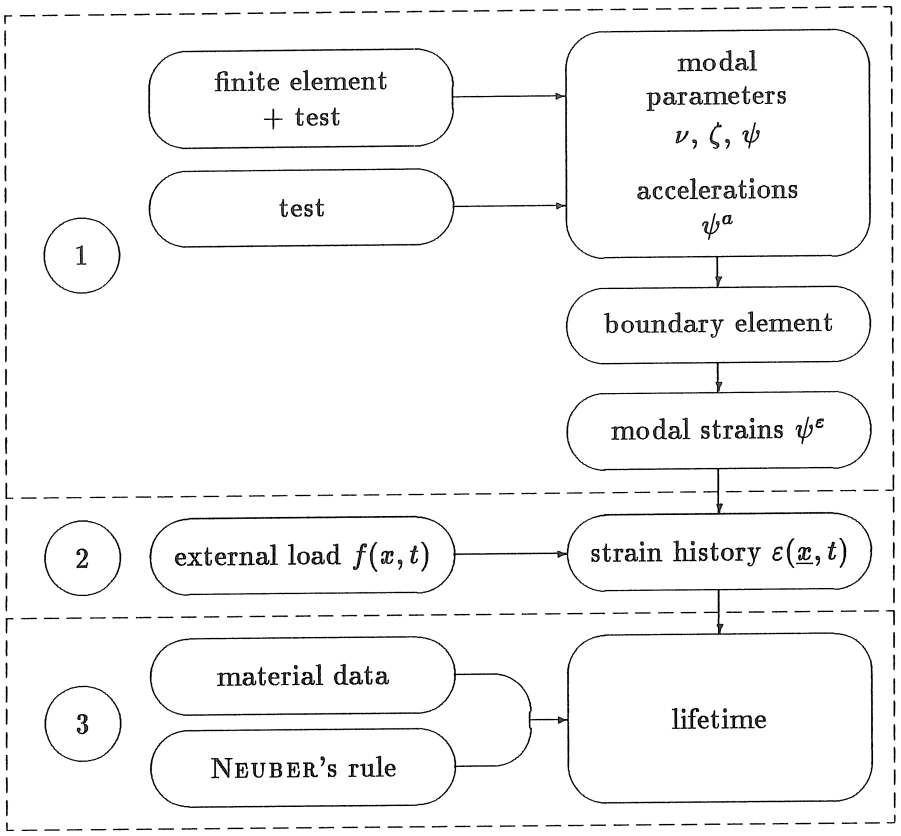

Figure 2.8: Modified scheme of the proposed method

maximum strain. In this case the strain tensor is a "nominal" strain tensor. It must be related, however, to the actual peak stress level. This relation is expressed by the elastic stress concentration factor K_t. All the input data is now ready to start the fatigue analysis.

2.3.3.1 Flowchart

Fig.2.9 gives a schematic overview of the consecutive steps of the analysis of strain histories. Basically the local strain approach is used. The final result is an estimation of fatigue lifetime.

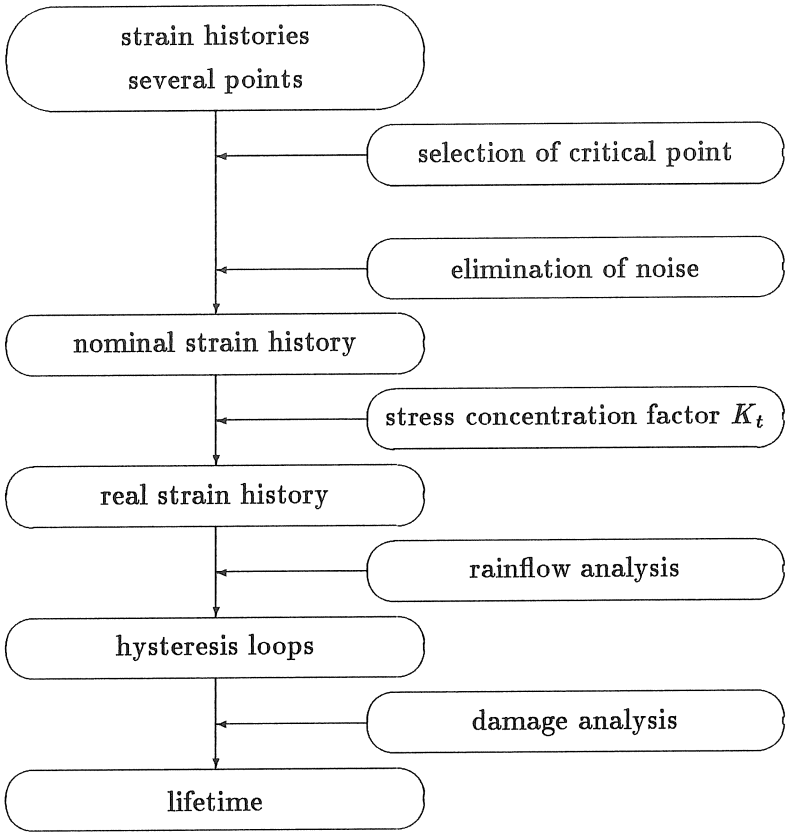

Figure 2.9: Scheme of the life prediction technique from several strain sequences

2.3.3.2 Selection of the critical areas on the structure

It is often intuitively clear which zone of the structure is most critical. Sometimes the structure or its loading is that complex that it is hardly possible to predict which location will suffer most from fatigue. Two different criteria can be utilized :

maximum nominal strain range : (fig.2.10) the critical point on the structure is characterized by the maximum difference between maximum strain and minimum strain

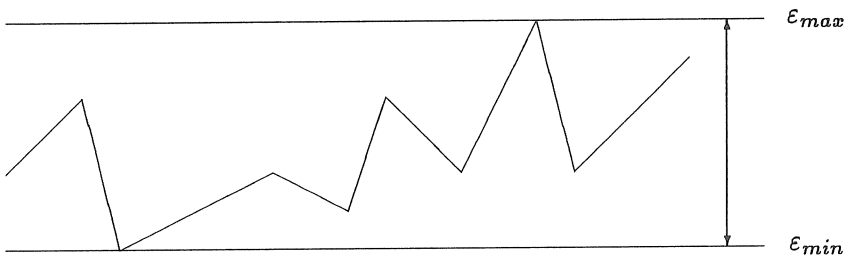

Figure 2.10: Criterion of maximum strain amplitude

maximum mean square differences : (fig.2.11) for each point on the structure the squares of the momentary differences $K_t\Delta\epsilon_{nom}$ are summed and divided by the number of terms :

$$\mathcal{S} = \frac{1}{n}\sum_{i=1}^{n}(K_t\Delta\varepsilon_{nom,i})^2$$

The critical point is characterised by the maximum $\mathcal{S}$-value.

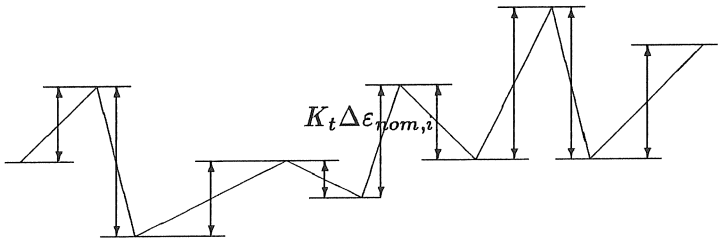

Figure 2.11: Determination of $\mathcal{S}$

It is rather difficult to compare both of these criteria in a general fashion. In case of a variation with a more or less constant amplitude, both criteria yield almost the same result. In case of a strongly variable amplitude, the criterion of maximum strain amplitude is closer to reality, since it recognizes large amplitudes which consume the most important portion of the component's lifetime. The criterion of maximum strain amplitude is utilized to extract the point on the structure where

the loading is most harmful. Subsequent analysis can be concentrated on this particular point.

The next step is the elimination of intermediate values from the full nominal strain sequence. Only the local extreme values are left. The frequency contents of a strain variation may contain several modes, which are superposed onto each other. Often a high frequency mode is superposed onto a mode of lower order. The amplitudes associated with the higher mode are generally lower than those of the lower mode. The resulting strain variation may be something like the variation presented in fig.2.12. The fatigue damage that is associated to this sequence is influenced very little by the small variations due to the higher mode. The sequence on the left hand side of the figure involves a lot more computations than the sequence on the right hand side. The amount of noise that is eliminated is defined as a fraction of the maximum amplitude of strain. Noise ratios up to 50% of the maximum amplitude have little influence on the expected lifetime.

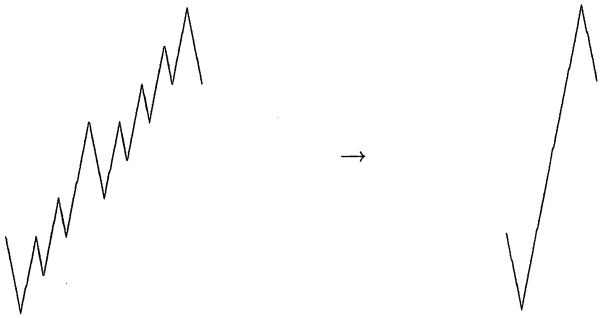

Figure 2.12: Elimination of noise on strain sequence

2.3.3.3 Conversion of nominal strain history to local strain history

After the reduction phase is terminated one ends up with a sequence of nominal strains which contains only alternating local minima and local maxima. These strains are nominal strains and in general, they differ from the real strains at the corresponding critical point. However, they are related to the real strains. Terminology of the local strain approach designates them as "local strains". Two criteria are used :

- the cyclic stress-strain -curve (equation 1.9)

- NEUBER's rule (equation 1.14)

Knowledge of the elastic stress concentration factor is necessary to express the relation between nominal strain and real strain. The stress concentration factor is determined from the same boundary element analysis that the modal strains are computed by. Section 1.3.2.2 explains how this set of equations is solved for local strains. Together with local strains, local stresses are computed. Starting from a nominal strain sequence, a local strain sequence and the corresponding local stress sequence are formed.

2.3.3.4 Resolution into distinct hysteresis loops

The sequence of local strains may be complex, for instance in random vibrations. The analysis must be capable of distinguishing the different cycles which cause the accumulation of damage. A complex history is reduced to a sequence of distinct events. A large number of procedures is proposed in literature : the "range-count" method, the "peak-valley" method, the "range-pair" method, the "rainflow" method, the "racetrack" method, ... The rainflow method is best suited since it corresponds best to physical reality. It will be shown in section 5.2.3.4 that it represents the memory behaviour of the material fairly well. The memory behaviour of the material governs the way local stress and local strain are related during cyclic loading. The rules imposed by the memory behaviour are explained in section 1.3.2.1.1. The graphical representation of hysteresis loops can be interpreted easily. A complex strain variation is reduced to a number of elementary rules each of which corresponds to one cycle on the plot of hysteresis loops. Extreme values of stress and strain are read quickly. A particular cycle is characterized completely by the set of maximum stress, stress amplitude and strain amplitude.

2.3.3.5 Evaluation of accumulated damage

Every single cycle is characterized by three quantites of stress and strain. The damage that is associated to it is found from the strain-life -relation 1.11, or, when mean stresses are taken into account, with the SMITH-TOPPER-WATSON -parameter 1.13. Each cycle has a certain amount of damage associated to it. The total damage is evaluated using MINER's linear rule 1.3.

2.3.4 Evaluation of design modifications

The proposed method is used to its full power when analysing design modifications. It was argued before that it is particularly well suited for evaluating modifications. Therefore the model has to be validated first. The procedure involves stepwise tuning of the model. Its results are compared to experimental results and it is updated in such a fashion that it may be used for detailed analysis :

- the modal parameters should coincide with the experimental values : if so the model is useful for modification analysis, if not, it should be updated towards a fair correspondence. Powerful model-updating procedures are presented by HEYLEN [77] and JANTER [76].
- modal strains are determined by boundary element analysis : when modal strains are measured experimentally, comparison is possible. The method of computing modal strains from modal accelerations automatically smooths the mode shape (section 4.3.4.3). The same analysis establishes the relation between nominal strain and real strain.
- dynamic stress response : if the computed response fails to match the measured response, this may be due to number of reasons :
  - static loading : static loading is responsible for mean stresses
  - dynamic loading : discrepancies between modelled and measured data may be caused by an imperfect model of dynamic loads
  - damping values : as eigenfrequencies and mode vectors are tuned, the only modal parameters that may be in discordance are damping values
  - number of modes : the number of modes that should be taken into account is determined by the frequency contents of the loading
- lifetime : the analytical result may be different from the measured lifetime. This correlation is usually most difficult to interpret, since this discrepancy may be due to a number of reasons,

material properties, residual stresses, local material conditions, environmental conditions, ... A pragmatic approach introduces a "damage parameter", which is defined as the right hand side of MINER's equation 1.3. In case of a perfect correspondence of analytical and experimental results, this constant is equal to 1.

All the steps of this validation procedure are run through consecutively. At that instant, the model is updated to match the real structure and its loading. It may subsequently be used in the prediction of design modifications.

2.3.5 Comparison of statistical methods with the proposed method

Problems that are treated using statistical methods can also be handled with the proposed method, provided that the time sequence of the load input is well defined. Some important differences, however, need further discussion :

random nature of excitation depending on the particular type of application, the random nature may be clearly different in two ways. Two examples are illustrative :

- the main direction of rough road excitation on an automobile is almost time invariant. Although transversal components of load should not be neglected, the vertical component of load is predominant. The load variation is random only with respect to time. Moreover, the driving habits of a particular driver are rather constant, and the maximum stress levels that occur during several trips will not vary significantly.
- the wave excitation of an offshore platform is much more complex. Amplitude information and directional information about the wave are equally important. Both variations are very unpredictable. Concepts like 10 year water wave and 50 year wave show up only in branches like offshore industry [78].

In the former case it is not very difficult to establish a time sequence of loads that is representative to a particular driver,

whereas in the latter case there is no alternative to statistical methods. A plethora of papers on the fatigue of offshore platforms use statistical considerations [79], [80], [81].

interpretability of results the interpretation of results may not be trivial as one obtains information only on the number of zero crossings and peak values and on the distribution of peak levels. The stress variation is not computed as such. This may be an awkward drawback, especially when evaluating structural modifications. One obtains only indirect information on how the structural response is modified. The proposed method uses intermediate results to update the model and ameliorate its performance. Statistical methods may act as a kind of black box approach while the results of the proposed method may be interpreted directly.

cyclic behaviour of the material statistical methods assume a linear material behaviour. Plastic deformation and the existence of fluctuating residual stresses are supposed not to exist. This is a valid assumption in a majority of problems of high cycle fatigue. Some theoretical restrictions are imposed on the applications of statistical methods.

sequence of loads statistical methods do not take the sequence of strains into account. As residual stresses arise from overloading, and as residual stresses affect the lifetime of a structure, the sequence of loads should be recognized correctly. PERRETT [82] illustrates different ways of reconstituting a strain sequence from a rainflow matrix. He generates two distinct time sequences, one of which corresponds to the maximum damage that is accumulated, the other one corresponds to the minimum damage.

single overloading single overloads may consume an extremely important portion of the lifetime of a structure. Statistical methods may not recognize the occurrence of an overload in the loading sequence correctly. It is therefore crucial that the statistical model represents the load variation correctly. Statistical models tend to estimate the load sequence well as far its mean value is concerned. When discrete overloads are expected beyond those

predicted by the model, it may be preferable to generate a load sequence manually.

The most important advantage of statistical methods is its speed, as it estimates the fatigue lifetime of a structure from a limited number of quantities. One should be well aware however of the limitations of the method and use the method in an adequate way.

2.4 Conclusion

This chapter presents an overview of a general approach of estimating fatigue lifetime of a structure on an analytical basis. An original approach links the boundary element method to a fast convolution algorithm using modal strains.

The proposed method is designed to allow a maximum interaction with experimental data, yet it is capable of running totally independent from any test setup. The main advantage of the method is that it models dynamic stresses and strains accurately, and that it superposes static and dynamic loads quickly. Three basic steps can be clearly distinguished, which are executed consecutively, such that all intermediate results can be interpreted easily. The model is updated in a way that is obviously intelligible.

The first step involves the computation of the "modal strains" that characterise the modes of a structure. Modal strains are computed from modal accelerations using the boundary element method. It is crucially important that the mode shapes be represented by their accelerations. This features facilitates the use of experimental modes, and it smooths modes in such a way that stresses vary in a more continuous way along the structure.

In the second step the dynamic response of the structure is computed. From the description of the dynamic behaviour of the structure, and from the knowledge of load variation, the transient response is determined in the time domain using a fast, new convolution algorithm. The dimensions of the response are immediately strains.

The third step uses theorems and criteria from the "local strain approach" and estimates the fatigue lifetime of the structure. The analytical result is used to update the model towards experimental data. Globally, the proposed method is perfectly capable of evaluating structural modifications.

The next three chapters will cover each aspect of the method separately :

- chapter 3 : response prediction
- chapter 4 : stress/strain analysis
- chapter 5 : estimation of lifetime

Chapter 3

Computation of the dynamic response of a structure

3.1 Introduction

Section 1.2 introduced the concept of resonance fatigue. It was stated there that the dynamic behaviour of the structure together with the frequency content of the load determine the transient response of the structure. Each cycle accumulates a certain amount of damage to the structure. It is of the utmost importance that the designer has a thorough understanding of the strain sequence at the critical zones of the structure. The relation between external load and deformation may be rather complex, especially when several load inputs act simultaneously in an independent way.

This chapter illustrates the main aspects of this transient computation :

- which factors is the computed lifetime most sensitive to ?
- which techniques are available ?
- how can these techniques be used to their full benefit ?

Not only the determination of the dynamic response is important here, but the data must be well prepared such that dynamic stresses and strains can be evaluated accurately.

3.2 A modal model of the structure

External load and dynamic behaviour constitute the two factors that determine the dynamic response of a structure. As the external load variation is a factor the engineer sometimes has only very little impact on, the dynamic behaviour of the structure itself is the sole parameter the designer can modify in order to make his product perform better. It is then crucially important for him to be able to model the dynamic behaviour of the structure in a useful way. This model will be called the "modal model". It must be capable of describing the effect of a certain dynamic load on the structure. The nature of the load does introduce a number of requirements to the model. A model that performs well for one particular load may be useless in the prediction of the response to another load. This section deals with how a modal model can be built within the framework of requirements set by the applied load and the service conditions.

3.2.1 Determination of modal parameters

The methods that are used for the determination of modal parameters are subdivided in two categories : analytical and experimental methods. The model that is established will in both cases be called the "modal model".

3.2.1.1 Analytical methods

This section summarizes the concepts of finite element theory as it is applied to problems of elastodynamics.

Consider a structure $\Omega+\Gamma$ consisting of a domain Ω and a boundary $\Gamma = \Gamma_u + \Gamma_p$. Displacements are imposed $\underline{u} = \underline{\tilde{u}}$ on the part Γ_u of the boundary and tractions $\underline{p} = \underline{\tilde{p}}$ are imposed on Γ_p. The domain is subdivided in N_e elements with N_n nodes. There are N_d degrees of freedom. The field of displacements is represented by the scalar function $u_i(\underline{x}, t)$:

$$\underline{u} = u_i(\underline{x}, t)\underline{e}_i$$

where $\underline{e}_i$ represents the unit vector in i-direction. The variation of displacements over an element is represented by the shape function φ_j

introduced by the usual separation of variables :

$$u_i(\underline{x},t) = \sum_{j=1}^{n_e} \varphi_j(\underline{x}) u_i^{(j)}(t)$$

where : n_e : the number of nodes per element
i : direction of degree of freedom
j : number of the node for that element

The degrees of freedom $u_i^{(j)}(t)$ are still functions of time t. All the degrees of freedom over the entire structure are grouped together in one vector $\{d\}$. The matrix of interpolation functions is commonly denoted $[N]$. Strains are obtained from displacements by derivation. Although the strain tensor $\underline{\underline{\epsilon}}$ and the stress tensor $\underline{\underline{\sigma}}$ are two-dimensional the values of strains and stresses are gathered in two vectors :

$$\{\epsilon\} = \{\epsilon_{xx} \ \epsilon_{yy} \ \epsilon_{zz} \ \epsilon_{xy} \ \epsilon_{yz} \ \epsilon_{zx}\}^t$$

$$\{\sigma\} = \{\sigma_{xx} \ \sigma_{yy} \ \sigma_{zz} \ \sigma_{xy} \ \sigma_{yz} \ \sigma_{zx}\}^t$$

In matrix notation one obtains :

$$\{\epsilon\} = [\partial].\{u\} = [\partial].[N].\{d\} = [B].\{d\}$$

$$\{\sigma\} = [D].\{\epsilon\}$$

where : $[\partial]$: matrix containing differential operators
$\{u\}$: column vector containing degrees of freedom in nodes adjacent to the element
$[D]$: matrix containing the mathematical expression of HOOKE's law

As for the loads, distinction should be made between volume loads $\underline{f}$ $[N/m^3]$ and surface tractions $\underline{p}$ $[N/m^2]$. Unlike displacements, the variation of loads is represented by discrete point forces, acting in the nodes of the model. Their values are grouped together in vectors :

$$\{p\} = \{p_x \ p_y \ p_z\}^t$$
$$\{f\} = \{f_x \ f_y \ f_z\}^t$$

The theory of elastodynamics is developed from HAMILTON's principle [83]. This principle states that equilibrium is obtained for that particular vector of displacements $\underline{u}$ that minimises the function $J(\underline{u})$:

$$\begin{aligned} J(\underline{u}) &= \int_0^t (\text{total potential energy} - \text{kinetic energy})\, dt \\ &= \int_0^t (P_i + P_e)\, dt - \int_0^t T\, dt \end{aligned} \tag{3.1}$$

where : P_i : elastic energy of internal forces
P_e : potential energy of external forces $\underline{f}$ and $\underline{p}$
T : kinetic energy

Elaborating each of these terms, first for one element of the entire structure :

$$\begin{aligned} P_i &= \frac{1}{2}\int_{\Omega_i} \underline{\underline{\sigma}} : \underline{\underline{\epsilon}}\, d\Omega = \frac{1}{2}\int_{\Omega_i} \{\sigma\}^t\{\epsilon\}\, d\Omega \\ &= \frac{1}{2}\{d\}^t \left(\int_{\Omega_i} [B]^t.[D].[B]\, d\Omega\right) \{d\} \\ P_e &= -\int_{\Omega_i} \underline{f}.\underline{u}\, d\Omega - \int_{\Gamma_{p,i}} \underline{p}.\underline{u}\, d\Gamma \\ &= -\int_{\Omega_i} \{f\}^t\{u\}\, d\Omega - \int_{\Gamma_{p,i}} \{p\}^t\{u\}\, d\Gamma \\ &= -\{d\}^t \int_{\Omega_i} [N]^t.\{f\}\, d\Omega - \{d\}^t \int_{\Gamma_{p,i}} [N]^t.\{p\}\, d\Gamma \\ T &= \frac{1}{2}\int_{\Omega_i} \rho\dot{\underline{u}}.\dot{\underline{u}}\, d\Omega = \frac{1}{2}\int_{\Omega_i} \rho\{u\}^t\{u\}\, d\Omega \\ &= \frac{1}{2}\{\dot{d}\}^t \left(\int_{\Omega_i} \rho[N]^t.[N]\, d\Omega\right) \{\dot{d}\} \end{aligned}$$

Gathering all of these representations in equation 3.1 :

$$\int_0^t \left(\frac{1}{2}\{\delta\}^t[K]_i\{d\} - \{d\}^t\{F\}_i - \frac{1}{2}\{\dot{d}\}^t[M]_i\{\dot{d}\}\right) dt$$

where : $[K]_i = \int_{\Omega_i}[B]^t.[D].[B]\, d\Omega$
: stiffness matrix for element i
$\{F\}_i = \int_{\Omega_i}[N]^t.\{f\}\, d\Omega + \int_{\Gamma_{p,i}}[N]^t.\{p\}\, d\Gamma$
: external load vector over element i
$[M]_i = \int_{\Omega_i} \rho[N]^t.[N]\, d\Omega$
: mass matrix for element i

Accumulating the contributions of all the elements of the entire model :

$$J = \int_0^t \left(\frac{1}{2}\{d\}^t[K]\{d\} - \{d\}^t\{F\} - \frac{1}{2}\{\dot{d}\}^t[M]\{\dot{d}\} \right) dt$$

$[K]$, $[M]$ and $\{F\}$ now apply to the entire structure. The matrices $[K]$ and $[M]$ do not vary with time. J is a function of $2N_d + 1$ variables :

$$J(\underline{u}) = \int_0^t \mathcal{J}\left(t, d_1, \dot{d}_1, \ldots, d_{N_d}, \dot{d}_{N_d}\right) dt$$

EULER's equations for this type of variational problems are [84] :

$$[K]\{d\} + [M]\{\ddot{d}\} = \{F\} \tag{3.2}$$

This is a set of N_d linear coupled differential equations. In order to obtain the structural resonance frequencies, a sinusoidal movement is considered, with all external forces $\{F\}$ equal to zero :

$$\{d(t)\} = \{\psi\} \sin \omega t$$

Equation 3.2 then reduces to :

$$\left([K] - \omega^2[M]\right)\{\psi\} = \{0\} \tag{3.3}$$

$[K]$ and $[M]$ being positive definite, the matrix $[K] - \omega^2[M]$ should have eigenvalues ω^2, that render its determinant zero. The square root of the k^{th} eigenvalue is the k^{th} eigenpulsation of the structure. Several algorithms have been developed that solve for the eigenvalues of the system. BATHE and WILSON [86] review four methods : Householder QR inverse iteration, generalized Jacobi transformation, determinant search, and subspace iteration. The inverse power method [85] searches for eigenvalues within a frequency band defined by the user. The subspace method [87,88,89] in its different versions, solves for eigenvalues after having transformed the system to a vector space of lower dimension. In an overview paper [90], GÉRADIN discusses the conditions under which each of these methods are most useful. After having solved for the eigenvalues, the corresponding mode shapes are obtained. A factor of proportionality should be taken into account. Analytical methods are not capable of determining damping characteristics. They should be determined independently. Appendix C provides some details on this topic.

3.2.1.2 Experimental methods

The modal parameters of a structure can be determined experimentally by performing a modal test on the actual structure. Linearity is always an implicit assumption. A basic test setup requires one or more exciters with load cells, response transducers and some signal processing hardware. Throughout the last two decades many excitation signals have been developed. They all have their own advantages and drawbacks. Several types of response transducers are available. Accelerometers yield results that are most accurate. It will be shown that these devices are best suited for obtaining modal strains.

A modal test involves the measurement of transfer functions between excitation and response in several points on the structure. Due to the principle of reciprocity [92], the measurement of only one row or column of the transfer function matrix is sufficient, unless closely spaced modes are expected to occur. In the parameter estimation phase of the test, the coefficients of the analytical expression 3.4 of the transfer functions are determined by curve fitting the experimental data :

$$H_{IJ}(\omega) = \sum_{k=1}^{N} \left[\frac{\psi_{Ik} L_{Jk}}{j\omega - \lambda_k} + \frac{\psi_{Ik}^* L_{Jk}^*}{j\omega - \lambda_k^*} \right] \tag{3.4}$$

where : ψ_{Ik} : component I of modevector k
L_{Jk} : modal participation factor for input location J and mode k
λ_k : complex pole for mode k
N : number of modes in the frequency band of interest

The user has to decide on the number of poles N he wants to take into account to describe the dynamic behaviour in the frequency band of interest. Depending on the complexity of the problem and on the quality of the measurements this may be a difficult task. The influence of modes outside the selected frequency is almost always neglected in practical applications, because there does not exist a method of taking them into account. Parameter estimation routines first compute the complex poles $\lambda_k = -\sigma_k + j\omega_{dk}$, yielding damping values and damped natural frequencies. From these results the mode shape components ψ_{Ik} are obtained.

3.2.2 Accuracy of modal parameters

The degree of accuracy of the obtained results depends on the quality of the modal model. The quality of the modal model is determined to an important extent by the experience and the know-how of the engineer.

The quality of a finite element model depends on the choice of the element types, the distribution of mass and stiffness over the model, the mesh quality, the boundary conditions, ... JANTER [76] demonstrates how an experienced modeller is able to determine the resonance frequencies of a structure within margins less than 1–2 %. Mode shapes are computed from previously obtained information on the resonance frequencies. The error on the overall mode shape is generally an order of magnitude higher than the error on the resonance frequencies.

A large number of sources of error affect the quality of an experimental model. Not only quality of the available hardware, but rather the selection of a proper excitation signal, the location of the measurement points, the choice of filters and windows have major repercussions. Techniques have been developed to establish confidence in the accuracy of the obtained result. JANTER states that accuracies of 0.1 *Hz* absolute or 1% relative — whichever of both is largest — on the eigenfrequencies is feasible. Errors on the individual components of mode shapes may reach and even exceed a level of 15%. Errors on damping may be still more significant, especially when damping values are low. A margin of 30% is considered acceptable. Appendix C provides some details on how damping characteristics should be estimated. The next five paragraphs (3.2.2.1–3.2.2.5) outline the requirements the modal model should meet in order to allow a fair estimation of dynamic strain history.

3.2.2.1 Sensitivity of spatial strain distribution to modal parameters

The modal parameters of a structure themselves do not have a direct influence on its fatigue lifetime. They do have an indirect influence, as they determine both spatial and temporal variations of the strain tensor. This section shows how the different modal parameters affect the strain variation. Consider the expression for the response in the

time domain, based on the parameters of the modal model :

$$x_I(t) = 2 \int_0^t \sum_{k=1}^{N} \left(U_{IJk} \cos \nu_k \tau - V_{IJk} \sin \nu_k \tau\right) e^{-\sigma_k \tau} f_J(t-\tau)\, d\tau$$

where : $x_I(t)$: response at response location I at time t
N : number of modes that is taken into account
U_{IJk} : real part of complex mode shape component
V_{IJk} : imaginary part of complex mode shape component
ν_k : damped resonance frequency for mode k
σ_k : damping factor for mode k
$f_J(t)$: load variation in time domain in location J

This expression is the time domain equivalent of equation 3.4. The response history is expressed as a rather involved relation of several parameters. Some of these parameters affect primarily the spatial variation while others more notably influence the temporal variation. The dynamic deformation of the structure is a linear combination of a number of modal deformations. It can be stated roughly that the mode shapes basically shape the spatial variations, and that resonance frequencies and damping values determine the temporal variation. The temporal variation of displacements is generally different at different points on the structure. This difference contributes most to straining of the structure. The influence of the temporal variation is analysed by the counting algorithm (section 5.2.3) at the instant of computing the stress–strain -cycles. The spatial variation of the response is investigated hereafter, and the influence of the modal parameters will be outlined consecutively :

resonance frequencies : numerical eigenvalue solvers and experimental parameter estimation routines both compute resonance frequencies first. Mode shapes are determined afterwards, using the obtained resonance frequencies. Resonance frequencies and mode shapes constitute a complete set of parameters together. In practice, the relationship is of a numerical kind, as an error on the former causes an error on the latter which may be much more significant.

damping factors : there is no direct interaction between damping factors and mode shapes. Damping values determine the ampli-

tude of deformation, so they are predominant in the scaling of the mode shape. The residue R_{IJk} is determined from the modal displacements by :

$$R_{IJk} = \frac{U_{IJk} + jV_{IJk}}{\sigma_k}$$

mode shapes : they may be expressed in terms of several quantities :

- strain : when strain gauges are used, the parameter estimation phase of the modal test gives the spatial distribution directly. This may seem to be an interesting feature. A number of drawbacks have to be mentioned, however :
  - the quality of the measurements may be poor, when "spikes" occur, peaks in measured data that are due to external effects and that have to be filtered out
  - sticking straingauges at or even near critical areas on the structure is a difficult task, that has to be performed meticulously by experienced technicians
  - interpolation for values of strains at intermediate points is theoretically impossible

  SONG et al. [91] report on modal analysis using strain gauge measurements. Although they claim the results to be good, careful comparison of experimental and analytical results reveals errors on individual mode shape components up to 50%.
- displacement : finite element analysis gives mode shapes expressed in terms of displacements, allowing for an easy visual interpretation. Strains are obtained from displacements by derivation, provided a continuous representation of displacements is available :

$$\varepsilon_{ij} = \frac{1}{2}\left(\frac{\partial u_i}{\partial x_j} + \frac{\partial u_j}{\partial x_i}\right)$$

  Since values of displacements are known only in the nodes of the modal model, numerical differentiation is used instead of mathematical derivation :

$$\varepsilon_{ij} = \frac{1}{2}\left[\frac{u_i(\underline{x} + \Delta x_j \underline{e}_j) - u_i(\underline{x})}{\Delta x_j} + \frac{u_j(\underline{x} + \Delta x_i \underline{e}_i) - u_j(\underline{x})}{\Delta x_i}\right] \tag{3.5}$$

where : $\underline{x}$: field point where strain is computed
Δx_i : increment of coordinate along i-axis
$\underline{e}_i$: unit vector in i-direction

It is a well established fact that numerical differentiation is a highly unstable mathematical procedure. A slight variation of the displacement at one coordinate may result in an important change of the value of strain. Especially when post-processing experimentally measured mode shapes, where accuracy is inherently lower, strain values that are computed using equation 3.5 tend to be absolutely irrelevant.

The same remark applies to variations of displacements obtained by curve fitting a number of discrete points. Quadratic interpolation is a commonly used procedure for representing the deformed shape of beams or plates. The curvature $\chi \approx \frac{\partial^2 u}{\partial x^2}$, that determines strain in the cross-section of the beam, is supposed to be constant (fig.3.1) :

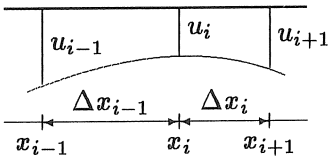

Figure 3.1: Assumption of constant curvature in beams

$$\chi = 2\frac{u_{i-1}\Delta x_i - u_i(\Delta x_{i-1} - \Delta x_i) + u_{i+1}\Delta x_{i-1}}{\Delta x_{i-1}\Delta x_i(\Delta x_{i-1} + \Delta x_i)}$$

The value of curvature is extremely sensitive to variations of the displacements u_{i-1}, u_i, u_{i+1}.

- accelerations : experimental mode shapes are expressed most often in terms of accelerations. For a particular mode k the inertial force $\underline{f}$ is proportional to the acceleration $\underline{a}$ at the same point :

$$\underline{f}(\underline{x}) = \rho(\underline{x})\underline{a}(\underline{x}) = -\rho(\underline{x})\nu_k^2\underline{u}(\underline{x}) \qquad (3.6)$$

where $\underline{x}$: any coordinate on the structure
$\rho(\underline{x})$: mass density of the material at location $\underline{x}$
ν_k : resonance frequency of mode k

The stress distribution in the entire structure can be computed with a static analysis by expressing static equilibrium of inertial forces and internal forces :

$$\begin{cases} \frac{\partial \sigma_{xx}}{\partial x} + \frac{\partial \sigma_{xy}}{\partial y} + \frac{\partial \sigma_{xz}}{\partial z} + f_x = 0 \\ \frac{\partial \sigma_{yx}}{\partial x} + \frac{\partial \sigma_{yy}}{\partial y} + \frac{\partial \sigma_{yz}}{\partial z} + f_y = 0 \\ \frac{\partial \sigma_{zx}}{\partial x} + \frac{\partial \sigma_{zy}}{\partial y} + \frac{\partial \sigma_{zz}}{\partial z} + f_z = 0 \end{cases} \tag{3.7}$$

The system of equations is solved using the boundary element method. In order to investigate the sensitivity of the strain distribution to individual mode shape coefficients, consider a case of uniaxial loading represented in fig.3.2.

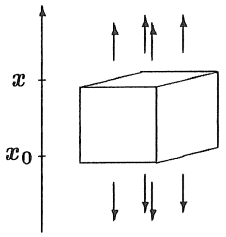

$$\sigma_x(x) = \sigma_x(x_0) + \left(\frac{d\sigma_x}{dx}\right)_{x=x_0} (x - x_0) + O\left((x - x_0)^2\right)$$

$f_x(x)$

$\sigma_x(x_0)$

Figure 3.2: Small cube of material subjected to uniaxial loading

Equation 3.7 reduces to :

$$\frac{d\sigma_x}{dx} + f_x = 0$$

Integration of the equation of equilibrium gives :

$$\sigma_x(x) = \sigma_x(x_0) - \int_{x_0}^{x} f_x(\xi)\, d\xi$$

The important point to be noticed here is that stresses and strains are obtained by integration, whereas in the previous case differentiation was necessary. Integration is a numerically stable procedure. Even when only a limited number of discrete points defines the variation of modal accelerations the spatial strain distribution can be represented fairly

well. This feature renders experimentally determined mode shape data suitable for stress–strain -analysis. The sensitivity of spatial strain distribution to modal accelerations is very low.

Finite element practice yields mode shapes in terms of displacements. Conversion of displacements to inertial forces is easy using the multiplication factor of equation 3.6.

The modal model can be updated efficiently based on the knowledge of the factors that spatial strain distribution is most sensitive to.

3.2.2.2 Correction of modal parameters

The accuracy individual mode shape components are determined with is rather poor. Still, they determine the strain distribution that corresponds to the mode. Local inaccuracies on the mode shape components yield erroneous values for the strain tensor. The global pattern of deformations should be modelled such that modal strains are as close to reality as possible. The overall strain distribution should not exhibit excessive peaks, except in locations of extremely high stress concentrations. The question arises how data that are not particularly smooth can be used to give a fair estimate of stress.

Consider a particular mode k that is characterized by its resonance frequency ν_k and its mode shape ψ_k^u. Both modal parameters may either be measured or computed analytically. Suppose that estimates $\nu_{k,e}$ and $\psi_{k,e}$ of the correct modal parameters are available. A good modal model is capable of determining the resonance frequency in a fairly accurate fashion, $\nu_{k,e}$ is supposed to be correct : $\nu_{k,e} = \nu_k$. The error on the mode shape is more significant. The mode shapes have to be adjusted such that modal strains can be derived. Some techniques which are generally referred to as "smoothing" and "completion" are presented in references [93,94,95,96].

The technique that is presented hereafter uses information from previous analytical or experimental work and processes these data in a boundary element computation.

Start with the estimated mode shape $\psi_1^u = \psi_{k,e}^u$ expressed in terms of displacements. First inertial forces are computed at each of the nodes of the modal model :

$$\psi_1^f = \rho \nu_k^2 \psi_1^u$$

With these inertial forces, which are essentially forces per unit volume, a static computation 3.7 is performed with the boundary element method. The deformed shape ψ_2^u that results from this set of equations is identical to the first estimate ψ_1^u, provided the mode shape is correct. When the original mode shape is not correct, the deformed shape ψ_2^u differs from the original shape ψ_1^u. It is a better estimate of the correct mode shape. The procedure now starts again from this new mode shape ψ_2^u, by first computing the corresponding inertial forces ψ_2^f. From these volume forces ψ_2^f a new deformed shape ψ_3^u is computed.

After a number of iterations convergence will occur and the exact mode shape will finally be obtained. This mode shape is an analytical mode shape. Starting from the originally estimated mode shape ψ_1^u, one gradually proceeds to the analytical mode shape. The information that is contained in the original mode shape is gradually replaced by the analytical data. Depending on the quality of the original mode shape and the boundary element model both original and final modes coincide more or less.

This procedure of "smoothing" and "completing" a mode shape is an extension to techniques developed by STODOLA [97] and ENGESSER - VIANELLO [47, Chap.25]. The basic idea behind this technique is used to update the originally estimated mode shape by performing one static computation with the original data. In this fashion the original information is not lost, yet local inaccuracies are smoothed, thus allowing for a reliable determination of modal strains.

3.2.2.3 Coarseness of the modal model

Stress analysis of structures with the finite element method uses structural models with very fine meshes in the critical areas. These models are characterized by a very high number of degrees of freedom. They can be used for dynamic computations at the cost of a very time consuming computational effort. In industrial practice, large structural models are simply not feasible for use in dynamic computations.

Unlike stress computations, which need only local information in the critical area, a dynamic model should incorporate the entire structure. Provided the selection of the type of elements is well considered by the engineer, a rather coarse model of the structure is generally suited for the analysis of the dynamic behaviour of the structure [98].

The only reason why a detailed model of the structure is necessary is the stress analysis. The method that is described in sections 3.2.2.1 and 3.2.2.2 is well suited for combining a rather coarse modal model with a detailed structural model for the analysis of stresses and strains in the critical areas. The structural model is described in detail in section 4.3.4.

3.2.2.4 Representation of the eigenmodes

Several types of representation of eigenmodes are discussed above. Measuring mode shapes with strain gauges introduces severe errors [91]. It is shown that mode shapes are expressed preferably in terms of accelerations. Both experimental and analytical techniques determine mode shapes in terms of displacements or accelerations. Inertial forces are easily derived. These inertial forces yield the distribution of modal strains via a static boundary element computation, including a discretisation of the volume. Finally the mode shapes are expressed in terms of modal strains, allowing a quick and straightforward computation of the strain history.

3.2.2.5 Example

Consider a homogeneous beam supported at its extremities (fig.3.3). Suppose the first mode shape is measured experimentally, it is represented by the polygonal line in fig.3.3. The correct mode shape is shaped sinusoidally. The strain distribution corresponding to the measured mode will be computed with both methods mentioned in section 3.2.2.1. The results will be compared to the correct results of the sinusoidal mode.

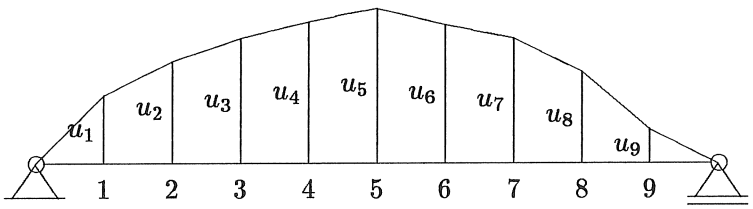

Figure 3.3: Hinged beam vibrating at 1^{st} resonance frequency, experimental mode shape

Its section has following properties :

E : modulus of elasticity $[MN/m^2]$
ϱ : mass per unit length $[kg/m]$
l : length of the beam $[m]$
h : distance from neutral fibre to upper fibre $[m]$
I : bending moment of inertia $[m^4]$

The natural frequency for the first mode is :

$$\omega = \left(\frac{\pi}{l}\right)^2 \sqrt{\frac{EI}{\varrho}}$$

and the theoretical mode shape :

$$\psi^u(x) = u_{max} \sin \frac{\pi x}{l} \tag{3.8}$$

where u_{max} is the amplitude of displacement at the middle of the beam $[m]$. These characteristics are computed explicitly, based on theoretical considerations. The strain distribution at the upper fibre is derived easily :

$$\psi^\epsilon(x) = \frac{\pi^2 h u_{max}}{l^2} \sin \frac{\pi x}{l} = \epsilon_{max} \sin \frac{\pi x}{l} \tag{3.9}$$

The modal model is shown in fig.3.3. There are nine equidistant measurement locations. The mode shape is represented by :

$$\{u\} = \{u_1 \ \ldots \ u_9\}^t$$

The two ways of computing the strain variation that are described in section 3.2.2.1 will be used here and their results will be compared to the correct values 3.9. The governing equations for both methods are :

- from displacements via direct differentiation :

$$\begin{aligned} \epsilon_i &= -100h \frac{u_{i-1} - 2u_i + u_{i+1}}{l^2} \\ &= -\frac{100}{\pi^2} \frac{\pi^2 h u_{max}}{l^2} \left(\frac{u_{i-1}}{u_{max}} - 2\frac{u_i}{u_{max}} + \frac{u_{i+1}}{u_{max}} \right) \\ &= -\frac{100}{\pi^2} \epsilon_{max} \left(\frac{u_{i-1}}{u_{max}} - 2\frac{u_i}{u_{max}} + \frac{u_{i+1}}{u_{max}} \right) \end{aligned} \tag{3.10}$$

- from inertial forces via integration :

$$\epsilon_i = \frac{M_i h}{EI} \tag{3.11}$$

with M_i the bending moment caused by the distribution of inertial forces $\{f\} = \{f_1 \ \ldots \ f_9\}^t = \varrho\omega^2\{u\}$. Linear interpolation is performed for intermediate points. The distribution of bending moments is obtained by double integration of inertial forces. The formulation introduced by DECHAENE [34] is used for the representation of inertial load and bending moment (see also fig.2.4) :

$$\langle x-a\rangle^n = \begin{cases} (x-a)^n & , \ x > a \\ 0 & , \ x \leq a \end{cases}$$

$$\langle x-a\rangle^{-1} = \begin{cases} \infty & , \ x = a \\ 0 & , \ x \neq a \end{cases}$$

Introducing the notations $\xi = x/l$, $\phi_i = f_i/f_{max}$, and $\phi_0 = \phi_{10} = 0$, the distributions $f(\xi)$ and $M(\xi)$ are written :

$$\begin{aligned} f(\xi) &= \frac{f_{max}}{100}\sum_{k=1}^{9}(10-k)\phi_k\langle\xi-0\rangle^{-1} \\ &- 10 f_{max}\left[\phi_1\langle\xi-0\rangle^1 + \sum_{k=1}^{9}(\phi_{k+1}-2\phi_k+\phi_{k-1})\langle\xi-\frac{k}{10}\rangle^1\right] \\ M(\xi) &= \frac{f_{max}l^2}{100}\sum_{k=1}^{9}(10-k)\phi_k\langle\xi-0\rangle^1 \\ &- \frac{5 f_{max}l^2}{3}\left[\phi_1\langle\xi-0\rangle^3 + \sum_{k=1}^{9}(\phi_{k+1}-2\phi_k+\phi_{k-1})\langle\xi-\frac{k}{10}\rangle^3\right] \end{aligned}$$

To investigate the sensitivity of the obtained results to errors on the original mode shape, three different estimates of the mode shapes ψ^u are considered :

- individual mode shape components are identical to the correct values 3.8, load 1 in table 3.1
- individual mode shape components different from correct values by alternatively -1% and +1%, load 2 in table 3.1

node	load 1	load 2	load 3
1	0.309	0.306	0.294
2	0.588	0.594	0.605
3	0.809	0.801	0.793
4	0.951	0.961	0.875
5	1.000	0.990	1.060
6	0.951	0.961	0.961
7	0.809	0.801	0.769
8	0.588	0.594	0.600
9	0.309	0.306	0.337

Table 3.1: Individual relative displacement components for each load

- individual mode shape components different from correct values by random value between -10% and +10%, load 3 in table 3.1

Table 3.2 summarizes the results for the different strain computations :

- the first column repeats the values of displacements for each load case (table 3.1), together with their relative difference with respect to the perfect sinusoid
- the second column shows the values of relative strain computed with equation 3.10, together with their relative differences with respect to the exact values
- the third column shows the values of relative strain computed with equation 3.11, together with their relative differences with respect to the exact values
- the fourth column shows the exact values of relative strain as they are computed with equation 3.9

Figure 3.4 gives a graphical representation of the same results. Load case 2 is compared to load case 1 on the left hand side of the graph, and load case 3 is compared to load case 1 on the right hand side. The top half of the graph shows the perfect sine wave load case 1 with the solid line, and the load cases 2 and 3 with the dashed lines with circles o. The bottom half of the graph shows the distribution of relative strain along the length of the beam : the dashed line with circles o

node no.	displacement table 3.1		strain					
			eq.3.10		eq.3.11		eq. 3.9	
	$\frac{u}{u_{max}}$ [-]	Δ [%]	$\frac{\epsilon}{\epsilon_{max}}$ [-]	Δ [%]	$\frac{\epsilon}{\epsilon_{max}}$ [-]	Δ [%]	$\frac{\epsilon}{\epsilon_{max}}$ [-]	
	load 1							
1	0.309		0.304	-2	0.307	-1	0.309	
2	0.588		0.588		0.583	-1	0.588	
3	0.809		0.800	-1	0.802	-1	0.809	
4	0.951		0.942	-1	0.943	-1	0.951	
5	1.000		0.993	-1	0.992	-1	1.000	
6	0.951		0.942	-1	0.943	-1	0.951	
7	0.809		0.800	-1	0.802	-1	0.809	
8	0.588		0.588		0.583	-1	0.588	
9	0.309		0.304	-2	0.307	-1	0.309	
	load 2							
1	0.306	-1	0.182	-41	0.307	-1	0.309	
2	0.594	+1	0.821	+41	0.583	-1	0.588	
3	0.801	-1	0.476	-41	0.803	-1	0.809	
4	0.961	+1	1.327	+41	0.944	-1	0.951	
5	0.990	-1	0.588	-41	0.992	-1	1.000	
6	0.961	+1	1.327	+41	0.944	-1	0.951	
7	0.801	-1	0.476	-41	0.803	-1	0.809	
8	0.594	+1	0.821	+41	0.583	-1	0.588	
9	0.306	-1	0.182	-41	0.307	-1	0.309	
	load 3							
1	0.294	-5	-0.172	-156	0.304	-2	0.309	
2	0.605	+3	1.246	+112	0.578	-2	0.588	
3	0.793	-2	1.074	+33	0.795	-2	0.809	
4	0.875	-8	-0.436	-146	0.936	-2	0.951	
5	1.060	+6	2.878	+188	0.988	-1	1.000	
6	0.961	+1	0.942	-1	0.940	-1	0.951	
7	0.769	-5	-0.233	-129	0.799	-1	0.809	
8	0.600	+2	0.952	+62	0.582	-1	0.588	
9	0.337	+9	0.750	+143	0.307	-1	0.309	

Table 3.2: Distribution of relative strain along the length of the beam

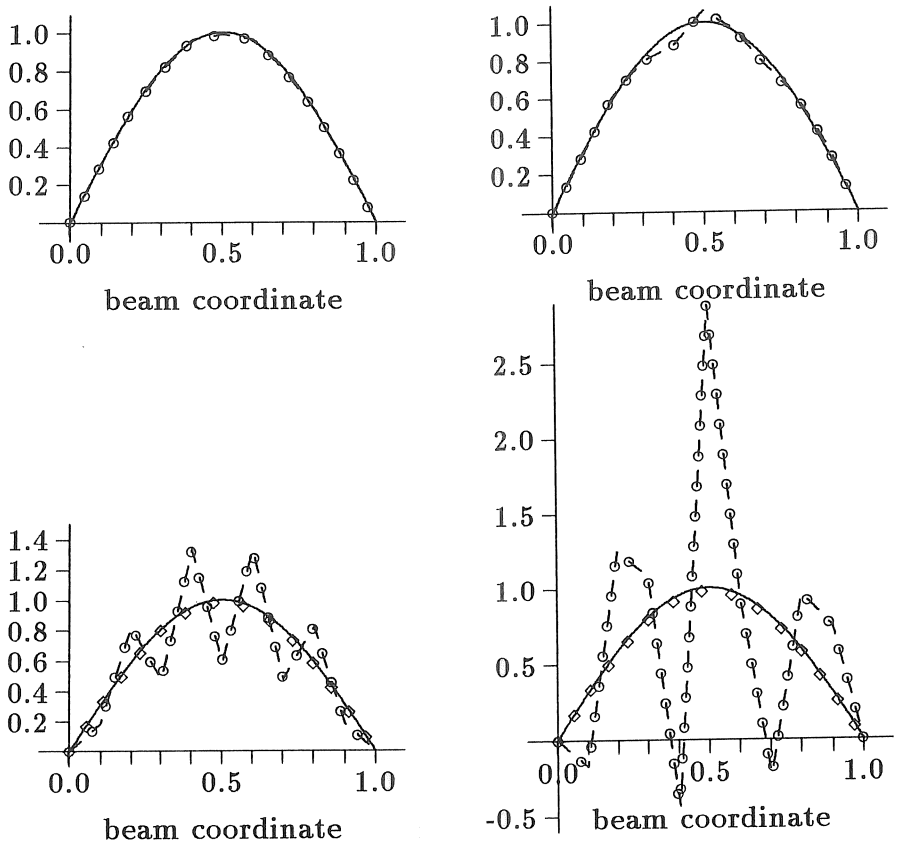

Figure 3.4: Load cases 2 and 3 and distribution of relative strain

shows the results obtained with equation 3.10, the dashed line with diamonds ◇ shows the results obtained with equation 3.11.

It is immediately obvious from the listed figures and pictures that the results of equation 3.10 are in no way reliable. The results of equation 3.11 on the contrary are very close to the correct values 3.9. This observation is valid for loadcases that exhibit significant differences from the correct mode shape.

3.3 Computation of the dynamic response

Basic theory of modal analysis shows that the deformation of a vibrating linear structure can be described by a certain number of vibration

modes. The number of modes is theoretically infinite. In practice a limited number suffices to represent the deformation patterns accurately. It depends on the frequency contents of the load, and to a lesser extent on the distribution of damping. Only those modes whose resonance frequencies remain within the frequency spectrum of the load should be taken into account.

The time response of the structure may then be found from the modal parameters. The following sections 3.3.1 and 3.3.2 will outline two distinct methods. A general structure is considered. The points on the structure where either experimental or analytical data is available, are indicated I, J, $K, \ldots = 1, 2, \ldots N$.

3.3.1 Frequency domain method

This method can be used only when experimental data is available. The transfer function for excitation in point J and response in point I is defined :

$$H_{IJ}(j\omega) = \frac{X_I(j\omega)}{F_J(j\omega)} \tag{3.12}$$

where : $X_I(j\omega)$: Fourier transform of the response in point I
$F_J(j\omega)$: Fourier transform of the input force in point J

After all transfer functions $H_{IJ}(j\omega)$ have been measured, the response in point I under any load in point J is found from :

$$X_I(j\omega) = H_{IJ}(j\omega).F_J(j\omega) \tag{3.13}$$

Equations 3.13 are grouped together for multiple excitation :

$$\{X(j\omega)\} = [H(j\omega)].\{F(j\omega)\} \tag{3.14}$$

The transfer function matrix $[H(j\omega)]$ and the load vector $\{F(j\omega)\}$ are known and the response vector $\{X(j\omega)\}$ has to be determined. The response $x(t)$ in the time domain is found by inverse Fourier transformation of equation 3.14 :

$$\{x(t)\} = \mathcal{F}^{-1}\left([H(j\omega)].\{F(j\omega)\}\right)$$

where $x(t)$: the vector of displacements at time t
Inverse Fourier transformation is a mathematical operation that is performed by standard routines.

The method which is based on direct frequency response measurements has a number of limitations :

- the time increment between successive deformation patterns of the structure is determined by the measurements
- it is impossible to make corrections for windows that are possibly used during measurements (e.g. exponential windows)
- measurements are partially incompatible due to measurement errors (e.g. shift of resonance frequencies due to the mass loading effect of the accelerometer)
- the computation of inverse Fourier transforms is time consuming

3.3.2 Time domain method

This method is based on modal parameters. They may be found either from experimental or from numerical analysis. If necessary, damping values have to be measured separately.

The response at point I for an excitation in point J is found from :

$$\frac{X_I(j\omega)}{F_J(j\omega)} = \sum_{k=1}^{N} \left(\frac{U_{IJk} + jV_{IJk}}{-\sigma_k + j(\omega - \nu_k)} + \frac{U_{IJk} - jV_{IJk}}{-\sigma_k + j(\omega + \nu_k)} \right) \tag{3.15}$$

where : I : response point
J : excitation point
k : mode number
N : number of modes that are taken into account
$j\omega$: purely imaginary variable
j : $\sqrt{-1}$
X_I : Fourier transform of response in point I
F_J : Fourier transform of load input in point J
U_{IJk} : real part of mode shape component k
V_{IJk} : imaginary part of mode shape component k
$\nu_k = \Im(\lambda_k)$: damped natural frequency for mode k
$\sigma_k = \Re(\lambda_k)$: damping value for mode k
λ_k : pole of transfer function

Equation 3.15 expresses the transfer function based on modal parameters. Mode shape components may be expressed in terms of displacements, velocities, accelerations, strains. The computed structural response has corresponding dimensions.

Until now it was assumed that the point where the load input is applied is identical to the excitation point used during the modal test. When they do not coincide the mode shape components have to be corrected for the new excitation point. Denoting the excitation point J, the mode shape component at point I for mode k is written $U_{IJk} + jV_{IJk}$. When the structure is loaded in point M, the relevant quantity is denoted $U_{IMk} + jV_{IMk}$. The relation between them is established easily :

$$\begin{aligned} U_{IJk} + jV_{IJk} &= \frac{2j}{a_k}\psi_{Ik}\psi_{Jk} \\ U_{IMk} + jV_{IMk} &= \frac{2j}{a_k}\psi_{Ik}\psi_{Mk} \\ &= \frac{2j}{a_k}\psi_{Ik}\psi_{Jk}\frac{\frac{2j}{a_k}\psi_{Mk}\psi_{Jk}}{\frac{2j}{a_k}\psi_{Jk}\psi_{Jk}} \\ &= \frac{(U_{IJk} + jV_{IJk})(U_{MJk} + jV_{MJk})}{(U_{JJk} + jV_{JJk})} \end{aligned} \tag{3.16}$$

Expression 3.16 is used for the computation of the mode shape component for load input in point M different from the excitation point J.

3.3.2.1 Impulse response

The impulse response function is the inverse Fourier transform of the transfer function. It is the response of the structure when it is excited with a Dirac-impulse $\delta(t - t_0)$ or $\langle t - t_0 \rangle^{-1}$:

$$\delta(t - t_0) = \langle t - t_0 \rangle^{-1} = \begin{cases} \infty & t = t_0 \\ 0 & t \neq t_0 \end{cases}$$

Thus :

$$x(t) = h(t) = \mathcal{F}^{-1}(H(j\omega))$$

Using equation 3.15 one obtains :

$$\begin{aligned} h(t) &= \\ &= \sum_{k=1}^{N} \left[(U_{IJk} + jV_{IJk})\, e^{(-\sigma_k + j\nu_k)t} + (U_{IJk} - jV_{IJk})\, e^{(-\sigma_k - j\nu_k)t} \right] \\ &= 2\sum_{k=1}^{N} (U_{IJk} \cos \nu_k t - V_{IJk} \sin \nu_k t)\, e^{-\sigma_k t} \end{aligned}$$

In industrial practice many cases are characterized by a type of load input which is roughly a Dirac impulse. Military equipment, for instance, consists of moving parts that hit each other instantaneously. Ground transportation vehicles riding over an isolated road asperity are subjected to a Dirac impulse. Sudden application of a static load also involves quasi-Dirac components. The load that is transferred by the landing gear of an aircraft at the instant of touchdown suddenly increases from zero to a constant level.

3.3.2.2 Arbitrary force input

Force functions may be very much different from a Dirac impulse. The response in the frequency domain is defined by equation 3.12 :

$$H_{IJ}(j\omega) = \frac{X_I(j\omega)}{F_J(j\omega)}$$

Inverse Fourier transformation of this equation yields the response of the structure in the time domain :

$$x_I(t) = 2\int_0^t \sum_{k=1}^{N} (U_{IJk}\cos\nu_k\tau - V_{IJk}\sin\nu_k\tau)\, e^{-\sigma_k t} f_J(t-\tau)\, d\tau \quad (3.17)$$

Evaluation of the convolution integral yields the response of the structure at time t in point I, for a load applied in point J.

3.3.2.3 Implementation of the algorithm

Thorough examination of equation 3.17 reveals a number of aspects that should be considered carefully :

- for every single timestep a separate computation has to be performed, evaluating the same integrand from time $t = 0$ to time t.
- every single integrand consists of a summation over N relevant modes of the structure and over all the components J of the load.
- the computation of sinusoidal and exponential functions is very intensive.

Quadrature schemes define a number of coordinates ξ_i in the integration interval $[a, b]$. In each of these coordinates the integrand $g(\xi_i)$ is evaluated and a weighting factor w_i is associated to it. The integral is then written :

$$\int_a^b g(\xi)\, d\xi = \sum_{i=1}^{m} w_i g(\xi_i) \qquad a \leq \xi_i \leq b$$

The integration coordinates ξ_i and the weighting factors w_i are taken from tables of numerical constants [171]. Standard quadrature schemes are used for finite, continuous and smooth functions $g(\xi)$, whereas special schemes are developed for singular functions of several types. The accuracy of the result depends on the number of integration points m. Especially when strongly varying integrands occur, a fair estimation of the integral is extremely time-consuming.

All of these considerations render numerical integration cumbersome and time-consuming. There is however a way to transform the integral in such a way that integration is accurate and fast.

The modal displacements occur as coefficients of two integrals, which are respectively the real and the imaginary part of following complex integral :

$$\mathcal{RS}_k(t) = \int_0^t e^{(-\sigma_k + j\nu_k)\tau} f(t-\tau)\, d\tau \tag{3.18}$$

$\mathcal{RS}_k(t)$ is the response function for mode k and force input $f(t)$. A recursion formula can be used.

$$\begin{aligned}
\mathcal{RS}_k(t+\Delta t) &= \int_0^{t+\Delta t} e^{(-\sigma_k + j\nu_k)\tau} f(t+\Delta t-\tau)\, d\tau \\
&= \int_0^{\Delta t} e^{(-\sigma_k + j\nu_k)\tau} f(t+\Delta t-\tau)\, d\tau \\
&\quad + \int_{\Delta t}^{t+\Delta t} e^{(-\sigma_k + j\nu_k)\tau} f(t+\Delta t-\tau)\, d\tau \\
&= \int_0^{\Delta t} e^{(-\sigma_k + j\nu_k)\tau} f(t+\Delta t-\tau)\, d\tau \\
&\quad + \int_0^{t} e^{(-\sigma_k + j\nu_k)(\tau'+\Delta t)} f(t-\tau')\, d\tau' \\
&= \int_0^{\Delta t} e^{(-\sigma_k + j\nu_k)\tau} f(t+\Delta t-\tau)\, d\tau \\
&\quad + e^{(-\sigma_k + j\nu_k)\Delta t} \mathcal{RS}_k(t)
\end{aligned} \tag{3.19}$$

Two distinct terms have to be evaluated separately. The first term on the right hand side involves an integration over the interval $[0, \Delta t]$. The integrand comprises information about the load input between time t and time $t+\Delta t$. It expresses the instantaneous influence of the load on the structure. The second term expresses the influence of the resonant character of the structure. No approximation is made, the values of both sides of the equation are identical. This recursive formulation can be taken full advantage of, since the integration interval is reduced to a much smaller size. The computational effort that is necessary in order to achieve an accuracy that is comparable to the accuracy of direct integration 3.18 is considerably lower. The whole procedure of computing a complete sequence of time responses involves the repeated evaluation of equation 3.19. The proposed recursive algorithm is much more efficient since it evaluates the direct influence of the load input in the time interval $[t, t + \Delta t]$ only once. This formulation is generally valid, regardless of the type of excitation force, and it is numerically exact.

Still, it may be cumbersome to obtain accurate values for the integral on the right hand side. Conventional quadrature schemes may give poor results, even when high-order integration formulas are used. For many types of load functions $f(t)$, however, the integral can be evaluated exactly and explicitly. First, the exponential factor may be written alternatively :

$$e^{(-\sigma_k + j\nu_k)\tau} = e^{-\sigma_k \tau}(\cos \nu_k \tau + j \sin \nu_k \tau) \tag{3.20}$$

Any function $g(t)$ that is written as a product of exponential, trigonometric or polynomial functions, such as :

$$g(x) = (a - x)^n e^{kx} \sin(\omega x - \phi) \tag{3.21}$$

where a, k, ω, ϕ are arbitrary real numbers and n a non-negative integer, may be integrated in an explicit fashion. Two successive partial integrations transform the undetermined integral I_n :

$$\begin{aligned} I_n &= \int (a - x)^n e^{kx} \sin(\omega x - \phi)\, dx \\ &= \frac{1}{\omega^2 + k^2} \{[\, - \omega (a - x)^n \cos(\omega x - \phi) \\ &\qquad - n(a - x)^{n-1} \sin(\omega x - \phi) \end{aligned}$$

$$+ k(a-x)^n \sin(\omega x - \phi)]\, e^{kx}$$
$$+ 2knI_{n-1} - n(n-1)I_{n-2}\} \qquad (3.22)$$

special cases : for $n = 0$: only 1^{st} and 3^{rd} terms
for $n = 1$: only 1^{st}, 2^{nd}, 3^{rd} and 4^{th} terms

This recursive expression is valid for any value of a, k, ω, ϕ and n ($= 0$, $1, \ldots$). Starting from integrals I_0, I_1, ..., higher orders are obtained successively.

Basic trigonometry shows that following identities hold :

$$\begin{aligned} \cos\alpha &= \sin(\tfrac{\pi}{2} + \alpha) \\ \sin\alpha \sin\beta &= \tfrac{1}{2}\left(\cos\tfrac{\alpha-\beta}{2} - \cos\tfrac{\alpha+\beta}{2}\right) \end{aligned} \qquad (3.23)$$

Introduction of 3.20, 3.21, 3.22 and 3.23 into equation 3.19 gives a formulation that allows an explicit, direct and accurate evaluation of time response. A general force input :

$$f(t) = A(t-t_p)^n e^{kt} \sin(\omega t - \phi)$$

with A, t_p, k, ω and ϕ arbitrary real numbers and n a non-negative integer, the integrand $e^{(-\delta+j\nu)\tau} f(t-\tau)$ is converted to a sum of four integrands that can each be handled explicitly with equation 3.22 :

$$\begin{aligned} e^{(-\delta+j\nu)\tau} f(t-\tau) = \frac{1}{2} A e^{kt} (t - t_p - \tau)^n e^{-(k+\delta)\tau} \\ . \quad \{\sin[(\omega+\nu)\tau - (\omega t - \phi - \pi)] \\ - \quad \sin[(\nu-\omega)\tau - (\phi + \pi - \omega t)] \\ + \quad \sin\left[(\nu-\omega)\tau - (\phi + \frac{\pi}{2} - \omega t)\right] \\ - \quad \sin\left[(\omega+\nu)\tau - (\omega t - \phi - \frac{3\pi}{2})\right]\Big\} \end{aligned} \qquad (3.24)$$

For cases where n, k, ω or ϕ are zero, the formulation may be even more simplified. Each of the terms on the right hand side of equation 3.24 has the same general shape of equation 3.22. The computational effort that is required is minimal. The integrands need to be computed only at the boundaries of the interval $[0, \Delta t]$. The most important conclusion that is drawn however, is the independency of the size of the time increment. The computed result is independent of the number

of time steps. The only factor that is determinative to the choice of the time increment Δt is its ability to represent the time history of the response in a sufficiently accurate fashion. It must not be any larger than the minimum time span between successive peaks and troughs of the response history. Neither is there a need for it to be much smaller.

3.3.2.4 Static loads and higher modes

The representation of transfer functions in a restricted frequency band involves two residual terms, one for lower modes and one for higher modes. The component (i, j) of the transfer function matrix is written 3.25 :

$$h_{IJ} = \sum_{k=1}^{N} \left[\frac{U_{IJk} + jV_{IJk}}{-\sigma_k + j(\omega - \nu_k)} + \frac{U_{IJk} - jV_{IJk}}{-\sigma_k + j(\omega + \nu_k)} \right] + \mathcal{UR}_{IJ} - \frac{\mathcal{LR}_{IJ}}{\omega^2} \tag{3.25}$$

where : $\mathcal{UR}_{IJ}$: upper residual term of transfer function
$\mathcal{LR}_{IJ}$: lower residual term of transfer function

The upper residual term $\mathcal{UR}_{IJ}$ represents the influence of higher modes on the estimation of the transfer function, and $\mathcal{LR}_{IJ}$ represents the influence of lower modes. The upper residual term is often called residual stiffness, the lower residual term is called residual mass. Loads characterized by a frequency content exceeding the frequency band of measurement excite the lower modes as if they were "rigid body" modes. This is the inertial effect for lower modes. Loads with a frequency content below the frequency band of interest are unable to excite the higher modes. The response of the structure is similar to the response of a static load.

The global influence of lower and upper residual terms can be modelled only in the frequency domain (section 3.3.1). Static loads are treated easily using conventional elastostatic theory. As the structure is supposed to be linear, superposition of static and dynamic effects is straightforward. High order modes cannot be handled easily. Their influence on the global deformation pattern is usually insignificant. The amplitude of high order frequencies is generally small and the static response of a structure to small loads is not significant.

Two important conclusions show up as to the number of modes that should be included in the analysis of time response (equation 3.15) :

- all of the lower modes of the structure must be included, even when the frequency content of the load is concentrated preponderantly in higher regions
- the highest mode that should be included corresponds to the highest frequencies of the load's spectral density, the influence of higher modes usually being insignificant

3.3.3 Comparison of frequency domain methods with time domain methods

It is essential that the strain history is defined in the time domain, in order to process it in an appropriate fashion. There are a number of phenomena that can be described only in the time domain :

- the actual strain history should be defined appropriately :
  - when static strains are present only in a portion of the entire duration of the strain history, they must be superposed explicitly to the dynamic strain pattern. This phenomenon can be described only in the time domain.
  - residual stresses influence the complete subsequent stress variation, so it is important to know when residual stresses are generated. Frequency domain data are not capable of conveying this information.
- the stress/strain history should be well prepared to allow post-processing regarding fatigue life assessment. Resolution of a complex strain into a number of distinct cycles is feasible only when the correspondance between strain amplitudes and the instantaneous peak levels of stress is uniquely defined. It is the interaction between both peak and mean quantities that is responsible for the accumulation of damage.

All of these arguments show that a time domain approach is necessary as far as the strain history is concerned. The possibility still remains to adopt a frequency domain approach for the response computation (section 3.3.1) and then inverse Fourier transform the response to the time domain. A comparison with the time domain approach (section 3.3.2) shows that the latter is preferable to the former in many regards.

3.3.3.1 Computational efficiency

The inverse Fourier transform is defined :

$$x(t) = \frac{1}{2\pi} \int_0^\infty X(j\omega) e^{j\omega t} \, d\omega \tag{3.26}$$

This approach is adopted only when the dynamic behaviour of the structure is defined in terms of transfer functions $H_{ij}(j\omega)$ 3.15. When the frequency content $X(j\omega)$ is known from previous computations, the original signal $x(t)$ is recovered by evaluating the complex integral 3.26. Standard routines exist for performing the integration numerically. These routines are approximative in a sense that values of $X(j\omega)$ are defined only at discrete values of frequency. The frequency resolution of the measurement setup is determinative for the number of frequencies that is taken into account. The integration over the frequency range ω is transformed to a summation over discrete frequency values. For each timestep t, a separate integration should be performed. Information about the deformation at time t can not be used for the computation of deformations at time $t + \Delta t$. The accuracy that can be obtained may be poor, when frequency resolution is insufficient.

The time domain approach is very much different as it is theoretically perfectly accurate, regardless of the value of the timestep Δt. It is a particularly interesting feature that deformations at time $t + \Delta t$ are computed from the corresponding values at the previous instant of time t. The interval of integration is narrow. For most types of loading, the integrals can be evaluated explicitly and accurately. The integral is written in a closed form. Its computation involves the evaluation of only a limited number of exponential, polynomial and trigonometric functions.

3.3.3.2 Influence of a particular mode

It is important for the designer to know the relative importance of a particular mode in the response of the structure. The location of nodes of a mode on the structure together with the damping value of the mode determine the amplitude of the response at a particular point on the structure. An area on the structure that is subjected to large amplitudes of strain on one mode may not be strained at all

on another mode. It may be helpful for the designer to modify the structure in such a way that only one or a few modes are altered.

The relative importance of a mode may be evaluated by leaving it out of the summations 3.15 or 3.17. As each of both formulations comprises a summation over all the relevant modes, they are both capable of revealing information about the distribution of the amplitudes of deformation over the different modes.

3.3.3.3 Influence of static loads

The importance of accurate superposition of static and dynamic loads is an issue that has been stressed repeatedly. Modelling the influence of static loads in a time domain approach is a straightforward procedure. The frequency domain approach is not capable of handling static loads, because static loads do not have a frequency. The lower residual term in equation 3.25 is merely a very rough approximation of dealing with static loads. The use of frequency domain approaches is not suitable of handling static loads. It would be a terminological contradiction.

3.4 Recent advances in dynamic modelling

Recent research in numerous domains of modal analysis resulted in several tools that are helpful in modelling the dynamic behaviour of a structure. Some of these advances have been made on technological issues while others involve theoretical developments. Some techniques may readily be used, others still need further investigation.

3.4.1 Model updating techniques

Section 3.4.1 explains how experimental and analytical procedures are combined in an attempt to analyse the dynamic behaviour of a structure thoroughly and consistently. Two distinct modal models are constructed, a model based on experimental data and a finite element model. Both models possess their own characteristics and generally, they represent the dynamic behaviour of the structure in different fashions. Nevertheless, a linear, time invariant structure has a unique set of modal parameters. It is assumed that the experimental modal characteristics are close to the real values on condition that two basic requirements are met. First, the experimental modal model has the

capability of representing the structure's dynamic behaviour in the frequency band of interest. Second, consecutive phases of the modal survey, including measurement setup, data acquisition and parameter estimation are executed in a well-considered manner.

The modal parameters found from numerical analysis not always coincide with the correct data. Therefore the finite element model should be updated in order for its modal characteristics to match the real values. Recently, some methods were developed that modify the model towards a fair correspondence of modal data. They are classified in three different levels :

- updating of individual elements of global mass and stiffness matrices [77]
- updating of proportional correction factors for submatrices of global mass and stiffness matrices [99]
- updating of input data of the finite element model [76,100]

In both the first and the second approach, the elements of the matrices $[K]$ and $[M]$ (equation 3.3) are altered directly, without reference to their physical meaning. Unexpected modifications may be suggested and the correlation between the physical meaning of the updated model and the actual structure may be totally lost. The results of the updating procedure are perfect in a mathematical sense but from a designer's point of view the model may be useless. The technique presented by JANTER [76] allows the designer to control and interpret the changes that are brought into the model. Direct physical input parameters that do have a tangible meaning to the designer are affected. A sensitivity analysis is used to predict the influence of the input parameters to the modal parameters. Via an iterative modification of the input parameters the computed modal characteristics gradually converge towards the desired values. A wide range of applications is presented and the author concludes that the technique is valid for a multitude of input parameter types, for small as well as for large models.

After the updating procedure is achieved successfully, the modal model is prepared to accurately predict the dynamic response of the structure to the applied load.

3.4.2 Error localization

In the previous section it was stated that analytical modal models often show discrepancies with the experimental modal model. There are two classes of errors. The first class regards the selected approach of modelling the structure, the selection of the type of elements, the way the structure is fixed, ... These errors are unlikely to be committed by a knowledgeable and experienced engineer, but when they occur they are very hard to recover. The second type of errors is related rather to the dedication of the finite element engineer and to the accuracy of the model. These errors concern the geometrical location of the nodes of the model, the definition of the material properties, the distribution of mass over the structure, the definition of constraints, ... These errors are rather likely to occur, but they can be corrected for fairly easily. The purpose of error localization techniques is to detect these errors consistently, by comparison of analytical modal parameters to experimental values.

LAMMENS et al. [101] give an overview of techniques that are presented in literature. The authors comment briefly on the basic reasoning behind each of those methods and they elaborate on two techniques.

The "Coordinate Modal Assurance Criterion COMAC" is developed by LIEVEN and EWINS [102]. It is a variant to ALLEMANG's MAC-criterion [103]. It compares the individual mode shape components of all corresponding analytical and experimental modes at a particular degree of freedom. A correlation factor is defined and it is stated that low correlation values give an indication of error at that location. Careful examination of some testcases shows that the COMAC-method is not capable of certified detection of errors.

The force balance method is presented by IBRAHIM and STAVRINIDIS [104]. It is based on the most fundamental law of physics, the expression of equilibrium. Equation 1.22 is expressed in terms of analytical mass and stiffness matrices $[M_a]$ and $[K_a]$ on the one hand and experimental parameters for mode k ω_{ek} and $\{\psi_{ek}\}$ on the other hand :

$$\left([K_a] - \omega_{ek}^2[M_a]\right).\{\psi_{ek}\} = \{E_k\}$$

Theoretically the right hand side of this equation should be zero. In case errors occur in the model, the non-zero elements of elements of vector $\{E_k\}$ give an indication of the location of errors. This technique

appears to be promising although some problems arise regarding the completion of experimental mode shapes, and the sensitivity to measurement errors.

The experience gathered so far by several researchers clearly shows that no single method has the right to claim consistent detection of errors. Although several methods may give some rough indications on the location of errors they can certainly not be automated as a reliable error detection technique. A large amount of experience and insight still has to be gained before error localization techniques can be accepted generally as a useful tool in the process of design and analysis.

3.4.3 Nonlinearities

One of the basic assumptions of modal analysis is the hypothesis of linear behaviour of the structure. For a majority of cases this assumption is valid, the influence of possible non-linearities being local and negligible in the overall characteristics of the structure. Still many applications exist where non-linearities disturb the linear behaviour of the structure : gaps, backlash, friction, plastic deformation, ... These and similar phenomena often occur in real life structures. The most common example is a mechanical joint, that has a significant influence on the overall behaviour of the structure. The engine mounting of an automobile does play an important role in the dynamic behaviour of the entire engine compartment.

Although many researchers are trying intensively to tackle the problem of nonlinearities, it has not left academic spheres yet. Current research tries to detect and identify the nonlinear behaviour of rather simple structures. Some methods were proposed to study small systems of one or a few degrees of freedom [105]. Modelling a real life component that exhibits a significant nonlinear behaviour is not yet feasible, if it will ever be. Probably researchers will soon be able to build models that describe the behaviour of specific and relatively simple systems. It is the writer's opinion however that a consistent approach of modelling mechanical components of even little complexity for use in dynamic computations is utopian.

The transient response of a structure can be determined using direct integration. Theoretically this method allows the modelling of some types of nonlinearities. Practical experience shows that the reli-

ability of this option may be doubtful with commercial finite element codes. Some codes have nonlinear springs in their element library. Again, the reliability was poor in a number of tests that were performed by the author.

The engineer has to resort to a pragmatic approach and use sound engineering judgment in constructing a model that comes as close to reality as possible. Each single source of nonlinearity should be studied carefully. Consider for instance a case of backlash, presented in fig.3.5. Denote by m the relative number (in %) of cycles during which no

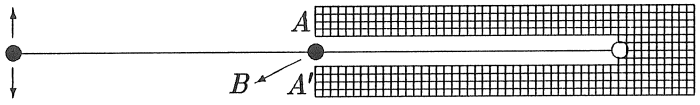

Figure 3.5: Vibrating beam with backlash

contact is made, and by n the relative number (in %) of contact-cycles. Distinction should be made between three cases, depending on the amplitudes of vibration at point B of the vibrating beam :

- $m \ll n$, B seldom hits stops A or A' : consider the stops to be nonexistent
- $m \gg n$, B hits stops A or A' almost always : consider the points A, A' and B to be coincident, and eliminate any relative displacement between those points
- $m \approx n$: determine the impulse response functions $h_1(t)$ and $h_2(t)$ for both cases, without and with contact and define the total impulse response $h(t)$ function in two parts :

$$h(t) = \frac{1}{100}\left(mh_1(t) + nh_2(t)\right)$$

For other types of nonlinearities, such as friction, practical solutions are less obvious.

3.5 Conclusion

This chapter elaborates on the details of response computation. A fast convolution method is combined with a static boundary element analysis in an original way to give strain response quickly and accurately.

Firstly, a review is given of how a modal model should be assembled. Some important aspects are mentioned related to the accuracy of the modal parameters. It is proved that the accuracy of the mode shape vectors is particularly important. Mode shape components should be expressed in terms of inertial forces or accelerations. Displacements are not directly suited as a representation of mode shapes. Modal strains are obtained from inertial forces by a static analysis. An example illustrates the insignificance of sensitivities of strain distribution to individual mode shape components, provided they are expressed in terms of inertial forces.

Secondly, two distinct methods of dynamic response computation are presented. The frequency domain method uses frequency response functions and subsequently inverse Fourier transformation. In the time domain method the convolution integral between the force function and the impulse response function is computed. A fast computation algorithm is developed. Comparison of the frequency domain approach to the time domain approach shows that the latter is preferable to the former in many regards.

Finally some recent advances in modal analysis applications are mentioned that may be helpful in the phase of designing a structure that is to be subjected to dynamic loading. The proposed methods are fast and accurate. The analytical model can be tuned perfectly so as to match its experimental characteristics.

Chapter 4

Strain computation in a dynamic context

4.1 Introduction

The previous chapter demonstrates how the principle of modal superposition converts a dynamic strain response computation to a number of static computations. The concept of modal strains is introduced. Modal strains are used to represent the mode shapes of the structure. Response computation utilizes modal strains and gives strain histories immediately. It is shown why the spatial strain distribution is extremely sensitive to the accuracy of modal vectors. Modal strains are therefore computed based on information about modal accelerations.

This chapter discusses the details of the computation of modal strains. The finite element method is used very often in the determination of stresses and strains. The capabilities of the finite element method in its traditional formulation and in some more advanced formulations is described thoroughly.

The boundary element method is established recently as an adequate alternative to the finite element method. Particularly in applications of stress and strain analysis it offers superior potentials of accuracy that are exploited fully in the proposed method. Especially for static computations the boundary element method is well suited. The proposed method introduces a way of using boundary element principles for dynamic analysis. Inertial forces are distributed essentially in the volume of the structure. Modelling of body forces is an

awkward procedure in a conventional boundary context. It is illustrated in the previous chapters that a rather coarse geometrical model of the volume of the structure is perfectly well suited for an accurate representation of body loads.

The last section of the chapter deals with the effects of plastic deformation. It is explained on what conditions elastic analysis can be used to compute stresses and strains in the plastic domain.

4.2 Numerical static elastic stress analysis

This section comments on two computational methods that are used for elastic stress analysis. First the finite element method and afterwards the boundary element method are described. Their standard formulations are given, together with some information on alternative capabilities which are less commonly used. Theoretical developments on the general aspects of both methods are kept strictly minimum. Attention is focussed on how stresses and strains are obtained. Some comments on the practical use of both methods are given. Finally it is argued why the latter is preferred to the former.

4.2.1 The finite element method

Finite element concepts are used for quite some years already. Many commercial software packages are available for a wide range of applications. Historically one of the first applications was elastic stress and strain analysis.

4.2.1.1 Basic features

For undamped dynamic computations the development of the matrix equation is presented in section 3.2.1.1. For static applications the same way of reasoning is adopted except for the inertia terms, which are of course nonexistent. The final matrix equation is similar :

$$[K]\{u\} = \{F\} \tag{4.1}$$

where : $[K]$: the stiffness matrix of the entire structure
$\{u\}$: vector of degrees of freedom in all nodes
$\{F\}$: vector of point forces applied in the nodes

The stiffness matrix $[K]$ is the same matrix as for dynamic computations. The vector of degrees of freedom contains components of displacements and in some cases components of rotational degrees of freedom. The type of degrees of freedom depends on the choice of the element type. The column vector $\{F\}$ contains components of point forces that are applied in the nodes. Depending on the type of analysis and on the particular choice of the element type moments can be included in the analysis. In the context of dynamic computations the loads consist of inertial forces that are distributed over the entire volume of the structure. Experimentally determined mode shapes do not include rotational degrees of freedom. Thus, moments occur only when analytical mode shapes are used.

An important point to notice is concerned with the representation of volume loads. In a finite element context forces are applied only in the nodes of the model. Point forces are expressed in Newton. For a particular element of the model, the components of the force vector $\{F\}_i$ are given by :

$$\{F\}_i = \int_{\Omega_i} [N]^t \{f\} \, d\Omega$$

where : Ω_i : volume, domain of element i
$[N]$: matrix of shape functions
$\{f\}$: vector of inertial forces per unit volume $[N/m^3]$

The components $\{F\}$ are the resultant forces in the nodes of the distributed volume loads. The same shape functions that are used for the displacements occur in the integrand. A continuous representation of volume loads $[N/m^3]$ is converted to a set of discrete point loads. In a finite element context the appropriate components of forces must be assigned to every single node. This property excludes experimental data from being used, unless they are completed for all the nodes of the model. Experimental models do not contain all the nodes of the analytical model. Techniques of mode completion are used to assign components of mode shapes to individual nodes [93,94,95,96].

Some details are given now on how stresses and strains are obtained from displacements. Consider a finite element problem of plane stress and suppose the first phase of the analysis completed. All the degrees of freedom have specific values. The subsequent discussion deals with the postprocessing of the primary data.

Consider one single element **5** with its adjacent nodes 6, 7, 10, 11. The mesh in the neighbourhood of the considered element **5** is represented in fig.4.1, left. The degrees of freedom in these nodes are gathered in vector $\{d\}$.

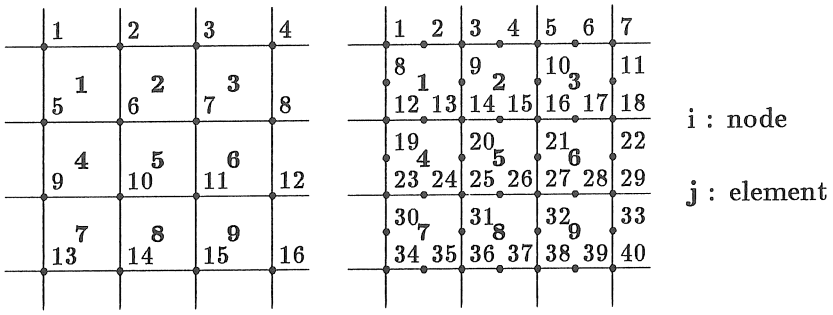

Figure 4.1: Linear and quadratic meshes of rectangular elements

Strains are found by derivation of displacements :

$$\varepsilon_{ij} = \frac{1}{2}\left(\frac{\partial u_i}{\partial x_j} + \frac{\partial u_j}{\partial x_i}\right) \tag{4.2}$$

The strain tensor is generally two-dimensional, finite element practice groups individual components in a 3×1 vector $\{\varepsilon\}$. The equivalent matrix formulation of equation 4.2 is :

$$\{\varepsilon\} = \begin{Bmatrix} \varepsilon_{xx} \\ \varepsilon_{yy} \\ \gamma_{xy} \end{Bmatrix} = \begin{Bmatrix} \varepsilon_{xx} \\ \varepsilon_{yy} \\ 2\varepsilon_{xy} \end{Bmatrix} = \begin{bmatrix} \frac{\partial}{\partial x} & 0 \\ 0 & \frac{\partial}{\partial y} \\ \frac{\partial}{\partial y} & \frac{\partial}{\partial x} \end{bmatrix} \cdot \begin{Bmatrix} u_x \\ u_y \end{Bmatrix}$$

$$= [\partial] \cdot \begin{bmatrix} N_1 & 0 & N_2 & 0 & N_3 & 0 & N_4 & 0 \\ 0 & N_1 & 0 & N_2 & 0 & N_3 & 0 & N_4 \end{bmatrix} \cdot \begin{Bmatrix} u_1 \\ v_1 \\ u_2 \\ v_2 \\ u_3 \\ v_3 \\ u_4 \\ v_4 \end{Bmatrix}$$

$$= [\partial].[N].\{\delta\} = [B].\{\delta\}$$

where : $[N]$: matrix of shape function

N_i : shape function for node i
$[\partial]$: matrix of differential operators
$[B]$: matrix of differences

The matrix $[B]$ depends only on the coordinates of the nodes of the element. Four-noded quadrilateral elements have linear shape functions. All the elements of the matrix $[B]$ are thus constant throughout the entire element. The state of strain in the whole element is characterised by a unique value. Stress and strain variations over elements are described by polynomials one degree lower than the shape functions N for displacement variations. Quadratic variations can also be used for modelling a structure (figure 4.1, right). The number of elements remaining the same, the number of nodes is roughly double. The matrix $[\partial]$ remains unchanged, while the vector $\{d\}$ is 16×1 and the matrix $[N]$ is 2×16. The elements of the matrix $[B]$ now exhibit a linear variation in the geometrical coordinates. Variations of strain over a single element can now be modelled. Quadratic elements offer clear advantages over linear elements for stress and strain analysis. Strains are computed exactly in some well-defined locations on the element. The points for Gaussian quadrature of an element for evaluation of strain differ from the Gauss-points for evaluation of the stiffness matrix $[K]$, because the degree of strain variation is one less than the degree of displacement variation. The locations of Gauss-points of the SYSTUS quadrilateral elements [106] are indicated on fig.4.2.

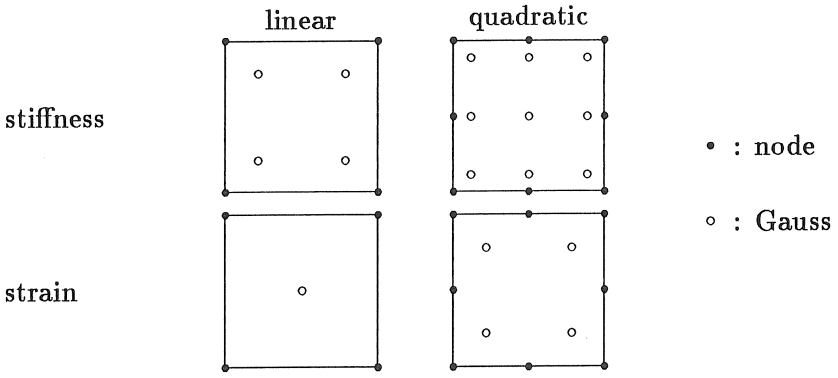

Figure 4.2: Location of Gauss-points in SYSTUS elements 2004 and 2008

The areas of high stress of a structure are usually located at the edge or surface of the structure. Peak values of strain in an element generally occur at the edge of the element. This value is obtained by an extrapolation of the strains at the Gauss-points. A problem arises concerning the uniqueness of strains at interface points. Node 14 (fig.4.1, right) belongs to elements **1**, **2**, **4** and **5**. The values of strain at node 14 assigned by extrapolation in each of the four elements probably do not coincide. An averaging procedure seems to be most significant in assigning a unique value to the node, although there is no physical support for it. BARLOW [107] proposes a procedure to rationalise the connection between optimal stress points and reduced integration.

4.2.1.2 Enhanced capabilities

The finite element method is used in a very wide range of applications. Some developments are made that enhance its capabilities in specific areas. This section briefly mentions the main features that improve its usefulness in static stress analysis.

4.2.1.2.1 Geometric mesh refinement

The most straightforward improvement of a finite element model for stress analysis is an optimization of the geometrical mesh. Especially in areas of high stress gradients significant improvements may be obtained. Elements are added or modified by adding, deleting or shifting nodes.

Routines exist that transport displacement data from a rather coarse mesh to a new, dense mesh that is defined only in a restricted zone around the critical area. The displacement data on the coarse mesh are imposed as boundary conditions to the dense mesh.

Research is developing nowadays automated procedures for optimizing the mesh. Mainly three different approaches are distinguished :

r-line refinement : the total number of nodes and elements remains unchanged, only the locations of the nodes are modified in search of an optimum distribution of potential energy over the elements

h-line refinement : elements are subdivided in a higher number of elements of the same type. Nodes are generated either on the

edges of the element, either in the interior of the element. Triangular and quadrilateral elements are subdivided in triangles and/or quadrilaterals of smaller dimensions.

p-line refinement : the total number of nodes and elements remains unchanged, only the degree of the polynomial shape functions is increased, thus allowing a stronger variation of displacements and strains on the edges of the element and inside it.

Some approaches are combined techniques, e.g. h-p-refinement.

4.2.1.2.2 Non-conforming elements

Basic theory of the finite element method assumes a certain degree of continuity over the adjacent elements' interfaces. The required continuity depends on the particular type of problem. The most common example is a four-noded rectangular thin plate bending element. Each node has three degrees of freedom, one transversal displacement w and two rotations $\partial w/\partial x$ and $\partial w/\partial y$. Intuition requires all three quantities to be continuous over the elements' boundaries. This requirement can impossibly be achieved in every point along the edges of the element with only twelve degrees of freedom. The element is called "non-conforming".

Nevertheless, non-conforming elements produce results that are often far superior to the results obtained with conforming elements. Theoretical explanations for this observation are not always as obvious. ZIENKIEWICZ [48, Chap. 11] makes a general statement that non-conforming elements do not have to follow the energy bounds inherent to perfectly continuous formulations, and that the non-conforming model has a greater freedom to take up the best shape. Effective use of non-conforming elements may be somewhat tricky, demanding a good amount of intuition. The user may convince himself of the consistency of an element's behaviour by verifying whether it passes the patch test [48, Chap. 11].

Two examples of non-conforming elements are presented in fig.4.3. MORLEY [108] developed a six-noded triangular plate bending element (fig.4.3, left). Six degrees of freedom are prescribed, displacement w at the corners and normal slope $\partial w/\partial n$ at the midsides. Both elements provide increased potentials of accuracy. The rectangular element on the right hand side is used in two-dimensional plane stress analysis.

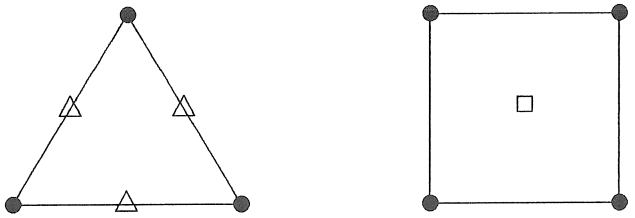

Figure 4.3: Two examples of non-conforming elements

Each corner has two translational degrees of freedom, and one internal node has two rotational degrees of freedom.

4.2.1.2.3 Hybrid elements

The traditional finite element formulation employs displacement quantities to describe the state of deformation of a structure, including the states of stress and strain, which are derived from displacements. Continuity is guaranteed on a displacement basis, stresses and strains are generally not continuous over adjacent elements' boundaries. Equilibrium is violated.

The conventional displacement formulation of the finite element method results from the principle of minimum potential energy :

$$\delta\Pi = \int_{\Omega} \sigma_{ij}\, \delta\varepsilon_{ij}\, d\Omega - \int_{\Omega} f_i\, \delta u_i\, d\Omega - \int_{\Gamma_p} \overline{p}_i\, \delta u_i\, d\Gamma = 0$$

Π : potential energy
$\delta\varepsilon_{ij}$: virtual strain distribution
δu_i : virtual displacement field

with introduction of constraints on Γ_u :

$$\delta\Pi' = \delta\Pi - \int_{\Gamma} \delta p_i (u_i - \overline{u}_i)\, d\Gamma$$

where δp_i are virtual reactions on Γ_u.

A so-called dual formulation or mixed approach works exactly the inverse way. This technique starts from approximations of the state of stress that explicitly obey equations of equilibrium in every element.

The dual approach requires the minimization of complementary energy :

$$\Pi_c = \int_\Omega \mathcal{B}(\sigma_{ij}) d\Omega - \int_{\Gamma_u} p_i \overline{u}_i \, d\Gamma + \int_\Omega \left(\frac{\partial \sigma_{ij}}{\partial x_j} + f_i \right) u_i \, d\Omega$$

where $\mathcal{B}(\sigma_{ij})$ represents elastic stress energy density. δu_i act as weighting functions in the minimization of the term between brackets, thus expressing internal equilibrium. The displacements are introduced as Lagrangian constraints in energy formulations. Finally an additional term is introduced :

$$\Pi_c' = \Pi_c + \int_{\Gamma_p} (p_i - \overline{p}_i) u_i \, d\Gamma$$

Many types of energy formulations exist [48, Chap. 12]. Each of them is used in specific situations where constraints on internal equilibrium and continuity over elements' interfaces are imposed.

The earliest equilibrium element for plane stress-strain analysis is described by FRAEYS DE VEUBEKE in 1963 [109]. A constant stress field is assumed inside each triangular element. On each side a two-component vector is defined that is associated with the displacements of a centrally placed node (fig.4.4). Displacements are constant over

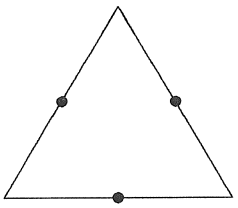

Figure 4.4: Hybrid element by FRAEYS DE VEUBEKE

the full length of the side on which they are defined. Thus, in a global sense, displacement is discontinuous.

SARIGUL and GALLAGHER [110] present a family of rectangular elements for two-dimensional elasticity with an increased accuracy of stress prediction. JIROUSEK [111] presents a new element with adjustable accuracy. It has an arbitrary polygonal form with a fixed number of degrees of freedom at the corner nodes and an optional number of degrees of freedom at the mid-side nodes. This is variant to the p-line mesh refinement technique.

A more thorough investigation of mixed formulations reveals that most of the elements designed originally as hybrid elements can be obtained also in a non-conforming formulation. In general hybrid elements thus have characteristics and capabilities that are closely related to those of non-conforming elements. They are particularly useful in analysis of complex stress fields. Only few commercial codes have libraries that contain hybrid or non-conforming elements. Their use is mainly confined to very special applications, most often in academic spheres.

4.2.1.3 Computational aspects

The elements that are contained in the library of a finite element code are characterized by a fairly simple relation between internal forces and deformation. These relations differ for each particular type of element but they are unique. The constitutive relations are determined once and for all. Probably many hundreds of types of elements have been developed throughout the last three or four decades. Many types are used very often, e.g. simple beams and plates, other elements are designed for use in very peculiar situations. The general shape of the stiffness matrices being constant, they depend only on the coordinates of the nodes of the element. The individual matrix coefficients may be expressed easily in terms of the coordinates. All the element stiffness matrices are assembled in the global stiffness matrix by routines that locate the degrees of freedom of the model that are connected to each other. The global stiffness matrix has a band structure and it is symmetrical. Although the size of the full matrix may be vast, only those coefficients that are different from zero are stored, thus reducing the memory and disc space that are required.

4.2.1.4 Comments on the use of the method

A number of practical aspects and recommendations are given concerning the construction of the model and the selection of computational options. It must be kept in mind that stress analysis imposes some stringent requirements. It is very hard to give some precise numbers on the shape of the mesh but some general principles should be mentioned :

- the use of two-dimensional or three-dimensional elements of a general continuous type is mandatory in areas of high stress gradients. Simple beam or plate elements are not suitable unless the areas of maximum stress are distant from geometrical concentrations.
- in areas of high stress gradients the mesh is extremely dense in each direction, in both or all three directions tangential to and perpendicular to the notch.
- the aspect ratio of any element does not exceed 3, i.e. the dimensions of an element along each of its local axes are comparable.
- the use of quadratic or higher order elements is compulsory, since linear elements seriously underestimate peak values of stress and strain.
- the geometrical shape of the element corresponds very closely to the actual geometry of the structure.
- triangular or tetrahedral elements are not used if stresses are to be computed in those elements.
- the local axes of the elements are oriented more or less along the principal stress and strain trajectories.
- the transition between small elements in highly stressed areas and bigger elements in less critical areas is smooth.

4.2.2 The boundary element method

Basic concepts of boundary integral formulations are known for a very long time already. Mathematical expressions are quite complex, however, and their evaluation requires powerful hardware. Only by the end of the seventies, research was directed towards the development of commercial codes. A limited number of packages are available nowadays. Industrial practice does not yet widely apply boundary element principles. A number of big companies invest in the development of their own software that is suited for their specific needs.

Boundary integral formulations may seem to be abstract and inaccessible to a novice. Closer consideration of the mathematical development quickly reveals the opportunities for accurate stress analysis.

4.2.2.1 Basic features

The boundary integral formulation of static elastic problems is developed in section A.2. The indirect formulation is more generally valid and can be extended easily to other applications. The direct formulation is more straightforward and intelligible to the intuition of a stress engineer. The equation that is essential to the whole approach is due to SOMIGLIANA [112] :

$$\begin{aligned} c_{ij}u_j(\underline{\xi}) &= \int_\Gamma u^*_{ij}(\underline{\xi},\underline{x})p_j(\underline{x})\,d\Gamma(\underline{x}) - \int_\Gamma p^*_{ij}(\underline{\xi},\underline{x})u_j(\underline{x})\,d\Gamma(\underline{x}) \\ &+ \int_\Omega u^*_{ij}(\underline{\xi},\underline{x})f_j(\underline{x})\,d\Omega(\underline{x}) \end{aligned} \tag{4.3}$$

where : $\underline{\xi}$: coordinates of the field point
$\underline{x}$: coordinates of the integration point
Ω : domain of the body
Γ : boundary of the body
$u_j(\underline{x})$: displacement in j-direction at point $\underline{x}$
$p_j(\underline{x})$: traction in j-direction at point $\underline{x}$
$f_j(\underline{x})$: volume force $[N/m^3]$ in j-direction at point $\underline{x}$
$u^*_{ij}(\underline{\xi},\underline{x})$: fundamental solution for displacement
: (equation A.8-A.9)
$p^*_{ij}(\underline{\xi},\underline{x})$: fundamental solution for traction
: (equation A.8-A.9)
c_{ij} : constant value $(0 \leq c_{ij} \leq 1)$ depending on
: the location of $\underline{\xi}$ with respect to Ω and Γ

These equation express relations between the displacements u_i and the traction p_i. These quantities appear only in the integrals on the boundary Γ. Even if body forces are present, the field of unknowns that has to be solved for is restricted to the boundary.

Section A.3 elaborates on the numerical implementation of this formulation. The introduction of discretizations and numerical integration leads to a matrix notation :

$$[H]\{u\} = [G]\{p\} + [V]\{f\} \tag{4.4}$$

where : $[H]$: matrix of influence coefficients for displacements
$[G]$: matrix of influence coefficients for tractions

$[V]$: matrix of influence coefficients for volume forces
$\{u\}$: vector of displacements at collocation points
$\{p\}$: vector of tractions at collocation points
$\{f\}$: vector of volume forces at nodes of volume model

In each direction i at each collocation point $\underline{\xi}$ either the displacement $u_i(\underline{\xi})$ or the traction $p_i(\underline{\xi})$ is imposed. The other quantity is unknown and has to be solved for. In the context of dynamic computations the load consists of inertial forces that are distributed over the entire volume of the structure. These loads are known from previous computations. The equations 4.4 are rearranged such that all the unknown quantities, tractions p_i or displacements u_i, are grouped together in one vector $\{x\}$. All the other terms together with the terms from $[V]\{f\}$ are gathered on the right hand side :

$$[A]\{x\} = \{y\} \tag{4.5}$$

where : $[A]$: system matrix of influence coefficients
$\{x\}$: column vector of unknowns
$\{y\}$: right hand side column vector of known quantities

The matrix $[A]$ depends on geometry, material properties, type of boundary conditions. It does not vary with load $\{f\}$. Only the right hand side vector $\{y\}$ varies with load $\{f\}$. Successive load vectors $\{y\}$ are handled easily by inversion of the system matrix $[A]$:

$$\{x\} = [A]^{-1}\{y\}$$

This equation is merely a symbolic representation of the actual mathematical operations that are performed. Matrix $[A]$ is not inverted explicitly, matrix reduction schemes are used to solve for the unknowns.

Some remarks should be made on how the influence of inertial forces is introduced in equation 4.4. Recollecting the third term on the right hand side of equation 4.3 :

$$\int_\Omega u^*_{ij}(\underline{\xi}, \underline{x}) f_j(\underline{x})\, d\Omega(\underline{x}) \tag{4.6}$$

The procedure for evaluating these integrals is described in section A.3. Two important remarks concern the subdivision of the domain Ω into volume cells. It is related to the way volume forces are defined

over the domain. Only discrete values of inertial forces are computed, either in the nodes of the experimental model, either in the nodes of the analytical model.

A limited number of nodes are usually sufficient to represent the modal deformations of a structure. Analytical mode shapes obtained by finite element analysis often provide superfluous data as the mode shape components are computed in more nodes than strictly necessary. There is no need to use acceleration data at nodes located inside the volume of the structure since they do not vary through the thickness of the structure. Definition of values on the surface provide sufficient information about what is happening inside the volume. Linear interpolation is used for intermediate nodes. Volume forces are represented by a vector $\{f\}$ of limited dimension. Appropriate shape functions are used.

The nodes of the volume model Ω do not have to coincide with the nodes of the boundary model Γ. Both integrals are totally independent, and this provides the stress engineer with the freedom of defining a volume model that is completely different from the structural boundary model. The volume model may be much coarser than the boundary model.

An example may be clarifying. Consider the first lateral bending mode of a clamped T-plate (fig.4.5). The plate is thin, so the volume is merely an expansion of a two-dimensional figure. Volume integrals are two-dimensional multiplied with a constant thickness. Figure *a* shows the geometry of the structure, *b* shows the finite element model used for computing resonance frequencies and mode shapes, *c* is the structural boundary element model, *d* is the volume model. The dashed box in figure *a* is neglected for a while. The first lateral bending mode of the structure is characterized by significant deformation in the vertical part of the "T". The horizontal part behaves more like mass, whereas its contribution to the global stiffness is limited. The finite element mesh *b* is dense in the vertical part and it is coarse in the horizontal part. The structural model *c* is constructed such that it is capable of computing stresses in the critical areas, i.e. the mesh is finer in the corners than it is along the straight edges. Inertial loads are most important in the horizontal part but their variation is close to linear. One four-noded element 1 conveys sufficient information about the distribution of inertial loads in the horizontal part of the "T". The

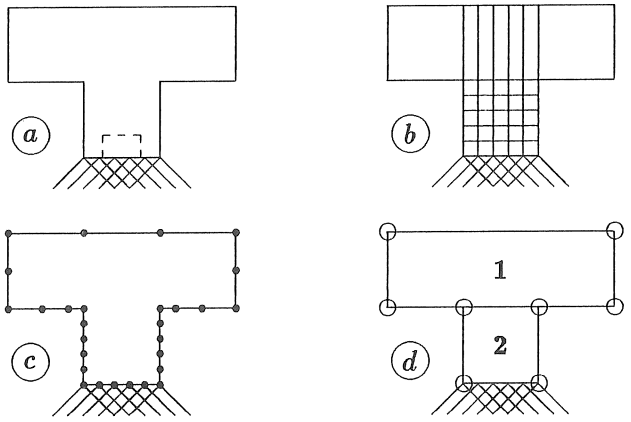

Figure 4.5: Models of clamped T-plate

second element **2** adds very little to the overall load represented in the right hand side of equation 4.5. It is remarkable that the nodes of the the volume elements **1** and **2** do not coincide. There is no reason why the volume model should cover the whole structure. Some parts may be uncovered or covered multiply, provided the overall distribution of inertial forces is close to reality. The same volume model can be used for a T-structure with an opening, represented by the dashed box in geometrical model *a*. The finite element model and the boundary element model must of course be modified.

After the basic equations 4.5 are solved values of stresses and strains are obtained by postprocessing. Stresses and strains are computed only on a node per node basis, i.e. they are computed only in those points that are required by the user. Two separate ways of computing stresses are feasible, depending on the location of the point of interest.

For points located inside the volume of the structure equation 4.3 is derived with respect to coordinates x_i and x_j, and these derivatives are introduced into HOOKE's law. Details are given in section A.4. The structure is considered to be continuous, and unlike finite element computations this procedure yields continuous stress distributions.

For points located on the boundary another procedure is followed. Stress and strain quantities are computed merely from local values. Displacements and tractions are known in the collocation points of the particular element. Shape functions define these quantities in in-

termediate points on the element. Strains are obtained by derivation of displacements, and again HOOKE's law is used. Surface tractions have to be taken into account too. Consider a point $\underline{\xi}$ located on a four-noded linear surface element parallel to the xy-plane (fig.4.6). Displacements $u_i^{(j)}$ and tractions $p_i^{(j)}$ are known in each of the nodes

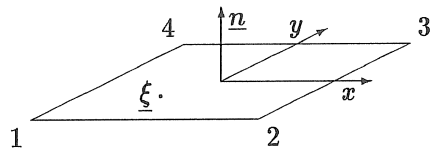

Figure 4.6: Four-noded linear surface element

$(i = 1, 2, 3; j = 1, 2, 3, 4)$:

$$u_i(\underline{\xi}) = \sum_{j=1}^{4} \varphi^{(j)}(\underline{\xi}) u_i^{(j)} \qquad p_i(\underline{\xi}) = \sum_{j=1}^{4} \varphi^{(j)}(\underline{\xi}) p_i^{(j)}$$

$$\begin{aligned} \varepsilon_{ij}(\underline{\xi}) &= \frac{1}{2}\left(\frac{\partial u_i}{\partial x_j} + \frac{\partial u_j}{\partial x_i}\right)_{\underline{x}=\underline{\xi}} \\ &= \frac{1}{2}\sum_{k=1}^{4}\left(\frac{\partial \varphi^{(k)}}{\partial x_j} u_i^{(k)} + \frac{\partial \varphi^{(k)}}{\partial x_i} u_j^{(k)}\right)_{\underline{x}=\underline{\xi}} \end{aligned}$$

Derivatives of shape functions are evaluated in the point of interest. For the stresses one obtains :

$$\begin{array}{lllll} \sigma_{xx} & = & \sigma_{11} & = & \frac{1}{1-\nu}\left[\nu p_3 + 2G(\varepsilon_{11} + \nu\varepsilon_{22})\right] \\ \sigma_{yy} & = & \sigma_{22} & = & \frac{1}{1-\nu}\left[\nu p_3 + 2G(\varepsilon_{22} + \nu\varepsilon_{11})\right] \\ \sigma_{zz} & = & \sigma_{33} & = & p_3 \\ \tau_{xy} & = & \sigma_{12} & = & 2G\varepsilon_{12} \\ \tau_{yz} & = & \sigma_{23} & = & p_2 \\ \tau_{zx} & = & \sigma_{13} & = & p_1 \end{array}$$

where : G : shear modulus
ν : POISSON coefficient

Several types of shape functions can be used. Commercial codes incorporate constant, linear and quadratic elements. The shape functions

for displacements and tractions may generally be different. Although this is not a strict requirement, it may be preferable to take the functions for tractions of one order less than those for the displacements. Obviously best results are obtained with quadratic elements. Other types of shape functions yield discontinuous stress distributions over the element boundaries.

4.2.2.2 Enhanced capabilities

The boundary element method presents some capabilities that the finite element method does not offer. Some of them are inherent to the basic boundary integral formulation while some others need a little more development.

A peculiar feature of the boundary integral formulation concerns the domain of integration. Infinite or semi-infinite regions are handled exactly the same way finite domains are treated. Green's theorem converts volume integrals to boundary integrals. Geometries with internal boundaries are handled easily even though their domains extend to infinity. Construction of a finite element model for such cases is difficult since the whole domain has to be covered. One should take care that the elements are followed in the correct sense of rotation, i.e. internal elements should be oriented in a clockwise sense when outward elements are oriented in a counter clockwise sense. MINDLIN developed special fundamental solutions for semi-infinite problems that are bounded by a straight line or a plane [113]. These functions automatically take into account the effect of the geometry being infinite.

Another case where special fundamental solutions have to be used is anisotropy. The starting boundary integral equation can be represented as before (eq.4.3) on condition that the elastic constants for the fundamental problem be the same as those in the actual problem. JOHN [114], VOGEL and RIZZO [115], and SYNGE [116] have arrived at an integral representation for the fundamental three-dimensional displacements. BREBBIA summarizes their conclusions [171, Chap. 5].

A particularly interesting feature is the development of discontinuous elements. It is mentioned earlier that constant shape functions can be used. It is proved that derivatives of the displacement are transferred from the approximate to the second loading function marked with * in section A.2. This produces discontinuities in displacements between elements which do not invalidate the convergence of the tech-

nique. The concept of constant elements is extended to a whole family of discontinuous elements. They are characterized by standard shape functions of first, second and higher orders and their nodes are located inside the elements. A constant and a quadratic element are shown in fig.4.7.

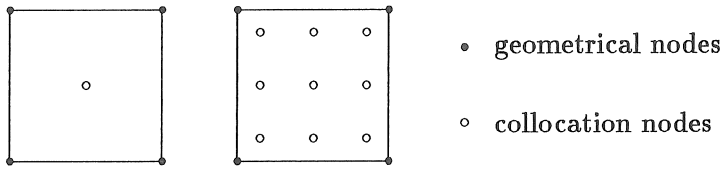

Figure 4.7: Constant and quadratic discontinuous surface elements

It should be noted that geometrical shape functions may be different from approximate functions for tractions and displacements. The functions for the unknowns should be of the same or higher order than the geometrical functions in order to satisfy rigid body type conditions. The constant element violates this requirement, but nevertheless it yields very good results. Another advantage of discontinuous elements is that different shape elements can be more easily combined since there are no continuity conditions between elements. Two examples of possible meshes are shown in fig.4.8. In both cases geometrical shape

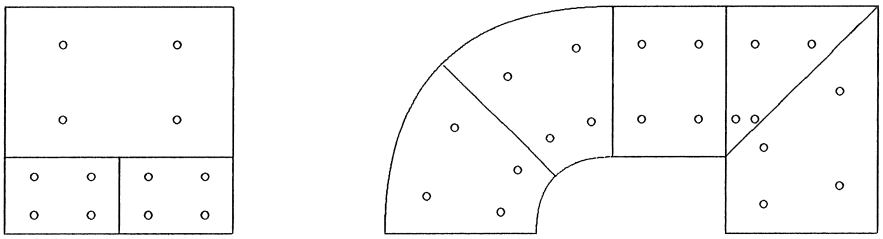

Figure 4.8: Examples of allowable linear surface meshes

functions and approximate functions are linear. The only requirement for discontinuous elements is that the surface of the structure is fully covered. These elements are of interest for problems in which the variation of displacement or traction is discontinuous between elements. The convergence of these elements is remarkably fast in many cases.

In a recent publication, RANK presents adaptive h-, p- and hp- versions for boundary integral element methods. These schemes optimize

the boundary element mesh for improved performance.

4.2.2.3 Computational aspects

Reasons of limited computational power have impeded the early breakthrough of boundary element software. Intensive computational efforts are needed in order for the matrices $[H]$, $[G]$ and $[V]$ (eq.4.4) to be constructed. They all involve the evaluation of quite complex integrands over the entire boundary Γ or the complete domain Ω. The major point of difficulty is the occurrence of singularities in the integrand. Depending on the type of analysis and on the matrix that is constructed, functions like $\ln r$ or negative powers r^{-n} $(n = 1, 2, 3)$ appear in the integrand. For elements that contain the collocation point of interest these functions tend to infinity. Techniques of moving the collocation points away from the boundary [118] render the integrands non-singular, but the resulting set of equations 4.5 may become ill-conditioned. Appropriate transformations of the integration domain are necessary in order to eliminate the singularity. The author developed a particular transformation that splits a two-dimensional element in four sub-elements, as represented in fig.4.9. A quadratic or higher

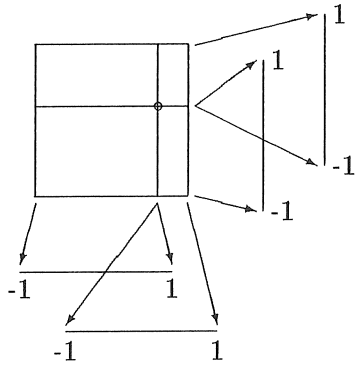

Figure 4.9: Transformation of integration domain

order transformation is defined such that the Jacobian produces the correct power of zero in the numerator that eliminates the singularity.

Explicit integration is generally not possible. Standard gaussian quadrature schemes are used [171, App. A]. Some improved schemes that take into account the effect of singularities may also be utilized.

The matrices are constructed by repetitive evaluation of boundary or domain integrals. Evaluation of volume integrals is more time consuming since they are one degree higher than boundary integrals. The size of the $[V]$ matrix is generally more reduced than that of the $[H]$- and $[G]$- matrices which are square.

4.2.2.4 Comments on the use of the method

In this section a number of practical aspects and recommendations are given concerning the construction of the model and the selection of computational options.

- the structure must be sufficiently massive. The ratio of the highest dimension to the lowest dimension must not exceed 10. In case it does, e.g. in beam-like structures, it must be subdivided in separate zones. After the influence matrices are computed for each zone successively, they are all grouped in one big system matrix.

- structures that contain several types of materials with different characteristics must also be subdivided in a number of zones.

- the order of quadrature formulas is chosen to be about 4 or 5. Only for the computation of stresses in internal points that are located close to the boundary higher order integration should be used.

- the use of discontinuous elements is always recommended. Apart of their extremely fast rate of convergence they have the added advantage that different shape elements can be more easily combined. They also eliminate the problems that are encountered in corners [119].

- geometric shape functions may be linear, whereas the approximate functions should at least be quadratic for the displacements and linear for the tractions. Lower order functions are not capable of describing the variation of stress within an element in a sufficiently accurate manner. Lower order approximate functions are allowable only where stresses at the boundary should not be computed and only stresses inside the volume are relevant. DEB and BANERJEE [120] show that quartic elements are more

reliable in accuracy than quadratic and cubic elements without being necessarily more expensive.

- the discretization of the volume may be coarse. Linear shape functions are usually capable of representing the variation of inertial loading in a sufficiently accurate manner.

4.2.3 Comparison of the boundary element method to the finite element method

The previous sections illustrate some of the characteristics of the finite element method and the boundary element method. The next four sections 4.2.3.1 to 4.2.3.4 compare both methods to each other. Advantages and drawbacks of both methods are commented on, from a practical point of view, from a computational point of view and also in relation to the required accuracy.

4.2.3.1 The preprocessing phase

The most intensive and time consuming phase in the development of a model regards the efforts that are needed for an accurate construction of the geometrical model. Both methods require an adequate description of the geometry of the boundary of the body. In the finite element method an additional discretization of the volume is needed. A finite element mesh is quite obviously much more complex than a boundary element mesh since the latter does not care about the interior of the structure. However, next to the structural boundary model a volume model of the interior of structure is constructed. It is stated repeatedly that this model can be coarse. A finite element model must not be coarse because it is to represent the structural behaviour.

Several techniques are used nowadays to facilitate the preprocessing task as much as possible. Most commercial software packages contain some sort of automatic mesh generators, for two-dimensional and even for three-dimensional modelling. Recently, research attention is paid to solid modelling. Some finite element companies have adopted a philosophy of defining every model in terms of solids. Particularly for stress analysis this is obviously a necessity. Consequently powerful modelling tools are developed that help the stress engineer in constructing a model. Practical experience shows that these procedures do not yet run in a particularly smooth way. The definition of

a model of a somewhat complex structure still is a troublesome task, and again, it is much more reduced in boundary element applications.

4.2.3.2 The continuous representation of geometry

The finite element method discretizes the volume of the structure. The structural model of the boundary element method comprises only a discretization of the boundary. The volume is implicitly considered as a continuous medium. This has some consequences on the computation of stresses and strains in points inside the volume. The boundary element method uses values of tractions and displacements on the entire boundary of the structure, whereas the finite element method uses data of the element around the point of interest. The modelling of body force terms occurs in different manners in both distinct techniques. It is explained thoroughly in section 2.3.2.2 how the boundary element method uses a continuous representation of inertial forces. The finite element method explicitly discretizes the distributed volume load to a number of discrete point loads.

4.2.3.3 The size of the matrices

The size of the matrices is determined by the number of degrees of freedom of the models. For a typical three dimensional analysis each finite element node has three degrees of freedom and each boundary element node has six degrees of freedom of which only three are unknown. The total number of degrees of freedom of a finite element model is clearly much higher than the number of degrees of freedom of a boundary element model. Practical experience has shown that in order to obtain comparable accuracy of results the number of nodes of a boundary element model may be lower than the number of boundary nodes in a finite element model. The size of the square matrices $[H]$ and $[G]$ (equation 4.4) is typically an order of magnitude lower than the size of the $[K]$ matrix (eq.4.1).

The contents of the matrices $[K]$ on the one hand and $[H]$ and $[G]$ on the other hand are completely different. The matrices $[H]$ and $[G]$ are fully populated and non-symmetrical. With a well considered mesh and numbering of the nodes the matrix $[K]$ is a band matrix. It is always symmetrical. The disc space that is needed to store the non-zero elements of the $[K]$- matrix may be much smaller than the

space for storing $[H]$ and $[G]$. The situation is a little different when the domain of the structure is subdivided in zones. Each zone has its own elementary $[H]$- and $[G]$- matrices and they are assembled to global matrices. These global matrices do contain zero elements, and they exhibit some kind of band structure, but they are not symmetrical. The nature of the system matrix, $[K]$ in finite elements, $[A]$ in boundary elements, determines the algorithm that should be used for solving the set of equations. The reduction of the symmetrical banded matrix $[K]$ requires only a fraction of the computational effort needed for matrix $[A]$.

4.2.3.4 Variables of mixed type

The traditional formulation of the finite element method uses displacement components as independent degrees of freedom. All quantities of stress and strain are computed from these data. Procedures of numerical differentiation give strains which are subsequently converted to stresses. Extrapolation of strains at Gauss-points to the edges of the element often underestimates the real values. Some problems of accuracy may arise concerning the values obtained by postprocessing. The margin of error on computed values increases with each supplementary operation. As one is interested in the values of strains, care should be taken as to establish confidence in the results that are obtained.

The boundary element method uses displacements and tractions as independent degrees of freedom. Differentiation of displacements is no longer necessary for the determination of strains at locations inside the volume. For points located on the boundary differentiation still is needed. However, boundary values are processed immediately and no extrapolation is necessary. Stress gradients that characterize stress concentrations are estimated accurately.

Hybrid elements in finite elements have capabilities that are similar to those of the boundary element method. Variables of mixed type occur next to other allowing for a particularly accurate determination of stresses and strains with a rather coarse model.

4.2.4 Example

An example illustrates the concepts that are mentioned in the previous sections. The stress concentration near an eccentric hole in a rotor disc

is analysed (fig.4.10). Only a quarter disc is considered. The geometrical characteristics and the material properties are indicated in table 4.1. The disc rotates at 6000 *rpm*, the material of the disc is loaded

material			geometry			
E	=	70 GN/m^2	rotor :	inner diam.	=	50 mm
ν	=	0.3		outer diam.	=	210 mm
ρ	=	2700 kg/m^3	hole :	diam.	=	25 mm
				eccentricity	=	87.5 mm

Table 4.1: Geometrical and material properties of rotor disc

by a centrifugal load $\rho\omega^2 r$, varying with radius from 53.3 MN/m^3 at the inner diameter to 223.8 MN/m^3 at the outer diameter.

This example is selected to allow comparison with analytical data that are provided in a paper by PAPE and BANERJEE [121]. Two particular values of stress are computed : tangential stress σ_{nom} at the inner edge of the disc, far away from the eccentric hole, and tangential stress σ_{max} at the outer edge of the eccentric hole. Stress concentration factor K_t is defined as the ratio of the latter to the former :

$$K_t = \frac{\sigma_{max}}{\sigma_{nom}}$$

Two models are constructed, they are both designed to produce acceptable accuracy on the stress values in the areas of interest. Fig.4.10a shows the finite element mesh, 4.10b the boundary element mesh, 4.10c the volume element mesh, and 4.10d the plot of iso-lines of equivalent VON MISES-stress. The finite element code SYSTUS is used, the elements are eight-noded quadrilaterals. The boundary element mesh consists of thirty three-noded discontinuous line elements. The volume mesh consists of two four-noded quadrilaterals with linear shape functions in the inertial loads. The results of both computations together with some data on the performances of both methods are summarized in table 4.2.

The obtained values of the stress concentration factors K_t are very close, compared to the analytical value. It is noticed however that the finite element method consistently underestimates peak values of stress.

The volume model can be represented in a more simplified yet accurate way, using a polar coordinate system. The variation of inertial

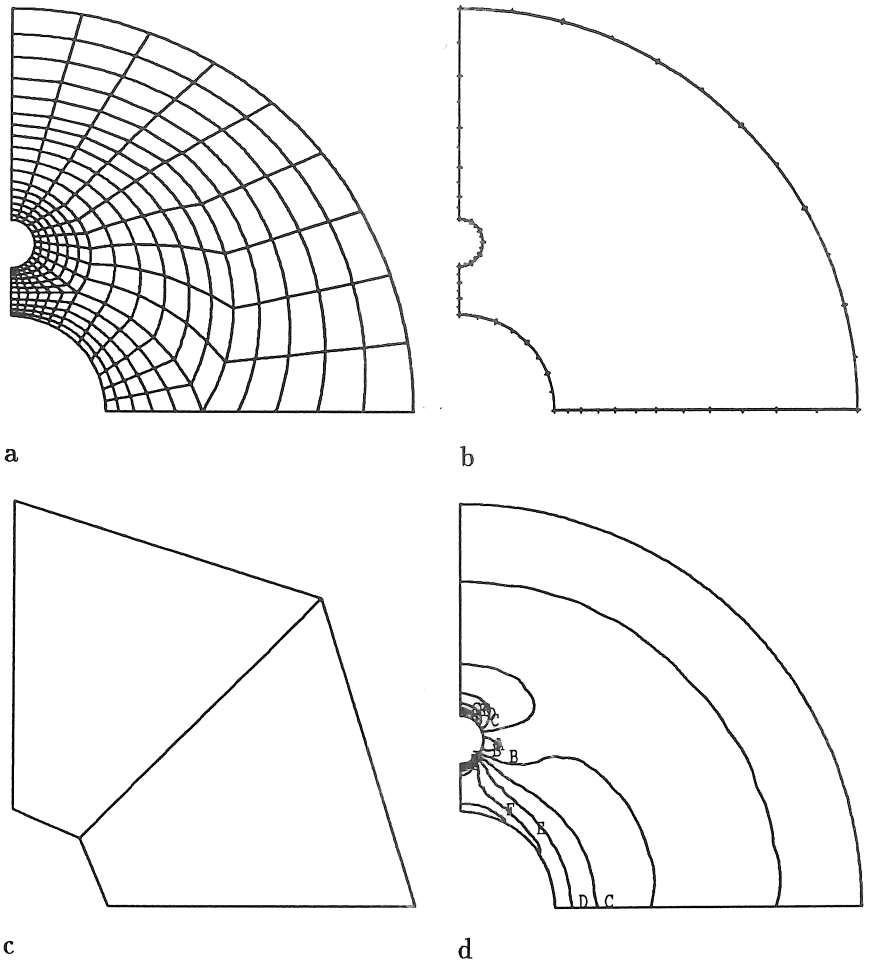

Figure 4.10: Models and stress distribution of rotor disc

	FE	BE
model preparation time (min)	48	5
preprocessing time (sec)	17.0	4.2
computation time (sec)	173	91
no. of degrees of freedom	1644	180
storage space ($kByte$)	564	260
nominal stress σ_{nom} $[MN/m^2]$	34.8	36.7
maximum stress σ_{max} $[MN/m^2]$	67.4	71.4
K_t-factor [-]	1.94	1.94

Table 4.2: Performance of FE and BE method on rotor disc

loads is then described by a constant-linear element. Inertial loads do not vary in the tangential direction. The shape function in the radial direction is linear, while the shape function for the tangential direction is constant By the way, it is worth mentioning here that a centrifugal type of loading can be handled in a pure boundary integral formulation using particular integrals [121].

4.3 Use of the boundary element method in elastic dynamic analysis

In the process of fatigue life assessment of a structure the dynamic stress response has to be determined. It is shown in the previous sections why the boundary element method offers some particularly interesting features for accurate computation of global stress patterns and stress concentrations. It still has to be investigated whether the method of modal representations is most appropriate. This section presents some techniques that use boundary integral formulations in the analysis of the dynamic behaviour of the structure.

4.3.1 Time dependent integral formulation

For the purpose of simplified representation, the displacement equation of motion is written :

$$\left(C_1^2 - C_2^2\right) \frac{\partial^2 u_i}{\partial x_i \partial x_j} + C_2^2 \frac{\partial^2 u_j}{\partial x_i \partial x_i} + \frac{1}{\rho} f_j = \frac{\partial^2 u_j}{\partial t^2} \qquad (4.7)$$

where : u_i : displacement in i-direction
f_i : volume load in i-direction
ρ : mass density
C_1, C_2 : material constants

C_1 and C_2 have the dimensions of velocity :

$$C_1 = \sqrt{\frac{\lambda + 2\mu}{\rho}} \qquad C_2 = \sqrt{\frac{\mu}{\rho}}$$

λ and μ are the LAMÉ-constants :

$$\lambda = \frac{E\nu}{(1+\nu)(1-2\nu)} \qquad \mu = G = \frac{E}{2(1+\nu)}$$

Combinations of the fundamental point source solution of equation 4.7 with the dynamic extension of BETTI's reciprocal theorem [122] leads to :

$$c_{ij}u_i(\underline{\xi}, t) = \int_\Gamma \left[U^*_{ij}(\underline{x}, t, \underline{\xi}) * p_i(\underline{x}, t) - P^*_{ij}(\underline{x}, t, \underline{\xi}) * u_i(\underline{x}, t)\right] d\Gamma(\underline{x})$$

It is assumed that initial displacements and velocities are zero. The fundamental solutions U^*_{ij} and P^*_{ij} are the displacements and tractions in point $\underline{x}$ at time t, resulting from a unit impulse of the form $\delta(t)$ at point $\underline{\xi}$. These functions do not only depend on the distance r between points $\underline{x}$ and $\underline{\xi}$, but also on time t. Mathematical expressions were proposed by ERINGEN and SUHUBI. They are listed in [123]. The operator $*$ denotes time convolution.

Since volume loads f_i are supposed to be nonexistent, this method is not applicable in dynamic analysis. This formulation can be extended to dynamic problems, at the cost of still more complex computations.

A time-stepping algorithm similar to that in section 1.4.1 is used. The time axis is discretized :

$$t_N = \sum_{n=1}^{N} n\Delta t$$

where Δt is the time step and t_N the total time. Both displacements and tractions are assumed to vary during a time step according to a

certain law that is defined in advance. This procedure is similar to the way geometrical variations of quantities are expressed by shape functions. Expressing the operation of convolution explicitly gives :

$$c_{ij}u_i(\underline{\xi}, t_m) = \int_\Gamma \left[\int_0^t U_{ij}^*(r, t_m - \tau) * p_i(\underline{x}, \tau)\, d\tau - \int_0^t P_{ij}^*(r, t_m - \tau) * u_i(\underline{x}, \tau)\, d\tau \right] d\Gamma(\underline{x}) \qquad (4.8)$$

This equation 4.8 expresses a linear relation between displacements and tractions at time t_m and all previous time steps t_{m-1}, ..., t_1. The coefficients that occur in this relation are computed by numerical integration. A generalised matrix equation is established now, that expresses the time convolution procedure :

$$[H]^{(1)}\{u\}^{(m)} + [H]^{(2)}\{u\}^{(m-1)} + \ldots + [H]^{(m)}\{u\}^{(1)} = [G]^{(1)}\{p\}^{(m)} + [G]^{(2)}\{p\}^{(m-1)} + \ldots + [G]^{(m)}\{p\}^{(1)} \qquad (4.9)$$

The matrices $[H]^{(i)}$ and $[G]^{(i)}$, and the vectors $\{u\}^{(j)}$ and $\{p\}^{(j)}$ have the same meaning as in equation 4.4, except that they vary with time. The superscripts pertain to the time step i, j. At time step i all quantities $i-1, \ldots, 1$ are known and the influence matrices $[H]^{(i)}$ and $[G]^{(i)}$ are computed. The procedure that is followed is then similar to the procedure used for static problems :

$$[A]\{x\}^{(i)} = \{y\}^{(i)} + \{z\}^{(i)}$$

where : $[A]$: system matrix
$\{x\}^{(i)}$: unknown tractions and displacements at time i
$\{y\}^{(i)}$: right hand side vector at time i
$\{z\}^{(i)}$: contribution of previous time steps $i-1, \ldots, 1$

The unknowns at time t_i are computed based on information about tractions and displacements at previous time steps $t_{i-1}, \ldots, t_1$. While the vectors $\{y\}^{(i)}$ and $\{z\}^{(i)}$ have to be computed all over again for each successive time step, only one matrix inversion takes place.

The time stepping nature gives the method the potential to tackle piecewise non-linear problems, a potential that is absent in the transform approaches. It requires only surface discretization, it accounts

for boundaries that extend to infinity and it is an unconditionally stable time-marching algorithm. The computation of successive influence matrices $[H]^{(1)}, [H]^{(2)}, \ldots, [G]^{(1)}, [G]^{(2)}, \ldots$ is extremely tedious. This statement is particularly relevant when higher order shape functions are used for spatial and temporal variation. Use of lower order functions reduces accuracy.

4.3.2 Transform formulations

In order to overcome the inadequacies of the time dependent formulation some authors propose transform formulations. AHMAD and BANERJEE [125] obtain the solution for the transient dynamic problem by first solving it in the Laplace domain and then performing the numerical inversion. Laplace transformation of equation 4.7 gives :

$$\left(C_1^2 - C_1^2\right) \frac{\partial^2 \mathcal{U}_i}{\partial x_i \partial x_j} + C_2^2 \frac{\partial^2 \mathcal{U}_j}{\partial x_i \partial x_i} + \frac{1}{\rho}\mathcal{F}_j - s^2 \mathcal{U}_j + s u_j^{(0)} + v_j^{(0)} = 0$$

where uppercase letters indicate transformed variables :

$$\mathcal{U}_i(\underline{x}, s) = \mathcal{L}[u_i(\underline{x}, t)] \qquad \mathcal{F}_i(\underline{x}, s) = \mathcal{L}[f_i(\underline{x}, t)]$$

and the initial velocity $v_j^{(0)}$ together with the initial displacement $u_j^{(0)}$ can be grouped with $\mathcal{F}_j$ in a modified body force term :

$$\mathcal{Q}_j = \mathcal{F}_j + \rho\left(s u_j^{(0)} + v_j^{(0)}\right)$$

Expressions for the fundamental solutions are developed by CRUSE and RIZZO [124] and are listed in [125, App. II]. $\mathcal{U}_{ij}^*$ and $\mathcal{P}_{ij}^*$ are the displacements and tractions at $\underline{x}$ resulting from a unit harmonic force of the form e^{-sT} at $\underline{\xi}$. These fundamental solutions have modified BESSEL functions embedded in them. The transformed dynamic boundary integral statement for the transformed internal displacements is written :

$$\begin{aligned} c_{ij}(\underline{\xi})\mathcal{U}_j(\underline{\xi}, s) &= \int_\Gamma \mathcal{U}_{ij}^*(r, s)\mathcal{P}_j(\underline{x}, s)\, d\Gamma - \int_\Gamma \mathcal{P}_{ij}^*(r, s)\mathcal{U}_j(\underline{x}, s)\, d\Gamma \\ &+ \int_\Omega \mathcal{U}_{ij}^*(r, s)\mathcal{Q}_j(\underline{x}, s)\, d\Omega \end{aligned} \tag{4.10}$$

Equation 4.10 gives rise to the classical boundary element equations which can be solved for a series of values of the transform parameter

s. Once this is done for a sufficient numer of values of the transform parameter, numerical inversion must be performed on the relevant variables. The boundary integral can also take account of internal viscous dissipation of energy. This is accomplished by replacing the elastic parameters of LAMÉ λ and μ by their complex counterparts λ^* and μ^* :

$$\lambda^* = \lambda(1 + 2j\zeta) \qquad \mu^* = \mu(1 + 2j\zeta)$$

with ζ the damping ratio. The same remarks that are made in section 3.3.3 apply here. Inversion of the solution in the Laplace domain is inefficient in this context.

Fourier transformations are used in the determination of resonance frequencies and natural modes of vibration. The same way of reasoning is adopted except that the Laplace parameter s is replaced by $j\omega$, that there are no initial conditions and that there is no body force term :

$$\begin{aligned} c_{ij}(\underline{\xi})\mathcal{U}_j(\underline{\xi},\omega) &= \int_\Gamma \mathcal{U}^*_{ij}(r,\omega)\mathcal{P}_j(\underline{x},\omega)\,d\Gamma - \int_\Gamma \mathcal{P}^*_{ij}(r,\omega)\mathcal{U}_j(\underline{x},\omega)\,d\Gamma \\ &+ \int_\Omega \mathcal{U}^*_{ij}(r,\omega)\mathcal{Q}_j(\underline{x},\omega)\,d\Omega \end{aligned} \tag{4.11}$$

As before, equations 4.11 are solved for a sufficient number of values of frequency ω and the variable $\mathcal{U}_j(\underline{x},\omega)$ is inverted to obtain the time dependent displacement $u_j(\underline{x},t)$. A direct consideration of the magnitudes of $\mathcal{U}_j(\underline{x},\omega)$ for different values of ω gives the natural modes of the body. A repeated computation of the influence matrices $[H(\omega)]$ and $[G(\omega)]$ is necessary and for each of them a separate system matrix is constructed. A separate matrix reduction has to be performed for each frequency. Resonance frequencies are characterized by peak values in the transfer function. Since the complete set of equations has to be reassembled and solved for each frequency, the procedure is very time consuming.

4.3.3 Nardini's method

The main disadvantage of the method of Fourier transformation for determining natural modes is that the analysis cannot be transformed into an algebraic eigenvalue problem because the fundamental solution is itself frequency dependent. NARDINI and BREBBIA present an alternative procedure [126]. Their approach is more straightforward

as it reduces the problem of free vibrations to an algebraic eigenvalue problem.

The static Kelvin fundamental solutions u^*_{ij} and p^*_{ij} (equations A.8 - A.9) are adopted instead of the frequency dependent ones. Inertial forces inevitably appear in the integral formulation. Not only the boundary but also the domain needs to be discretized, unless the volume integrals can be transformed to boundary integrals :

$$\begin{aligned} c_{ij}(\underline{\xi})\mathcal{U}_j(\underline{\xi},\omega) &= \int_\Gamma u^*_{ij}(r)\mathcal{P}_j(\underline{x},\omega)\,d\Gamma - \int_\Gamma p^*_{ij}(r)\mathcal{U}_j(\underline{x},\omega)\,d\Gamma \\ &+ \rho\omega^2 \int_\Omega u^*_{ij}(r)\mathcal{U}_j(\underline{x},\omega)\,d\Omega \end{aligned} \tag{4.12}$$

NARDINI approximates the internal displacement amplitudes :

$$\mathcal{U}_j(\underline{x},\omega) = \sum_{k=1}^{N} \alpha_j^{(k)} q^{(k)}(\underline{x}) \tag{4.13}$$

where : $\mathcal{U}_j(\underline{x},\omega)$: amplitudes of motion at frequency ω
$q^{(k)}(\underline{x})$: approximate functions $(k = 1, \ldots, N)$
$\alpha_j^{(k)}$: unknown coefficients

The volume integral in equation 4.12 becomes :

$$\int_\Omega u^*_{ij}\mathcal{U}_j\,d\Omega = \sum_{k=1}^{N} \alpha_j^{(k)} \int_\Omega u^*_{ij} q^{(k)}\,d\Omega$$

It is the objective that the domain integral is converted to a boundary integral. The procedure to achieve this is similar to the technique used in standard static analysis. The functions $q^{(k)}$ are associated to fields of displacements $\psi_{lj}^{(k)}$ and corresponding stress fields $\sigma_{ljm}^{(k)}$ such that :

$$\frac{\partial \sigma_{ljm}^{(k)}}{\partial x_m} = \delta_{lj} q^{(k)}$$

where δ_{lj} represents the Kronecker δ. The tractions on the boundary are computed from :

$$p_{lj}^{(k)} = \sigma_{ljm}^{(k)}$$

Equation 4.12 is then written :

$$c_{ij}\mathcal{U}_j + \int_\Gamma p^*_{ij}\mathcal{U}_j \, d\Gamma - \int_\Gamma u^*_{ij}\mathcal{P}_j \, d\Gamma = \rho\omega^2 \sum_{k=1}^{N} \alpha_l^{(k)} \left(-c_{ij}\psi_{lj}^{(k)} + \int_\Gamma u^*_{ij} p_{lj}^{(k)} \, d\Gamma - \int_\Gamma p^*_{ij}\psi_{lj}^{(k)} \, d\Gamma \right) \quad (4.14)$$

Discretization is done in the standard form, the boundary integrals that correspond to the inertia term only include known expressions and can be computed numerically. The same shape functions already adopted to interpolate $\mathcal{U}_j$ and $\mathcal{P}_j$ are used to represent the boundary variation of $\psi_{lj}^{(k)}$ and $p_{lj}^{(k)}$. The same standard matrices $[H]$ and $[G]$ are obtained. If the total number N of functions $q^{(k)}$ is chosen to be the number of nodal points, the unknown coefficients $\alpha_l^{(k)}$ (equation 4.13) are obtained as functions of the boundary displacement amplitudes in the form :

$$\{\alpha\} = [Q]^{-1}\{\mathcal{U}\}$$

where : $\{\alpha\}$: vector of coefficients α
$[Q]$: matrix containing the values of $q^{(k)}$ at the nodes
$\{\mathcal{U}\}$: vector of boundary displacement amplitudes

NARDINI claims that this procedure produces accurate results, despite the approximation in the inertia. The choice of the functions $q^{(k)}$ is not always as trivial as it is in the examples that are given. Literature provides little evidence of good results obtained with this method.

4.3.4 Method based on modal parameters

It is shown why boundary element formulations present superior capabilities for static stress analysis. Many of those advantages turn into disadvantages when dynamic analyses have to be performed because of the occurrence of the volume integral. Several methods are presented that deal with these complications.

The most efficient way to analyse the dynamic behaviour of a structure is the use of modal analysis principles. Boundary element methods are not particularly suited for determining modal parameters whereas the finite element method provides some very powerful capabilities. A pragmatic approach joins the best of both techniques, by modelling the dynamic behaviour with a finite element model and performing

the stress computation in a boundary element model. The approach of combining two separate models is acceptable because they are both very simple.

For the purpose of quick and easy postprocessing of strain data, a time domain approach offers most advantages. Strain response is computed directly with equation 3.17.

4.3.4.1 Description of inertial loads

A finite element model of the structure is constructed. It should meet the following requirements :

- the full structure has to be modelled, or at least a part that is totally independent from the rest of the structure as far as its dynamic behaviour is concerned

- distribution of mass and stiffness : beam and plate elements are appropriate for describing the dynamic behaviour of the structure, rather than two-dimensional or three-dimensional volume elements. Addition of lumped mass and the use of isolated springs are permitted. The influence of mass and stiffness preponderates over the influence of geometry. A well-designed equivalent model is sometimes much more useful than a model that accurately represents the structure's geometry.

- connections to environment : the definition of constraints should match the actual situation. A number of degrees of freedom should be fixed, depending upon whether the structure is free, hinged, clamped, ... When the structure is in a free-free condition, a numerical shift on the eigenvalues must be introduced in an appropriate way. Hinges that possibly occur in the structure must be modelled accurately.

- frequency band of interest : computed resonance frequencies should lie in a frequency band that is sufficiently wide and that comprises all lower order frequencies. The coarseness of the mesh is determined by the "wavelength" of the modes. The distance between two successive nodes of the highest mode of vibration that is considered should comprise at least three or four nodes.

A number of sets of modal parameters are found as a results of the eigenvalue computation. Damping values have to be measured separately. The modes of vibration are generally expressed in terms of displacements or rotations. Multiplication of these quantities by the square of the resonance frequency and by the mass density of the material expresses the mode shapes in terms of translational and angular accelerations.

4.3.4.2 The concept of modal strains

The mode shape components that occur in equation 3.17 may be expressed in any type of variable. Since subsequent analysis essentially employs strain data, strains are most appropriate for representing mode shapes. Computation of response immediately yields strains at the areas of interest.

Conversion of conventional mode shapes to modal strains is rather critical however. Section 3.2.2.1 shows how very sensitive the spatial strain distribution is to modal parameters. An original technique is presented there for computing modal strains in an accurate way. The superior capabilities of the boundary element method are used to their full benefit. Two distinct models are constructed :

- a boundary model expresses the relation between the local structure's deformation external loading : it must be capable of describing the state of stress and deformation in the areas close to the point of interest. There is no need for the model to encompass the entire structure. Only a restricted area should be included in the model.
- a volume model describes the variation of inertial loads over the structure.

4.3.4.2.1 Restriction of analysis to critical areas

This section shows why the boundary element analysis does not need to include areas of the structure that are distant from the area of interest. An example clarifies this idea. Consider a notched beam vibrating at its lowest resonance frequency (fig.4.11). The critical area in this beam obviously is located at the notch, and modal strains have to be computed at that point. The state of stress and strain at the critical area is governed only by the state of deformation in the material

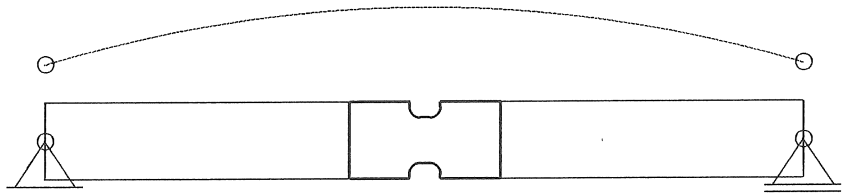

Figure 4.11: Notched beam vibrating at 1^{st} resonance frequency

that surrounds it. The analysis is largely simplified if only the zone with the thicker lines is included in the analysis.

The restricted domain is indicated by Ω and its boundary is denoted Γ, Ω^* being the entire domain and Γ^* its boundary. The strain distribution that corresponds to mode shape ψ and resonance frequency ω is sought, only in the restricted domain Ω. The governing equations are :

$$\begin{array}{ll} \text{equilibrium :} & \frac{\partial \sigma_{ij}}{\partial x_j} + \rho\omega^2\psi_i = 0 \quad \forall \underline{x} \in \Omega \\ \text{boundary conditions :} & \begin{cases} u_i = \overline{u}_i & \forall \underline{x} \in \Gamma_u \\ p_i = \overline{p}_i & \forall \underline{x} \in \Gamma_p \end{cases} \\ \text{boundary tractions :} & \sigma_{ij} n_j = p_i \quad \forall \underline{x} \in \Gamma \end{array}$$

It will be discussed later what the particular boundary conditions are or should be. The distinction between Γ_u and Γ_p will be explained as well. The values $\overline{u}_i$ are the amplitudes of motion of the considered mode shape $\overline{u}_i = \psi_i$. The equations are fulfilled in an approximative sense by a weighted residual formulation :

$$\int_\Omega \left(\frac{\partial \sigma_{ij}}{\partial x_j} + \rho\omega^2\psi_i \right) u_k^* \, d\Gamma = \int_{\Gamma_p} (p_k - \overline{p}_k) u_k^* \, d\Gamma + \int_{\Gamma_u} (\overline{u}_k - u_k) p_k^* \, d\Gamma \qquad (4.15)$$

The weighting functions are chosen to be equal to the KELVIN fundamental solutions for static elastic stress analysis of an infinite body (equations A.8 - A.9). Integrating by parts twice and regrouping terms leads to :

$$-\int_\Omega \frac{\partial \sigma_{jk}^*}{\partial x_j} u_k \, d\Omega = \int_\Omega \rho\omega^2 \psi_k u_k^* \, d\Omega + \int_{\Gamma_u} p_k u_k^* \, d\Gamma$$

$$+\int_{\Gamma_p} \overline{p}_k u_k^* \, d\Gamma - \int_{\Gamma_u} \overline{u}_k p_k^* \, d\Gamma - \int_{\Gamma_p} u_k p_k^* \, d\Gamma \qquad (4.16)$$

The particular choice of weighting functions eliminates the volume integral on the left hand side of equation 4.16 :

$$\frac{\partial \sigma_{jk}^*}{\partial x_j} = -\Delta_k \quad \Rightarrow \quad -\int_\Omega \frac{\partial \sigma_{jk}^*}{\partial x_j} u_k \, d\Omega = c_j u_j$$

The weighted residual formulation 4.15 is converted to SOMIGLIANA's identity A.10. The formulation 4.16 that results is nothing else but the conventional boundary element relation. The boundary conditions still have to be defined. In other words, the parts Γ_u and Γ_p still have to be defined. Theoretically displacements are known throughout the entire body Ω^* and thus also on the body Ω. As the modal model is coarse, the general shape of deformation is close to correct. However, significant discrepancies may occur locally. It is therefore unwise to impose deformations obtained for Γ^* to the entire boundary Γ. It was shown in section 3.2.2.1 that spatial strain distribution is much more sensitive to imposed displacements than it is to imposed loading. It is thus preferable to make the part Γ_p of the boundary as large as possible, and to limit the part Γ_u to what is strictly necessary. In any case, the part Γ_p should include those parts of the boundary Γ that belong to the free surface. As to the rest of the boundary $\Gamma - \Gamma^*$ where the body Ω is attached to the remainder of Ω^*, the choice depends on the availability of data :

- if stress resultants are known at these sections, they should be imposed as $\overline{p}_k$. This is usually the case when the finite element model comprises elements of the family of beams or shells. Due to the principle of DE SAINT-VENANT, the stress distribution under the imposed stress resultants has only little importance, provided the section is distant from the considered point where strains are computed. Still, it is necessary to assign a few points to the part Γ_u, only to avoid rigid body movements and make the system matrix non-singular.

- if stress resultants are not known at sections belonging to $\Gamma - \Gamma^*$, which may occur with some types of elements or when only experimental mode shapes are available, displacements have to be imposed $u_k = \overline{u}_k$. This is a rather critical operation, since the

strain distribution is extremely sensitive to imposed displacements. Minor changes of $\overline{u}_k$ introduce significant modifications of strains. Extreme care should be taken that boundary conditions are modelled correctly.

The principle of restricting strain analysis to a limited part $\Omega + \Gamma$ of the entire body $\Omega^* + \Gamma^*$ is particularly interesting when cases of large and complex domains are encountered. Only one or maybe a few small sections of the structure need to be modelled.

4.3.4.2.2 Practical aspects

A number of practical aspects should be considered thoroughly when preparing the boundary element model. A number of stringent requirements should be met :

the structural model

- it coincides closely with the actual geometry
- the mesh is sufficiently dense
- the use of quadratic or higher order elements is compulsory
- in case the aspect ratio of the domain is too high, the domain is subdivided in zones

the volume model

- it does not need to accurately represent geometrical details of the structure
- the mesh can be very coarse
- linear or sometimes constant shape functions are acceptable
- a small number of elements is sufficient

4.3.4.3 Smoothing techniques

The procedure developed in section 3.2.2.1 smooths the mode shapes. The smoothing process has to be performed in order for the strain data to be reliable. The internal states of stress and deformation are computed from forces rather than from displacements. When only a restricted area of the domain is considered for the determination of

modal strains, the correct boundary conditions have to be imposed. Particular care must be taken that the displacements on the boundary Γ_u are introduced correctly. Not only translational but also rotational degrees of freedom have to be taken into account.

4.4 Computation of the effects of plasticity

Fatigue phenomena always involve a certain amount of plastic deformation. The cyclic nature of the load induces effects of plasticity much earlier than a static type of loading. Even when cyclic load is not excessively high and the corresponding macroscopic stress does not exceed yield limit, some grains of the material experience plastic deformation.

An engineering approach employs macroscopic stresses rather than microscopic stresses which are largely unpredictable. Fatigue phenomena are classified roughly in two categories. High-cycle fatigue corresponds to long lives (10^7 - 10^8 cycles) and is characterized by stresses that remain essentially in the elastic domain. Low-cycle fatigue (10^3 - 10^4 cycles) corresponds to short lives and is characterized predominantly by plastic deformation on a macroscopic level. In intermediate areas, effects of plasticity may also be significant. The question whether the effects of plasticity should be taken into account in fatigue analysis still remains unanswered. In case the answer is positive stress analysis must be able to compute plastic deformations. In a well-designed structure effects of plasticity occur only very locally. The overall behaviour of the structure remains linear. As to the local aspects of stress and strain computation, the analysis is no longer linear, thus gravely complicating numerical procedures.

4.4.1 Use of the finite element method

The general formulation in finite element terminology remains unchanged :

$$[K]\{u\} = \{F\} \tag{4.17}$$

The difference consists in the dependence of the material's stiffness on load. The matrix $[K]$ is no longer constant, it is a function of displacements $\{u\}$. In the formulation of the principle of virtual work this dependence is expressed by the term due to the virtual work of

the internal stresses :

$$\frac{1}{2}\int_{\Omega}[B][D]^t[B]\,d\Omega$$

where the matrix $[D]$, that expresses the relation between stress and strain, is not constant. Several types of constitutive equations exist, depending on the behaviour of the material itself and on the type of loading. Some relations express stress in terms of strain, others express strain in terms of stress.

The dependency of stiffness $[K]$ on displacements $\{u\}$ causes the problem to be non-linear. The set of equations 4.17 has to be solved using iterative techniques. The solution procedure depends on how the matrix $[D]$ relates stress to strain. The computation of plastic deformation can only be done by splitting the load path into a number of intervals. Small load increments are imposed successively and at each step the stiffness is evaluated. Solution of the set of equations gives displacements and subsequent computation of strains allows an estimation of stiffness for the next interval.

Due to the non-linearity of the problem an incremental approach has to be adopted. An iterative procedure is employed usually, since the initial stress rates are unknown at the outset.

Computation of the stress and strain in case of plastic deformation is obviously very time consuming. Yet it is feasible for fairly simple geometries with only a limited number of degrees of freedom, for load histories that are relatively short in time, and when the plastic area is not too vast.

4.4.2 Use of the boundary element method

The key element of boundary integral methods is the use of fundamental solutions. The expressions of the fundamental solutions, either for the KELVIN-type (equation A.8 - A.9), or for the MINDLIN-type [113], are developed once and for ever. They are used essentially for elastic deformations. The coefficients of the material's constitutive equations, YOUNG's modulus E and POISSON's coefficient ν are implicitly supposed to be constant. In the region of plastic deformation, the material's stiffness varies with applied load, and so the fundamental solution can no longer be used. The boundary element method in its original form is not valid any more. BREBBIA presents a modified formulation [171, Chap. 6] that is very much similar to the elastic

one (equation A.10). A volume integration of the initial stress rate seriously complicates mathematical operations.

4.4.2.1 Coupling with the finite element method

A very elegant approach that is receiving considerable attention in recent years is the coupling of the finite element method with the boundary element method [127]. The basic idea behind it is very simple : one portion of the structure is discretized in a conventional finite element model and the remainder is modelled using boundary elements. The edges where both parts of the structure are attached, are included in the boundary element model.

In a sense the part of the domain that is modelled with a boundary element mesh can be considered as one large superelement. Each of those superelements have a corresponding generalized stiffness matrix that expresses the relation between loads on the boundary and displacements. An expression for the stiffness matrix is derived, starting from the traditional boundary integral discretization :

$$[H]\{u\} = [G]\{p\}$$

Premultiplying both sides with the non-singular matrix $[G]^{-1}$:

$$[G]^{-1}[H]\{u\} = \{p\} \tag{4.18}$$

Vector $\{p\}$ describes the variation of tractions on the boundary of the structure. They are distributed over the boundary. In the conventional displacement formulation, finite element methods use only discrete point forces. Distributed tractions are converted to point forces using shape functions $[N]$. Transformation of tractions to point forces is expressed by the matrix $[M]$:

$$\{F\} = [M]\{p\}$$

Introducing this into equation 4.18 leads to :

$$[M][G]^{-1}[H]\{u\} = [\tilde{K}]\{u\} = \{F\}$$

Unlike stiffness matrices in conventional finite element approaches the matrix $[\tilde{K}]$ is generally not symmetrical. The non-symmetrical part of $[\tilde{K}]$ is removed by the definition of $[K]$:

$$[K] = \frac{1}{2}\left([\tilde{K}] + [\tilde{K}]^t\right)$$

Matrix $[K]$ is used instead of $[\tilde{K}]$ as stiffness matrix for the superelement. Although this process of symmetrization introduces errors, all authors consider this operation to be necessary. Firm justification gives evidence of this operation. Following quite different approaches, GEORGIOU [128] and ZIENKIEWICZ [129] obtain the same result.

Coupling both methods is very useful in the analysis of plasticity. The entire domain is subdivided such that the areas where plastic deformation occurs are modelled with finite element models and the areas that remain in an elastic state are modelled with boundary models. Such a procedure uses the capabilities of both methods in the best possible combination.

4.4.2.2 Banerjee's technique involving particular integrals

This paragraph briefly discusses a technique developed by BANERJEE [130] that employs the concept of particular integrals. It is mentioned to illustrate the wide variety of techniques that are presented in literature. Each of those methods can be used in particular applications.

The governing differential equation for incremental elastoplasticity is expressed in terms of incremental displacement $\dot{u}_i$ as :

$$\begin{aligned} \mathcal{L}(\dot{u}_i) &= (\lambda+\mu)\frac{\partial^2 \dot{u}_j}{\partial x_j}\partial x_i + \mu\frac{\partial^2 \dot{u}_i}{\partial x_j}\partial x_j \\ &= \frac{\partial \dot{\sigma}_{ij}^{(0)}}{\partial x_j} \\ &= \left(D^e_{ijkl} - D^{ep}_{ijkl}\right)\dot{\varepsilon}_{kl} \end{aligned}$$

where : $\dot{\sigma}_{ij}^{(0)}$: initial stress rate
λ, μ : constants of LAMÉ
$\dot{\varepsilon}_{kl}$: total strain rate
D^e_{ijkl} : elastic constitutive tensor
D^{ep}_{ijkl} : elastoplastic constitutive tensor

The solution of this equation is represented as the sum of a complementary function $\dot{u}_i^c$ that satisfies the homogeneous equation and a particular integral $\dot{u}_i^p$ that satisfies the inhomogeneous equation. As to the complementary function the differential equation is similar to

the case of elastostatics, mutatis mutandis :

$$c_{ij}(\underline{\xi})\dot{u}_i^c = \int_\Gamma u_{ij}^*(\underline{x},\underline{\xi})\dot{p}_i^c \, d\Gamma - \int_\Gamma p_{ij}^*(\underline{x},\underline{\xi})\dot{u}_i^c \, d\Gamma$$

Different fundamental solutions from the ones presented in equations A.8 - A.9 have to be used now. The particular integral is expressed in terms of a fictitious tensor density $\dot{\phi}_{ij}(\underline{\xi})$ as an infinite series using a global shape function $C(\underline{x},\underline{\xi})$. Details can be found in [130]. Obviously, this method demands extremely high computational effort. Although the authors present some results of fair accuracy, future perspectives are not very promising, because of the high degree of complexity.

4.4.3 Estimation of plastic deformation using elastic analysis

NEUBER establishes a theoretical relation between stress and strain in the vicinity of geometrical concentrations [30]. He studies the complicated behaviour of stress and strain in a notched prismatical body subjected to pure shear (fig.4.12).

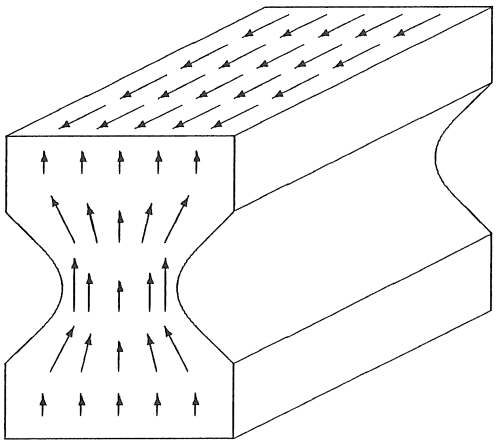

Figure 4.12: Model of prismatic notch effect

The only non-zero component of the stress tensor is shear stress τ. The corresponding value of shear strain is sought. The general law of the material's deformation is denoted :

$$F = F(\tau)$$

with the restricting condition :

$$\lim_{\tau \to 0} F(\tau) = \tau$$

The solution for the stress function is represented by a superposition of two conformal mappings. The lines of constant warping and the lines of constant stress are orthogonal. The stress trajectories are shown on fig.4.12. Equilibrium of stresses is expressed on the edges of an elementary curvilinear square. Next to the Hookian elastic stress concentration factor, stress and strain concentration factors are defined :

$$K_t^\sigma = \frac{\tau_{max}}{\tau_{nom}} \qquad K_t^\varepsilon = \frac{\gamma_{max}}{\gamma_{nom}}$$

NEUBER observes :

$$\begin{aligned} F > \tau \quad &\Rightarrow \quad K_t^\varepsilon > K_t > K_t^\sigma \\ F < \tau \quad &\Rightarrow \quad K_t^\varepsilon < K_t < K_t^\sigma \end{aligned}$$

and he derives that there exists a function, which is neither stress nor strain, but a certain combination of both with the quality, that its concentration factor has the same value for all stress–strain laws. Consequently this function, which NEUBER calls the "leading function" $L(\tau)$, must be equal to the Hookian stress concentration factor. A final relation is obtained :

$$L(\tau) = \sqrt{\tau . F(\tau)}$$

or, stated alternatively :

$$K_t = \sqrt{K_t^\varepsilon . K_t^\sigma}$$

The leading function is the geometrical mean value of stress and deformation. In a general state of uniaxial stress, the most useful formulation of this approximation provides a relation between local or real and nominal stress and strain quantities :

$$\sigma_{real}\varepsilon_{real} = E(K_t\varepsilon_{nom})^2 \frac{(K_t\sigma_{nom})^2}{E}$$

In conjunction to the constitutive law of the material this rule allows the determination of real stress and real strain at the location of the stress concentration. The direct computation of plastic stress

and strain quantities is no longer necessary. An elastic computation is sufficient. It is however imperative that the factor K_t is determined accurately. In the plastic domain, a small increase of the stress concentration factor corresponds to a much more important increase of local strain. It is shown in the next chapter that the influence on fatigue life is even more important.

4.5 Conclusion

This chapter describes some important techniques that are used in numerical stress and strain analysis. The boundary element method is selected because of its superior capabilities of accuracy. Although conventional wisdom rejects the method when volume loads are important, it is well suited in an application of computing modal strains quickly and accurately.

The finite element method is best known. It is shown how discretisation of the domain leads to a set of equations that the unknown displacements can be computed from. Strains are found by numerical differentiation of displacements. This procedure may considerably underestimate peak values of strain at locations of high stress gradients, unless an extremely dense mesh is used. Unlike the conventional displacement formulation, the dual formulation employs rather coarse meshes to obtain fair estimations of stress and strain. Non-conforming elements also offer improved capabilities.

The boundary element method is essentially very different. The accuracy of stress concentrations is improved significantly with respect to the finite element method. This is due to the fact that displacements and tractions appear next to each other in the discretized equations. Another advantage is the simplicity of the boundary element model, even when volume loads have to be taken into account. Computational aspects on the other hand are more demanding.

As to the dynamic effects of strain response, the use of boundary integral formulations is less evident than it is in cases of elastostatics. The methods that are presented in literature are rather complex and their areas of application are limited. An original concept of modal strains is presented. In combination with an efficient dynamic response computation, it leads to an accurate and quick computation of strain history.

Plastic computations are reviewed very briefly. Existing methods are extremely demanding, because of the high degree of complexity and because of a non-negligible computational effort. A more pragmatic approach uses linear analysis.

Chapter 5

Estimation of fatigue lifetime

5.1 Introduction

This chapter discusses the ultimate step in the fatigue analysis procedure. Postprocessing of the computed or measured strain response finally gives an estimation of lifetime. The local strain approach is well established as a powerful tool in fatigue life assessment.

The first section discusses why the local strain approach is useful in fatigue life prediction of notched mechanical structures. The basic features of the method are reviewed briefly and it is shown how the different steps fit into the global approach. An accurate determination of material characteristics is essentially important, and some remarks on this matter are given. In order for the analysis of consecutive cycles to be reliable yet not excessively expensive, appropriate preprocessing of strain data is necessary. Some relevant techniques are developed that are complementary to the well known "rainflow" method. The local strain approach handles cases of plasticity in a very elegant way. The background of this technique is described thoroughly.

The local strain approach is developed essentially for problems of uniaxial fatigue. Cases where the state of stress and strain is biaxial or sometimes even triaxial are much more complex. A wide variety of techniques and numerical models are presented in literature. Their use is computationally extremely demanding. A more pragmatic approach can be used in a majority of problems of engineering practice.

A third section deals with how the local strain approach is used in practice. Its relevance with respect to experimental data is discussed and some major factors that influence the accuracy of the computed result are mentioned. Finally it is shown how the fatigue life prediction model is tuned based on experimental data.

5.2 Local strain approach

The local strain approach is used to predict the number of cycles a component can be subjected to before it fails. Distinction is made here between the number of cycles to crack initiation and the crack propagation rate. The assumption of absence of initial flaws is valid in a wide range of applications. It is assumed explicitly that no initial cracks occur. The computed fatigue life is the number of cycles to initiation of a flaw. For all types of the structures mentioned in section 2.2.1.1 the major portion of the life is consumed in the initiation phase.

5.2.1 Basic features

In a well-designed component the gross deformations are related to the applied loads in a linear-elastic manner. The overall state of stress and strain is mainly elastic while some local areas may exhibit plastic straining. Suppose that a strain measurement is done in the notch, where the strains are highest. If plastic deformation occurs at the notch, the local strain history is qualitatively similar to the load history, but the two are not proportional. The non-linearity between stress and strain causes strain to increase much faster than stress, even under overall load-deflection behaviour which is linear elastic. The local strain approach relates the fatigue life of a structure to cyclic strain rather than to cyclic stress. A measured strain sequence that is enforced upon an unnotched axial test specimen subjects the material to the same accumulation of damage as the original component. The life of a notched specimen is expected to be equal to that of an unnotched specimen if failure is defined in both as a common small crack size.

The basic features of the local strain approach are described in section 1.3.2.2. It is divided into two principal steps. First the local stress and strain must be predicted, and, second, the life resulting from these sequences must be estimated. The first step is most difficult and

time-consuming as it requires specific handling of the complex non-linear relationships between load, strain and stress.

The local strain approach is designed to be a valuable engineering tool in the analysis and design of real-life mechanical structures. The main reason why it is so effective is the fact that it relies only on experimental data that are case-independent. It provides a rational basis for accounting for interactions among material behaviour, geometry, and load history. Only the material characteristics have to be evaluated experimentally. This consists entirely of data that are obtained from laboratory specimens. This is a major advantage for components which can not be tested conveniently. The measured material behaviour together with the influence of geometry and the load sequence produce the local strain sequence which is characteristic to the accumulation of damage. This is possible only because the real material's situation of stress and strain is compared to the situation that occurs in an unnotched specimen. The use of notched component data necessitates a wide variety of conditions to cover all possibilities. This feature of the local strain method allows to define sensitivity coefficients of the computed life to several parameters. The influence of each parameter can be investigated separately. Life predictions that are based on local strain and that result to be somewhat far removed from the actual component can be corrected for by modifying input parameters appropriately. This suggests that local strain fatigue analysis should be used in conjunction with any available component test results or service history information.

5.2.2 Material properties

The material's characteristics are the only data that have to be determined experimentally. Extreme care must be taken when the relevant quantities are being measured. The accuracy they are evaluated with is a critical factor to the success of the local strain fatigue analysis. Section 1.5.2 summarises the major factors that influence the validity of an experiment.

5.2.2.1 Cyclic properties of the material

It is observed experimentally that the cyclic material's constitutive law deviates considerably from the monotonic relation. An experimental

law is found to be most representative :

$$\varepsilon = \frac{\sigma}{E} + \left(\frac{\sigma}{K'}\right)^{\frac{1}{n'}} \tag{5.1}$$

where : ε : local strain amplitude
σ : local stress amplitude
E, K', n' : material constants

Equation 5.1 defines a relation between the amplitudes of stress and strain during cyclic loading. A material is said to exhibit a MASING-description when the hysteresis loops are described by the cyclic stress–strain -curve magnified by a factor of two. This relation emerges as the critical element of life prediction based on local notch behaviour. It is important simply because no reasonable estimate of local notch behaviour can be made without considering both stress and strain.

Extensive research efforts have been made in the investigation of different material's behaviour. WINTER [131] studies the behaviour of a simply supported flat circular aluminum plate under reversed cyclic central loads. He finds ample evidence of the serious errors that are induced in the theoretical prediction of cyclic strain range when using the monotonic stress–strain -curve. The extreme complexity encountered in obtaining a valid model is due to the wide variety of materials that are used and to the fact that each material behaves differently.

Two types of transient cyclic stress–strain behaviour occur in virtually all metals :

- cyclic hardening or softening : it is generally sufficient to know simply the stable stresses and strains which prevail during most of the fatigue life. The notch is subjected to a type of loading that is similar to the way the unnotched specimen is strained. It is agreed that in points that are located close to but not in the notch the material's behaviour may not be considered negligible, as stress and strain distributions are affected only in a minor way. For engineering metals which exhibit an extreme degree of cyclic hardening or softening, such as annealed austenitic stainless steels, some caution is advisable.

- creep or relaxation : both aspects occur simultaneously during plastic deformation at notches. Whereas the mean strain is governed by the surrounding elastic material, relaxation of mean

> stress is generally more important. This phenomenon can be studied only when material creep data are measured independently. A more pragmatic approach computes the life twice, once with accounting for mean stress, which is considered not to relax, and once with neglecting the influence of mean stress. The more conservative result is probably acceptable, if at all there is a difference.

More refined methods are presented, that take into account every peculiarity of the material behaviour. MILLER [132] presents a technique where the work-hardening coefficient K' is made a function of the stress at reversal of a cycle. The author claims that an improved simulation of normal and anomalous BAUSCHINGER-effects is thus possible. The physical relevance of the presented modifications is discussed in terms of annihilation of dislocation loops and decreases in dislocation density.

Two classes of materials are identified. Some materials do not follow a MASING-type description. JHANSALE and TOPPER [133] propose an approach for describing the loop shapes of a non-MASING material. Carbon low alloy steel ASTM A-516 GR 70 for instance shows positive peaks of the half-life hysteresis loops that do not fall on a monotonically increasing unique curve [134]. Most technical materials however do obey the MASING-relation within reasonable margins of error. ELLYIN has also investigated the effect of tensile mean strain on cyclic properties of the above mentioned material [135]. The effect of relaxation seems to be significant. For a cyclic strain amplitude that was kept constant and a mean strain varying from 0 to 6 %, there is quite a noticeable mean stress relaxation during the softening phase. After one hundred cycles the mean stress drops to 30 % of its initial value whereas after one thousand cycles it reaches to about 10 % of its initial magnitude. The rate of mean stress relaxation is greater for higher values of mean strain.

5.2.2.2 Strain–life -relation

It is clear for quite a long time already that phenomena of high cycle and low cycle fatigue are essentially different. For each of both cases fair approximations are proposed that relate the number of cycles to failure to load amplitude, either in terms of stress or in terms of strain. Fatigue behaviour in the high cycle region is governed by quantities like

yield strength and ultimate stress. The state of deformation is grossly elastic. In the low cycle area the material ductility preponderates. It is the merit of the local strain approach that both phenomena can be handled in a global approach. Strain amplitude is related to the number of cycles via :

$$\frac{\Delta\varepsilon}{2} = \frac{\sigma'_f}{E} N^b + \varepsilon'_f N^c \tag{5.2}$$

where : $\frac{\Delta\varepsilon}{2}$: strain amplitude
σ'_f : fatigue strength coefficient
b : fatigue strength exponent
ε'_f : fatigue ductility coefficient
c : fatigue ductility exponent

An alternative approach relates the number of cycles to failure to the total absorbed plastic strain energy [134]. During a high strain low cycle fatigue test most of the irrecoverable plastic strain energy is dissipated as heat. The plastic strain energy per cycle ΔW is the area of the hysteresis loop. The energy per cycle is found by evaluation of the integral :

$$\Delta W = \int_{\varepsilon\nearrow} \sigma \, d\varepsilon - \int_{\varepsilon\searrow} \sigma \, d\varepsilon$$

For MASING-type of materials :

$$\begin{aligned} \Delta W &= \left(\frac{1-n'}{1+n'}\right) \Delta\sigma \Delta\varepsilon^p \\ &= 4\sigma'_f \varepsilon'_f \left(\frac{c-b}{c+b}\right) N^{b+c} \end{aligned}$$

Each material has the capacity to dissipate a certain amount of energy, and when this limit is attained cracks propagate and failure results. In most cases the hysteresis loops stabilize after a few cycles and thus the strain energy per cycle can be assumed to be constant during the fatigue life. ΔW being the plastic strain energy per cycle, the total accumulated energy at failure W_f is obtained by multiplication with the number of cycles N_f :

$$W_f = 4\sigma'_f \varepsilon'_f \left(\frac{c-b}{c+b}\right) N_f^{1+b+c} \tag{5.3}$$

Non-MASING behaviour suggests that the proportional stress range in the linear region is not constant but increases with the size of the loop. JHANSALE and TOPPER [133] propose a correction to the formula valid for MASING materials. Again they obtain an explicit relationship between W_f and N_f. Supplementary material constants K and α occur in the final formulation of the general shape :

$$W_f = K N_f^{\alpha}$$

The authors provide experimental data validating their theories.

5.2.2.3 Measurement of the material properties

The measurement of the material properties that pertain to the cyclic behaviour of a material is not a standard procedure. It is however essential to the success of the method that the material properties, particularly the cyclic properties are evaluated correctly. Smooth cylindrical specimens with a measurement basis that is about twice the diameter of the specimen, are subjected to cyclic axial loading. Smoothly curved transitions towards the shoulders must not create any stress concentrations (fig.5.1). An extensometer or sometimes a

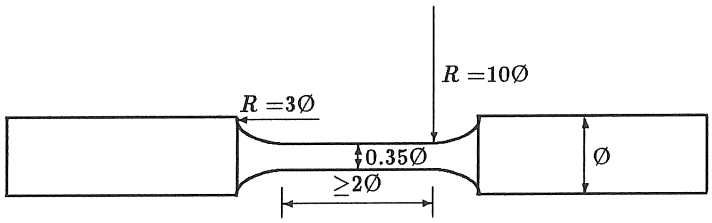

Figure 5.1: Specimen for measurement of cyclic material properties

strain gauge is used to measure deformation in the central cylindrical part where stress and strain are supposed to be uniformly distributed. During the experiment the strain variation is controlled. A certain cyclic displacement is imposed and the corresponding force or stress is measured. Usually push-pull load variations are imposed, the mean value of strain for each cycle being zero. Due to the hardening and softening behaviour of the material a certain number of cycles of constant amplitude deformation is necessary before cyclic force reaches

a stable value. Only after stabilisation is achieved the force or stress value is recorded. This value corresponds to the imposed strain. One thus gradually proceeds throughout the entire range of strain amplitudes, e.g. 0.05%, 0.1%, ... To prevent the material from heating low frequencies are imposed particularly in the high strain area (0.5 - 1 - 2 *Hz*).

As to the succession of strain amplitudes that are imposed to the specimen two strategies can be followed. The first strategy, which is most correct, employs a new specimen for each load increment. At each stage of loading, the specimen is cycled until it fails and the evolution of stress response is recorded throughout the entire life. The stress amplitude at mid life is taken to be representative. When the imposed strain is so small as not to cause failure, loading continues for a number of cycles at least two or three times the number of cycles needed to achieve stabilisation. A complete experiment is obviously very time-consuming and expensive. The second strategy therefore uses only a small number of specimens. At each stage of loading, the strain amplitude is kept constant until the stress response reaches a stable value. This value is recorded and the strain amplitude is increased using the same specimen. This strategy is as accurate as the first one in the area of low strain amplitudes. In regions of higher strain plastic deformation occurs and subsequent stages may be influenced by preceding ones. Damage accumulated during anterior cycling may cause the specimen to break unexpectedly early. The risk of failure due to buckling has to be considered especially when strain gauges are used. In the elastic region the strain increment can be taken higher than in the plastic domain. In the plastic domain the stress increment that corresponds to a certain strain increment is much smaller than in the elastic domain, but it takes much more cycles before stabilisation of stress is obtained.

After the test is completed for the last stage of loading one disposes of a number of corresponding strain and stress amplitudes and hysteresis loops. The corresponding stress and strain amplitudes are plotted in the σ–ε -diagram and the best fit of the general form 5.1 is fit through those points. Appendix B discusses how the material coefficients E, K' and n' can be determined. In case the obtained stress–strain -curve is similar to the measured hysteresis loops, the material exhibits a MASING-behaviour.

Measurement of the fatigue characteristics of a material is more a standard procedure. Several types of testing machines are developed for axial loading, three-point bending, four-point bending, torsion. The geometry of the specimen is generally different from the one used for the determination of cyclic properties. There is only one area in the specimen where the cross-section is minimum. Fig.5.2 shows an example of a test specimen used for rotary bending. Tests are per-

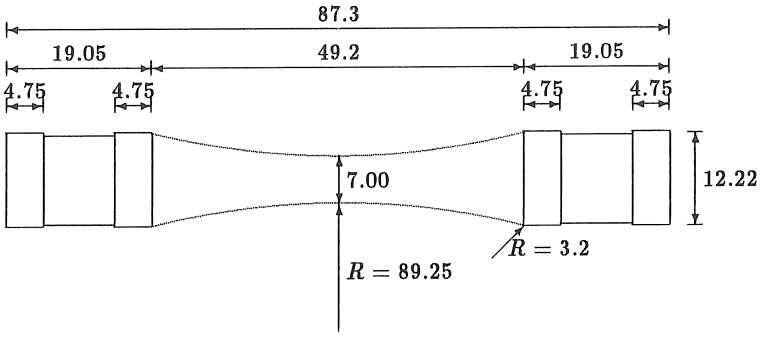

Figure 5.2: Fatigue test specimen type "Moore"

formed usually on a stress controlled basis. A constant load amplitude is imposed and the specimen is cycled until it fails. Every single test on a specimen results in one single point in the ε–N -curve. Depending on the type of machine the loading frequency can reach as high as 10 - 50 - 100 *Hz*. In areas of high-cycle fatigue the total test time still is very long. The variance on measurement data may be significant. Especially in the area of long lives the standard deviation of cycles can be very high. A complete fatigue test therefore provides a set of curves that correspond to different probabilities of failure.

Theoretical relations exist between the cyclic stress–strain coefficients E, K', n' on the one hand and the fatigue characteristics σ'_f, ε'_f, b, c on the other hand. YOUNG's modulus of elasticity can be determined based on static computations since the static modulus coincides with the cyclic factor.

$$\frac{\Delta\varepsilon}{2} = \frac{\Delta\sigma}{2E} + \left(\frac{\Delta\sigma}{2K'}\right)^{\frac{1}{n'}} = \frac{\sigma'_f}{E}N^b + \varepsilon'_f N^c$$

Comparison of corresponding terms quickly shows :

$$n' = \frac{b}{c} \qquad K' = \frac{\sigma'_f}{\varepsilon'^c_f}$$

MORROW and TULLER [136] suggest relations between b, c and n' :

$$b \approx -\frac{n'}{1+5n'} \qquad c \approx -\frac{1}{1+5n'}$$

Another set of approximations relates the fatigue strength coefficient σ'_f and ductility coefficient ε'_f to the monotonic tension test fracture properties :

$$\sigma'_f \approx \sigma_f \qquad \varepsilon'_f \approx \varepsilon_f$$

LANDGRAF [137] shows that ε'_f may vary between $0.35\varepsilon_f$ to ε_f depending on the particular type of material.

Section 1.5.1.2 explains that these relations can be used in the evaluation of the parameters. It is however preferable that all the parameters are determined independently, without explicitly using those relations.

Both the cyclic curve and the fatigue curve have to be determined separately. Section B.1 describes how K' and n' are evaluated and section B.2 explains how the fatigue characteristics are determined.

In some cases it appears to be very hard to fit a curve of the general shape 5.2 through the measured data. The flexibility that is contained in the freedom of determining four parameters always allows to produce a good fit in a large domain along the horizontal axis. However either in the low-cycle area, either in the high-cycle area or in the transition zone some deviation may exist. It is then up to the user to select the area that is most important. If only a few or even one cycle of very high amplitude is expected to occur extreme care must be paid that a good fit is obtained in the low-cycle area since this cycle consumes a major portion of the life. If the loading amplitude is about constant and close to the fatigue limit, the strain–life -curve in the high-cycle region has to be modelled accurately. A general statement can be made that most attention should be paid to the highest strain amplitudes that are expected to occur.

5.2.3 Counting methods

Counting methods separate a complex strain-history into a number of discrete cycles. Each of these cycles will subsequently be treated independently.

Counting methods are also used to reduce the storage space of recorded data. Independent load cycles are identified and are stored in a loads matrix. The contents of this matrix can be used for different purposes :

- the computation of the portion of the fatigue life that is consumed during the period of measurement
- the reconstitution of a sequence of loads which, although it may be different from the original sequence, is required to have the same contents of fatigue damage

Most of the commonly used counting algorithms observe the load variations rather than absolute load levels, since the damage due to fatigue depends primarily on the amplitude. The basic characteristics and the use of these so-called "range"-methods is discussed hereafter.

In view of a clear visualisation of the third method the time-axis of the load-variation is drawn vertically. A similar representation is used for the other methods so as to allow an easy comparison of the individual methods.

5.2.3.1 Peak-valley method

The counting of single ranges is illustrated in fig. 5.3.
Each variation from a peak to a valley or from a valley to a peak is counted as half a cycle. This method is simple and straightforward, but it is very sensitive to small load variations, as indicated by fig. 5.4.

Analysis of the signal on the left results in the counting of a large number of relatively small ranges. If the signal passes through a filter suppressing the small load variations, as it appears on the right hand side, only one range is counted. The fatigue life consumed by only one cycle of large amplitude is much more important than the life consumed by a number of cycles of a smaller amplitude.

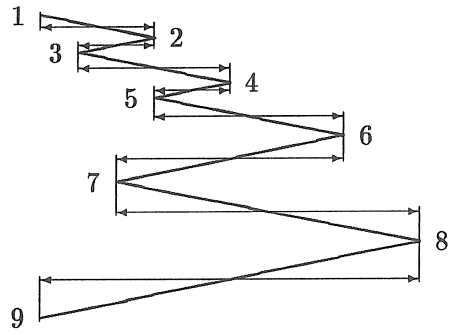

Figure 5.3: The peak-valley method

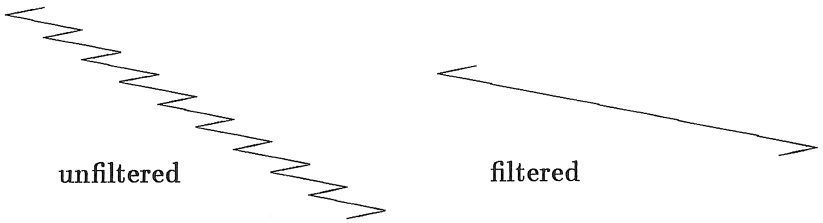

Figure 5.4: Sensitivity of the peak-valley method to small load variations

5.2.3.2 Range-pair method

This method was presented by DE JONGE (refs. [138], [139]). It is illustrated in fig. 5.5.
At first, the smaller cycles are counted and their points of reversal are eliminated from the subsequent analysis. The same procedure then applies to the reduced sequence. It is repeated until only one cycle is left. This cycle has the largest amplitude.

5.2.3.3 Rainflow method

This method was presented by MATSUISKI and ENDO (ref. [140]). It is illustrated in fig. 5.6. The graphical representation of its rules is very similar to the flow of raindrops. First the cycle with the largest amplitude is eliminated, then the second cycle, and so on, ...

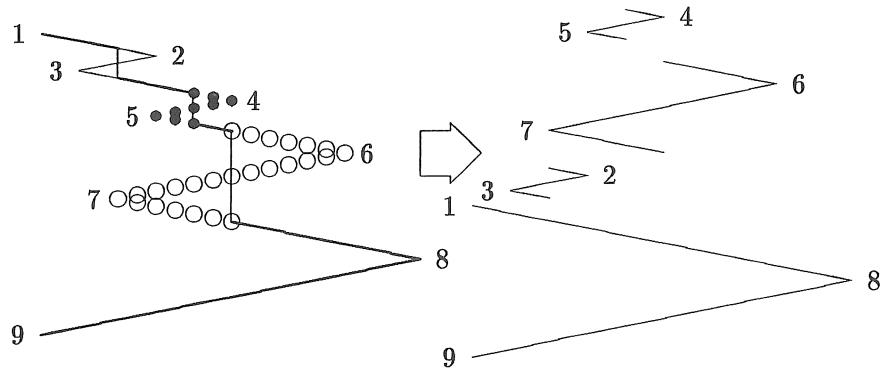

Figure 5.5: The range-pair method

5.2.3.4 Discussion of different methods

Of the various counting techniques currently available, the rainflow method provides the most complete description of the loads data. It is capable of detecting large discontinuous load transitions that can be missed by other techniques. It is also compatible with the stress-strain behaviour associated with fatigue critical areas such as the material near the tip of a fatigue crack, which is subjected to cyclic plasticity. History dependent closed loops are identified by the technique. It is primarily for these reasons that rainflow counting is the favoured technique for application in fatigue analysis.

5.2.3.5 Storage of data

The rainflow counting algorithm is a moderately complicated procedure that uses computer processing time inefficiently. PERRETT [141] has shown that the range-pair algorithm recognises the same load cycles as the rainflow method, but uses a much simpler computer algorithm. DE JONGE [142] and PERRETT [82] present a detailed description of the algorithm. The popular implementation of the method uses a four-point algorithm to extract complete cycles from the sequence for storage in a range-mean or a peak-trough matrix. The range-mean matrix should be used preferably for the evaluation of the consumed lifetime, while the peak-trough matrix is favoured for the storage in view of a reconstitution of the sequence.

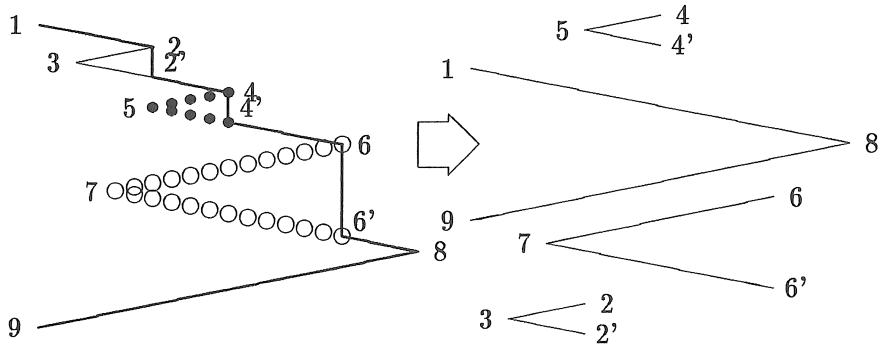

Figure 5.6: The rainflow method

The range-mean matrix is obtained by dividing the full range from minimum load P_{min} to maximum load P_{max} in a number n of intervals of equal length $\frac{P_{max}-P_{min}}{n}$. In this way n classes $\frac{P_{max}-P_{min}}{n}$, $2\frac{P_{max}-P_{min}}{n}$, ..., $P_{max} - P_{min}$ are defined. Similarly, n levels of mean values $P_{min} + \frac{P_{max}-P_{min}}{2n}$, $P_{min} + 3\frac{P_{max}-P_{min}}{2n}$, $P_{min} + 5\frac{P_{max}-P_{min}}{2n}$, ..., $P_{min} + (2n-1)\frac{P_{max}-P_{min}}{2n}$ are defined. The classes of amplitude are represented in the rows of the matrix and the classes of mean values are represented in the columns of the matrix. Each cycle that is obtained from the counting algorithm is put on a particular element of the matrix. The element a_{ij} of the matrix gives the number of counted cycles with amplitude class i and mean level j.

The peak-trough matrix has a size $(n+1) \times (n+1)$. The columns of the matrix represent the levels from which a particular cycle starts and the rows of the matrix represent the levels on which a particular cycle ends. The element a_{ij} of the matrix gives the number of counted variations from level j to level i.

5.2.3.6 Reduction of noise

In order to reduce the processing time that is needed for the estimation of the fatigue lifetime it is often desirable to eliminate cycles of a small amplitude from the analysis. These cycles cause only a minor amount of damage and so they do not influence the accuracy of the analysis.

Several methods exist which eliminate the smaller amplitudes. The

"racetrack"-method defines a racetrack with a certain width and the same profile as the original sequence. Only the points of reversal where the racer switches upward and downward movement are preserved for subsequent analysis. The width of the track determines the amplitude of the cycles that are eliminated. Reversals that are maintained, should also keep the actual values they had originally.

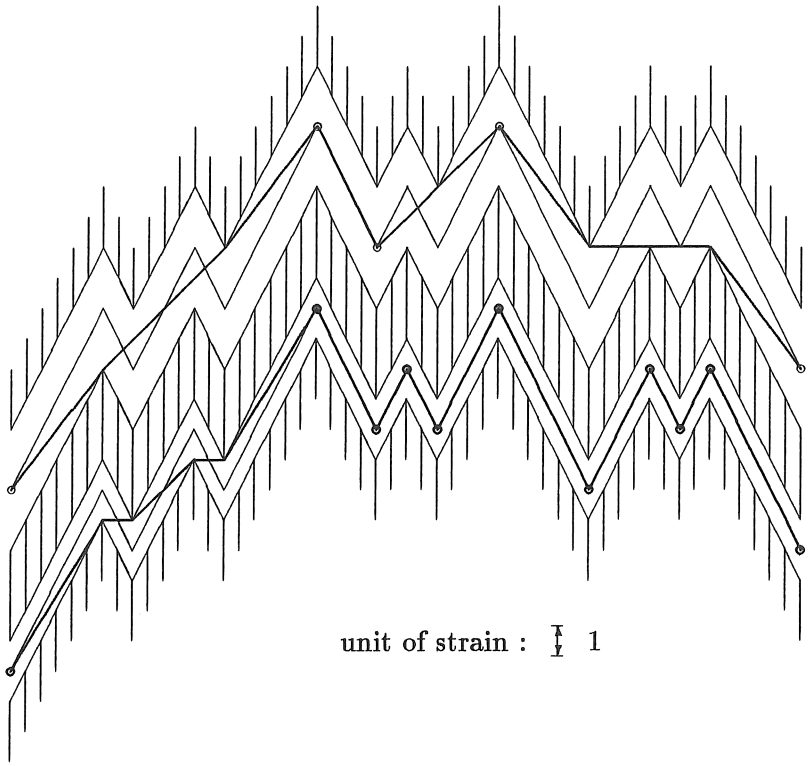

Figure 5.7: Application of "racetrack"-method for reduction of noise

The example in fig.5.7 shows two applications, the upper one has a bandwidth of 4, the lower one has a bandwidth of 2. Starting from 15 reversals, the upper reduction has 5 reversals left and the lower one 11 reversals.

5.2.4 Influence of plasticity

In general, strains can not be measured easily at the critical location. Analytical methods have to be used to determine strain. Elastoplastic finite element methods can be applied for this purpose. Section 4.4 describes some methods that can be used. They are all very demanding. Simple stress-strain analyses of the notch root are desirable for practical implementations. Section 4.4.3 briefly explains the approach that is adopted by NEUBER. A well designed mechanical component exhibits plastic deformation only in very small areas, if at all. The surrounding material remains in a state of elastic stress, thereby imposing bounds on local plastic deformation. NEUBER gives theoretical evidence of his approach for computing plastic behaviour based only on elastic analysis. Although some materials behave in a slightly different way, the approximation is found to be acceptable for most technical metallic materials. Elastic strain data are used in an area that surrounds the critical location. The relation between maximum elastic stress in the critical area and nominal stress in the surrounding material is expressed by the elastic stress concentration factor K_t :

$$\Delta\sigma_{real}\Delta\varepsilon_{real} = \frac{(K_t\Delta\sigma)^2}{E} \tag{5.4}$$

Combination with the cyclic stress–strain -relation results in a set of nonlinear equations presented in section 1.3.2.2. Graphical representation is given in fig. 5.8a. In some applications an alternative approach is used. It is assumed that local strain is equal to nominal strain multiplied by the elastic stress concentration factor :

$$\varepsilon_{real} = K_t\varepsilon_{nom}$$

The graphical representation of the alternative approach is shown in fig. 5.8b. NEUBER's method is used preferably to evaluate plastic stress and strain. The alternative method does not have any physical background. It simply appears to give good results in some cases.

5.3 Multiaxial fatigue

All the fatigue theories that are dealt with so far are valid only for cases of uniaxial loading. Only one diagonal component of the two-dimensional stress tensor differs from zero. This limits the range of

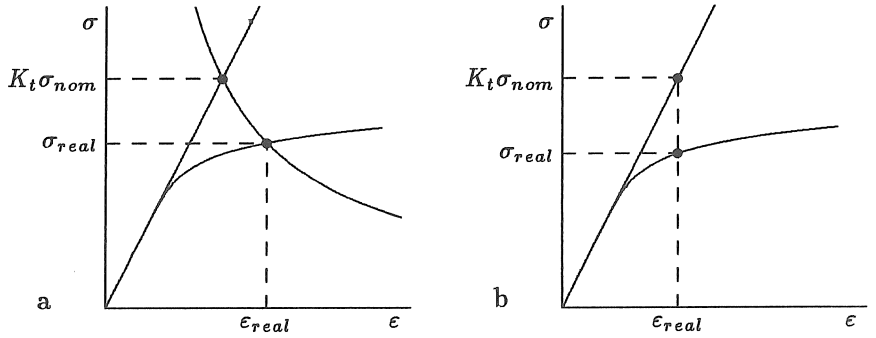

Figure 5.8: Local strain computation - a - NEUBER - b - alternative

applications of the local strain approach. However, many cases of industrial practice are classified in a category of uniaxial states of stress. In most cases the critical area of fatigue is located at a free surface. Still two components of principal stress may be different from zero.

Most experimental fatigue data pertain only to uniaxial states of stress. A question arises as to whether those data are useful in the analysis of multiaxial states of stress. If so, how do different components have to be combined in an equivalent quantity ? Or is there a need for special theories to handle such conditions ? Another important issue concerns the frequency difference and the phase shift that possibly separate both components of principal stress. In this context, a uniaxial state of stress of variable direction is considered to be a case of multiaxial stress, because the axis of principal stress is rotating.

Two different types of loading are identified. A graphical representation is used in a general vector space of individual stress tensor components. For biaxial loading, the vector space is three-dimensional with axes σ_x, σ_y, τ. For triaxial loading, the vector space is six-dimensional with axes σ_x, σ_y, σ_z, τ_{xy}, τ_{yz}, τ_{zx} :

proportional loading the individual components of the stress tensor vary in a proportional way. The principal axes of the stress tensor remain constant throughout an entire load cycle. This type of loading is represented in the general vector space of stress components by a straight line that passes through the origin (fig. 5.9a).

nonproportional loading the individual components of the stress tensor vary in a way that is not proportional. The principal axes

of the stress tensor vary during a single load cycle. This type of loading is represented by any load path that differs from a single line going through the origin. An example is shown in fig. 5.9b.

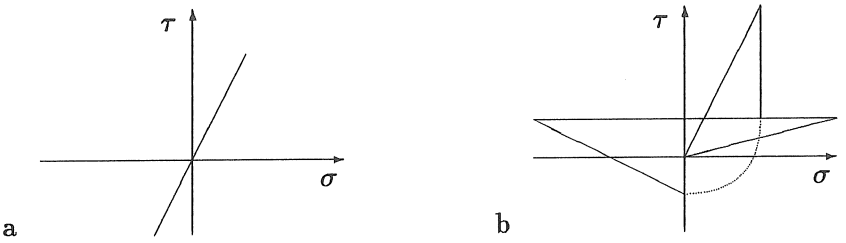

Figure 5.9: Examples of proportional and nonproportional loading

Both types of loading cause the material to behave differently when it is subjected to cyclic loading. Appropriate stress-strain analysis has to be performed and suitable fatigue criteria have to be applied.

5.3.1 Failure mechanisms under multiaxial straining

The orientation of the stress- strain field with respect to the surface is a feature omitted from all classical theories (section 1.3.1). MILLER and BROWN [143] explain some mechanisms that initiate and propagate cracks. First cracks invariably initiate at or very close to the surface, and second, the orientation to the surface of a crack plane, which is dependent on the three-dimensional field obviously affects lifetime. Just as in the local strain approach, strain rather than stress is invoked to correlate fatigue data. The bulk deformation in the surrounding material controls the stress-strain field of crack tips and strain is more representative of material behaviour, especially after yield.

The theory is best understood by considering both the size and the position of MOHR's circles of strain (fig. 5.10, $\varepsilon_1 > \varepsilon_2 > \varepsilon_3$). The radius of the largest circle has a size equal to the true shear strain. The position from the origin of the circles is given by the centre of the largest circle $\frac{\varepsilon_1+\varepsilon_3}{2} = \varepsilon_n$, which is the tensile strain on the plane of the maximum shear strain. Both these parameters differentiate between two fundamentally different cracking systems. The cracks in the top half of fig. 5.11 grow along the surface plane, while those in the bottom half grow on planes perpendicular to the surface.

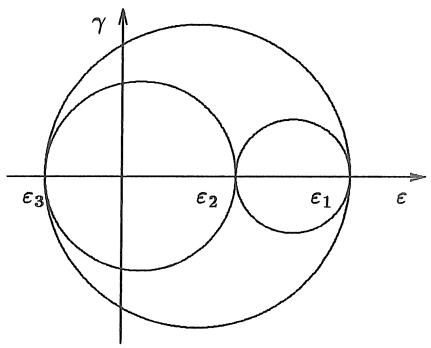

Figure 5.10: MOHR's circle for strains

5.3.2 High cycle multiaxial fatigue

In most practical cases multiaxial states of stress that lead to failure are biaxial. Cracks usually initiate at the surface of an element. Individual stress tensor components are σ_{11}, σ_{22} and σ_{12}. Principal stresses are denoted σ_1 and σ_2.

5.3.2.1 Proportional loading

The situation in proportional loading is similar to a problem of multiaxial static loading. For ductile materials the VON MISES criterion is a generally accepted indicator of plastic deformation. In cyclic proportional loading it is always the same fibre of material that is subjected to maximum stress applied in the same direction. SAWERT [144] proposed a criterion that is very similar to the VON MISES criterion. Failure occurs when the square root of the second invariant of the stress deviator of the stress amplitude exceeds a certain constant characteristic of the material :

$$\sqrt{\frac{3}{2}J_2'} = \frac{1}{2}\sqrt{\sigma_1^2 + \sigma_2^2 - \sigma_1\sigma_2} \geq \tau_{crit}$$

SINES and OHGI [145] propose that effects of mean stress are taken into account via the invariant of static stress :

$$J_1 = \sigma_1 + \sigma_2$$

They propose a criterion which includes the effect of different combinations of alternating stress with static stress. For stresses which do

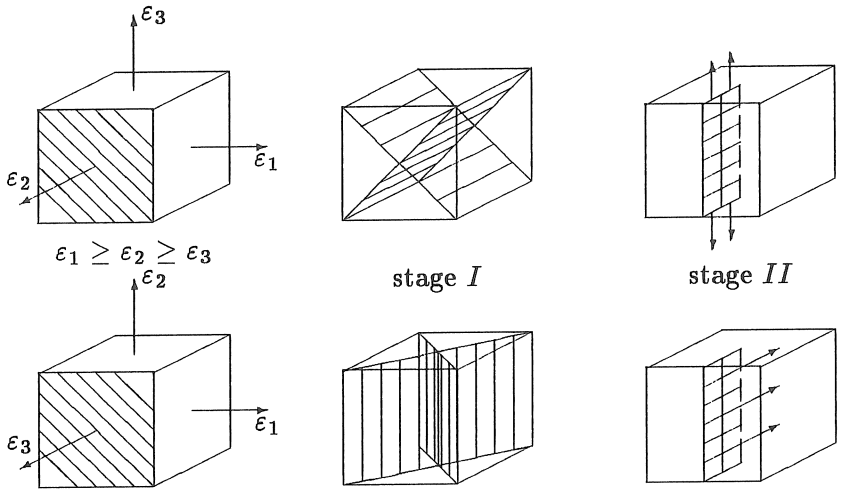

Figure 5.11: Planes and directions of stages I and II crack growth

not excessively exceed yield it appears from their measurement data a simple linear relationship is reasonable :

$$\sqrt{J'_{2,alt}} + \alpha J_{1,stat} \geq \sqrt{\frac{2}{3}}\tau_{crit} \tag{5.5}$$

where : $_{alt}$: refers to the alternating portion of stress
$_{stat}$: refers to the static portion of stress
α, τ_{crit} : functions of the number of cycles

The criterion is claimed to be valid for lives greater than 10^5. To find the values of τ_{crit} and α for a given life experimental determinations of the desired fatigue life are necessary from tests having two different values of $J_{1,stat}$. Insertion in the criterion of the two different stress states gives two simultaneous algebraic equations in τ_{crit} and α which are easily solved. The physical interpretation of the criterion is that for a given cyclic life, the permissible amplitude of alternation of the root mean square of the shear stress over all planes is a linear function of the static normal stress averaged over all planes. The general shape of the proposed relation is similar to the criterion of HAIGH–SODERBERG for uniaxial stresses (equation 1.1).

SINES [145] modifies his criterion for cases of high mean stresses. When the maximum stress of the cycle exceeds the yield strength con-

siderably, the linear behaviour no longer continues and a supplementary term is added to account for the macroscopic inelastic effects :

$$\sqrt{J'_{2,alt}} + \alpha_1 J_{1,stat} + \alpha_2 {J'_{2,stat}}^{a} \geq \sqrt{\frac{2}{3}}\tau_{crit}$$

where the exponent a is an experimental parameter.

LEIS and TOPPER [146] compare analytical results of the VON MISES criterion in fatigue to experimental data. They define K_f to be the ratio of fatigue resistance of the unnotched specimen over the fatigue resistance of the notched specimen :

$$K_f^t = \frac{\sigma_{v,\text{unnotched}}}{\sigma_{v,\text{notched}}}$$

The notation for the biaxiality ratio α is defined as :

$$\alpha = \frac{\Delta\sigma_2}{\Delta\sigma_1}$$

where $\Delta\sigma_i$ is the variation of the principal stress along the i-axis. The VON MISES criterion is expressed as :

$$\Delta\sigma_{eq} = \Delta\sigma_1\sqrt{1 - \alpha + \alpha^2}$$

where $\Delta\sigma_{eq}$ is the variation of equivalent stress. LEIS and TOPPER have taken measurements on two types of geometries, circularly notched thick plates loaded in uniaxial tension and circumferentially V-notched bars loaded in uniaxial tension or pure bending. The comparison of analytical data to experimental data gives excellent results.

5.3.2.2 Nonproportional loading

In the previous section concerning proportional loading it becomes clear that it is often unnecessary to modify the VON MISES citerion in order to obtain valid predictions. For nonproportional cycling however section 5.3.1 proves why the VON MISES criterion is theoretically not correct.

MILLER, OHJI and MARIN [147] developed a modified octahedral shear stress failure theory that considers rotating principal stress axes and nonsynchronous stresses. This theory assumes that fatigue damage occurs on the octahedral plane containing the maximum octahedral shear stress. The shear stress on this reference plane is examined

during one complete cycle of stress. The resultant stress on the reference plane during a cycle is resolved into a normal stress and a shear stress (fig.5.12a). The shear stress has a line of action that coincides with the maximum shear stress in the reference octahedral plane. The variation of octahedral shear stress over a full cycle is considered (fig.5.12b) :

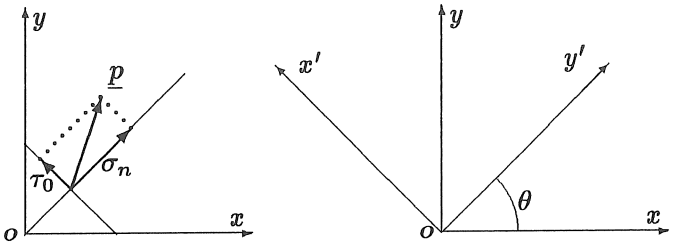

Figure 5.12: a. Octahedral plane – b. Variation of τ_0 with θ

Its maximum value is denoted τ_0', with instantaneous stress values σ_1', σ_2' :

$$\tau_0' = \max[\tau_0(\theta)] = \frac{\sqrt{2}}{3}\sqrt{\sigma'^2_1 + \sigma'^2_2 - \sigma'_1\sigma'_2}$$

The projection of the resultant stress vector :

$$\underline{p} = p_x\underline{e}_x + p_y\underline{e}_y$$

where $p_x = \sigma_1 \cos\theta$ and $p_y = \sigma_2 \cos\theta$ onto a line S coincident with and in the direction of τ_0' is required. The components of τ_0' along x- and y- axis are :

$$\tau'_{0,x} = \frac{2\sigma_1' - \sigma_2'}{3\sqrt{3}} \qquad \tau'_{0,y} = \frac{2\sigma_2' - \sigma_1'}{3\sqrt{3}}$$

The projection τ_p on S is :

$$\tau_p = \frac{1}{9\tau_0'} \quad \{ \quad S_1[\sigma_1 \cos\theta(\cos\theta + \sin\theta) - \sigma_2 \sin\theta(\cos\theta - \sin\theta)]$$
$$+ \quad S_2[\sigma_1 \sin\theta(\cos\theta + \sin\theta) + \sigma_2 \cos\theta(\cos\theta - \sin\theta)]\}$$

with : $S_1 = 2\sigma_1' - \sigma_2'$ and $S_2 = 2\sigma_2' - \sigma_1'$. Once the maximum and minimum values of τ_p are obtained, the alternating and mean components

can be computed. Both of these components are in the octahedral shear stress plane and have the same line of action as the minimum octahedral shear stress.

LEIS and LAFLEN investigate some techniques and criteria that are used in damage analysis under nonproportional cycling [148]. They conclude that while such damage measures may be valid for mildly nonproportional histories, their successful application to general nonproportional problems is unlikely. Difficulties are encountered because the damage process under nonproportional cycling causes damage on many planes with different orientations with possibly different directions. Nonproportional cycling induces path dependent multiaxial effects which give rise to significantly different damage states than those characterised by conventional techniques. Synthesised deformation histories show evidence of the path dependent nature of the damage process. Two basic types of problems are observed :

- segments of the history involve aspects that are not characterised by the simple reference damage data base. In the case of a circular load path in two-dimensional straining for instance, equivalent VON MISES- stress remains constant, whereas the directions of principal stress rotate. Correlation of such variations to conventional uniaxial cycles is questionable.

- the damage parameter fails to reflect the multidimensional path dependent nature of the process. Correlation of spatial variations to temporal variations is not straightforward.

Except for strongly nonproportional load paths and high amplitude cycling the modified octahedral shear stress theory is accepted by many authors.

5.3.3 Low-cycle fatigue

Phenomena of low-cycle fatigue are characterised essentially by plastic deformation. Stress quantities are no longer capable of representing plastic states of deformation. It is thus no longer feasible to apply octahedral shear stress theory to cases of low-cycle fatigue. Detailed analysis has to be made to evaluate both spatial and temporal variations of stress and strain quantities. Theory of plasticity in multiaxial states of loading is quite complicated. Considerable progress has been

made in modelling cyclic plasticity. They all use concepts of stress and strain increments rather than instantaneous values. They are all based on DRUCKER's postulate [149].

5.3.3.1 Constitutive equations

PRAGER [150] presents a kinematic model that describes a rigid perfectly plastic behaviour, a rigid work-hardening behaviour or an elastic perfectly plastic behaviour in two-dimensional straining. The states of

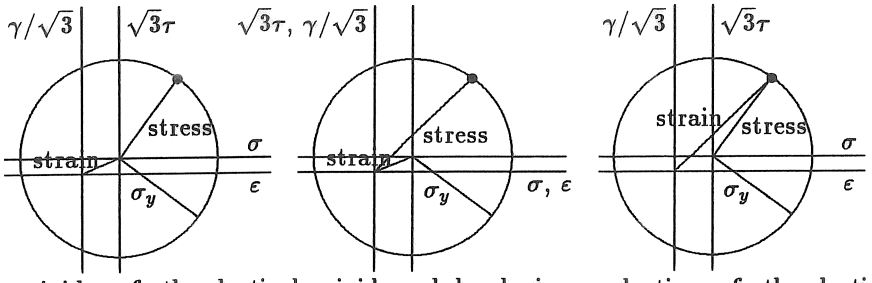

a. rigid perfectly plastic b. rigid work-hardening c. elastic perfectly plastic

Figure 5.13: PRAGER's models for plastic behaviour

stress and strain are represented in the diagrams 5.13. The material's yield limit is denoted σ_y. The appearance of the factor $\sqrt{3}$ in the numerator of shear stress τ and in the denominator of shear strain γ scales VON MISES' ellipse to a circle. The instantaneous state of stress and strain is indicated by the dot. In the kinematic model the dot is considered to be a frictionless pin and the circle is a rigid ring. As stress and strain vary the pin moves inside the ring. When it touches the ring, the ring slides without friction. Depending on the particular type of behaviour of the material the values of stress and strain are indicated in the appropriate coordinate system.

Each of PRAGER's models corresponds to an idealised description of the material's behaviour with for instance a constant rate of work-hardening. MROZ [151] presents a more general approach, that models the BAUSHINGER effect more realistically [149]. The BAUSHINGER effect is the phenomenon that under reversed loading plastic deformation occurs at a lower stress increment than yield limit. The model of the material is assumed as a composition of elasto-plastic subelements, as in fig. 5.14.

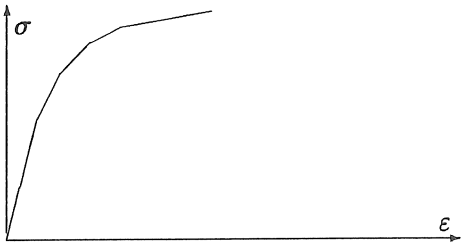

Figure 5.14: Piecewise linear stress–strain -law

Each stage of loading has a certain work-hardening modulus assigned to it. In multiaxial loading, this corresponds to a series of yield surfaces f_0, f_1, ...that each have a particular work-hardening modulus. Each surface f_i has an associated value of yield limit $\sigma_y^{(i)}$. For an isotropic material f_0, f_1, ...are similar and concentric, enclosing the origin O (fig. 5.15a). When the stress point • moving from O towards

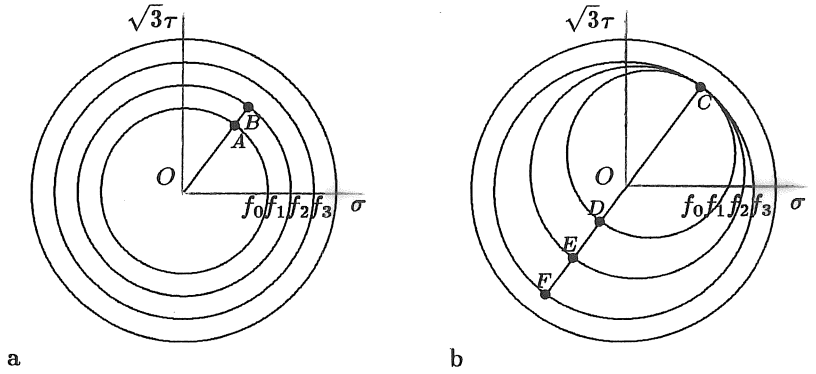

Figure 5.15: Yield surfaces during proportional loading

C reaches f_0 at A, the surface f_0 starts to translate with the stress point towards B. From B the two surfaces f_0 and f_1 move together until the point C is reached. The field of work-hardening moduli after reaching C is presented if fig. 5.15b. During reverse loading the surface f_0 starts to translate backwards when the stress point reaches D and from E the two surfaces f_0 and f_1 move together to F. For nonproportional variation of stress it is assumed that the surfaces f_0, f_1, ...do not intersect but consecutively contact and push each other. MROZ provides some numerical expressions that give the location of

the surfaces and corresponding stress values. As a further extension to this theory and to be able to describe transitory phenomena, the surfaces f_0, f_1, ...are allowed to expand or contract during plastic deformation. The parameter λ describes the amount of plastic deformation :

$$\lambda = \sqrt{\frac{2}{3}} \int_0^t \left(\dot{\varepsilon}_{ij}^p \dot{\varepsilon}_{ij}^p \right)^{\frac{1}{2}} \, dt$$

Yield surfaces vary as a function of λ :

$$\sigma_y^{(i)} = \sigma_y^{(i)}(\lambda)$$

KRIEG [152] further extended MROZ' theory with a continuum of intermediate loading surfaces where the distribution of these surfaces is analytically described a priori. The loading surface moves and grows continuously. A limit surface is introduced which grows and moves independently and encloses the loading surface. It is taken to have hardening rules which are identical to those of an elastic, linearly hardening, combination isotropic-kinematic plasticity theory. The hardening of the loading surface depends upon a distance vector from the stress state to the limit surface. The stiffness of the limit surface increases smoothly with the distance from the stress state to the limit surface. Three distinct zones are identifiable during a loading process. The elastic zone is associated with small recoverable strains. In the asymptotic plastic zone the system adopts the stiffness of the limit surface. The in-between zone is characterised by a variable stiffness. KRIEG's theory has some definite advantages over MROZ' theory. Since the model is continuous, it can more easily be implemented in a computer program. The actual selection of material constants describing the hardening behaviour is cumbersome and critical.

Many extensions to MROZ' and KRIEG's models are proposed in literature. It is generally acknowledged however that the major aspects of a material's behaviour are included in these models. Very peculiar phenomena that are specific to a certain material may not be described, but most authors consider the above theories as reference models. MCDOWELL [153] develops some advanced mathematical formulations based on kinematic hardening rules of MROZ and PRAGER for the yield and limit surfaces. LAMBA and SIDEBOTTOM [154] conducted extensive experiments on annealed copper under cyclic nonproportional strain histories. They conclude that a model that appears

to be extremely reliable is a combination of a TRESCA yield surface translating according to the MROZ hardening rule, inside a stationary TRESCA limit surface.

Literature provides ample evidence of additional cyclic hardening due to out-of-phase loading that is not found in simple proportional tests [155,156,157]. For equal cyclic strain effective stress can even be doubled during nonproportional loading. This increase in stress must be included in the damage parameter, e.g. via the SMITH-TOPPER-WATSON -parameter.

5.3.3.2 Low-cycle multiaxial fatigue criterions

Several attempts were made to correlate experimental data with the maximum octahedral shear strain range theory. KANAZAWA, MILLER and BROWN [158] conducted tests on CrMoV -steel under combined cyclic axial and torsional loads with various phase relationships. They found that fatigue cracks initiate on that plane of maximum shear strain range which experiences the greatest amplitude of normal strain. The shear strain range and the amplitude of normal strain on the plane of maximum shear govern fatigue endurance in out-of-phase fatigue tests. Both the TRESCA and the octahedral shear strain criteria are nonconservative however under out-of-phase cyclic loading. Nonproportional loading conditions where the axes of principal strain rotate, phase angles of 90° are most harmful, whereas in-phase cyclic strains give highest endurances. Their experience once more proves that clear distinction should be made between proportional and nonproportional load paths.

The approach of relating fatigue life to absorbed plastic strain energy that is mentioned briefly in section 5.2.2.2 is used by many authors. One of the first publications on this method is by LEFEBVRE, NEALE and ELLYIN [159]. This approach can be used for uniaxial states of deformation as well as for multiaxial states. The basic idea behind this approach relates the total amount of damage that can be accumulated by a material to the total amount of energy that can be dissipated before failure occurs. During one cycle of loading a certain portion of strain $\Delta\varepsilon_p$ cannot be recovered. The energy that is dissipated is equal to $\sigma\Delta\varepsilon_p$. The plastic energy dissipated per unit volume during a given loading cycle for an element subjected to a cyclically

varying stress and strain history σ_{ij} and ε_{ij} is :

$$W = \oint \sigma_{ij}\, d\varepsilon_{ij} \tag{5.6}$$

Because of the incompressibility during plastic deformation $d\varepsilon_{kk} = 0$, this relation is also expressed as :

$$W = \oint s_{ij}\, d\varepsilon_{ij}$$

where $s_{ij} = \sigma_{ij} - \delta_{ij}\frac{\sigma_{kk}}{3}$ is the deviatoric stress tensor. For multiaxial states of stress and for proportional stressing, the plastic strain according to VON MISES -theory is given by :

$$\varepsilon_{ij}^{p} = \frac{3}{2}\left(\frac{1}{E_s} - \frac{1}{E}\right) s_{ij}$$

where $E_s = \frac{\tilde{\sigma}}{\tilde{\varepsilon}}$, $\tilde{\sigma}$ and $\tilde{\varepsilon}$ being defined as :

$$\tilde{\sigma} = \sqrt{\frac{3 s_{ij} s_{ij}}{2}} \qquad \tilde{\varepsilon} = \sqrt{\frac{3 \varepsilon_{ij} \varepsilon_{ij}}{2}}$$

Equation 5.6 then takes the form :

$$W = \oint \tilde{\sigma}\, d\tilde{\varepsilon}^{p}$$

where $d\tilde{\varepsilon}^{p}$ is the increment of equivalent plastic strain $\tilde{\varepsilon}^{p}$:

$$d\tilde{\varepsilon}^{p} = d\tilde{\varepsilon} - \frac{\tilde{\sigma}}{E}$$

With the generalised cyclic stress–strain -relation :

$$\Delta\tilde{\varepsilon}^{p} = K\,(\tilde{\sigma})^{\frac{1}{n'}}$$

the plastic energy dissipated during one steady state cycle of multiaxial loading :

$$W = K\frac{1 - n'}{1 + n'}\Delta\tilde{\sigma}^{1+\frac{1}{n'}}$$

The total energy dissipated at fracture is :

$$W_f = K\frac{1 - n'}{1 + n'}\Delta\tilde{\sigma}^{1+\frac{1}{n'}} N_f$$

Another estimate of the plastic energy at fracture U is obtained from the monotonic stress–strain -curve and from test results in uniaxial fatigue :

$$U_u = \frac{\varepsilon_u \sigma_u}{1+n}$$

where : ε_u : plastic strain at fracture
σ_u : ultimate stress
n : monotonic strain hardening coefficient

For biaxial loading the plastic strain energy U is related to U_u. In uniaxial fatigue the plastic strain energy at fracture is :

$$W_{fn} = A\, U_u\, N_f^{\alpha}$$

where A and α are functions of monotonic and cyclic material mechanical properties. Combining all equations together finally a relation of the form is obtained :

$$\Delta\tilde{\varepsilon}^p \Delta\tilde{\sigma} = kN^c$$

where : $\tilde{\varepsilon}^p$: equivalent plastic strain amplitude
$\Delta\tilde{\sigma}$: equivalent stress amplitude
N : number of cycles to failure
k, c : material properties

The constants are expressed in terms of monotonic and cyclic mechanical characteristics of the material. Some mathematical formulas are presented in [159].

GARUD [160] simultaneously developed a similar theory, in combination with a computation of incremental plasticity according to MROZ. The approach is found to be in good agreement with general results on fatigue under complex loading with moving principal stress axes. A fair correlation between plastic work per cycle and fatigue life was obtained for a set of tests under axial and torsional strains with different phase angles.

Similar results are found in [161,162,163]. ELLYIN and KUJAWSKI [162] extend the criterion with corrections for non-MASING materials. GOLOS and ELLYIN [163] present a unified theory that is also applicable in high-cycle fatigue. The damage criterion is based on the total strain energy density per cycle, being the sum of plastic and tensile elastic strain energy.

5.3.4 A pragmatic approach

SOCIE [164,165] investigated the fundamental failure mechanisms of several materials under proportional and nonproportional loading. For each type of loading the location and the orientation of cracks are observed. Together with their evolution from nucleation to early growth and failure the major portion of the lifetime is consumed in the crack growth phase from $0.01mm$ to $1mm$.

Three different types of material behaviour under cyclic loading are identified. They each correspond to a particular mechanism of crack nucleation and growth :

1. failure mode is dominated by shear crack growth. Cracks initiate in slip bands and at grain boundaries. Once initiated, the cracks become more distinct but show no significant increase in length.

2. cracks are initiated by a mechanism of shear crack nucleation. Shearcrack growth consumes only a small fraction of fatigue life. Cracks predominantly grow on planes of maximum principal strain.

3. the major portion of the life is consumed in the nucleation phase. Cracks form within single grains but they are unable to propagate into neighbouring grains.

Experiments show that for a particular case the failure mechanism is determined by the type of loading, the amplitude of loading and by the material itself. Difference of one of these three characteristics may cause a different failure mechanism to be active. SOCIE observed the behaviour of 304 stainless steel and Inconel 718 in axial and torsional loading. At low torsional loading amplitudes mechanism 2 is active for 304 stainless steel whereas mechanism 1 is active for Inconel 718. At high axial tension loading amplitudes mechanism 2 is active for 304 stainless steel and mechanism 1 for Inconel 718. Mechanism 3 is encountered only at low amplitude axial loading in 304 stainless steel. In torsional loading and in Inconel 718 mechanism 3 occurs only at load amplitudes that are close to fatigue limit.

In a next step physical damage phenomena are quantified in a fatigue damage map fig.5.16. The vertical axis is plotted in terms of hydrostatic stress normalised by maximum principal stress. This format allows representation of all the stress states from torsion to

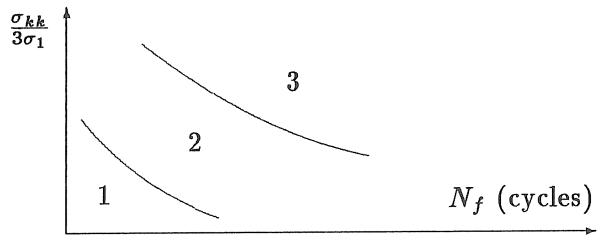

Figure 5.16: Fatigue damage maps

biaxial tension on a single diagram. The fatigue damage maps are used to estimate the type of failure that is expected for any state of stress. The regions indicated by 1, 2, 3 correspond respectively to the failure mechanisms 1, 2, 3.

Once the failure mode has been identified the appropriate life estimation model can be selected. Each region requires a separate damage model that is based on the observed failure mode :

1. mechanism 1, shear crack growth is predominant [166]

$$\hat{\gamma} + \hat{\varepsilon}_n + \frac{\hat{\sigma}_{n0}}{E} = \frac{\tau'_f}{G} N^b + \gamma'_f N^c$$

where : τ'_f : shear fatigue strength coefficient
γ'_f : shear fatigue ductility coefficient
b : fatigue strength exponent
c : fatigue ductility exponent
G : shear modulus
N : number of cycles to formation of a $1.0mm$ surface crack
$\hat{\gamma}$: maximum shear strain amplitude
$\hat{\varepsilon}_n$: tensile strain perpendicular to the maximum shear strain amplitude
$\hat{\sigma}_{n0}$: mean stress perpendicular to the maximum shear strain amplitude
E : YOUNG's elastic modulus

2. mechanism 2, crack growth predominantly on planes of maxi-

mum principal strain

$$\sigma_1^{max}\varepsilon_1 = \frac{\sigma_f'^2}{E}N^{2b} + \sigma_f'\varepsilon_f' N^{b+c}$$

where : ε_1 : maximum principal strain amplitude
σ_1^{max} : maximum principal stress on ε_1 -plane

This criterion is an extension of the SMITH-TOPPER-WATSON -parameter to multiaxial loading.

3. mechanism 3, nucleation phase predominant

$$\hat{\tau} + \hat{\sigma}_n = \sigma_f' N^b$$

where : $\hat{\tau}$: maximum shear stress amplitude
$\hat{\sigma}_n$: maximum stress on $\hat{\tau}$ -plane

This criterion is an extension of the strain–life -relation for low amplitude loading to combined axial and torsional loading. It is proposed by FINDLEY [167].

The quantities $\hat{\gamma}$ in equation 1, σ_1^{max}, ε_1 in equation 2 and $\hat{\tau}$ in equation 3 should be taken equal to the overall maximum value over an entire cycle. For nonproportional loading σ_1^{max} and ε_1 may not occur simultaneously.

Material constants in each of these equations are determined from tension and torsion tests. The fatigue strength and ductility exponents b and c are often nearly the same in tension and torsion.

If both tension and torsion data are available, good life estimates can be made by considering both tensile and shear failure models. The shear model overestimates the life in situations dominated by tensile crack growth and the tensile model overestimates the life for situations dominated by shear crack growth. A valid engineering approach is to calculate the three damage parameters and estimate the life from each one. The expected life will then be the lower of the two estimates.

5.4 Comparison of the computed lifetime to experimental results

Accuracy of fatigue computations is a matter of serious concern. Standard deviation on both computed and measured lifetimes tend to be very high. Values that range from 33% up to 300% of the "correct" value are considered acceptable. This statement is valid for both analytical and experimental results. Even for specimens with very simple geometry that are subjected to well defined loading, variance of measured lifetime usually is significant. This is due to material deficiencies on a microscopic scale.

These considerations do not imply however that fatigue analyses are doomed to scientific oblivion. The approach that is presented in previous chapters and sections is perfectly capable of revealing tendencies. Appropriate modelling of different influence factors allows a sensitivity analysis. It is then up to the user to decide on how accurate models and parameters need to be, depending on the results that are expected.

5.4.1 Sensitivity of the computed lifetime to variations of some parameters

In numerical analysis the computed result is sensitive to variations of each of the parameters that are involved. This relation is merely theoretical for a number of parameters, while for some others, sensitivity may be extremely significant. Subsections 5.4.1.1 to 5.4.1.3 enumerate the most important relations that the user has to define carefully. It is always assumed that all other quantities remain unchanged.

5.4.1.1 Material properties

Two classes of material properties are identified. The constitutive relations describe the stress–strain behaviour in elastic and plastic regions, and the strain–life -relation expresses the fatigue characteristics of the material. Three constant numbers fully describe the constitutive relation. Uncertainty on the value of the elastic modulus E is usually insignificant, since this parameter is well known for almost all materials. The plastic modulus K' and exponent n' on the other hand are seldom accurately determined. Appendix B shows why the evaluation

of these constants is more complex than the evaluation of E. Consequently one needs to have an idea of the influence these coefficients have on the computed lifetime. In the area of high-cycle fatigue the influence is nonexistent since no plastic straining occurs. In the plastic area the slope of the cyclic curve is determined by n' and the height of the curve is given by K'. The influence of both parameters on the computed lifetime is rather low.

An example that is taken from common practice illustrates the effects these parameters have on computed life. An age-hardened cast aluminum Gk AlSi7Mg specimen is axially loaded in constant amplitude push-pull conditions. Purely elastic deformation, purely plastic deformation and transitory effects are modelled by varying the stress concentration factor K_t. The material coefficients, that are taken from GRUBISIC [168], and data on the loading conditions are presented in tables 5.1. The computed life is given for different combinations of K'

material constants	
E	75 GN/m^2
K'	233 MN/m^2
n'	0.072
σ'_f	277.5 MN/m^2
ε'_f	0.018
b	-0.07
c	-0.46

loading conditions	
$\frac{\Delta\varepsilon_{nom}}{2}$	0.1%
$\varepsilon_{nom,mean}$	0%
elastic	$K_t = 1.25$
transition	$K_t = 1.75$
plastic	$K_t = 2.25$

Table 5.1: Material properties and loading conditions

and n' in every stage of deformation (table 5.2).

The influence of the fatigue characteristics is more readily clear. The coefficients σ'_f and ε'_f determine the height of the strain–life - curve whereas b and c describe its slope. Life obviously increases with σ'_f and ε'_f and decreases with b and c. The influence of σ'_f and b is predominant in the high-cycle fatigue area, ε'_f and c preponderate in the low-cycle region. Evaluation of the coefficients is not straightforward as parameters appear in an exponential relation. Further, variation on measurement results complicates the mathematical operation of curve-fitting the data. Confidence levels are employed to account for the variation on experimental results.

		K'		
	n'	95%	100%	105%
$K_t = 1.25$	95%	6.21×10^6	6.27×10^6	6.30×10^6
	100%	6.11×10^6	6.22×10^6	6.27×10^6
	105%	5.97×10^6	6.14×10^6	6.22×10^6
$K_t = 1.75$	95%	51290	63830	74820
	100%	44060	56240	67610
	105%	37670	48980	60400
$K_t = 2.25$	95%	1795	2312	2931
	100%	1589	2042	2582
	105%	1409	1807	2280

Table 5.2: Sensitivity of computed life to K' and n' for different K_t

5.4.1.2 Mean stress level

Several models have been designed to take the effect of mean stress into account. It is observed experimentally that tensile mean stresses tend to reduce the number of cycles a material can be subjected to before it fails. Compressive mean stress may have a beneficial effect on lifetime. A conservative approach neglects this phenomenon.

The influence of mean stress is significant only in the area of high-cycle fatigue. In low-cycle fatigue mean stress effects are almost nonexistent, since high strain amplitudes tend to relieve mean stresses. Only amplitude is determinative for lifetime. It is thus important to take mean stress into account especially when the number of cycles to failure is high. The results obtained for example 5.1 are compared to a similar case with mean value of nominal strain equal to 0.1%. Table 5.3 summarises the computed lives. It is demonstrated that :

- the SMITH-TOPPER-WATSON -parameter recognises the absence of mean stresses

- influence of mean stress is significant for low-amplitude loading

These considerations illustrate the importance of static loads and residual stresses.

$\varepsilon_{nom,mean}$		0%	0.1%
$K_t = 1.25$	no mean stress	6.22×10^6	6.22×10^6
	SMITH-TOPPER-WATSON	5.88×10^6	0.31×10^6
$K_t = 1.75$	no mean stress	56230	56230
	SMITH-TOPPER-WATSON	68710	18540
$K_t = 1.75$	no mean stress	2042	2042
	SMITH-TOPPER-WATSON	4198	2018

Table 5.3: Influence of mean stress

5.4.1.3 Cyclic stress level

The most important factor that influences the computed life is the cyclic strain level. The amplitude of straining is related directly to the number of cycles to failure. It is shown easily that computed life is extremely sensitive to strain amplitude :

$$\frac{\Delta\varepsilon}{2} = \frac{\sigma'_f}{E} N^b + \varepsilon'_f N^c$$

In low-cycle fatigue a fair approximation is obtained with $(c < 0)$:

$$\varepsilon = \varepsilon'_f N^c$$

$$\frac{d\varepsilon}{dN} = c\varepsilon'_f N^{c-1}$$

Thus :

$$\frac{d\varepsilon}{\varepsilon} = c\frac{dN}{N}$$

Consequently a relative error on ε is multiplied by a factor $1/|c|$. In the other extreme case of high-cycle fatigue the sensitivity is even more important. Relative errors on ε are multiplied by a factor $1/|b|$, a number that is often greater than 10.

The factor of prime importance in fatigue analysis is thus the stress concentration factor K_t, that is computed numerically by boundary element analysis. This consideration justifies why so much careful attention has to be paid to the computation of modal strains and the stress concentration factor. Some practical examples are presented in table 5.4, using the same data as in table 5.1. For this case an increase of only 5% of the stress concentration factor reduces the life to half its original value.

K_t	95%	100%	105%
1.25	12.6×10^6	6.22×10^6	3.19×10^6
1.75	118300	56240	27860
2.25	3724	2042	1200

Table 5.4: Sensitivity of computed life to stress concentration factor K_t

5.4.1.4 Comments on the accuracy of the computed lifetime

The final result of a fatigue life analysis is one single number. One should be well aware of what that number means. It can obviously not be expected to represent the correct number of cycles before failure occurs. The obtained result is valuable however, provided the model is well suited and the final result is interpreted soundly. The reasons why it is not correct are multiple.

Firstly, it is often hard or even impossible to account for all the environmental conditions that exist in service. Laboratory conditions during testing and measurement of material characteristics can be significantly different from real service conditions. Simulation of service conditions can be difficult.

Secondly, local structural behaviour can cause minor discrepancies from the modelled behaviour. Phenomena like friction and backlash can introduce local nonlinear behaviour, possibly influencing crack initiation in the fatigue critical area. When these phenomena are significant, some other approach has to be used to estimate the fatigue life of the affected area.

Thirdly, there is no physical law that validates MINER's rule. Damage accumulation may not follow a linear law. Variable amplitude loading generates variable crack opening stress levels. The stress amplitude that is responsible for damage accumulation is difficult to predict. The succession of high and low amplitudes or vice versa does affect damage accumulation. The effects of this can be quite important (ELBER, section 1.3.3.2.1). MINER's law does not recognise this phenomenon.

These shortcomings are responsible for a rather high degree of variance on results. Numerical values are considered acceptable when they differ from experimental values by a factor of three. Apart from these phenomena, the influence of which can hardly be quantified, some uncertainty may exist on the actual values of the parameters. It is always

wise to investigate the influence of these parameters, by checking sensitivities. For the influence of mean stress for instance, it is advisable to verify their influence by performing several computations. Comparison of the computed life without mean stress, with HAIGH-SODERBERG's criterion, with the SMITH-TOPPER-WATSON -parameter, ...allows a critical evaluation of the actual situation. As to the material characteristics and the K_t-factor, sensitivity analysis reveals the parameters one should be confident about.

5.4.2 Tuning of the model

It would be very brave and foolhardy to credit the approach proposed by the author in the previous chapters with the merit of rendering experiments superfluous. The factors mentioned in the previous subsection are not taken into account by analytical theories. Their influence may be significant. The only way to have an idea on the repercussions they have is a test. This test should preferably be performed under real service conditions and not in laboratory simulation.

Experimental evidence thus remains an essential element in a practical fatigue analysis. It can easily be integrated in the numerical approach, thus accounting for all the factors of uncertainty that should be incorporated. The nominal value of the right hand side constant in MINER's rule is 1. When performing a fatigue test under service conditions it is rather unlikely that the left hand side sum of the MINER accumulation rule at failure would equal the theoretical value. This is a strong suggestion that for all cases that are similar to the one tested, the right hand side constant should be equal to the experimental value. By doing so all the factors of uncertainty together are handled in a sort of black box approach. This is an efficient way of updating the model to physical reality. The flowchart of the updating procedure is presented in figure 5.17.

5.5 Conclusion

This chapter covers the methods that are used in the prediction of fatigue life that corresponds to a given strain sequence. The basic elements of the local strain approach are incorporated in a global method that allows sensitivity analysis and updating of the fatigue life prediction model. The local strain approach is adopted. Its basic features

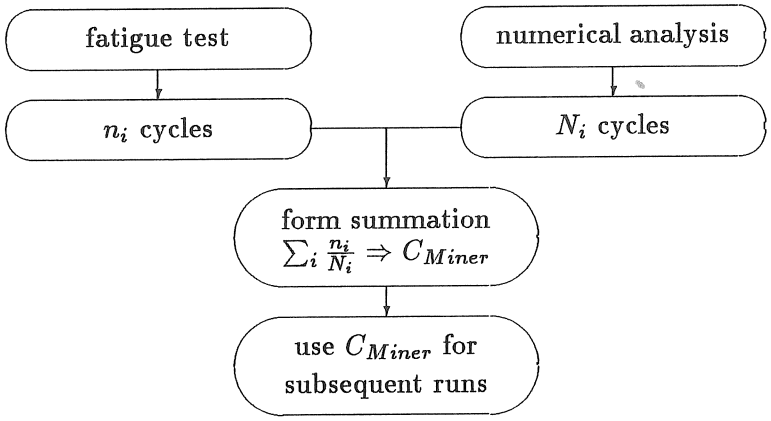

Figure 5.17: Flowchart of fatigue updating procedure

are briefly summarised and some counting procedures are discussed. It is shown that the approach is based on a number of idealisations on the stress–strain behaviour of a material and on the spatial distribution of stress and strain in the neighbourhood of a geometrical discontinuity. These assumptions are valid for a very wide range of metallic materials and loads in practical applications. The rainflow technique is found to be closest to reality.

For situations of multiaxial stress the local strain technique is not directly applicable. Quite voluminous effort has been spent by researchers all over the world in devising theories and methodologies that are capable of modelling the peculiar effects of multiaxial states of stress and strain. For high-cycle fatigue a modified octahedral shear stress theory is developed. For low-cycle fatigue the situation is much more difficult, especially when load paths are nonproportional. SOCIE presents an approach that is essentially similar to the conventional strain–life -relation from local strain approach. Three different damage mechanisms are identified that each have a particular damage parameter associated to it. The damage mechanism that is most harmful in the considered situation will be active.

In order to establish confidence in the obtained results the user should know which parameters are most critical to the computed lifetime. Sensitivity analysis quickly reveals that cyclic strain levels do

have the largest influence on lifetime. Relative errors on cyclic strain are multiplied by a factor equal to the reciprocal of the slope of the strain–life -curve in a logarithmic diagram. This observation explains why such diligent care has to be taken in the strain computation phase. Material characteristics n' and K' have an important effect too, when high load amplitudes occur. Measurement of these parameters is rather critical.

A large number of uncertainties on local material and service conditions affect the fatigue behaviour. Those effects can almost not be taken into account. They cause the MINER sum at failure to be different from the theoretical value 1. Modification of this value based on experimental results allows tuning of the model. In subsequent analysis, it is then reasonable to assume that all the effects one is uncertain about can be neglected.

Chapter 6

Practical examples

6.1 Introduction

Two examples illustrate the concepts that are developed in the theoretical chapters 2–5. Although both cases appear to present only low degree of complexity at first sight, some special considerations apply to each one of them. It will be shown that very specific details of the problem govern the entire fatigue behaviour. In the first example geometric characteristics are responsible for fracture, whereas in the second example the dynamic behaviour preponderates.

In both cases analytical predictions of the fatigue life are compared to experimentally measured lives. In the first example, the cause of the discrepancy between both quantities is discussed and it is shown how the model is updated. In the second example the structure is modified to exhibit improved fatigue resistance.

6.2 Notched cantilever beam

A practical problem of fracture of a notched beam is examined. The component is loaded by a sinusoidally varying force at resonance. Experimental and analytical modal analysis are performed and the analytical model is updated manually. Stress analysis is done with the boundary element method. The predicted life is compared to the experimentally measured life. It turns out that predicted values do not match with experimental results. Closer examination of geometry reveals the sources of error and the numerical model is updated

efficiently.

6.2.1 Description of the problem

A beam with square cross-section ($10 \times 10mm^2$) made of steel DIN 14NiCrMo13 is clamped on an electrodynamic vibration exciter. The geometry of the beam together with the clamping is shown in fig.6.1. An enlarged view of the notched section of the beam is given in fig.6.2.

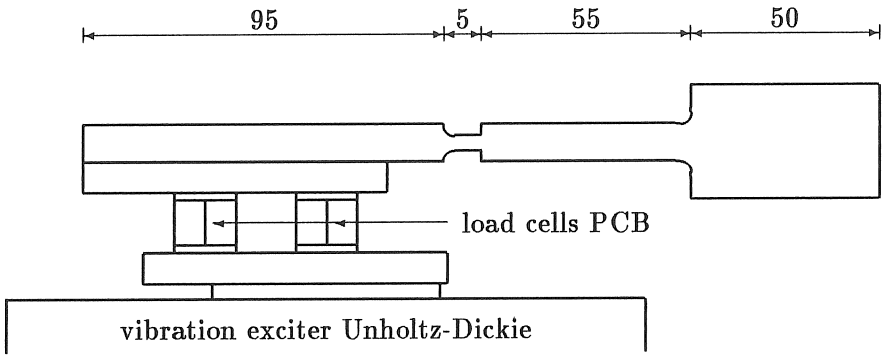

Figure 6.1: Geometry of clamped beam

The radii of the notches are 3 *mm* at the left hand side **a** of the notch

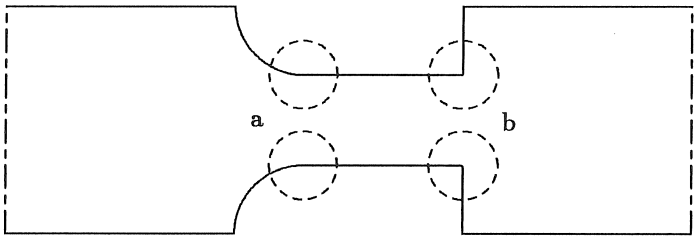

Figure 6.2: Enlarged view of notched area

and 0.1 *mm* at the right hand side **b**.

The structure is loaded with a sinusoidally varying force at the second resonance frequency. The amplitude of vibration is a displacement of 1.5 *mm* at the free end of the beam. Two areas are potentially critical, one on the left hand side **a** of the notch and another one on the right hand side **b**.

6.2.2 Dynamic analysis

6.2.2.1 Experimental modal analysis

An experimental modal analysis of the structure is performed. The structure is mounted on an electrodynamic vibration exciter Unholtz-Dickie. A burst random excitation signal is applied. Load input is measured with two load cells PCB. Addition of both signals gives a measure of the vertical force that is developed by the exciter. Subtraction of both signals gives a measure of the moment generated in the clamping device. The response of the structure is measured with a light-weight accelerometer Kistler. The response transducer is placed at fourteen locations successively. The frequency range that is used is 50 – 350 *Hz*, because only the second mode of the structure is of importance here.

First the addition of both load signals is considered. Parameter estimation gives following results :

$$\nu_2 = 146.1\ Hz \qquad \zeta = 2.31\%$$

The mode shape is represented in an amplitude format in fig.6.3. Visual interpretation of animated mode shape data on the screen shows

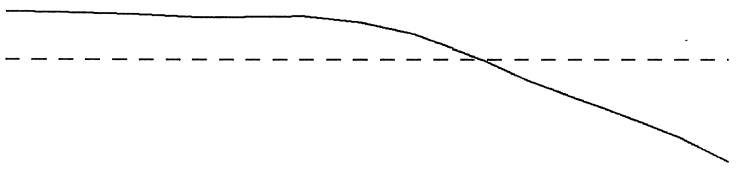

Figure 6.3: Experimental mode shape

that phase shifts are not significant. The deformation of the mode is concentrated mainly in the notch.

Subtraction of signals is considered afterwards. Frequency response functions between exciting moment and response at any location are almost flat, revealing that the clamping device has some quite rigid characteristics. Rotations are zero in the nodes located at the clamping device.

6.2.2.2 Numerical modal analysis

A finite element model of the structure is constructed using MSC-Nastran. The beam is modelled with 43 grids and 43 CBAR elements

having appropriate cross-sectional properties. The clamping is modelled with 17 scalar CELAS3 elements with a stiffness which is a priori unknown. The mass loading effect of the clamping device is modelled with 17 scalar CMASS3 elements over which the total added mass is distributed. Rotational degrees of freedom are constrained at the nodes on the clamping device. The finite element model is shown in fig.6.4. Beam elements are well suited for modelling both the stiffness

Figure 6.4: MSC-NASTRAN finite element model

and the mass distributions along the beam. It is learnt in experimental analysis that constraining rotational degrees of freedom in the clamping device is a valid assumption. The only parameter that one is uncertain about is the stiffness characteristic of the CELAS3 elements. Fig.6.5 shows the variation of second resonance frequency with stiffness of the spring elements. In order to obtain correlation with experimental data stiffness properties of the scalar springs are taken to be 7.45 kN/m. The scaling option is selected such that displacement

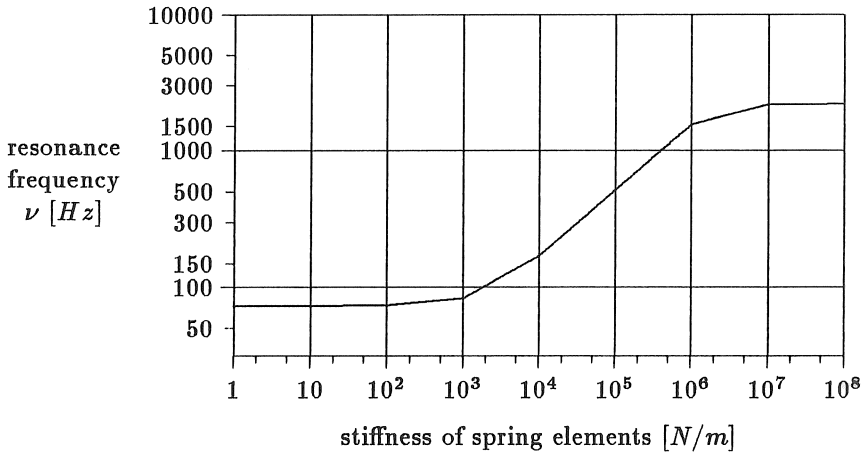

Figure 6.5: Variation of resonance frequency with spring stiffness

is equal to 1 at the free end of the beam.

6.2.3 Modal strains

Acceleration mode shape data are used to compute the distribution of inertial loads over the structure. Analytical data obtained with the updated model are used to determine inertial loads. Mode shapes are scaled to the desired amplitude of 1.5 mm at the free end of the beam. The factor which is applied is then :

$$\frac{a}{u} = -\omega_2^2 = (2\pi \times 146.1)^2$$

The total conversion factor from displacements to inertial loads is :

$$\rho\omega^2 = 7850\ kg/m^3 \times (2\pi \times 146.1)^2/s^2$$

Inertial load f_i at node i is thus given by :

$$f_i = \rho\omega^2 \frac{u_i}{u_{end}} \times 1.5\ mm \tag{6.1}$$

where : u_i : displacement amplitude as scaled originally
u_{end} : displacement amplitude at free end as scaled originally

Strain analysis is performed with a two-dimensional boundary element model. Two cross-sections of the beam are potentially critical. The remainder of the structure does not have to be examined. Strain analysis is restricted to an area that encloses the notched sections. The area shown in fig.6.2 is used. Because only part of the beam is modelled cross-sectional stress resultants have to be taken into account. The same factor of proportionality 6.1 which is used for inertial loads applies here to bending moments and shear forces. The stress distribution that both cross-sections have to be subjected to is more or less arbitrary. A linear distribution for normal stresses and a quadratic distribution for shear stresses are most conventional. An isostatic set of displacement boundary conditions is used. In order to describe the variation of volume loads a separate model is constructed using four linear four-noded quadrilateral elements. Geometry is modelled only with a very rough approximation. Inertial loading, cross-sectional loading and boundary conditions are presented in fig.6.6.

Because of the extremely small radius of the notch a very dense mesh of boundary elements is constructed. A total of 216 discontinuous

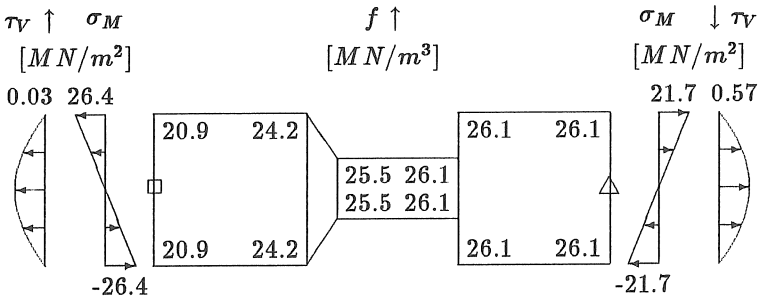

Figure 6.6: Boundary conditions and inertial loading

quadratic elements are defined with minimum size at the critical areas. The ratio of the dimensions of adjacent elements does not exceed 1.16. The boundary element code BE is used. It shows that maximum strains are found in the circular elements, close to the transition to straight elements.

$$\varepsilon_a = 0.095\% \qquad \varepsilon_a = 0.224\%$$

6.2.4 Fatigue life prediction

Two strain sequences are analysed, one in section **a** and one in section **b**. The selection of the most critical area is straightforward as the amplitude of vibration is kept constant.

The cyclic characteristics and the fatigue properties of the material are evaluated with the procedures discussed in appendix B. Detailed description of these tests is found in [175] and [176]. The values of the relevant material characteristics are summarised in table 6.1.

Both strain sequences are analysed with the program FATAN. The predicted lives together with intermediate results are summarised in table 6.2.

The computed lives are the numbers of cycles before a crack initiates at the particular area.

6.2.5 Fatigue life experiment

A complete fatigue test is performed using the same setup as in the modal test 6.2.2.1. A constant load amplitude is applied at resonance frequency 146.1 *Hz*. The response of the beam is monitored with

STEEL 14NiCrMo13		
property	symbol	value
Young's modulus	E	203 GN/m^2
Poisson coefficient	ν	0.3
yield stress	σ_y	600 MN/m^2
ultimate stress	σ_u	760 MN/m^2
plastic modulus	K'	1006 MN/m^2
cyclic exponent	n'	0.076
fatigue strength coefficient	σ'_f	821.1 MN/m^2
fatigue ductility coefficient	ϵ'_f	0.069
fatigue strength exponent	b	-0.0422
fatigue ductility exponent	c	-0.5554

Table 6.1: Material properties of steel 14NiCrMo13

	zone **a**	zone **b**
local strain [%]	0.095	0.225
local stress $[MN/m^2]$	190	445
number of cycles	2.3×10^{15}	1.98×10^6

Table 6.2: Predicted life of notched beam

an accelerometer mounted at the free end of the beam. The load amplitude is tuned such that the desired amplitude of deformation is obtained.

After six minutes of cycling it is observed that the amplitude of deformation has decreased with respect to the starting conditions. The frequency of the excitation signal is modified in search of resonance. Frequency is tuned manually to 138 *Hz*. After three more minutes resonance frequency has shifted again visibly. Frequency is tuned to 129 *Hz*. The response signal of the accelerometer deviates from a perfect sinusoidal shape at the maximum level, whereas it variation is sinusoidal at the minimum level. This is a first indication that a crack is initiating. Still visual inspection is unable to detect any cracks. Only after 20 minutes of cycling, with a frequency of 82 *Hz*, a crack becomes apparent at the upper surface of the beam in section **a**. The measured response signal is highly irregular. Cycling is continued until failure occurs after 29 minutes at a final frequency of 45 *Hz*. The crack has then extended over 3.5 *mm* of the total height of the beam of

4 *mm*. The fact that failure occurs in section **a** rather than in section **b** is unexpected. The number of cycles to initiation of the crack is taken 75000. All subsequent cycles should be analysed with fracture mechanics theories.

6.2.6 Justification of observed phenomena

Experimental results do not show any correlation with predicted values. The validity of the results of the fatigue tests can be considered to be beyond doubt. There has to be some aspect of the problem that is overlooked in theoretical modelling.

The deviation is caused by an imperfect milling of the specimen. Close examination of the milled notch shows both radii of 3 *mm* in zone **a** and 0.1 *mm* in zone **b** are manufactured accurately. The transition between the 3 *mm* notch and the straight section on the contrary is quite imperfect. A shoulder with a height of 0.05 *mm* and a very sharp notch cause an extremely high stress concentration to occur. The radius is so sharp that it can almost be considered as an initiated crack. The profile of the notch is shown in fig.6.7 with a magnification of 100×. A plaster cast of the notch is made and slices of it are

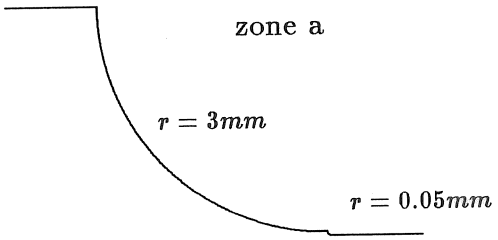

Figure 6.7: Profile of the milled notch

measured in a projector.

6.2.7 Updating of the model

The fatigue life prediction model can be updated in two ways :

- updating of the MINER-constant : it is observed that failure occurs in zone **a**, the predicted value in zone **a** is 2.3×10^{15}. The MINER-constant should therefore be set to $1/(2.3 \times 10^{15})$ instead of 1.

- updating of the stress concentration factor : in the computation that is described above modal strains are equal to maximum strains in the critical areas. Application of a stress concentration factor greater than 1 yields a computed life below the originally computed life. The stress concentration factor can be determined inversely such that predicted life equals the experimental value of 75000 :

$$K_t = 4.14 \tag{6.2}$$

Both methods can be applied independently. The latter provides a means of correlating data to physical quantities. Correlation is desirable since, in reality, the sharp notch does introduce stress concentrations.

6.2.8 Modification of the setup

A modified setup is made in order to allow comparison with the first test. The setup is largely the same as in fig.6.1, except for three modifications :

- the load cells and some mass are removed
- the beam is shifted by 15 *mm* with respect to the clamping device
- the material is carbonised

The modified setup is shown in fig.6.8.

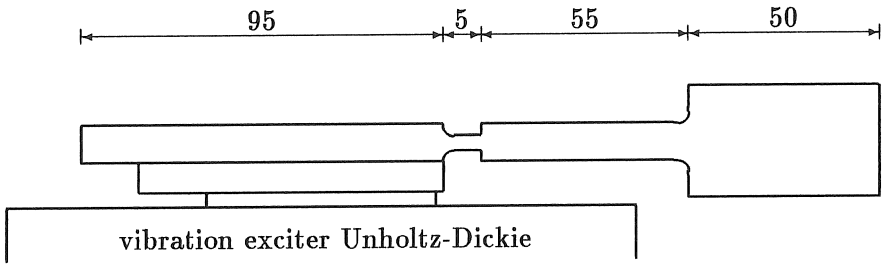

Figure 6.8: Modified setup of clamped beam

The notch is milled with exactly the same procedure as before. The imposed amplitude of vibration of the free end of the beam is 1.8 *mm*.

Because of the geometric modifications of the clamping resonance frequencies shift a little upward. However, since the notched beam in its second modal deformation behaves grossly as a single degree of freedom mass-spring system, resonance frequency is altered only slightly :

$$\nu_2 = 148.4\ Hz$$

The strain computation of the previous case is repeated with modified loading conditions. It is found that modal strain at the critical area is 0.1077% for the imposed amplitude. The elastic stress concentration factor obtained in equation 6.2 is applied. Properties of the carbonised material are summarised in table 6.3. Local stress and

STEEL 14NiCrMo13		
property	symbol	value
Young's modulus	E	203 GN/m^2
Poisson coefficient	ν	0.3
plastic modulus	K'	1306 MN/m^2
cyclic exponent	n'	0.042
fatigue strength coefficient	σ'_f	917 MN/m^2
fatigue ductility coefficient	ϵ'_f	1.417
fatigue strength exponent	b	0
fatigue ductility exponent	c	-0.7238

Table 6.3: Material properties of carbonised material

strain are computed :

$$\varepsilon_{real} = 0.4517\% \qquad \sigma_{real} = 893\ MN/m^2$$

The estimated number of cycles to failure is 120000. The alternative updating procedure omits the stress concentration factor but introduces a scaling constant in MINER's rule. When the stress concentration factor is omitted, however, strain levels remain below the fatigue limit and computed life is infinite.

The experimental determination of fatigue life is done in much the same way as for the previous test. The crack is initiated after about 270000 cycles. Correlation between predicted and measured lives is thus fair. During the crack propagation phase the measured response is highly irregular. Final failure occurs after 150000 more loading cycles.

6.2.9 Conclusion

Two important conclusions are drawn :

- minute geometric details affect life tremendously
- updating procedures are most efficient when physical reality, in this case the stress concentration factor, is modelled accurately

Clear distinction should be made between crack initiation and propagation. In this case the initiation phase constitutes the most important portion of the entire fatigue life.

6.3 Hammer of a machine

A practical problem of fracture of the hammer of a machine is examined. The component is loaded by a series of multiple impulses, giving rise to high frequency vibrations, and finally to resonance fatigue failure. The dimensions of the object are very small and so modal analysis has to be performed using the finite element method. Stress analysis is done with the boundary element method. Several design modifications are presented. It is shown why structural modifications are unable to increase the life of the structure unless the frequency contents of the load input is altered. The lifetime remains unacceptably low. Other measures have then to be taken and the only modification that is able to increase the lifetime significantly is the choice of material with better fatigue properties.

6.3.1 Description of the problem

The structure under consideration is shown in fig.6.9. It is the hammer of a machine. It has an axis of rotation C that is perpendicular to the plane of the page. It is uniformly made out of steel 14NiCrMo13. A normal cycle of operation consists of 6 phases (fig.6.10) :

1. before operation starts, the tail of the hammer is clamped against the force F_s of a spring.
2. after releasing the clamping, the spring makes it rotate in a counter-clockwise sense over an angle of about 90°.

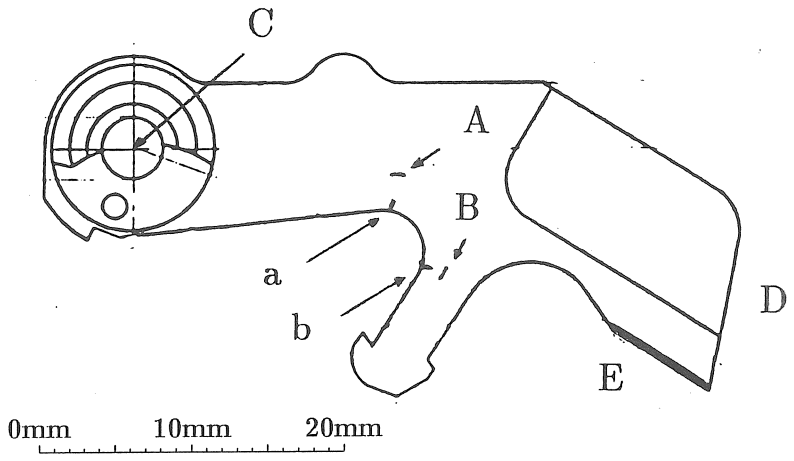

Figure 6.9: Geometry of the hammer

3. this counter-clockwise rotation is stopped by hitting another moving part M of the machine, that accelerates to the left. This contact is symbolized by an impact force F_1.

4. after a while the moving part M that was pushed to the left retreats and strikes in its turn the hammer. This contact force that hits the hammer is symbolized by the force F_2.

5. the clockwise motion of the hammer is stopped when it strikes a fixed axis X. This impact is symbolized by the force F_3.

6. the clamping device then locks the hammer in its starting position.

The angular velocity of the hammer in phases 2 and 4 is 175 rad/s, the linear velocity at contact in phase 5 is 7 m/s.

The problem of fatigue occurs in zones a and b (fig.6.9). After a number of cycles, typically 2000 to 4000, fracture occurs either in the body a, either in the tail b of the hammer. Cracks originate at the surface a or b and extend into the body towards zone A or into the tail towards zone B. Five specimens were tested up to failure, results are mentioned in table 6.4.

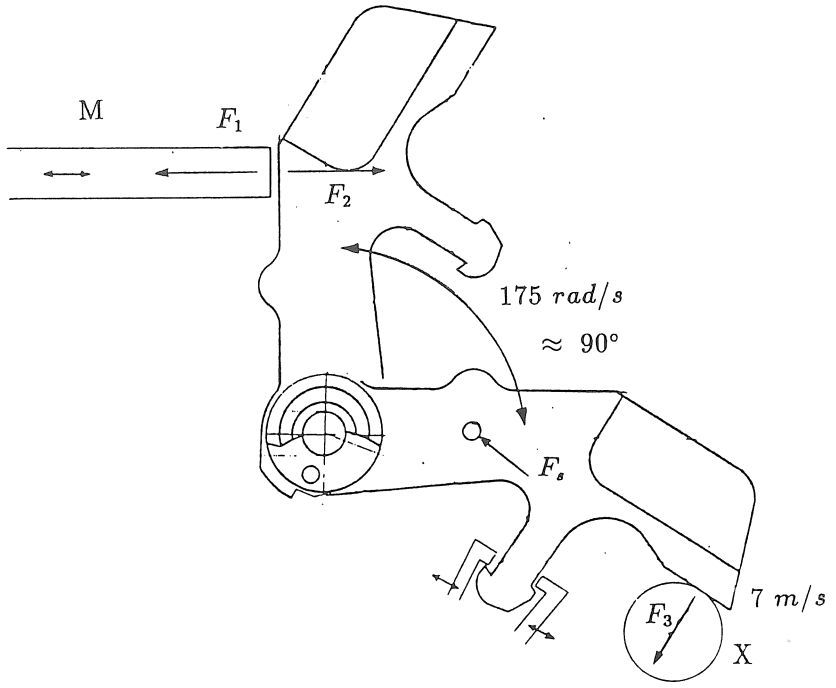

Figure 6.10: Different phases of a cycle of operation of the hammer

6.3.2 Fatigue analysis

For the present case the fatigue data have been measured on a R. R. Moore high speed fatigue testing machine. The type of loading was rotary bending with a constant bending moment. Test specimens had a diameter of 5.5 *mm*. The frequency of the test machine was 10000 *rpm*. The results of the tests are shown in the Wöhler–curve fig. 6.11.

The values of the relevant material characteristics are summarized in table 6.5.

Two different strain sequences are evaluated. They are obtained by measurement with straingauges. In most cases, like this one, it is difficult to stick straingauges in the critical areas. Moreover, most straingauges are not guaranteed to withstand high values of cyclic strain

specimen no.	number of cycles	location of failure
1	3820	body
2	2410	body
3	1970	tail
4	4020	tail
5	3050	body

Table 6.4: Lives of test specimens to failure

STEEL 14NiCrMo13		
property	symbol	value
Young's modulus	E	203 GN/m^2
Poisson coefficient	ν	0.3
yield stress	σ_y	1210 MN/m^2
ultimate stress	σ_u	1450 MN/m^2
plastic modulus	K'	1306 MN/m^2
cyclic exponent	n'	0.042
fatigue strength coefficient	σ'_f	1513.2 MN/m^2
fatigue ductility coefficient	ϵ'_f	0.000969
fatigue strength exponent	b	-0.0359
fatigue ductility exponent	c	-0.1476

Table 6.5: Material properties of steel 14NiCrMo13, CN 0.20

(3000 to 7000 μstrain) for several hundreds of cycles. The gauges are then placed as close as possible to the areas of fracture. A generalized stress concentration factor then expresses the relation between measured strain values and real strain values at the critical locations. The locations A and B are indicated on fig.6.9. With this configuration of straingauges the bending strains in both the body of the hammer and the tail are measured. The measured strain sequences are plotted in figs.6.12, 6.13.

The values are nominal values. The real values of the stresses that occur in the critical areas a and b (fig.6.9) of the hammer are obtained by multiplication of the measured nominal values with the appropriate stress concentration factor $K_{t,a}$ and $K_{t,b}$:

$$\sigma_a = K_{t,a}\sigma_A \qquad \sigma_b = K_{t,b}\sigma_B$$

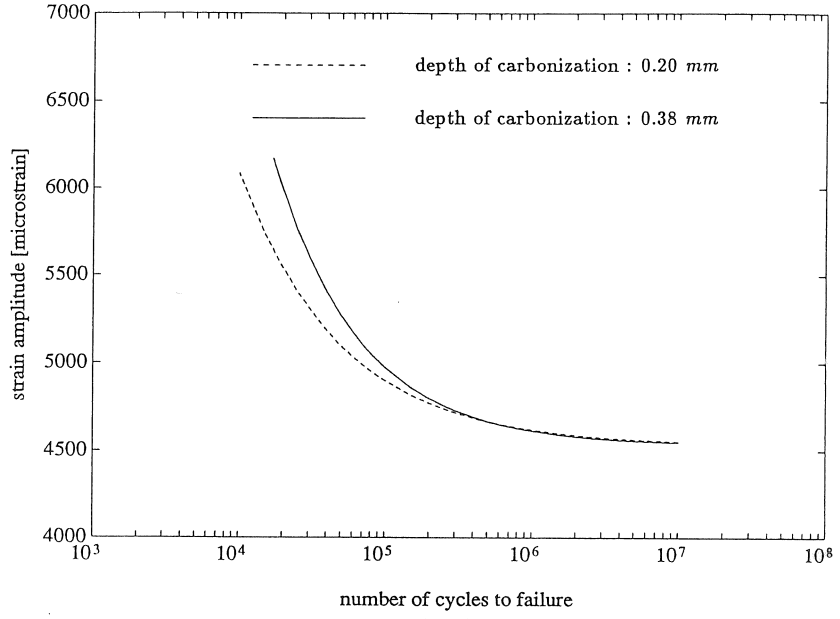

Figure 6.11: Relation between cyclic strain amplitude and number of cycles to failure

The stress concentration factors for dynamic loading are equal to those for static loading. Therefor one static computation is sufficient to obtain both $K_{t,a}$ and $K_{t,b}$. The loadcase that is considered is presented in fig.6.14. Both ends of the hammer are fixed and a static load is applied to the end of the tail of the piece.

Because of its superior capabilities in stress analysis, the boundary element method is used. The result of the analysis is presented in fig.6.15. The values of the stress concentration factors are then :

$$K_{t,a} = \frac{\sigma_a}{\sigma_A} \qquad K_{t,b} = \frac{\sigma_b}{\sigma_B}$$

This yields :

$$K_{t,a} = 2.81 \qquad K_{t,b} = 8.49$$

Application of the local strain approach with material characteristics as mentioned in table 6.5 consecutively yields local stresses and strains, hysteresis loops and accumulated damage. The hysteresis loops that occur in the critical area a of the body of the hammer are displayed in fig.6.16. As always in cyclic loading, the material behaviour exhibits plastic deformation at stress values far below static yield stress σ_y =1210 MN/m^2.

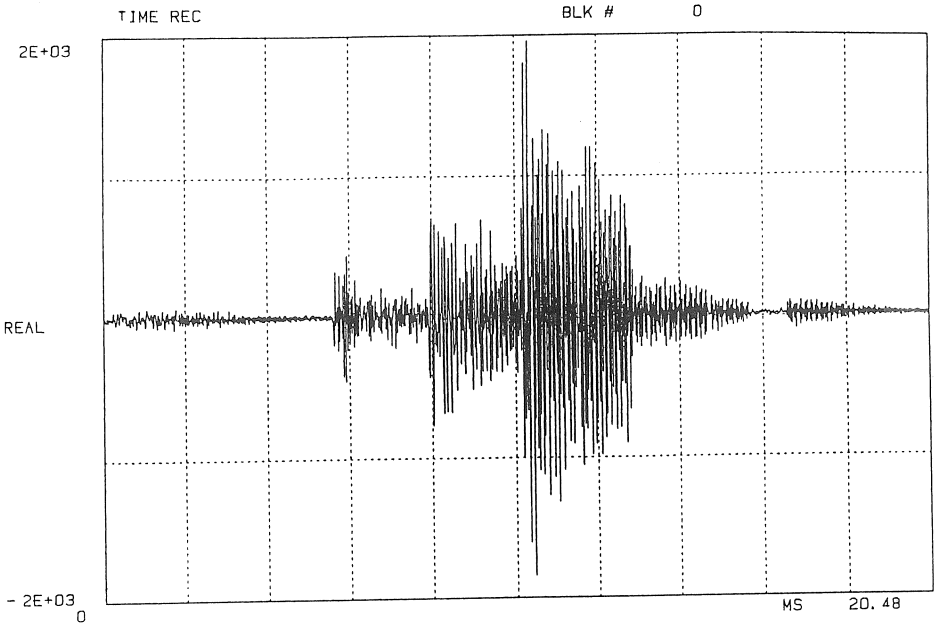

Figure 6.12: Measured strain sequence in point A

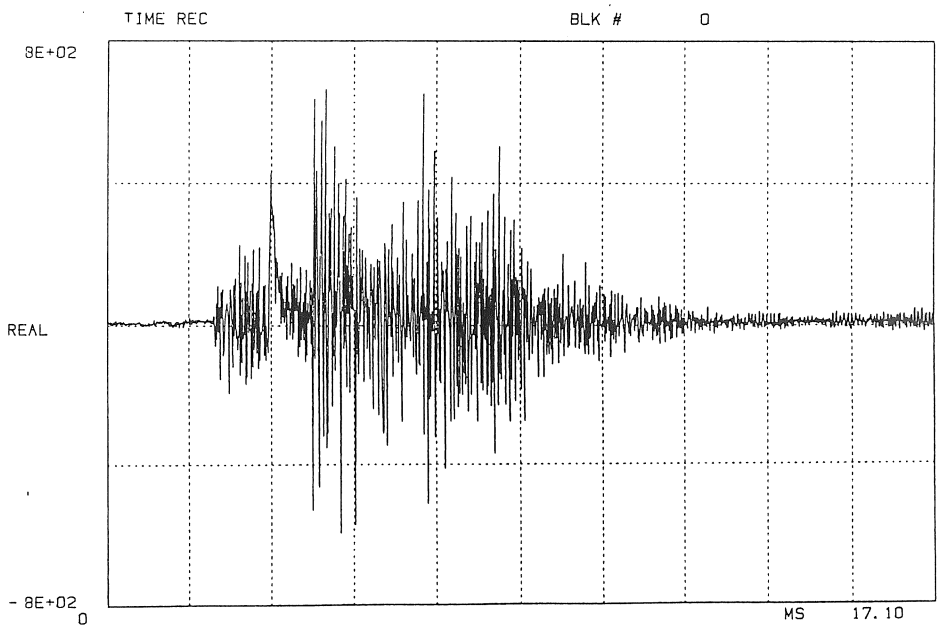

Figure 6.13: Measured strain sequence in point B

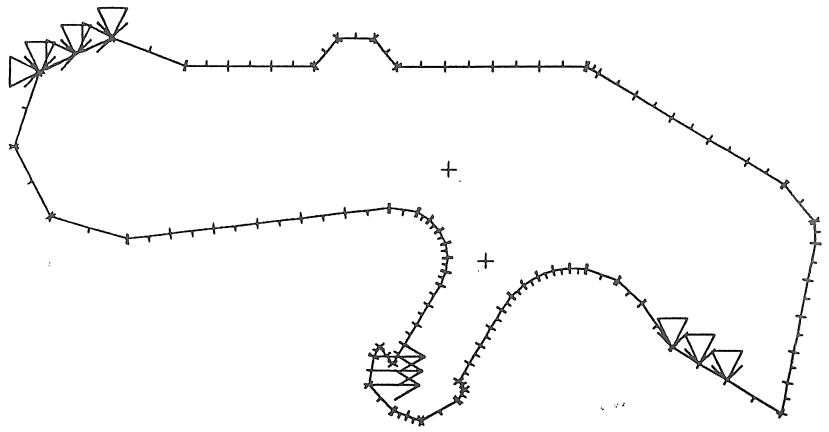

Figure 6.14: Static loadcase for determination of stress concentration factors

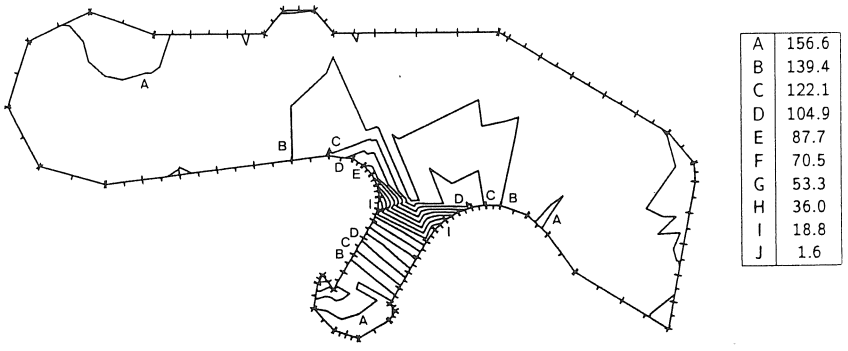

Figure 6.15: Iso-contour of equivalent VON-MISES -stress

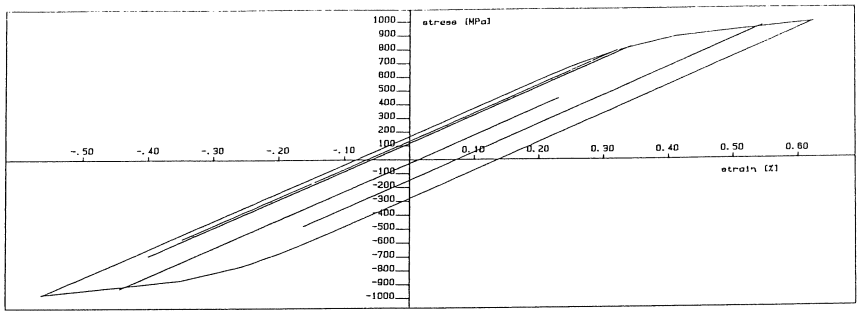

Figure 6.16: Hysteresisloops in the critical area a of the body of the tail

Finally the computed values of expected lifetime are found :

$$\begin{array}{ll} \text{zone a :} & N = 3820 \\ \text{zone b :} & N = 1940 \end{array}$$

These values represent the number of cycles (figs.6.12, 6.13) the hammer is able to withstand. These values should be compared to the lives that were obtained experimentally (table 6.4). With these data fracture would occur at the root of the tail of the hammer. However, with other specimens, fracture occurs in the body of the hammer (table 6.4). This is due to the fact that not all impacts F_2 (fig.6.2) have equal magnitude. Consequently, modes 1 and 2 are not always excited to the same proportion. This explains the variance that is found in experimental data. Anyway, the order of magnitude of the life predictions coincides with the experimental results. Relatively high numbers of variance are inherent to all fatigue life computations and experiments.

6.3.3 Resonance fatigue

Consider the measured strain sequences in each of both measurement points (figs.6.12, 6.13). These quickly varying signals are the response of the hammer to the applied load input. Their Fourier-transforms are presented in figs.6.17, 6.18. They reveal two peaks, one at 9.8 *kHz* and

another one at 21.0 *kHz*. These peaks suggest the existence of resonance frequencies of the structure. The peak at 21.0 *kHz* is dominant in the signal measured in point B, the peak at 9.8 *kHz* on the other hand appears in point A (fig.6.9).

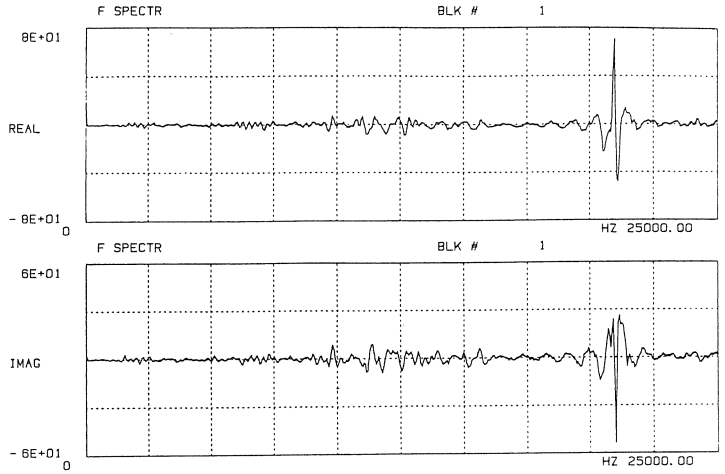

Figure 6.17: Fourier transform of measured strain sequence point A

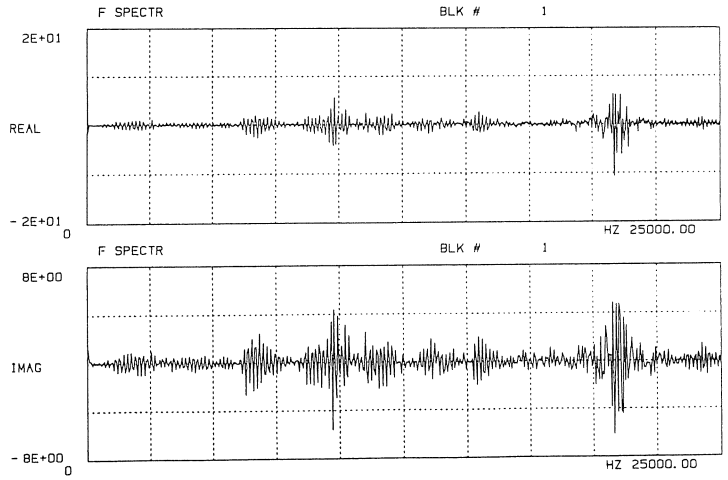

Figure 6.18: Fourier transform of measured strain sequence point B

The first measurements that were done, covered a frequency range up to 100 *kHz*. Some higher resonance frequencies appeared to exist in the neighborhoods of 54 *kHz* and 81 *kHz*, however, the stress levels

that characterized these modes, are considerably lower, so they could be left out of further analysis.

In conclusion, these plots give a strong supposition of resonance fatigue : the dynamic behavior of the hammer is responsible of a multiplication of the number of hysteresis loops with respect to the number of load cycles. This strongly reduces the life of the structure. A thorough analysis of the problem will have to start with an investigation of the dynamic characteristics of the hammer.

6.3.4 Resonance frequencies and modeshapes

Due to its very small dimensions, an experimental modal analysis of the hammer is hard to perform. Numerical modal analysis yields only resonance frequencies and modeshapes of the structure. Damping values can not be obtained without testing. However, damping is not primarily important for this problem.

Because the excitation of the hammer is in the plane of the structure, only the modes in this plane are relevant. An analytical modal analysis was performed, using the finite element package SYSTUS. A two-dimensional finite element model of the hammer was constructed using plane membrane elements. The model has a constant thickness. The mesh is shown in fig.6.19.

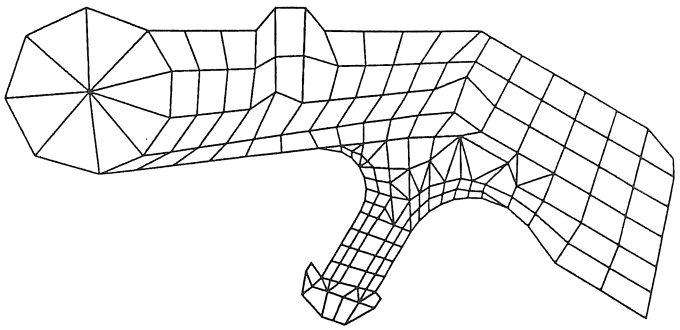

Figure 6.19: Finite element mesh

There are two degrees of freedom per node, namely the displacements of the node in both directions. The elements are quadrilateral or triangular, they are all linear. The structure is constrained at two

points, near the axis of rotation C, and at the extreme end D of the body of the hammer (fig.6.9). The first three resonance frequencies are summarized in table 6.6 and the corresponding modeshapes are shown in figs.6.20, 6.21 and 6.22.

mode no.	frequency $[kHz]$	type of deformation
1	7.7	bending of the body
2	18.4	bending of the tail
3	29.0	combination bending of tail and stretching of body

Table 6.6: Resonance frequencies

Only the first and the second eigenmode are important. These frequencies correspond with the peaks of the frequency spectra (figs.6.17–6.18). The third mode is less important since the direction of excitation in each of the phases 3, 4, 5 (section 6.3.2) is transversal to the main axis CD (fig.6.9) of the hammer, while the major direction of this mode is longitudinal.

6.3.5 Stress distribution

Each modeshape has its own stress distribution. This stress pattern is computed by imposing inertial forces from the modeshapes as an external static load. Each mode is characterised by the corresponding modal strain distribution.

The modal strain distributions for each mode are obtained from a static boundary element computation. The mode shapes computed in the finite element run are expressed in terms of displacements. Modal displacements are converted to inertial forces by multiplication with $\rho\omega^2$. The inertial forces are applied as a static load to the structure. Two computations were performed, one for the first and one for the second modeshape (figs.6.23, 6.24).

For the first modeshape, essentially bending of the body of the hammer, the area of maximum stress values is located in the body of the component, near the root of the tail. For the second mode, which is almost a pure cantilever bending of the tail, the area of maximum stress values is located in the tail, near its root. This is a confirmation of the supposition in section 6.3.3 that the first mode is primarily

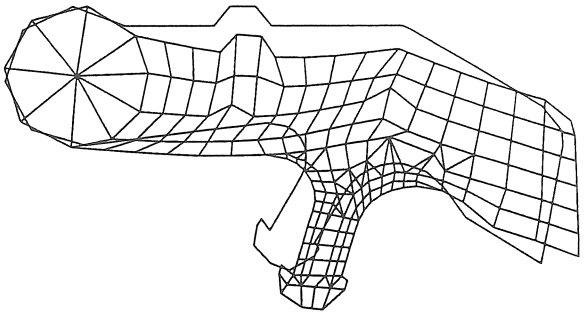

Figure 6.20: Deformation of mode 1

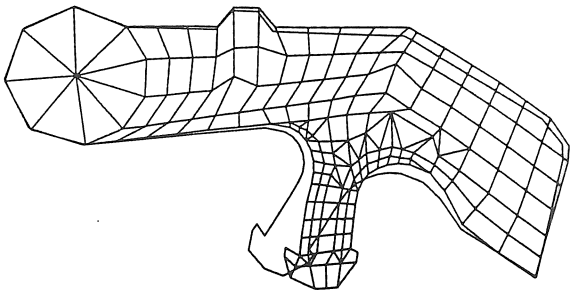

Figure 6.21: Deformation of mode 2

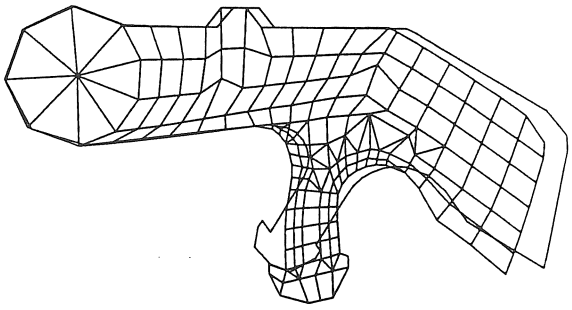

Figure 6.22: Deformation of mode 3

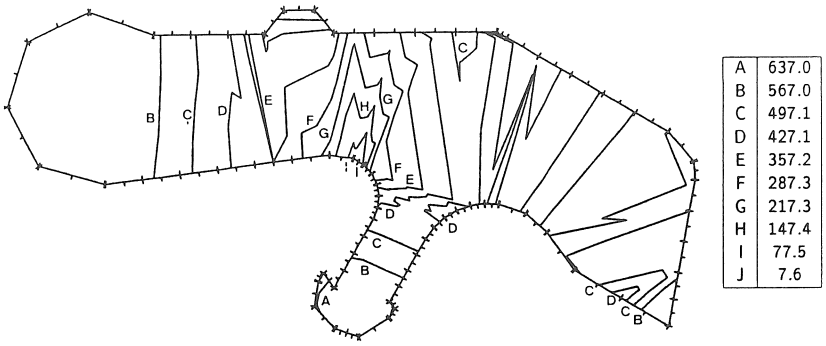

Figure 6.23: Iso-contour of equivalent VON-MISES -stress for mode 1

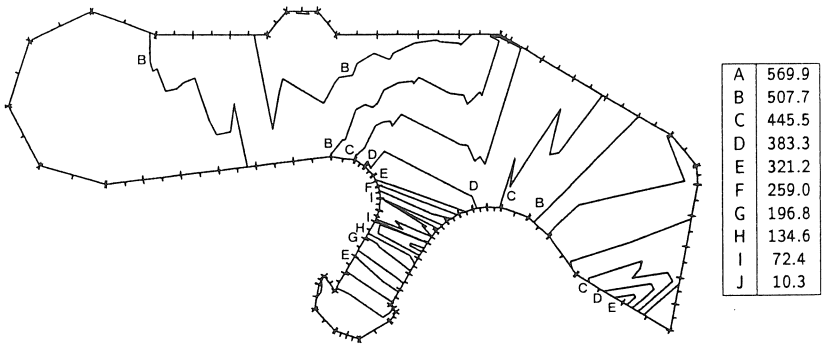

Figure 6.24: Iso-contour of equivalent VON-MISES -stress for mode 2

responsible for fracture of the body of the hammer, and the second mode for fracture of the tail.

6.3.6 Design modifications

Design modifications were absolutely necessary in order to obtain a reliable and well-functioning product. Several types of modifications are possible :

1. increase of radius of curvature of the root of the tail
2. increase of damping values
3. mass and/or stiffness modification in view of a shift of resonance frequencies
4. modification of load input
5. different material with better fatigue properties

6.3.6.1 Radius of curvature

The radius of curvature is sufficiently large. It can still be increased somehow, thus slightly reducing the stress concentration factor for zone A (fig.6.9). The peak stress in zone B under the first modeshape is almost independent of the radius of curvature. The gain in lifetime is only minor.

6.3.6.2 Damping

An important theoretical possibility to reduce the stress levels in a dynamically loaded structure is the introduction or the increase of damping. In the present case it is hard to evaluate damping in practice.

However, it is intuitively clear that the actual damping values are low : very few damping mechanisms are present. Friction only occurs in a limited area, moreover, friction is only activated in the first mode. The second mode is characterized by a cantilever bending vibration of the tail. Damping here is essentially material damping.

The only way to introduce significant damping is a coating of the material.

However, resonance frequencies will still be excited, and due to the impulse type of loading peak values of stress will be only slightly reduced.

6.3.6.3 Mass/stiffness modification

Mass or stiffness modifications are easily possible. For instance, some experiments have been performed with a thicker tail. Its thickness is increased from 4.30 *mm* to 5.05 *mm*. This modification results in an important increase of stiffness, and also an increase of mass of the tail.

The finite element computation, which is described in section 6.3.4 is repeated for this modified design. The values that were found are mentioned in table 6.7.

mode no.	frequency $[kHz]$	original frequency $[kHz]$
1	8.9	7.7
2	22.5	18.4
3	31.4	29.0

Table 6.7: Resonance frequencies of modified hammer

The general deformation patterns for the different modes remain unchanged.

This modification has an important effect on the resonance frequency of the second mode. However, both frequencies are still excited, because of the impulse type of loading, and so peak values of stress response are not altered considerably. The impulse response function $h(t)$ of the hammer is given by :

$$h(t) = |A_1|\, e^{-\zeta_1 \nu_1 t} \cos(\nu_1 t + \alpha_1) + |A_2|\, e^{-\zeta_2 \nu_2 t} \cos(\nu_2 t + \alpha_2)$$

where ν_1, ν_2 : resonance frequencies
ζ_1, ζ_2 : damping ratios
α_1, α_2: phase shift ($\approx 90°$)

A slight shift of the second resonance frequency ν_2 modifies only the argument of the exponential function, and as damping values do not vary with mass/stiffness modifications, the final result $h(t)$ remains approximately unchanged.

6.3.6.4 Load input

A useful design modification is a modification of the load input. The frequency spectrum of the load input is very broad. Due to the hardness of the materials the impulse approximates a theoretical Dirac-impulse closely, as far as its frequency contents is concerned. It was found that the resonance frequencies remain present in the Fourier transform of the response as if the load input were a theoretical Dirac-impulse. No matter what the resonance frequencies of the structure are they will always be excited by this load input. Only in the areas of high frequency 50 kHz and over, the frequency contents begins to decline.

From the readings of the straingauges (fig.6.12, 6.13) it is clear that stress reaches its highest values in phase 5 of the cycle of the hammer (section 6.3.2), when the hammer strikes the fixed axis X (fig.6.9). This phase is responsible for the largest portion of the accumulated damage. So it would be most helpful if this particular phase of the cycle could be changed.

The idea now rises to alter the load input in such a way that its frequency contents covers a much smaller range. This goal can be reached by a reduction of the hardness of the contact area of the hammer. It is done by covering the metallic head with an elastomer cushion E (fig.6.9). This reduces the frequency spectrum of the impulse to a much smaller range, thus avoiding the excitation of high resonance frequencies to a considerable extent. The critical frequencies are still present in the spectrum of the new impact load, but their level of excitation is reduced significantly. The straingauge readings in zone A (fig.6.9) are presented in fig.6.25. The peak values of stress are reduced to almost half of their original values. The lifetime increases tremendously : $N = 1.93 \times 10^{13}$.

However, the contact area between the elastomer head and the metal axis is small and geometrically very sharp. Moreover, impact occurs with a velocity of 7 m/s. After roughly 1000 cycles the elastomer cushion is completely worn out, and after that, contact occurs again between metal and metal. The gain in lifetime is limited to the number of cycles during which the elastomer head functions properly. For this particular structure, it would be a very awkward procedure to replace the elastomer head at regular intervals. This design modification is unacceptable for practical reasons.

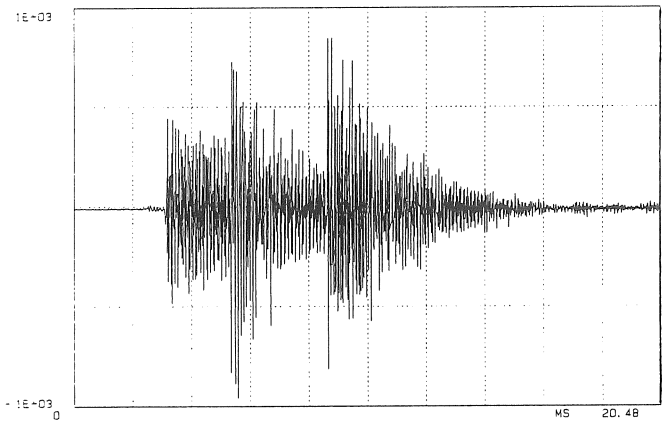

Figure 6.25: Measured strain sequence in point A, hammer with elastomer cushion

6.3.6.5 Different material

Only one solution to the problem is now left. A different material with better fatigue properties has to be used. Alternatively, the same material may be employed if, by an appropriate material treatment, better fatigue characteristics are obtained. The original material was already treated by carbonization. It still is possible to extend the depth of the layer of material that is carbonized. Originally, the thickness of this layer was about 0.20 mm, a more intensive carbonization of the material extends the influenced zone to a depth of about 0.38 mm. The static characteristics of strength and stiffness of the material remain almost unchanged. Fig. 6.11 shows that the fatigue characteristics are considerably better in the area of high strain, and that they remain almost unchanged in the area of lower strain.

The life of the hammer is now increased to an acceptable level : $N = 23000$.

6.3.7 Conclusion

It is shown that the problem of fracture of the present structure at the critical locations is caused by its dynamic behavior. The stress response is a history of free decay after multiple impulses. The areas where fracture occurs are the areas of maximum modal strain. The

lowest two eigenmodes of the structure are responsible for its early fracture. Fatigue life of the structure is estimated with the local strain approach.

Several possible design modifications are examined and it is explained why all structural modifications will fail unless the load input, caused by the impulse is altered. An elastomer head is used in place of a metal head in order to reduce the frequency contents of the load input to a much smaller range.

However, an appropriate material treatment is necessary in order to increase the life of the structure sufficiently.

Conclusions and ideas for future development

A global methodology is developed that enables the engineer to simulate the fatigue behaviour of dynamically loaded structures. The proposed method handles all the different aspects that determine the process of fatigue crack initiation in a structure. Dynamic effects are taken into account and superposed to effects of static loading, geometry is modelled efficiently in areas of stress concentrations and advanced fatigue criteria are applied. Although the proposed approach functions in a step by step procedure the consecutive modules smoothly fit in a global and integrated methodology. The modular outfit allows easy interpretation of intermediate results. Moreover, at every level of the analysis experimental data can be used to validate numerical results. For each level updating procedures are provided that tune the numerical model to experimental values. In this way analytical and experimental data are complementary and together they form a unified basis for thorough understanding of the behaviour of the structure. Environmental effects and service conditions that affect fatigue behaviour are covered in a kind of black box approach. From a user point of view the method is easy to apply. The engineer still has to take some rather critical decisions on how to run his analysis. Preprocessing time is limited due to the simplicity of the structural boundary element model.

For every step of the analysis an efficient technique is presented that models physical reality closely without overcomplicating mathematical operations. An original combination of boundary element techniques with modal analysis methods is developed and a fast convolution algorithm is presented. The local strain approach is extended

with some complementary tools that allow the user to gain a thorough understanding of the problem he is facing. The parameters of main importance in fatigue behaviour are easily revealed by sensitivity analysis.

Future developments that are most urgent can be classified largely in two categories. Some methods that are used to describe the behaviour of the structure in one of the phases of the complete analysis still need to be improved, and on the other hand the different modules have to be integrated even more in one package that is still more accessible to a non-specialist user. Developments of the former type are required in the description of the dynamic behaviour of structures. Modelling of damping behaviour and nonlinearities is still rather awkward in numerical simulation. Validation of multiaxial fatigue theories and criteria still needs extensive research both on the numerical and on the experimental side. The material's database which is being updated continuously should be even more elaborated and accessible to non specialist users. Some degree of standardisation in data acquisition and representation of material characteristics is highly desirable. Another matter of growing interest is the applicability of fatigue theories to plastics and composite materials. As to the developments of the latter type it should be attempted to come up with a totally unified approach that allows a user with basic engineering understanding to perform an analysis successfully. Although fatigue analysis does require a large amount of experience of the engineer it should be endeavoured to facilitate his tasks as much as possible and to provide ample support in taking crucial decisions in his analysis.

Appendix A

Basic features of the boundary element method

A.1 Introduction

The boundary element method is a very useful tool in the numerical analysis of potential problems, diffusion problems, problems of heat transfer, problems of electro-magnetism, problems of elasticity, ... From a user point of view, it has basically the same capabilities as the finite difference method and the finite element method. The theoretical background is very different, though. This appendix outlines the theoretical fundamentals of the method.

A.2 Boundary integral formulation of a problem of elastostatics

There are two ways of introducing the boundary integral formulation. One of them employs the concept of weighted residuals and their minimization. The other approach starts from the general formulation of the principle of reciprocity. This approach is more intelligible since it is closely related to the engineer's intuition and to his way of understanding physical reality.

Consider an elastic body which is defined by its domain Ω and its boundary Γ (fig.A.1). The body Ω may be three-dimensional, and then the boundary Γ consists of two-dimensional plane or curved patches.

The body may be two-dimensional and then the boundary consists of one-dimensional straight or curved lines. The boundary must be continuous and piecewise smooth. The domain may contain holes. A normal vector $\underline{n}$ is defined which is pointing out of the domain, or into the internal holes, if any.

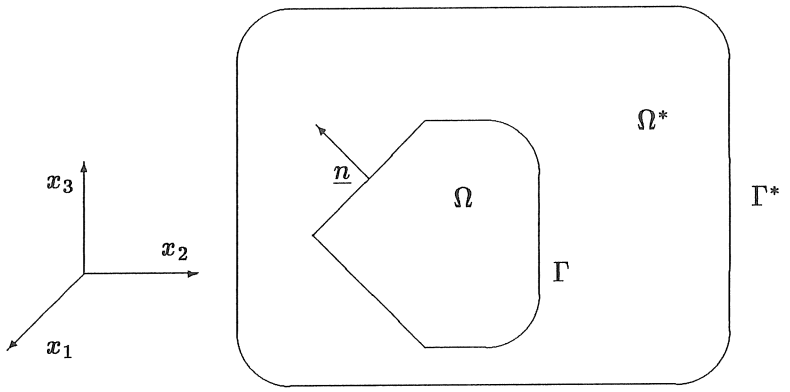

Figure A.1: Geometry of the bodies Ω and Ω^*

The body is in a state of static equilibrium under some imposed loads and displacements. This state is governed by the equations (A.1, A.2, A.3, A.4) :

$$\text{equilibrium :} \quad \begin{cases} \frac{\partial \sigma_{ij}}{\partial x_j} + f_i = 0 & \text{domain } \Omega \\ \sigma_{ij} n_j = p_i & \text{boundary } \Gamma \end{cases} \tag{A.1}$$

$$\text{deformation :} \quad \epsilon_{ij} = \frac{1}{2}\left(\frac{\partial u_i}{\partial x_j} + \frac{\partial u_j}{\partial x_i}\right) \tag{A.2}$$

$$\text{Hooke's law :} \quad \sigma_{ij} = C_{ijkl}\epsilon_{kl} \tag{A.3}$$

$$\text{boundary constraints :} \quad \begin{cases} u_i = \overline{u}_i & \text{boundary } \Gamma_u \\ p_i = \overline{p}_i & \text{boundary } \Gamma_p \end{cases} \tag{A.4}$$

The boundary Γ consists of a part Γ_u where the displacements $\overline{u}_i$ are imposed and another part Γ_p where the tractions $\overline{p}_i$ are imposed : $\Gamma = \Gamma_u + \Gamma_p$. The different types of loading are :

f_i : volume force (e. g. gravity, inertial load, ...)
$\overline{u}_i$: displacements on Γ_u
$\overline{p}_i$: surface load on Γ_p

The unknowns are the displacements u_i, the tractions p_i, the stresses σ_{ij} and the strains ϵ_{ij}.

Assume now another elastic body with domain Ω^* and boundary Γ^* that contains the body $\Omega + \Gamma$ (fig.A.1). This body is subjected to a load f_i^*. The state of displacement and stress is described by u_i^*, p_i^*, σ_{ij}^* and ϵ_{ij}^*. The shape of the body $\Omega^* + \Gamma^*$ and the load f_i^* will be described later. At this moment it is sufficient to require that the conditions of static equilibrium are fulfilled.

If one supposes purely elastic deformation, Maxwell's theorem then states :

$$\int_\Omega \sigma_{ij}\epsilon_{ij}^* \, d\Omega = \int_\Omega \sigma_{ij}^*\epsilon_{ij} \, d\Omega \tag{A.5}$$

Using equations A.1 both sides of the equation A.5 can be integrated by parts :

$$\begin{aligned} \int_\Omega \sigma_{ij}\epsilon_{ij}^* \, d\Omega &= \int_\Gamma p_i u_i^* \, d\Gamma + \int_\Omega f_i u_i^* \, d\Omega \\ \int_\Omega \sigma_{ij}^*\epsilon_{ij} \, d\Omega &= \int_\Gamma p_i^* u_i \, d\Gamma + \int_\Omega f_i^* u_i \, d\Omega \end{aligned}$$

Equation A.5 can thus be written as follows :

$$\int_\Gamma p_i u_i^* \, d\Gamma + \int_\Omega f_i u_i^* \, d\Omega = \int_\Gamma p_i^* u_i \, d\Gamma + \int_\Omega f_i^* u_i \, d\Omega \tag{A.6}$$

This equation is generally valid, irrespective of the choice of the body force f_i^*. Now is the time to define a specific shape for the body $\Omega^* + \Gamma^*$ and a specific function for the load f_i^*. Ω^* is assumed to fill the entire elastic space and its boundary Γ^* is taken to infinity. As to the load f_i^*, a special choice is made :

$$f_i^* = \Delta(\xi, x)e_i$$

where $\Delta(\xi, x)$ is the singular Dirac–function with ξ the point where the Dirac–function is applied and x the field point :

$$\Delta(\xi, x) = \begin{cases} 0 & \xi \neq x \\ \infty & \xi = x \end{cases}$$

Physically this corresponds to a positive unit point load applied at point ξ and pointing in direction $+i$. This particular choice of f_i^* then simplifies the second integral term on the right-hand side of equation A.6 :

$$\int_\Omega f_i^* u_i \, d\Omega = \begin{cases} u_i(\xi) e_i & , \quad \xi \in \Omega - \Gamma \\ 0 & , \quad \xi \notin \Omega + \Gamma \end{cases} \tag{A.7}$$

The corresponding functions u_i^* and p_i^* can now be written explicitly. They are called the fundamental solutions. The case of an infinite elastic medium Ω^* corresponds to the fundamental solution due to Kelvin (ref. [170]), and the appropriate expressions for the fundamental displacements and tractions are given by refs. [171,172] :

$$\begin{aligned} u_i^* &= u_{ji}^*(\xi, x) e_j \\ p_i^* &= p_{ji}^*(\xi, x) e_j \end{aligned}$$

The fundamental solutions are different depending upon the dimension of the problem (equations A.8, A.9) :

- Ω is a two-dimensional domain :

$$\begin{aligned} u_{ij}^*(\xi, x) &= -\frac{1}{8\pi(1-\nu)G} \left[(3-4\nu)\delta_{ij} \ln r - \frac{\partial r}{\partial x_i} \frac{\partial r}{\partial x_j} \right] \\ p_{ij}^*(\xi, x) &= -\frac{1}{4\pi(1-\nu)r} \left\{ \left[(1-2\nu)\delta_{ij} + 2\frac{\partial r}{\partial x_i} \frac{\partial r}{\partial x_j} \right] \frac{\partial r}{\partial n} \right. \\ &\quad \left. -(1-2\nu) \left(\frac{\partial r}{\partial x_i} n_j - \frac{\partial r}{\partial x_j} n_i \right) \right\} \end{aligned} \tag{A.8}$$

- Ω is a three-dimensional domain :

$$\begin{aligned} u_{ij}^*(\xi, x) &= \frac{1}{16\pi(1-\nu)Gr} \left[(3-4\nu)\delta_{ij} + \frac{\partial r}{\partial x_i} \frac{\partial r}{\partial x_j} \right] \\ p_{ij}^*(\xi, x) &= -\frac{1}{8\pi(1-\nu)r^2} \left\{ \left[(1-2\nu)\delta_{ij} + 3\frac{\partial r}{\partial x_i} \frac{\partial r}{\partial x_j} \right] \frac{\partial r}{\partial n} \right. \\ &\quad \left. -(1-2\nu) \left(\frac{\partial r}{\partial x_i} n_j - \frac{\partial r}{\partial x_j} n_i \right) \right\} \end{aligned} \tag{A.9}$$

In both cases, u^*_{ij} and p^*_{ij} represent the displacement and the traction in the j-direction at point x corresponding to a unit point force acting in the i-direction applied at point ξ. The other notations that are used are the following :

$$\begin{aligned} r_i &= x_i(x) - x_i(\xi) \\ r &= \sqrt{r_i r_i} \\ n_k &= k^{th} \text{ component of outward normal} \\ &= \underline{n}.\underline{e}_k \end{aligned}$$

Resuming equation A.6 and introducing equation A.7, one obtains :

$$\begin{aligned} c_{ij}u_j(\xi) &= \int_\Gamma u^*_{ij}(\xi,x)p_j(x)\,d\Gamma(x) - \int_\Gamma p^*_{ij}(\xi,x)u_j(x)\,d\Gamma(x) \\ &+ \int_\Omega u^*_{ij}(\xi,x)f_j(x)\,d\Omega(x) \end{aligned} \tag{A.10}$$

Equation A.7 shows that the value of the coefficient c_{ij} depends upon the location of the point ξ with respect to the body Ω. If the point ξ is located on the boundary Γ, then the value of c_{ij} depends upon the smoothness of the boundary at this particular location. Ref. [171] shows how this value can be computed for points which are located on the boundary. It is equal to 0.5 in case of a smooth boundary.

Equation A.10 is known as Somigliana's identity. It corresponds to one particular choice of ξ and i. An unlimited number of similar equations can be written by selecting another point ξ and a different direction i.

They all express a relation between the displacements u_i and the tractions p_i. It is noteworthy, however, that these quantities appear only in the integrals on the boundary Γ of the domain Ω. So, even if body forces $f_j(x)$ are present, the field of unknowns that has to be solved for is restricted to the boundary of the problem. This equation is the basis of the boundary element formulation.

A.3 Numerical implementation

This section shows how a set of equations A.10 can be used in the analysis of an elastostatic problem. Six consecutive steps are necessary

in order to come up with an algebraic representation of the problem :

1. **discretization of the boundary** In order to provide an accurate description of the geometrical characteristics of the boundary, a number N_m of distinct mesh points is defined on the boundary. The i^{th} coordinate of node j is denoted by $x_i^{(j)}$. The whole boundary is covered with elements :

$$\Gamma = \sum_{i=1}^{N_e} \Gamma_i$$

In case of a two-dimensional analysis the elements are straight or curved lines, joining the nodes. In case of a three-dimensional analysis, the elements are plane or curved patches. The shape of the elements is determined by the order of the interpolation functions φ_j : they can be linear, quadratic, cubic, ... The coordinates of a particular point on an element are written as a linear combination of the coordinates of the mesh points :

$$\underline{x} \in \Gamma_k \quad : \quad x_i = \sum_{j=1}^{n_m} \varphi_j x_i^{(j)}$$

where n_m is the number of mesh points per element, and N_m is the total number of mesh points on the full structure.

Some examples of interpolation functions φ_j are given in chapter 3 of ref. [171].

2. **discretization of the volume** In order to be able to compute the domain integral on the right hand side of equation A.10 the entire domain of the body has to be discretized in a number of volume-cells :

$$\Omega = \sum_{i=1}^{N_v} \Omega_i$$

The total number of nodes that are necessary for the definition of the volume-cells is denoted by N_n. In each of these points all the components of the body force f must be known. There are N_f components of body loads.

This discretization is exactly the same as the one used in finite element theory. This step is only necessary when body forces have to be taken into account.

3. **discretization of the field of unknowns** The variables u and p as they appear in equation A.10 are functions of the geometrical coordinate x. This coordinate varies only on the boundary. Similarly to step 1, a number N_c of discrete points is selected on the boundary. They are called the collocation points. The unknown functions $u(x)$ and $p(x)$ are written as a linear combination of the values at the collocation points :

$$\underline{x} \in \Gamma_k \quad : \quad \begin{cases} u_i &= \sum_{j=1}^{n_c} \phi_j u_i^{(j)} \\ p_i &= \sum_{j=1}^{n_c} \phi_j p_i^{(j)} \end{cases} \qquad \text{(A.11)}$$

where n_c is the number of collocation points per element, and N_c is the total number of collocation points.

There is no necessity for the collocation points to coincide with the mesh points. The only requirement that should be met in order to ensure accurate modelling of rigid-body displacements is that the number of mesh points per element n_m must not exceed the number of collocation points per element n_c : $n_m \leq n_c$.

Furthermore, the collocation points may not be located on the edges of the element. Discontinuous elements are allowable, they can even yield perfectly accurate results. The most common example is the constant element, which has only one collocation point, located in the middle of the element. Another example of discontinuous elements is shown in fig.A.2.

The definition of the elements, together with the choice of the degree of the interpolation function ϕ for the unknowns determine the total number of degrees of freedom of the problem. The number of degrees of freedom (dof) for two-dimensional and three-dimensional problems is indicated in table A.1.

4. **computation of the influence coefficients** Equation A.10 is a relation between all quantities u_i and p_i throughout the entire body. The coefficient of each variable is obtained by evaluation of the appropriate integral. Advanced numerical integra-

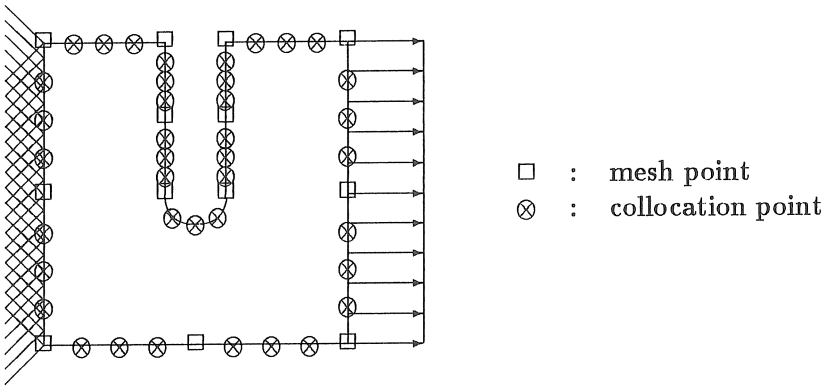

Figure A.2: Example of discontinuous elements in two-dimensional analysis (clamped square plate with notch subjected to tension)

type of analysis	2-D	3-D
no. of displacements per node	2	3
no. of tractions per node	2	3
total no. of displacements	$2N_c$	$3N_c$
total no. of tractions	$2N_c$	$3N_c$
total no. of dof	$4N_c$	$6N_c$

Table A.1: Number of degrees of freedom (dof)

tion schemes like Gauss-integration are used. Details of these procedures are provided in refs. [171,172].

Special attention should be paid to the evaluation of singular integrals. These singularities arise from the presence of a power of the distance r in the denominator of the fundamental solutions A.8, A.9. For field points close to the collocation point the integrand tends to infinity. Special integration schemes exist for an accurate evaluation of the integrals. Alternatively, an appropriate transformation of the integration variable eliminates the singularity. The author has modified the technique presented by MUSTOE (ref. [173]) for use in two-dimensional and three-dimensional problems.

This procedure of computing the influence coefficients in the three integrals of equation A.10 is repeated for each point ξ and each direction i. It will be shown that a number of N_d differ-

ent equations A.10 have to be written in order to come up with a set of equations that has a unique solution. Physically, this corresponds to consecutively applying a unit point load in each direction in each collocation point.

After having performed the evaluation of all the integrals over the boundary Γ and the domain Ω for each equation, one ends up with a set of N_d equations, that can be written in matrix notation A.12 :

$$[H]\{u\} = [G]\{p\} + [B]\{f\} \tag{A.12}$$

The order of these influence matrices and vectors is given in table A.2 :

matrix	dimension	contents
$[H]$	$N_d \times N_d$	coefficients of displacements
$[G]$	$N_d \times N_d$	coefficients of tractions
$[B]$	$N_d \times N_f$	coefficients of body forces
$\{u\}$	$N_d \times 1$	nodal displacements
$\{p\}$	$N_d \times 1$	nodal tractions
$\{f\}$	$N_f \times 1$	nodal body force components

Table A.2: Dimension of influence matrices and vectors

The matrices $[H]$, $[G]$ and $[B]$ contain only information on the geometry and the material properties of the body. They are independent of the boundary conditions and the body loads.

5. definition of boundary conditions The system of equations A.12 consists of N_d equations and it contains $2N_d$ variables u and p. A number of N_d variables is defined in advance. In a particular collocation point and in a certain direction, either the displacement or the traction is fixed. In case the displacement is imposed, the traction, which holds the body at the imposed displacement, is unknown. In case the traction is imposed, the displacement of the body at this collocation point is unknown.

The second terms on the right-hand sides of equations A.12 are constant. They depend only on the body forces that are applied.

One can rearrange all the equations A.12 in such a way that all the unknowns are on the left-hand side of the equations. All the terms that involve imposed boundary conditions and body forces are summed on the right-hand side. The matrix notation then becomes :

$$[A]\{x\} = \{y\}$$

The order of this matrix and these vectors is given in table A.3 :

matrix	dimension	contents
$[A]$	$N_d \times N_d$	coefficients of unknowns
$\{x\}$	$N_d \times 1$	unknowns
$\{y\}$	$N_d \times 1$	right-hand side coefficients

Table A.3: Dimension of the set of equations

6. solution of the system of equations Matrix equation A.12 contains a set of N_d equations with N_d unknowns. This system of equations can be solved for the vector x using standard solution schemes. It should be noted, however, that the matrix $[A]$ is generally fully populated and non-symmetric. This observation imposes some severe constraints on the algorithm that should be used to solve this set of equations. Some commercial powerful algorithms are available however that solve these problems in a fast and accurate manner (ref. [75]). Depending upon the type of the boundary condition, the unknown x_k is a displacement or a traction.

After having completed all of these steps, the basic problem is solved. At this moment only the values at the collocation points are known. The values of the displacements and tractions at any point on the boundary Γ are found from a linear superposition of the values at the collocation points.

A.4 Displacements and stresses at points located inside the domain or on the boundary

A.4.1 Internal points

Equation A.10 is a continuous representation of displacements at any point ξ that belongs to the domain Ω. It is used for the computation of the displacements at internal points of the domain, which are obtained from the displacements and the tractions at the boundary Γ. Introduction of equation A.10 into A.2 and A.3 leads to an expression for the stresses in internal points of the domain :

$$\begin{aligned}\sigma_{ij}(\xi) &= \int_\Gamma u^*_{ijk}(\xi,x)p_k(x)\,d\Gamma(x) - \int_\Gamma p^*_{ijk}(\xi,x)u_k(x)\,d\Gamma(x) \\ &+ \int_\Omega u^*_{ijk}(\xi,x)f_k(x)\,d\Omega(x) \qquad \text{(A.13)}\end{aligned}$$

Ref. [171] provides an explicit formulation for the fundamental solutions u^*_{ijk} and p^*_{ijk} :

$$\begin{aligned}u^*_{ijk} &= -\sigma_{ijk} \\ &= \frac{1}{4\alpha\pi(1-\nu)r^\alpha}\left\{(1-2\nu)\left(\frac{\partial r}{\partial x_i}\delta_{jk}+\frac{\partial r}{\partial x_k}\delta_{ij}-\frac{\partial r}{\partial x_j}\delta_{ki}\right)\right. \\ &\left.+\beta\frac{\partial r}{\partial x_i}\frac{\partial r}{\partial x_j}\frac{\partial r}{\partial x_k}\right\} \\ p^*_{ijk} &= \frac{G}{2\alpha\pi(1-\nu)r^\beta}\left\{\beta\frac{\partial r}{\partial n}\left[(1-2\nu)\delta_{ij}\frac{\partial r}{\partial x_k}-\gamma\frac{\partial r}{\partial x_i}\frac{\partial r}{\partial x_j}\frac{\partial r}{\partial x_k}\right.\right. \\ &\left.+\nu\left(\delta_{ik}\frac{\partial r}{\partial x_j}+\delta_{jk}\frac{\partial r}{\partial x_i}\right)\right]+\beta\nu\left(n_i\frac{\partial r}{\partial x_j}\frac{\partial r}{\partial x_k}+n_j\frac{\partial r}{\partial x_i}\frac{\partial r}{\partial x_i}\right) \\ &\left.+(1-2\nu)\left(\beta n_k\frac{\partial r}{\partial x_i}\frac{\partial r}{\partial x_j}+n_j\delta_{ik}+n_i\delta_{jk}\right)-(1-4\nu)n_k\delta_{ij}\right\}\end{aligned}$$

with :

two dimensions : $\alpha = 1, \beta = 2, \gamma = 4$
three dimensions : $\alpha = 2, \beta = 3, \gamma = 5$

A.4.2 Stresses on the boundary

The general equation A.13 may be used here. However, singularities occur as the load point goes to the boundary and the distance r goes to zero. Another approach is preferable since it does not involve any integration.

Assume a general three-dimensional boundary element with a local cartesian coordinate system tangent to its surface. The interpolation functions A.11 express the displacements u_i and tractions p_i in any point on the boundary element Γ_k in terms of the nodal values $u_i^{(j)}$ and $p_i^{(j)}$. The three components of the strain tensor over the surface of the boundary can be obtained by (i and j refer to the axes in the local coordinate system) :

$$\varepsilon_{ij} = \frac{1}{2}\left(\frac{\partial u_j}{\partial x_i} + \frac{\partial u_i}{\partial x_j}\right) \qquad i, j = 1, 2$$

These equations are used in addition to the equations of equilibrium A.1 and Hooke's law A.3 :

$$\begin{aligned}
\sigma_{11} &= \frac{1}{1-\nu}\left[\nu\sigma_{33} + 2G(\varepsilon_{11} + \nu\varepsilon_{22})\right] \\
\sigma_{12} &= 2G\varepsilon_{12} \\
\sigma_{22} &= \frac{1}{1-\nu}\left[\nu\sigma_{33} + 2G(\varepsilon_{22} + \nu\varepsilon_{11})\right] \\
\sigma_{13} &= p_1 \\
\sigma_{23} &= p_2 \\
\sigma_{33} &= p_3
\end{aligned}$$

In this way stresses at the boundary are obtained directly from displacements.

Appendix B

Numerical evaluation of material characteristics

This appendix describes the numerical procedure used for the evaluation of cyclic and fatigue material properties.

B.1 Cyclic material properties

The material behaviour is described by the constitutive relation B.1.

$$\frac{\Delta\varepsilon}{2} = \frac{\Delta\sigma}{2E} + \left(\frac{\Delta\sigma}{2K'}\right)^{\frac{1}{n'}} \tag{B.1}$$

Three coefficients E, K' and n' describe the cyclic behaviour of the material completely. They should be extracted from a number of measurements of corresponding $(\Delta\sigma, \Delta\varepsilon)$ values. As the purely elastic behaviour is equal in both cyclic and monotonic loading the modulus of elasticity can be assumed to be constant. For most technical materials this coefficient is well known. In case it is not, a number of simple static tests at low amplitude suffice to determine this quantity. It is the slope of the regression line between stress and strain.

The remaining constants K' and n' are computed without making use of equation B.1 directly. Rather the plastic term of this equation is written :

$$\frac{\Delta\varepsilon_p}{2} = \left(\frac{\Delta\sigma}{2K'}\right)^{\frac{1}{n'}}$$

Taking the logarithm of both sides leads to :

$$n' \log \frac{\Delta\varepsilon_p}{2} = \log \frac{\Delta\sigma}{2} - \log K'$$

Since $\Delta\varepsilon_p = \Delta\varepsilon - \Delta\varepsilon_e$ this expression is written :

$$n' \log \frac{\Delta\varepsilon - \Delta\varepsilon_e}{2} = \log \frac{\Delta\sigma}{2} - \log K'$$

$$n' \log \frac{\Delta\varepsilon - \frac{\Delta\sigma}{E}}{2} = \log \frac{\Delta\sigma}{2} - \log K'$$

This equation is written in a general shape :

$$\alpha x_i + \beta_i = y_i \tag{B.2}$$

where : $\alpha = n'$: the slope of the regression line
$\beta = \log K'$: the constant of the regression line
$x_i = \log \frac{\Delta\varepsilon - \frac{\Delta\sigma}{E}}{2}$: computed from measured quantities
$x_i = \log \frac{\Delta\sigma}{2}$: computed from measured quantities

The coefficients α and β are obtained directly from equations in section 1.6.2 [174]. An example of this analysis is given in [175].

B.2 Fatigue properties

B.2.1 General procedure

The general strain–life -curve is expressed :

$$\frac{\Delta\varepsilon}{2} = \frac{\sigma'_f}{E} N^b + \varepsilon'_f N^c \tag{B.3}$$

Four coefficients σ'_f, b, ε'_f, c describe the fatigue behaviour of the material. They should be extracted from a number of measurements of corresponding $(\Delta\varepsilon, N)$ values. The cyclic constitutive law B.1 is used in conjunction with equation B.3 :

$$\frac{\Delta\varepsilon}{2} = \frac{\Delta\varepsilon_e}{2} + \frac{\Delta\varepsilon_p}{2} = \frac{\Delta\sigma}{2E} + \left(\frac{\Delta\sigma}{2K'}\right)^{\frac{1}{n'}} = \frac{\sigma'_f}{E} N^b + \varepsilon'_f N^c$$

Elastic and plastic terms of both equations are set equal :

$$\frac{\Delta\varepsilon}{2E} = \frac{\sigma'_f}{E} N^b \qquad \text{and} \qquad \left(\frac{\Delta\sigma}{2K'}\right)^{\frac{1}{n'}} = \varepsilon'_f N^c$$

$$\log \frac{\Delta\sigma}{2} = \log \sigma'_f + b \log N \tag{B.4}$$

$$\frac{1}{n'} \log \frac{\Delta\sigma}{2K'} = \log \varepsilon'_f + c \log N \tag{B.5}$$

Both formulations have the same shape as equation B.2. In the elastic equation B.4, b is the slope α of the regression line and $\log \sigma'_f$ the constant β, $\log N$ is the measured x_i, and $\log \frac{\Delta\sigma}{2}$ the measured y_i. In the plastic equation B.5, c is the slope α of the regression line and $\log \varepsilon'_f$ the constant β, $\log N$ is the measured x_i and $\frac{1}{n'} \log \frac{\Delta\sigma}{2K'}$ the measured y_i. As for the constitutive equations (section B.1), the coefficients α and β are obtained directly [174].

B.2.2 General remarks

Scatter on measured fatigue data is significant, particularly in the area of high-cycle fatigue. The curve that is obtained by application of the above procedure corresponds to a probability of failure of 50%. The effect that life is predicted in an unconservative way is overcome either by selecting only the points that correspond to the shortest life at a certain strain level, either by applying a reduction factor on the life that is finally obtained using the entire data set.

It is stated in section 5.2.2.3 that the strain–life -curve should provide accurate data in that portion of the curve where maximum strain amplitudes are expected. These cycles are most damaging in the entire lifetime. This implies that particular attention should be paid to the low-cycle fatigue portion of the strain–life -curve for load variations in the low-cycle area or the transition area. The high-cycle fatigue portion of the curve is then less important. The high-cycle portion of the curve should be modelled accurately when maximum amplitudes of the complete strain sequence exceed the fatigue limit only slightly. Materials that exhibit a true fatigue limit below which no damage accumulation occurs can often be modelled by explicitly setting c equal to 0.

B.3 Statistical analysis

Similar operations are required to determine the different data sets (n', K'), (b, σ'_f), (c, ε'_f). In the determination of (b, σ'_f) and (c, ε'_f) a single measurement point is obtained for each specimen. Conventional statistical analysis is used to estimate mean values and standard deviations on (b, σ'_f) and (c, ε'_f). The measurement of cyclic characteristics is different in a sense that several measurement points are used for a single specimen. Statistical analysis is a little more complex. A complete test comprises several specimens, each specimen being sampled multiple times. It is thus not a priori obvious that all the measurement points can be gathered in a single data set. The statistical characteristics of each separate specimen have to be compared in order to investigate if all the measurements belong to a unique distribution. A FISHER-test on standard deviation and a STUDENT-test on mean values reveal whether the difference between individual specimens are significant or not. Details of these tests are described in [174, Chap.5]. An example of a complete statistical analysis on steel 14NiCrMo13 is presented in [175].

Appendix C

Measurement of structural damping characteristics

The damping properties of a structure play a particularly important role when problems of resonance fatigue occur. The damping characteristics determine the amplitude of vibration. This is why weakly damped structures are extremely sensitive to phenomena of resonance fatigue. Reliable determination of damping properties is therefore an essential element of the fatigue analysis.

Numerical modal analysis does not provide the damping characteristics of the structure, they have to be measured separately. When performing experimental modal analysis, parameter estimation routines solve for damping values. Depending on the time windows that are used on the response channels correction factors have to be applied to eliminate artificial damping. This corrective action is extremely inaccurate when damping values are low. An independent measurement procedure is necessary to estimate damping.

C.1 Logarithmic decrement method

Consider an impulse response function $h(t)$ of a single degree of freedom system (fig.C.1) :

$$h(t) = e^{-\sigma t} \sin \nu t = e^{-\zeta \nu t} \sin \nu t$$

where : σ : damping value

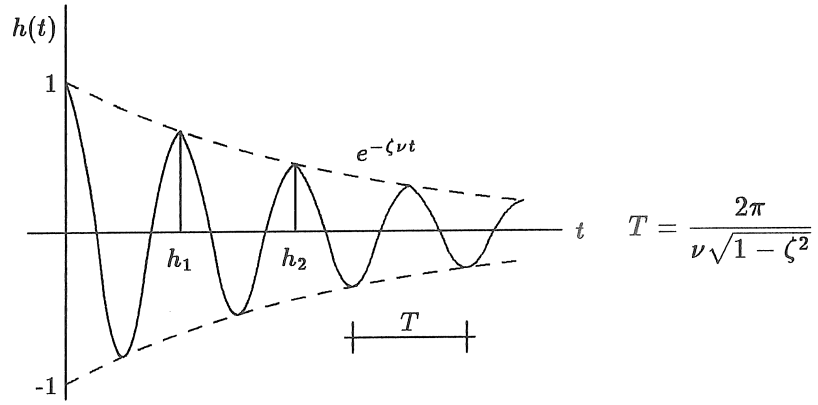

Figure C.1: Impulse response function

ζ : damping ratio
ν : damped resonance frequency

The function $h(t)$ expresses the time response for an excitation with a DIRAC-impulse. Taking the responses at times t_1 and $t_2 = t_1 + T$, the ratio of responses is given by :

$$\frac{h(t_2)}{h(t_1)} = e^{-\zeta\nu T}$$

Defining A as the logarithm of this ratio :

$$A = \ln\frac{h(t_2)}{h(t_1)} = -\zeta\nu T = \frac{2\pi\zeta}{\sqrt{1-\zeta^2}}$$

For most structures $\zeta < 0.2$, and thus a good approximation is obtained with $\sqrt{1-\zeta^2} \approx 1$:

$$A \approx \frac{A}{2\pi}$$

In practice it is more accurate to measure the amplitude after an elapse of a number of periods, and then :

$$\zeta \approx \frac{1}{2\pi n}\ln\frac{h(t_1)}{h(t_2)}$$

This approximation is valid only when damping is low. When $\zeta = 0.3$, the above substitution introduces an error of 6%.

For a multiple degree of freedom system, a DIRAC-impulse theoretically excites all the modes of the structure. The response signal

has to be filtered in order to eliminate all the components due to other modes. The filter must, however, be wide enough so as not to affect the free vibration decay in the selected mode. The filtering procedure introduces leakage which may distort the measured response signal. Widening the filter increases the possibility of multimodal response. A free decay with two closely spaced modes can not be analysed accurately by the logarithmic decrement method.

C.2 Practical application

The logarithmic decrement method is applied to a high pressure tube with geometry presented in fig.C.2 [178,179]. Experimental modal

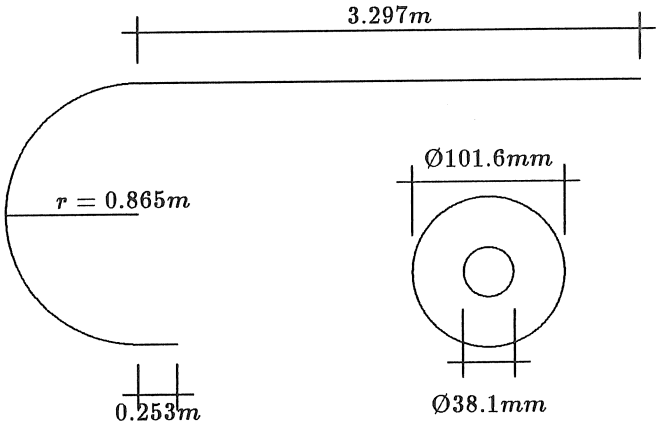

Figure C.2: Geometry of high pressure tube

analysis is performed using hammer excitation. Damped resonance frequency of the second out of the plane bending mode is 42.9 *Hz*. Use of an exponential window introduces artificial damping and parameter estimation yields a damping ratio of 0.597%. Application of a correction factor for the exponential window gives damping of negative sign. This is obviously impossible. In the logarithmic decrement method with a high-pass filter at 35 *Hz* and a low-pass filter at 50 *Hz* the time is measured that it takes the response to decrease to half its value : $t_{\frac{1}{2}} = 20.5s$. The number of cycles is n 879 and the damping ratio ζ is 0.013%.

Appendix D

Practical implementation

This appendix describes an example of a complete fatigue simulation software. It is complementary to the theoretical developments in chapters 2 – 5. No fundamentally new items are introduced. It explains how data are handled in each module and how data communication and transmission between modules is organised. Practical aspects are mentioned regarding preparation of data and construction of models.

D.1 General overview

After data have been prepared appropriately, three major modules are identified, in accordance with the theoretical developments :

1. modal strain : boundary element code BE
2. dynamic response : code RSPNS
3. fatigue life estimation : code FATAN

The flowchart fig.D.1 shows which data are processed, which input is needed in each stage and which results are obtained at each level of computation. Subsequent sections comment briefly on the input that has to be provided for each module and on the computational options that are available. Some practical information is given.

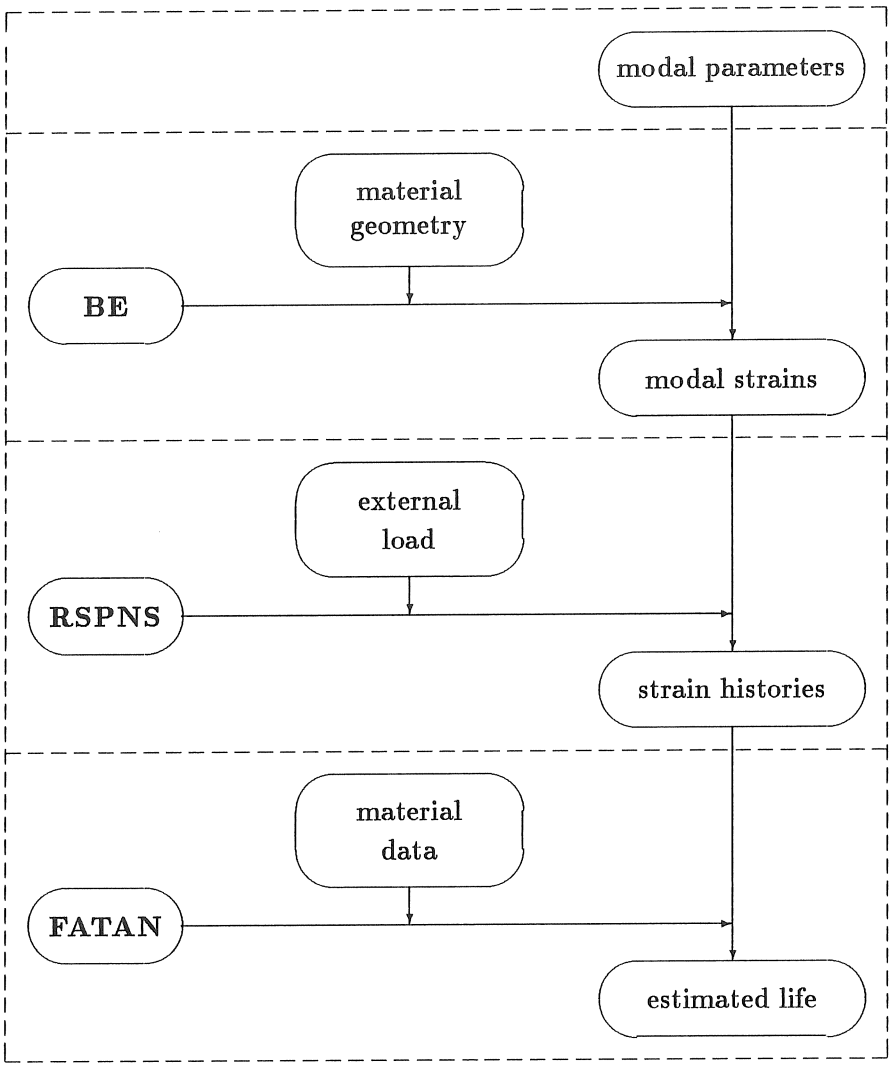

Figure D.1: Global scheme of computation

D.2 Data preparation

The dynamic behaviour of the structure determines its response to a certain external load. Resonance frequencies, damping characteristics and mode shapes constitute the full set of modal parameters describing the structure's dynamic behaviour.

Any major commercial finite element code provides the capabilities required to perform this analysis. Some simple tests have to be done to determine the damping characteristics of the structure. Alternatively, modal testing yields a complete set of modal parameters at once. Each of both approaches can be used separately in the present implementation. It is advisable, however, that both numerical and experimental data sets are completed, in order to build confidence in the obtained results. Experimental data are then very useful in updating the numerical model for optimum performance. Depending on whether mode shapes ψ are expressed in terms of displacements ψ^u, velocities ψ^v or accelerations ψ^a, conversion of quantities is still necessary. It is shown in section 3.2.2 that mode shapes are expressed preferably in terms of accelerations ψ^a or inertial forces ψ^f. This is done simply by a scaling procedure :

displacement modes	:	$\psi^f = \rho\omega^2\psi^u$
velocity modes	:	$\psi^f = \rho\omega\psi^v$
acceleration modes	:	$\psi^f = \rho\psi^a$

When only a portion of the structure is studied, the consideration made in section 4.3.4.2.1 are applicable. It is no longer sufficient to dispose of mode shape data in terms of inertial forces or accelerations only. Stress resultants at the cross sections where the studied portion is linked to the remainder of the structure need to be available as well. The quantities are expressed in terms of forces or moments. The same factor of proportionality that is used for inertial forces is applied to stress resultants. Knowledge of stress resultants is sufficient, rather than the actual stress distribution in the cross section. When information of the latter type is available it should be kept for further use.

When the complete set of modal parameters ω_k, ζ_k, ψ_k^f and if applicable, the stress resultants at the cross sections, are available, all the data are prepared to start the analysis.

D.3 Modal strain computation

The boundary element code BE computes the spatial strain distribution in a two- or three-dimensional solid, in areas on the boundary or inside the volume of the solid. The strain tensor is two-dimensional and principal components are computed as well. Theoretical background is described in sections 2.3.2 and 4.3.4.

D.3.1 Input data

A geometric model of the structure or the studied portion is constructed first. Multiply contiguous domains containing holes are allowed. A two-dimensional domain is bounded by a closed counter clockwise contour. Holes are bounded by clockwise contours. The boundary consists of straight lines and circular segments. The geometry of the elements is described by linear single parameter elements. Approximate functions are quadratic with one node placed centrally and two nodes located at a distance d $(0 \leq d \leq 1)$ at both sides of the centre. The elements are discontinuous. Three-dimensional structures are bounded by plane or curved patches. The geometry of the element is described by quadratic two parameter elements. Geometrical nodes are located at the corners and at the mid-sides of the elements. Approximate functions are quadratic with one node placed centrally and eight nodes at distances d $(0 \leq d \leq 1)$ from the element local axes. The elements are discontinuous. The geometrical or structural model should be constructed with due attention being paid to geometrical discontinuities, especially when load paths are expected to be disturbed by them. The size of the elements should be sufficiently small and the ratio of the dimensions of adjacent elements should not exceed 2.

The volumetric model can be constructed with much greater freedom. It only serves as a basis for representation of inertial loads and strictly, there is no further link to the real structure. Variations over the structure of inertial loads corresponding to the lower modes are generally fairly smooth. This statement is valid only when variations are considered over the global structure rather than on a local basis. The global distribution of inertial loads preponderates over local variations. Linear shape functions are suited for representing the variation of inertial loads over an element. It is noteworthy that the

volume model should correspond to the actual structure only on a global basis. Some parts of the structure can be covered multiply and some parts can be uncovered. Discontinuities of inertial loads over the elements' bounds are allowed. For two-dimensional structures, the volume model is also two-dimensional with an implicit assumption of constant variation over the third dimension of the structure. Inertial loads $[N/mm^3]$. All elements are quadrilateral. For three-dimensional structures the elements are eight-noded bricks.

The influence matrices $[H]$, $[G]$ and $[W]$ are computed. They depend only on geometry of the structure and on the material properties E and ν. They do not depend on loading and boundary conditions. The matrices $[H]$, $[G]$ and $[W]$ are saved on three separate files.

Next to geometry and material characteristics of the structure, inertial loads and boundary conditions have to be defined. Inertial loads are described by linear shape functions over an element. The values of inertial loads at the nodes have to be specified completely, i.e. each node should have two or three load components assigned to it, depending on the dimension of the problem.

The definition of boundary conditions in boundary element applications differs essentially from finite element concepts. Whereas in finite element practice reaction forces and moments are applied in discrete nodes, the boundary element method distributes the total resulting force or moment over an element. Further the boundary element method in its general two- or three-dimensional does not recognise rotations, but only translational degrees of freedom. Both aspects have some important consequences in modelling boundary conditions. As to the distributed character of boundary conditions, according to the principle of DE SAINT-VENANT [34] perturbations of the correct stress and strain patterns occur only in a region close to the boundary, while in remote areas the states of stress and strain gradually converge to the correct values. The modeller thus has some freedom in defining imposed tractions over the boundary. He should endeavour, though, to define a variation of imposed tractions that is as close as possible to the actual one, especially when points of interest are close to the boundary. As to the absence of rotational degrees of freedom, displacements at neighbouring nodes have to be computed such that the prescribed angle of rotation results.

A minimum number of displacement degrees of freedom has to

be imposed in order for the computation of modal strains to be feasible. The structure, or its isolated component, should be fixed in space. Two-dimensional structures are fixed by two constraints in one coordinate direction and one constraint in the other coordinate direction. Three-dimensional structures are fixed by three constraints in one direction, two constraints in another direction and one in the third direction.

The module of strain computation terminates with the storage of modal strain components in one or several points on the structure for all the nodes that are expected to be relevant for response analysis.

D.3.2 Computational options

All the areas that are potentially critical have to be examined by boundary element analysis. Depending on the number and on the size of critical areas the entire structure has to be modelled or, only one or a few sections have to be examined. It is advisable that following rules are obeyed when defining the structural models :

- geometry of the modelled structure or its portion should be simple
- geometry of the modelled structure or its portion should as much as possible resemble a square (two-dimensional) or a cube (three-dimensional) : the ratio of its boundary to its domain should be as low as possible (2D : ratio of the perimeter to the area of the domain, 3D : ratio of the area of the boundary surface to the volume of the domain)
- parts that behave more or less like independent components of the complete structure should be isolated preferably
- cross sections that link isolated parts to the remainder of the structure should be kept strictly minimum
- cross sections should not be taken in areas where stress concentrations occur

The decision as to whether the complete structure should be modelled depends mainly on the availability of data at cross sections. It is shown in section 4.3.4.2.1 that stress resultants or stress distributions

should be used preferably at cross sections. In structures composed of rods and beams, axial forces, shear forces, bending moments and torsional moments are easily available. In membrane, plate and shell type elements these quantities are also computed by the finite element code. Stress results in three-dimensional applications are more difficult to handle. Two examples are illustrative :

- the crankshaft of a combustion engine is a geometrically fairly complex structure. Modelling it with beam elements having six degrees of freedom per node is feasible, although many stress concentrations occur. Stress concentrations are recovered by isolating a well considered portion of the shaft and imposing relevant stress resultants in the boundary element analysis. The isolated portion is shown in fig.D.2.

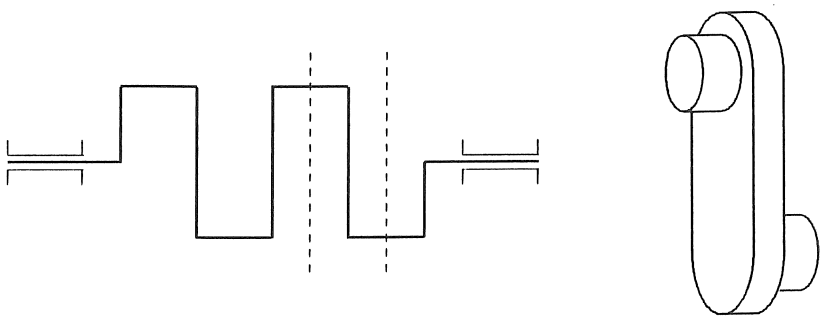

Figure D.2: Isolated portion of crankshaft

- the behaviour of a blade of a turbine engine is conventionally done with three-dimensional finite elements. The aspect ratio of some elements can be extremely bad. Stress quantities in sections near the root of the blade are quite difficult to handle. A dynamic model of the blade should therefore consist of shell elements with six degrees of freedom per node, each element possessing an appropriate value of thickness, or, if available, variable thickness. These elements provide improved capabilities of modelling global structural behaviour and stress resultants are easily computed. The stress resultants are converted to imposed tractions in the three-dimensional boundary element analysis.

D.3.3 General remarks

When one or several modes are not real, two separate computations have to be performed for this mode. The first computation uses only the imaginary part of mode shape data and the second computation uses only the real part. Complex modal strains are reconstituted by combining imaginary and real components of strain in $U_{IJk} + jV_{IJk}$.

The actual loading sequence is sometimes described by a measured nominal stress sequence. The only quantity that is necessary for the computation of the local stress and strain histories is the elastic stress concentration factor between stress at the measurement location and stress at the critical location. In order for this type of analysis to be feasible, a unique relation must exist between nominal strain and maximum strain. A static load consisting of imposed load or imposed strain can be applied.

D.4 Computation of dynamic response

The module RSPNS computes the dynamic response expressed in terms of strain at one or several locations on the structure. Theoretical background of this computation is described in sections 2.3.3 and 3.3.

D.4.1 Input data

Several data have to be provided as input to the program :

- the number of modes that is relevant to the applied load variation and in case an incomplete set of modes is used, the identification of the modes
- for each mode :
  - resonance frequencies ω_{dk}
  - damping ratios ζ_k
  - modal strains at the critical locations ψ_k^ε
- description of load variation : the function $f(t)$ should be described completely. Several options are available :
  - a DIRAC-impulse

– any function of the general shape :

$$f(t) = A(t - t_0)^n e^{kt} \sin(\omega t - \phi)$$

or a function comprising only one or two of its factors

– a random sequence, defined by a series of corresponding values (t_i, f_i). The time increment is not necessarily constant. Linear variation of load in intermediate time points is assumed and the discrete sequence is converted to a series of linear intervals.

- description of time interval for response computation. Three quantities have to be defined separately, start of time interval, end of interval and time increment between successive steps. Strictly, there are no upper nor lower bounds on the values of the increment. However, in order for the highest mode to be represented in an acceptable way, a value of 1/10 to 1/8 of the period of the highest mode should not be exceeded.

D.4.2 Computational options

Experience shows that the lower modes that are active in a considered area of the structure contribute significantly to the overall response at a particular location, unless some very local modes are unusually important. It can be argued on the other hand that only the modes with low associated damping values contribute to the process of damage accumulation. Sound engineering practice investigates the influence of every single mode in the frequency range of interest that is not obviously negligible.

When static loads are present the corresponding static strains have to be superposed to the alternating strains resulting from dynamic excitations. The values of strains should be added to the computed time sequence from the time the static load is applied.

D.4.3 General remarks

The strain tensor $\underline{\underline{\varepsilon}}$ generally comprises six independent components. When the point of interest is located at a free edge two or three components are approximately zero. Only three independent components

are left, when the state of deformation is plane strain and four components are non-zero when the state of stress is plane stress. Modal strain tensors are expressed by complex numbers when phase shifts occur in modes. The time variation of the strain tensor at a certain point is always real.

The factors of prime importance in the computation of dynamic response are the damping ratios of the different modes. These factors determine the amplitudes of vibration and thus the levels of dynamic strains that are reached. It is however extremely difficult to assess damping characteristics of a structure consistently. For modes with moderate (1%) to low (0.1%) damping the computed fatigue life is very sensitive to changes of damping ratios.

The module terminates with the storage of sequences of individual strain tensor components. Time information may be omitted here because it is no longer relevant to subsequent fatigue analysis.

D.5 Fatigue life estimation

The module FATAN computes the life of a structure subjected to a certain applied strain sequence. Theoretical background of this computation is described in sections 2.3.3, 5.2 and 5.4.

D.5.1 Input data

Several data have to be provided as input to the program :

- cyclic material parameters expressing the material's constitutive law and strain–life -relation
- one or several sequences of loading expressed in terms of nominal strain. Several points on the structure may be analysed at the same time. Only one complete fatigue life prediction is performed, however.
- one or several stress concentration factors expressing the relation between nominal strain and maximum elastic strain at the critical area. If several strain sequences are defined in the strain file, the corresponding values of concentration factors have to be provided. When the sequence that is provided is identical to

the maximum strain, a concentration factor equal to 1 has to be specified.

- a number of computational options, mentioned explicitly in section D.5.2.

In the present implementation the nominal strain sequences are either measured or computed. They are obtained as the result of the response computation explained in section D.4.

D.5.2 Computational options

Especially in the module of life prediction, some computational options are extremely important because they can give the user a feeling of which factors and which parameters are preponderant. The basic elements of the local strain approach are used throughout this implementation. It may be helpful for the user to compare his results with values obtained from alternative less conventional techniques which are not strictly applicable in the local strain method.

The program prompts the user for input on each of the options available. It is always possible to restart the analysis from a certain point and use the results obtained at that point. Four different levels are identified :

1. new computation
2. start from current nominal sequence
3. start from current local sequence
4. start from current hysteresis loops

This is an interesting feature in evaluating the influence of certain parameters without having to start all over again.

Several questions have to be answered successively, depending on the level one wants to start from. If a new computation is started, following questions appear on the screen :

dimension of analysis , default equal to 1

critical point three options are available :

- user-defined

- maximum amplitude of nominal strain
- maximum quadratic deviation

both the second and the third options are explained extensively in section 2.3.3.2

nature of the signal

- periodic : the number of periodic intervals to failure is computed
- non-periodic : the amount of decimal accumulated damage is computed

local strain computation two options are available :

- NEUBER approach
- hypothesis of local strain equalling nominal strain

both options are described in section 5.2.4.

sensitivity analysis sensitivities are computed for three parameters K_t, K' and n'. The maximum differences from the nominal value have to be specified. The computation is repeated for every combination of intermediate values with an increment of 1%. Finally a table is given with the lives for each combination of values of K_t, K' and n'.

counting algorithm two options are available :

- peak-valley counting
- rainflow counting

both options are explained extensively in section 5.2

amount of noise , expressed in percent of maximum nominal strain range

fatigue criterion modelling the material's fatigue behaviour :

- strain–life -relation
- MANSON-approximation
- COFFIN-approximation

the first option is described thoroughly in section 5.2.2.2. The second and the third alternatives are in the traditional method section 1.3.1.1.2.

Miner's constant

- equal to 1
- different from 1

a value different from 1 can be introduced for reasons of tuning the model with experimental data (section 5.4.2).

mean stress four options are available :

- no influence
- HAIGH-SODERBERG approximation
- MORROW approximation
- SMITH-TOPPER-WATSON parameter

the second option is explained in section 1.3.1.1.3, the third and the fourth options in section 1.3.2.1.3. It is advisable to always use the first and the fourth options and to compare both results.

After all necessary selections have been made, data are processed and intermediate results are stored on file.

D.5.3 General remarks

In order to gain fair understanding of the factors that have an important effect on lifetime it is advisable not to limit the analysis to a single run. Parameters like K_t, K' and n' and mean stress have a significant influence. Several runs should be tried with different combinations of parameters, and above all, results should be interpreted carefully.

As to the amount of noise that is eliminated, the user should be aware of the relative importance of smaller amplitudes with respect to the entire strain sequence. When the sequence is white noise, strain ranges up to 50% of maximum amplitude affect life only slightly. When the sequence is more or less constant amplitude and overloads occur only sparsely, the damage accumulated by the many smaller cycles may be more important than the damage due to the larger amplitudes.

Perhaps the most important element in the whole method is the material's database. For a very wide range of engineering materials data have been collected by thousands of companies and research institutes. Every material's scientist has his own methods of acquiring and analysing data and materials have been tested in all kinds of service conditions. Whereas monotonic tests have become standard procedures, this is not quite true with cyclic tests. Although some considerable progress has been made in recent years, there is still a lack of standardisation. Data provided in literature should still be handled with extreme care. Fatigue life characteristics of the material depend particularly strongly on the general conditions of loading. The type of loading may be bending, axial loading, torsion, or a combination, and the curve that is provided may be a 50%-curve, a 95%-curve, ... The notch effect is important in cases where S/N-data are taken. Heat treatments modify the material's properties drastically. It may then well be necessary to investigate the behaviour by experiment. The procedures for performing such tests and processing measurement data are described in section 5.2.2 and appendix B.

Bibliography

[1] W. HANISCH, *Termination of development to production stage*, Internal Report EXPPP, December 1988, Dr. Ing. H. C. F. Porsche, Weissach, Germany

[2] R. H. PARSONS, *History of the institution of mechanical engineers*, Institution of Mechanical Engineers, London, 1947

[3] G. M. VAN DIJK, J. B. DE JONGE, *Introduction to a fighter aircraft loading standard for fatigue evaluation "Falstaff"*, National Aerospace Laboratory NLR, Report NLR MP 75017 U

[4] M. HÜCK, W. SCHÜTZ, *Generating the Falstaff load history by digital mini computers* (Part II), IABG, Ottobrunn, Germany

[5] J. BRANGER, *Influence of the difference between genuine and generated load sequences, effect of ground-load variations of Falstaff-like programs*, Swiss Federal Aircraft Establishment

[6] D. SCHÜTZ, J. J. GERHARZ, *Enstaff a standard test sequence for composite components combining load and environment*, presented at the 14^{th} ICAF Symposium Ottawa, Canada, June 1987

[7] T. SWIFT, *Damage tolerance in pressurized fuselages*, presented to the 14^{th} ICAF Symposium, Ottawa, Canada, June 1987

[8] P. W. MARSHALL, *Strategies for fatigue design of deepwater platforms*, Transactions of ASME, Journal of Offshore Mechanics and Arctic Engineering, May 1988, Vol. 110, pp. 117-123

[9] K. J. MARSH, *Full-scale fatigue testing of components and structures*, Butterworths, London - Boston - Singapore - Sydney - Toronto - Wellington, 1988

[10] A. KOBAYASHI, I. SUSUKI, *A review of aeronautical fatigue investigations in Japan*, 20^{th} ICAF-conference, June 1987, Ottawa, Canada

[11] R. SNOEYS, D. ROESEMS, U. VANDEURZEN, P. VANHONACKER, *Survey of modal analysis applications*, Annals of the CIRP, Vol.28/2/1979, pp.497–510

[12] R. W. LANDGRAF, *Applications of fatigue analyses : transportation*, 3rd International Conference on Fatigue and Fatigue Thresholds, Charlottesville, Va., 1987, June 28 – July 3, pp.1593–1610

[13] D. ROESEMS, *Schadensanalyse und Lebensdauermodellierung bei Schwingfestigkeitsproblemen*, Porsche Internal Report VB EES Nr.1479

[14] W. EIFF, *Dynamische Betriebsfestigkeit SEAT Ibiza*, Porsche Internal Report VB EES No.1473

[15] C. J. TIVEY, *The utilization of fatigue life prediction techniques in support of a major vehicle project*, Proceedings of the Institution of Mechanical Engineers, Vol.200, No.D5, 1986, pp.S87–S94

[16] H. WOLTER, D. Zimmermann, *Fatigue life prediction within body engineering*, Ford Internal Report EJA No.800

[17] G. E. TOWNLEY, J. W. KLAHS, *Using test and system dynamic analysis for component life prediction*, Proceedings of IMAC4, Los Angeles, Ca., Feb.1986, pp.656–662

[18] R. SNOEYS, *Dimensioneren tegen vermoeiing*, 1988, Acco, Leuven, Amersfoort, 1988

[19] J. E. SHIGLEY, *Mechanical engineering design (first metric edition)*, McGraw-Hill Book Company, New York, London, 1986

[20] M. A. MINER, *Cumulative damage in fatigue*, Journal of Applied Mechanics, Trans. ASME, Vol. 12, Sept. 1945, pp. A-159–164

[21] CETIM, *Calcul des pièces à la fatigue, méthode du gradient*, © CETIM, 1980, ISBN 2-85400-022-6

[22] R. W. LANDGRAF, N. R. LAPOINTE, *Cyclic stress-strain concepts applied to component fatigue life prediction*, SAE 740280, Automotive Engineering Congress, Detroit, Mi., Feb.1974

[23] N. E. DOWLING, W. R. BROSE, W. K. WILSON, *Notched member fatigue life predictions by the local strain approach*, Westinghouse Research Laboratories

[24] N. E. DOWLING, *Fatigue failure predictions for complicated stress-strain histories*, Journal of Materials, Vol.7, No.1 March 1972, pp.71–87

[25] H. H. E. LEIPHOLZ, T. TOPPER, M. EL MENOUFY, *Lifetime prediction for metallic components subjected to stochastic loading*, Computers and Structures, Vol.16, No.1–4, 1983, pp.499–507

[26] JD. MORROW, D. SOCIE, *The evolution of fatigue crack initiation life prediction methods*, College of Engineering, University of Illinois, Urbana, Illinois, USA

[27] W. D. IWAN, *On a class of models for the yielding behaviour of continuous and composite systems*, Journal of Applied Mechanics, Trans. ASME, Sept. 1967, pp. 612–617

[28] F. ELLYIN, *Effect of tensile-mean-strain on plastic strain energy and cyclic response*, Journal of Engineering Materials and Technology, Trans. ASME, Vol. 107, April 1985, pp. 119–125

[29] R. N. SMITH, P. WATSON, T. H. TOPPER, *A stress-strain -function for fatigue of metals*, Journal of Materials JMLSA, Vol. 5, No. 4, 1970, pp. 767–778

[30] H. NEUBER, *Theory of stress concentration for shear-strained prismatical bodies with arbitrary nonlinear stress-strain law*, Journal of Applied Mechanics, Trans. ASME, December 1961, pp. 544–550

[31] J. BEAUFRONT, *Strain measurements with strain gauges and brittle lacquers*, Eurotest, International Scientific Association, Brussels

[32] M. F. KANNINEN, C. H. POPELAR, *Advanced fracture mechanics*, Oxford Engineering Science Series, Oxford University Press, New York, Clarendon Press, Oxford, 1985

[33] P. C. PARIS, G. C. SIH, *Stress analysis of cracks*, American Society for Testing and Materials, STP 381, 1965, pp. 30–81

[34] R. DECHAENE, *Sterkteleer en elasticiteit*, cursustekst 1982-83, Rijksuniversiteit Gent

[35] H. TADA, P. C. PARIS, G. IRWIN, *The stress analysis of cracks handbook*, Del Research Corporation, Hellertown, Pa., 1973

[36] G. C. SIH, *Handbook to stress intensity factors*, Lehigh University, 1973

[37] D. P. ROOKE, D. J. CARTWRIGHT, *Stress intensity factors*, Her Majesty's Stationary Office, London, 1976

[38] Y. MURAKAMI, *Stress intensity factors handbook (2 Vols.)*, Pergamon Press, New York, 1987

[39] W. ELBER, *The significance of fatigue crack closure*, American Society for Testing and Materials, STP 486, 1971, pp. 230–242

[40] H. NOWACK, R. MANSSEN, *Fatigue crack propagation of short and long cracks : physical basis, prediction methods and engineering significance*, Fatigue '87 (3 Vols.), Eds. R. O. Ritchie and E. A. Starke, Jr., EMAS, Warley, U.K., 1987

[41] J. D. WILLENBORG, R. M. ENGLE, H. A. WOOD, *Crack growth retardation model using an effective stress concept*, AFFDL-TM-FBR-71-1, Air Force Flight Dynamics Lab., 1971

[42] J. P. GALLAGHER, T. F. HUGHES, *Influence of yield stress on overload affected fatigue crack growth behaviour in 4340 steel*, AFFDL-TR-74-27, Air Force Flight Dynamics Lab., Ohio 1974

[43] O. E. WHEELER, Journal of Basic Engineering, Trans. ASME, March 1972, pp. 181–186

[44] P. D. BELL, A. WOLFMAN, *Mathematical modeling of crack growth interaction effects*, American Society for Testing and Materials, STP 595, 1976, pp. 157–171

[45] H. FÜHRING, T. SEEGER, *Structural memory of cracked components under irregular loading*, American Society for Testing and Materials, STP 677, 1979, pp. 144–167

[46] J. SCHIJVE, *Fatigue crack growth predictions for variable amplitude and spectrum loading*, Delft University of Technology, Faculty of Aerospace Engineering, Report LR-526, May 1987

[47] D. VANDEPITTE, *Berekening van constructies*, (3 Vols.), Wetenschappelijke Uitgeverij Story-Scientia, Gent - Antwerpen - Brussel - Leuven, 1982

[48] O. C. ZIENKIEWICZ, *The finite element method*, Third Edition, 1985, ISBN 0-07-084072-5

[49] R. DECHAENE, *De eindige elementen-methode in de toegepaste mechanica*, cursustekst 1981-82, Rijksuniversiteit te Gent

[50] R. D. COOK, *Concepts and applications of finite element analysis*, Second Edition, John Wiley and Sons, New York - Chichester - Brisbane - Toronto - Singapore, 1981

[51] T. J. R. HUGHES, *The finite element method*, Prentice-Hall International Editions, 1987

[52] MASSONNET, *Méthode des éléments de surface*, Third Cycle Course on the Boundary Element Method, Université Libre de Bruxelles, 1986

[53] D. DE VIS, W. HENDRICX, H. VERELST, C. DELLO, *Fatigue analysis of impact loaded structures*, 13^{th} International Modal Analysis Seminar, Leuven, September 1988

[54] S. H. CRANDALL, W. D. MARK, *Random vibrations in mechanical systems*, 1963, Academic Press, London - New York

[55] J. D. ROBSON, *An introduction to random vibration*, 1963, Edinburgh University Press, Elsevier Publishing Company, Amsterdam

[56] S. KARLIN, *A first course in stochastic processes*, 1966, Academic Press, New York - London

[57] R. L. KASHYAP, A. RAMACHANDRA RAO, *Dynamic stochastic models for empirical data*, 1976, Academic Press, New York - London

[58] D. E. NEWLAND, *Random vibrations and spectral analysis*, 1975, Longman Group Limited, London, ISBN-0-582-46334-3

[59] L. GRISARD, *Étude numérique d'une structure soumise à vibrations aléatoires*, Internal Report Belgian Army, TDLM, 1988

[60] J. W. MILES, *On structural fatigue under random loading*, Journal of Aeronautical Science. Vol.21, No.11, November 1954, pp. 753–762

[61] P. H. WIRSCHING, E. B. HAUGEN, *A general statistical model for random fatigue*, Transactions of ASME, Journal of Engineering Materials and Technology, Vol.96, No.1, January 1974, pp.34–40

[62] P. H. WIRSCHING, E. B. HAUGEN, *Probabilistic design for random fatigue load*, American Society of Civil Engineers, Journal of the Engineering Mechanics Division, Vol.99, EM6, December 1973, pp.1165–1179

[63] A. H. -S. ANG, W. H. MUNSE, *Practical reliability basis for structural fatigue*, American Society of Civil Engineers, National Structural Engineering Conference, April 1975

[64] K. G. NOLTE, J. E. HANSFORD, *Closed form expressions for determining the fatigue damage of structures subjected to ocean waves*, Proceedings of the Offshore Technology Conference, OTC Paper No.2606, May 1976, pp.861–872

[65] R. M. WETZEL, *A method of fatigue damage analysis*, Scientific Research Report No.SR-71-107, Ford Motor Company, Dearborn, Michigan, September 1971

[66] J. P. GALLAGHER, H. D. STALNAKER, *Methods for analyzing fatigue crack growth rate behaviour associated with fatigue loading*, AIAA Paper No.74-367, 15^th Structures, Structural Dynamics and Materials Conference, Las Vegas, April 1974

[67] J. N. YANG, W. J. TRAPP, *Reliability analysis of aircraft structures under random loading and periodic inspection*, AIAA Journal, Vol.2, No.12, December 1974, pp.1623–1630

[68] P. H. WIRSCHING, A. MOHSEN SHEHATA, *Fatigue under wide band random stresses using the rainflow method*, Transaction of ASME, Journal of Engineering Materials and Technology, July 1977, pp.205–211

[69] H. FENECH, A. R. RAO, *Statistical analysis of fatigue failure due to flow noise excitations*, Transactions of ASME, Journal of Vibration, Acoustics, Stress, and Reliability in Design, July 1986, Vol.108, pp.249–254

[70] J. N. YANG, E. HEER, *Analytical procedure for estimating reliability of randomly excited structures*, NASA Technical Brief 71-10189, 1971

[71] W. H. HARTT, N. K. LIN, *A proposed stress history for fatigue testing applicable to offshore structures*, International Journal of Fatigue, Vol. 8, No. 2, April 1986, pp. 91-93

[72] A. G. HERNRIED, K.-L. LAU, *Dynamic response of secondary systems in structures subjected to earthquake excitation*, Journal of Modal Analysis, January 1988, pp. 20-25

[73] E. VANSEVENANT, *A subsurface integrity model in grinding*, Ph.D. Dissertation, Faculty of Applied Science, KU Leuven, 1987, 87D3

[74] C. C. GROSJEAN *Numerieke analyse*, course, Rijksuniversiteit Gent, 1981

[75] N., *Nag Fortran mini manual, Mark 11, An introductory guide to the Nag Fortran manual*, Numerical Algorithms Group Ltd., 256 Bansbury Road, Oxford OX2 7DE, UK, 1984

[76] T. JANTER, *Construction oriented updating of dynamic finite element models using experimental modal data*, Ph.D. Dissertation, Faculty of Applied Sciences, KU Leuven, 1989, 89D1

[77] E. HEYLEN, *Optimization of model matrices of mechanical structures using experimental modal data*, Ph.D. Dissertation, Faculty of Applied Sciences, KU Leuven, 1987, 87D5

[78] J. THEUNS, *Waterbouwkundige werken II*, course, Rijksuniversiteit Gent, 1984

[79] S. R. BISHOP, L. M. LEUNG, L. N. VIRGIN, *Predicting incipient jumps to resonance of compliant marine structures in an evolving sea-state*, Transactions of ASME, Journal of Offshore Mechanics and Arctic Engineering, Vol.109, August 1987, pp. 223–228

[80] R. P. NORDGREN, *Analysis of high-frequency vibration of tension leg platforms*, Transactions of ASME, Journal of Offshore Mechanics and Arctic Engineering, Vol.109, May 1987, pp. 119–125

[81] P. W. MARSHALL, *Strategies for fatigue design of deepwater platforms*, Transactions of ASME, Journal of Offshore Mechanics and Arctic Engineering, Vol.110, May 1988, pp. 117–123

[82] B. PERRETT, *An evaluation of a method of reconstituting fatigue loading from rainflow counting*, RAE, Farnborough, U.K., 14^{th} ICAF-Symposium, June 1987, Ottawa, Canada

[83] J. DE RIES, *Mechanische trillingen*, Course Rijksuniversiteit Gent, 1984

[84] F. KULIASKO, H. VAN KEER, *Variatierekening in de analyse*, Course, RUGent, 1982

[85] J. H. WILKINSON, C. REISCH, *Linear Algebra*, Springer Verlag, Berlin, Heidelberg, New York, 1971

[86] K. J. BATHE, E. L. WILSON, *Solution methods for eigenvalue problems in structural mechanics*, International Journal for Numerical Methods in Engineering, 1973, Vol. 6, pp.213–226

[87] K. J. BATHE, E. L. WILSON, *Large eigenvalue problems in dynamic analysis*, Journal of the Engineering Mechanics Division, ASCE, 1972, Vol. 98, pp. 1471–1485

[88] K.-J. BATHE, E. L. WILSON, *Numerical methods in finite element analysis*, Prentice-Hall Inc., Englewood Cliffs, New Jersey, 1976

[89] H. A. KAMEL, E. L. WILSON, *Microcomputers in finite element analysis*, Vols. I-II, Institut pour la promotion des sciences de l'ingénieur, Paris, June 7–9, 1983

[90] M. GÉRADIN, *Une étude comparative des méthodes numériques en analyse dynamique des structures*, Bulletin de l'Association Technique Maritime et Aéronautique, No.78, Paris, 1978

[91] T. X. SONG, P. Q. ZHANG, W. Q. FENG, T. C. HUANG, *Experimental strain modal analysis by space time regression method in the time domain*, International Journal of Modal Analysis, January 1989, Vol. 4, No.1, pp.15–19

[92] D. FORMENTI, *Experimental modal analysis*, University of Cincinnati, Ohio, short course, 1977

[93] B. HAISTY, W. SPRINGER, *A simplified method for extracting rotational degree-of-freedom information from modal test data*, International Journal of Modal Analysis, 1/3, July 1986, pp.35–39

[94] R. GUYAN, *Reduction of stiffness and mass matrices*, AIAA-Journal, 3/2, February 1965, p.380

[95] J. O'CALLAHAN, I.-W. LIEU, C.-M. CHOU, *Determination of rotational degrees of freedom for moment transfers in structural modifications*, Proceedings of 3^{rd} IMAC, Orlando, Fl., Febraury 1985

[96] J. O'CALLAHAN, P. AVITABILE, I.-W. LIEU, R. MADDEN, *An efficient method for determining rotational degrees of freedom from analytical and experimental modal data*, Proceedings of 4^{th} IMAC, Los Angeles, Ca., February 1986, pp.50–58

[97] T. VAN DER WAETEREN, *Mechanische trillingen*, course, KU. Leuven

[98] P. Sas, M. De Smet, T. Janter, H. Van Brussel, *Intelligent meshing facility for dynamic finite element calculations*, Proceedings of the 14^{th} International Seminar on Modal Analysis, September 1989, Katholieke Universiteit Leuven

[99] H. G. Natke, *Einführung in die Theorie und Praxis des Zeitreihen und Modalanalyse*, F. Vieweg und Sohn Verlag, Braunschweig 1983

[100] M. Wei, T. Janter, *Optimization of mathematical models via selected physical parameters*, Proceedings of 6^{th} IMAC, Orlando, Fl., February 1988

[101] S. Lammens, H. Platteau, *Lokalisatie van modelfouten bij dynamische eindige-elementenberekeningen, gebruik makend van experimentele modale analyse*, KUL, 89EP13

[102] N. A. J. Lieven, D. J. Ewins, *Spatial correlation of mode shapes, the coordinate modal assurance criterion COMAC*, Proceedings of 6^{th} IMAC, Kissimmee, Fl., February 1988, pp.690–695

[103] R. J. Allemang, D. L. Brown, *A correlation coefficient for modal vector analysis*, Proceedings of 1^{st} IMAC, Orlando, Fl., February 1982, pp.110–116

[104] E. Fissette, C. Stavrinidis, S. Ibrahim, *error location and updating of analytical dynamic models using a force balance method*, Proceedings of 6^{th} IMAC, Kissimmee, Fl., February 1988, pp.1063–1070

[105] G. R. Tomlinson, *A comparison of procedures for identifying nonlinear systems without a priori information*, 13^{th} International Seminar on Modal Analysis, KUL, September 1988

[106] N., *Systus user manual, version 230*, Framasoft, Division of Framatome, Paris

[107] J. Barlow, *More on optimal stress points – reduced integration, element distortions and error estimation*, International Journal for Numerical Methods in Engineering, Vol.26, July 1989, pp.1487–1504

[108] L. S. D. MORLEY, *The triangular equilibrium element in the solution of plate bending problems*, Areo Quarterly, Vol.19, pp.149–169, 1968 ; *On the constant moment plate bending element*, Journal of Strain Analysis, Vol.6, No.20, 1971

[109] B. FRAEYS DE VEUBEKE, *Displacement and equilibrium models in the finite element method*, Stress Analysis, Eds. O. C. Zienkiewicz and G. S. Holister, Wiley, 1965

[110] N. SARIGUL, R. H. GALLAGHER, *Assumed stress function finite element method : two-dimensional elasticity* International Journal for Numerical Methods in Engineering, Vol.26, July 1989, pp.1577–1598

[111] J. JIROUSEK, *A new finite element model with adjustable accuracy*, FEM'87 Congress, Baden-Baden, November 1987, Edited by IKOSS GmbH

[112] C. SOMIGLIANA, *Sopra l'equilibrio di un corpo elastico isotropo*, Il nuovo ciemento, 1886, pp.17–19

[113] R. D. MINDLIN, *Force at a point in the interior of a semi-infinite solid*, 1936, Physics 7, pp.195–202

[114] F. JOHN, *Plane waves and spherical means applied to partial differential equations*, Interscience Publishers, New York, 1955

[115] S. K. VOGEL, F. J. RIZZO, *An integral equation formulation of three dimensional anisotropic elastostatic boundary value problems*, Journal of Elasticity 3, 1973, pp.203–216

[116] J. L. SYNGE, *The hypercircle in mathematical physics*, Cambridge University Press, Cambridge, 1957

[117] E. RANK, *Adaptive h-, p- and hp- versions for boundary integral element methods*, International Journal for Numerical Methods in Engineering, Vol.28, June 1989, pp.1335–1349

[118] J. L. WEARING, M. A. SHEIKH, *Three dimensional stress analysis using an indirect discrete boundary method*, Proceedings of 1^{st} European Boundary Element Meeting, Ed. J.L. Migeot, SDRC, Paris, May 1988

[119] J. L. MIGEOT, *Problems of edges, corners and multiple media*, 3^{rd} cycle course on the Boundary Element Method, 1986, ULB

[120] A. DEB, P. K. BANERJEE, *A comparison between isoparametric Lagrangian elements in 2D BEM*, International Journal for Numerical Methods in Engineering, Vol.26, July 1989, pp.1539–1555

[121] D. A. PAPE, P. K. BANERJEE, *Treatment of body forces in 2D elastostatic BEM using particular integrals*, Transactions of ASME, Journal of Applied Mechanics, Vol.54, December 1987, pp.866–871

[122] A. C. ERINGEN, E. S. SUHUBI, *Elastodynamics Vol. II : Linear theory*, Academic Press, London, 1975

[123] G. D. MANOLIS, S. AHMAD, P. K. BANERJEE, *Boundary element method implementation for three-dimensional transient elastodynamics*, Developments in Boundary Element Methods – 4, Eds. P. K. Banerjee and J. O. Watson, Elsevier Applied Science Publishers, London - New York

[124] T. A. CRUSE, F. J. RIZZO, *A direct formulation and numerical solution of the general transient elastodynamic problem, I*, J. Math. Anal. Appl. 22, 1968, pp.244–259

[125] S. AHMAD, P. K. BANERJEE, *Multi-domain BEM for two-dimensional problems of elastodynamics*, International Journal for Numerical Methods in Engineering, Vol.26, 1988, pp.891–911

[126] D. NARDINI, C. A. BREBBIA, *A new approach to free vibration analysis using boundary elements*, Boundary Element Methods in Engineering, Ed. C. A. Brebbia, Springer Verlag, Berlin, 1982

[127] J.L. MIGEOT, *Coupling of the boundary element method with the finite element method*, 3^{rd} cycle course on the Boundary Element Method, 1986, ULB

[128] P. GEORGIOU, *Coupling of the direct boundary element method with the finite element displacement technique in elastostatics*, Ph.D. Dissertation, University of Southampton, 1981

[129] O. C. ZIENKIEWICZ, D. W. KELLY, P. BETTESS, *The coupling of the finite element method and boundary solution procedures*, International Journal of Numerical Methods in Engineering, Vol.11, 1977, pp.355–375

[130] D. P. HENRY JR., P. K. BANERJEE, *A new boundary element formulation for two- and three-dimensional elastoplasticity using particular integrals*, International Journal of Numerical Methods in Engineering, Vol.26, 1988, pp.2079–2096

[131] R. WINTER, *Cyclic plastic deformation of a circular plate with work hardening*, Transactions of ASME, Journal of Pressure Vessel Technology, November 1984, Vol.106, pp.336–341

[132] A. K. MILLER, *Modelling of cyclic plasticity with unified constitutive equations : improvements in simulating normal and anomalous Bauschinger effects*, Transactions ASME, Journal of Engineering Materials and Technology, April 1980, Vol.102, pp.215–222

[133] H. R. JHANSALE, T. H. TOPPER, *Engineering analysis of the inelastic strain response of a structural metal under variable cyclic strains*, ASTM STP 519, 1973, pp.246–270

[134] D. LEFEBVRE, F. ELLYIN, *Cyclic response and inelastic strain energy in low cycle fatigue*, International Journal of Fatigue, Vol.6, No.1, January 1984, pp.9–15

[135] F. ELLYIN, *Effect of tensile mean strain on plastic strain energy and cyclic response*, Transactions of ASME, Journal of Engineering Materials and Technology, April 1985, Vol.107, pp.118–125

[136] JD. MORROW, R. F. TULLER, *Low-cycle fatigue evaluation of Inconel 713C and Waspalloy*, Transactions of ASME, Journal of Basic Engineering, Vol.87, No.2, 1965, pp.275–289

[137] R. W. LANDGRAF, *The resistence of metals to cyclic deformation*, ASTM STP 467, 1970, pp.3–36

[138] J. B. DE JONGE, *Fatigue load monitoring of tactical aircraft*, 29^{th} meeting of the AGARD SMP, Istanbul 1969, NLR Report, TR 69063 U, August 1969

[139] J. B. DE JONGE, *The monitoring of fatigue loads*, ICAS-Congress, Rome, Sept. 1970, NLR Report MP 70010

[140] M. MATSUISKI, T. ENDO, *Fatigue of metals subjected to varying stress*, Kyushu district meeting of the Japan Society of Mechanical Engineers, March 1968

[141] B. PERRETT, *The effect on fatigue performance and life estimation of load sequence reconstitution, methods applied to aircraft load histories*, RAE Technical Memorandum, Mat/Str 1058

[142] J. B. DE JONGE, *The analysis of load-time histories by means of counting algorithms*, National Aerospace Laboratory NLR, The Netherlands

[143] K. J. MILLER, M. W. BROWN, *Multiaxial fatigue : a review*, KVIV-studiedagen Metaalvermoeiing, KUL, 1979

[144] W. SAWERT, *Verhalten der Baustaehle bei wechselnder mehrachsiger Beanspruchung*, Z VdI 87, No.39/40, 1943, pp.609–615

[145] G. SINES, G. OHGI, *Fatigue criteria under combined stresses or strains*, Transactions of ASME, Journal of Engineering Materials and Technology, Vol. 103, April 1981, pp. 82-90

[146] B. N. LEIS, T. H. TOPPER, *Long-life notch strength reduction due to local biaxial state of stress*, Transactions of ASME, Journal of Engineering Materials and Technology, July 1977, pp. 215–221

[147] W. R. MILLER, K. OHJI, J. MARIN, *Rotating principal stress axes in high-cycle fatigue*, Transactions of ASME, Journal of Basic Engineering, March 1967, pp. 76-80

[148] B. N. LEIS, J. H. LAFLEN, *Problems in damage analysis under nonproportional cycling*, Transactions of ASME, Journal of Engineering Materials and Technology, January 1980, Vol. 102, pp. 127–134

[149] R. DECHAENE, *Plasticiteit*, cursustekst 1981-82, Rijksuniversiteit te Gent

[150] W. PRAGER, *The theory of plasticity : a survey of recent achievements*, paper presented in London, January 1955

[151] Z. MRÓZ, *An attempt to describe the behaviour of metals under cyclic loads using a more general workhardening model*, Acta Mechanica 7, 1969, pp. 199-212

[152] R. D. KRIEG, *A practical two surface plasticity theory*, Transaction of ASME, Journal of Applied Mechanics, September 1975, pp. 641-646

[153] D. L. MCDOWELL, *A two surface model for transient nonproportional cyclic plasticity : development of appropriate equations*, Transactions of ASME, Journal of Applied Mechanics, June 1985, Vol. 52, pp. 298-302

[154] H. S. LAMBA, O. M. SIDEBOTTOM, *Cyclic plasticity for nonproportional paths : cyclic hardening, erasure of memory, and subsequent strain hardening experiments*, Transactions of ASME, Journal of Engineering Materials and Technology, Vol. 100, January 1978, pp. 96-103

[155] Y. OHASHI, M. KAWAI, T. KAITO, *Inelastic behaviour of type 316 stainless steel under multiaxial nonproportional cyclic stressings at elevated temperature*, Transactions of ASME, Journal of Engineering Materials and Technology, April 1985, Vol. 107, pp. 101–109

[156] P. M. NAGHDI, D. J. NIKKEL JR., *Two-dimensional strain cycling in plasticity*, Transactions ASME, Journal of Applied Mechanics, December 1986, Vol.53, pp.821–830

[157] D. L. MCDOWELL, *An evaluation of recent developments in hardening and flow rules for rate-independent, nonproportional cyclic plasticity*, Transactions ASME, Journal of Applied Mechanics, June 1987, Vol.54, pp.323–334

[158] K. KANAZAWA, K. J. MILLER, M. W. BROWN, *Low-cycle fatigue under out-of-phase loading conditions*, Transactions of ASME, Journal of Engineering Materials and Technology, July 1977, pp. 222–228

[159] D. LEFEBVRE, K. W. NEALE, F. ELLYIN, *A criterion for low-cycle fatigue failure under biaxial states of stress*, Transactions of ASME, Journal of Engineering Materials and Technology, January 1981, Vol.103, pp.1–6

[160] Y. S. GARUD, *A new approach to the evaluation of fatigue multiaxial loading*, Transactions of ASME, Journal of Engineering Materials and Technology, Vol.103, April 1981, pp.118–125

[161] F. ELLYIN, B. VALAIRE, *High-strain multiaxial fatigue*, Transactions of ASME, Journal of Engineering Materials and Technology, July 1982, Vol.104, pp.165–173

[162] F. ELLYIN, D. KUJAWSKI, *Plastic strain energy in fatigue failure*, Transaction of ASME, Journal of Pressure Vessel Technology, November 1984, Vol. 106, pp. 342-347

[163] K. GOLOS, F. ELLYIN, *A total strain energy density theory for cumulative fatigue damage*, Transactions of ASME, Journal of Pressure Vessel Technology, Vol. 110, February 1988, pp. 36-41

[164] D. SOCIE, *Multiaxial fatigue damage models*, Transactions of ASME, Journal of Engineering Materials and Technology, October 1987, Vol. 107, pp. 293-298

[165] D. SOCIE, *Fatigue damage maps*, June 1987, Fatigue '87, Vol. II, Eds. R. O. Ritchie and E. A. Starke Jr., EMAS Ltd., Warley, West Midlands, UK, pp.599–616

[166] D. SOCIE, L. E. WAIL, D. F. DITTMER, *Biaxial fatigue of Inconel 718 including mean stress effects*, Multiaxial fatigue, ASTM STP 853, 1985, pp.463–481

[167] W. N. FINDLEY, *Journal of Engineering for Industry*, Transactions of ASME, Series B. Vol.81, pp.301–306

[168] V. GRUBISIC, H. LOWAK, *Fatigue life prediction and test results of aluminum alloy components*, Fatigue Prevention and Design, EMAS Ltd., ISBN-0-947817-27-1, July 1986, Ed. J. T. Barnby

[169] D. VANDEPITTE, P. SAS, C. LIEFOOGHE, F. SEYS, *Case study of fracture of a mechanical component due to resonance fatigue*, presented at IMAC7, 1989, Las Vegas, pp.1508–1515

[170] A. E. H. LOVE, *A treatise on the mathematical theory of elasticity*, Dover, New York, 1944

[171] C. A. BREBBIA, J. C. F. TELLES, L. C. WROBEL, *Boundary element techniques, theory and applications in engineering*, Springer-Verlag, Berlin, Heidelberg, New York, Tokyo, 1984

[172] F. VAN DER WEEËN, *Application of boundary elements to structural analysis*, National Contact Group on the Boundary Element Method, Third Cycle Course on the Boundary Element Method, Brussels, 1986

[173] G. G. W. MUSTOE, *Advanced integration schemes over boundary elements and volume cells for two and three dimensional non-linear analysis*, Developments in Boundary Element Methods – 3, Eds. P. K. Banerjee and S. Mukherjee, Elsevier Applied Science Publishers, London and New York

[174] J. PETERS, R. GOBIN, *Statistiek in de werkplaats en meettechniek*, 1983, Course, Katholieke Universiteit Leuven

[175] C. LIEFOOGHE, F. SEYS, D. VANDEPITTE, P. SAS, *Détermination expérimentale du comportement cyclique du matériau*, Final Report project IRSIA 4764, November 1988, Appendix 7

[176] H. VERELST, E. HEUBLEIN, *Détermination des courbes de* WÖHLER *de l'acier 74.1*, Final Report project IRSIA 4764, November 1988, Appendix 6

[177] J. SOOVERE, M. L. DRAKE, *Aerospace structures technology, damping design guide*, AFWAL-TR-84-3089, Wright Patterson Air Force Base, Ohio 45433

[178] T. JANTER, D. VANDEPITTE, P. SAS, *Studie tot het verminderen van restspanningen in hogedrukpijpen door trillingsexcitatie*, December 1985, Internal Report KUL-BP, 85R23

[179] P. BIELEN, M. DE SMET, T. JANTER, D. VANDEPITTE, P. SAS, *Studie tot het verminderen van restspanningen in hogedrukpijpen door trillingsexcitatie*, March 1988, Internal Report KUL-BP, 88R7